DIGITALCOMMONS
@WAYNESTATE

Wayne State University

Wayne State University Dissertations

1-1-2017

Evaluation Of Earth-Abundant Monometallic And Bimetallic Complexes For Catalytic Water Splitting

Kenneth Kwame Kpogo
Wayne State University,

Follow this and additional works at: https://digitalcommons.wayne.edu/oa_dissertations

Part of the Inorganic Chemistry Commons, and the Oil, Gas, and Energy Commons

Recommended Citation
Kpogo, Kenneth Kwame, "Evaluation Of Earth-Abundant Monometallic And Bimetallic Complexes For Catalytic Water Splitting" (2017). *Wayne State University Dissertations*. 1826.
https://digitalcommons.wayne.edu/oa_dissertations/1826

This Open Access Dissertation is brought to you for free and open access by DigitalCommons@WayneState. It has been accepted for inclusion in Wayne State University Dissertations by an authorized administrator of DigitalCommons@WayneState.

www.manaraa.com

EVALUATION OF EARTH-ABUNDANT MONOMETALLIC AND BIMETALLIC COMPLEXES FOR CATALYTIC WATER SPLITTING

by

KENNETH KWAME KPOGO

DISSERTATION

Submitted to the Graduate School

of Wayne State University,

Detroit, Michigan

in partial fulfillment of the requirements

for the degree of

DOCTOR OF PHILOSOPHY

2017

MAJOR: CHEMISTRY (Inorganic)

Approved By:

_____

Advisor Date

_____

_____

_____

www.manaraa.com

© COPYRIGHT BY

KENNETH KWAME KPOGO

2017

All Rights Reserved

www.manaraa.com

DEDICATION

I dedicate this dissertation to Nicole and my lovely family for encouraging me to pursue my dreams and completing this work. You are the love of my life.

www.manaraa.com

ACKNOWLEDGEMENTS

To say that Dr. Claudio Verani is a great mentor and advisor would be an understatement. He is the best to have. My wonderful encounter with Dr. Verani began in March of 2012 when I was visiting with Wayne State as part of my admission process. Dr. Verani was then the Graduate recruiting committee chairman. I was very skeptical about coming to school in Detroit but he did a great job in allaying all my fears. He personally convinced me that Wayne State was the best choice I could possibly make for my academic career. I found his enthusiasm in talking about Wayne State endearing. I have to say he was to a large extent the reason why I chose to come to Wayne State for my Ph.D. I naturally chose to join his research group when it was time to select mentors and advisors and I have not regretted my decision. Dr. Verani's passion for science is second to none. He exemplifies science in everything he does. He has an ability to answer and explain my scientific questions in depth and yet simplifies them with an interdisciplinary point of view that makes them easier to understand. His unassuming personality makes him approachable. He always has an open office door as well as an open mind for conversation. I have spent many hours discussing a wide variety of subjects with Claudio (he insists everyone calls him by his first name). He is a true friend to all his students He genuinely cares about us as individuals and serves as my life mentor as well as an academic mentor. He helps me find my drive and passion for education and research and I consider him as my role model. It has been a worthwhile experience to have Dr. Verani's guidance these past five years and I am looking forward to more years of having him as a mentor even after my graduation.

My appreciation goes to my dissertation advisory committee, Professors Matthew J. Allen, Jennifer L. Stockdill, and Eranda Nikolla for gracefully accepting to be my academic mentors during my Ph.D. program. I am grateful to you all for time and energy you sacrificed in meeting

www.manaraa.com

with me on numerous occasions. Your tenacity of purpose, patience and special attention you paid to my oral document, pre-defense document, and dissertation is second to none. Thank you.

Scientific breakthroughs mostly occur through collaborative efforts, and the Verani group at WSU is noted for having long-standing collaborations. The first and perhaps the longest one is the one with the Schlegel group at WSU. I was a beneficiary of this collaboration and I thank Professor Schlegel, Drs. Mazumder, and Thapa for their professionalism in helping me with computational calculations. I appreciate your patience during the long discussions and your insightful conversations, points of view and advice. Professor John Endicott is acknowledged for the discussions regarding the photochemistry of ruthenium and other questions and the numerous times I 'invaded' his office with general questions.

External collaborations are a testament to the visibility of research efforts. I want to thank Professor Adam T. Fiedler for recognizing the quality of work the Verani group does and deciding to collaborate with us. I am grateful for the steadfastness and professionalism exhibited by Prof. Fiedler during the collaborative work in general and the preparation of the manuscript. Dr. Denan Wang is acknowledged for synthesizing the compounds for our work. Dr. Oleg Poluektov and Dr. Jens Niklas from Argonne National Laboratory are acknowledged for their help with EPR spectroscopy.

My stay in the Verani group would not have been successful without the camaraderie and professional cohesion that exists in the laboratory. From the moment I joined the lab, I was met with senior students such as Drs. Dakshika Wanniarachchi, Dajena Tomco, Lanka Wickramasinghe and Debashis Basu who exuded scientific confidence and guided me when I was still 'green'. I appreciate all their help in transforming me from a synthetic organic chemist to an expert in physical inorganic chemistry. I learned a lot from my other colleagues with whom I spent

www.manaraa.com

the last five years. To Dr. Sunalee Gonawala, thank you for your calm assertiveness and the knowledge you imparted when we were collaborating on the corrosion project. To Habib Baydoun, buddy thank you for your valuable criticisms, they challenged me in ways you could not imagine. To Pavithra Hettiarachchi, Danushka Ekanayake, Nour El-Harakeh, Krista Kulesa, Jordyn Burdick and Isuri Weeraratne I thank you all for encouraging me, helping me in all our scientific endeavors. I feel I am losing a great team but I know you will be there for me for a long time. I appreciate all the strong bonds of friendship that we held. To Pavithra and Danushka, it was really great collaborating with you on the nickel and copper projects as well because you brought excellent professionalism to our discussions despite us being friends. Thank you. To Fredericka and Samudra, You have already shown that you will be assets to the Verani group. Fredericka, I know you will bring the same dedication and strong work ethic that you are known for to the Verani group, and I am sure Samudra will as well, I appreciate you all.

I want to acknowledge the indefatigable Mrs. Melissa Rochon, for her immense help during my entire stay in the Chemistry department at Wayne State University. You always had time for my questions and helped me with all my problems. I am grateful to Ms. Jacqueline Baldyga and the entire front office staff, I am forever indebted to you. I would like to express appreciation to the business office staff and the professors I taught undergraduate chemistry for. Professors, Barber, Zibuck, Munk and Matti, you imparted excellent teaching skills during my time as a graduate teaching assistant. Thank you.

Thanks to the entire Lumigen Instrument Center staff for helping with data analysis, especially Drs. Judy Westrick, Lew, Phil Martin, Yuri Danylyuk, Mei, Bashar Ksebati, and Johnna Birbeck, Nestor Ocampo, and all the science store staff.

www.manaraa.com

To Nicole Lenca and my family, words cannot express my gratitude for all that you have sacrificed for me during these difficult times. Your patience, care, and affection are greatly treasured. We made it!!

Last but not the least, I am grateful to the Chemistry Department and Graduate School, Wayne State University for offering me teaching assistantships and tuition support at various points during my study. I acknowledge the Department of Energy (DOE) and the National Science Foundation (NSF) for providing the necessary funding for my research and stipend with various grants. I want to thank Dr. Paul Schaap and his wife, the Mary Gorny Wood Foundation, and the Thomas Rumble Foundation for supporting me with Fellowships during my Ph.D. Your financial support made graduate school bearable. Thank you.

www.manaraa.com

TABLE OF CONTENTS

www.manaraa.com

www.manaraa.com

www.manaraa.com

www.manaraa.com

www.manaraa.com

LIST OF FIGURES

www.manaraa.com

www.manaraa.com

www.manaraa.com

www.manaraa.com

LIST OF TABLES

www.manaraa.com

LIST OF SCHEMES

www.manaraa.com

CHAPTER 1:

INTRODUCTION

Water Splitting

$$2H_2O \longrightarrow O_2 + 2H_2$$

www.manaraa.com

CHAPTER 1: INTRODUCTION

1.1. Background to Global Demand for Alternative Energy

Global population increase and pollution of the environment are major concerns.[1] According to the United Nations, about 89% of global energy sources are based on carbon sources. The use of these fuels produces byproducts such as carbon dioxide (CO_2) and other harmful greenhouse gases. It is expected that, at the turn of the century, more than 13.3 gigatonnes of carbon per year (GtC/yr) would be produced and have a harmful effect on our environment.[2] More alarming is the fact that carbon-based energy sources are not renewable and their substantial use will lead to their depletion by 2055 unless new sizable reserves are found.[3] This crisis, therefore, requires the search for an alternative energy source.[4] Hydrogen production from water using the Sun as an energy source is considered the answer to this looming global fuel crisis.[5] Water splitting involves a series of thermodynamically demanding redox reactions in which water is converted into its basic components, namely, dihydrogen and dioxygen, as shown in equations 1 to 3.[6-8]

$$2H_2O \rightarrow 2H_2 + O_2 \qquad (1)$$

$$2H_2O \rightarrow O_2 + 4H^+ + 4e^- \qquad E^0 = 1.23\ V \qquad (2)$$

$$4H^+ + 4e^- \rightarrow 2H_2 \qquad E^0 = 0\ V \qquad (3)$$

However, there is a thermodynamic barrier of 1.23 V for converting water into dihydrogen and dioxygen.[9] In order to overcome this energy barrier, an efficient, robust and affordable catalyst capable of offering a milder mechanistic pathway to obtain the desired products is needed. The development of water-splitting catalysts incorporating transition metals is of immense scientific interest. So far the most efficient water-splitting catalysts are noble metals such as ruthenium[10,11,12] and iridium.[13] Yet, in the past decade, commercial availability and Earth-abundance have become the overriding factors necessary to finding effective alternatives to these noble-metal catalysts. The

www.manaraa.com

development of electrocatalysts based on low-cost materials made of Earth-abundant metals such as cobalt,[14-21] nickel,[22-25] copper,[26-27] and iron,[28-30] is therefore perceived as an indispensable step towards the generation of efficient photocatalysts.

1.1.1 Hydrogen as an Energy Source

It is expected that hydrogen will eventually reduce the Earth's dependence on crude oil for its energy needs due to its high efficiency and low polluting nature.[1, 31,32] It can be easily stored in large quantities and transported with relative ease. Hydrogen can be obtained from the electrolysis of water, or the steam reformation of hydrocarbons such as methane. While steam reformation is currently the cheapest method of producing dihydrogen, it uses fossil fuels and contributes to greenhouse effects. It is therefore not a sustainable alternative to the use of coal.

The electrolysis of water to produce hydrogen, however, involves using electric current to 'split' water into its constituent elements, dihydrogen and oxygen gas. This process is unfortunately extremely expensive because it requires the use of electrical energy as well.

1.1.2 Oxygen as an Energy Source

To produce dihydrogen by electrolysis, water must be oxidized according to Equation 2. This process is energetically unfavorable as it requires 238 $kJmol^{-1}$ of energy to occur. The scientific community has invested effort in solving this 'bottleneck' over the past two decades.[11, 33-42] Nature, however, has perfected the process of oxidizing water to dioxygen through photosynthesis. Plants oxidize water to oxygen by utilizing a series of proton-coupled-electron-transfer (PCET) steps that include the formation of an essential O – O bond in the photosystem II (PS II).[43]

In the (PS) II, a central pair of chlorophylls, P_{680} is excited by energy from the sun and transfers an electron to the acceptor system Q_A, which subsequently reduces CO_2. The oxidized

www.manaraa.com

form, $P_{680}^{\bullet+}$, which is a strong oxidant with an oxidation potential of *ca.* +1.2 V versus the normal hydrogen electrode (vs NHE),[44] then recovers the electron from a Mn_4Ca-cluster in the oxygen-evolving complex (OEC) via a tyrosine bridge.

After four consecutive electron abstractions from the OEC, two molecules of H_2O are oxidized to generate one molecule of O_2 and four protons as shown in equation 3 above. Numerous research efforts have been directed at mimicking this process. However, these efforts have been quite daunting due to the non-trivial multi electronic nature of producing hydrogen through photosynthesis, and the mechanistic intricacies associated with the photosynthetic process. There is, therefore, an urgent need to focus attention on some persisting design and mechanistic questions in order to develop a system optimized to support photocatalysis.

1.2. Methods of Water Splitting Catalysis

The process of converting water into dioxygen and dihydrogen, using a catalyst can be broadly categorized into two main categories.

1.2.1 Water Reduction Catalysis

A) **Electrocatalytic Proton/Water Reduction:** The catalytic reduction of weak organic acids in organic solvents, or of water, with a catalyst is known as electrocatalytic proton/water reduction. Typical acid sources for proton reduction are CH_3COOH and CF_3COOH, while water serves as the proton source for water reduction. An efficient proton/water reduction catalyst undergoes successive electron reductions to attain a monovalent state when an appropriate electrochemical potential is applied. The monovalent species is then nucleophilic enough to attract a proton and form a metallo-hydride and subsequently, produces hydrogen.

B) **Photocatalytic Water Reduction:** Water reduction by a catalyst, and photosensitizer in the presence of a sacrificial electron donor. Here also, the photosensitizer absorbs light radiation

www.manaraa.com

of an appropriate wavelength, is excited, and quenched by the electron donor. The photosensitizer subsequently transfers an electron to reduce the catalyst. Hydrogen is subsequently produced.

1.2.2 Water Oxidation Catalysis

A) **Chemical water oxidation:** This is a method of catalysis where a chemical substance is used as a sacrificial oxidant. In this type of water oxidation, the catalyst of choice, the substrate (water) and the chemical oxidant are reacted and the evolution of gas (oxygen) is observed and quantified after a specified period of time. An efficient chemical oxidant must have a reduction potential sufficient enough to oxidize the water oxidation catalyst.[45] Chemical oxidants such as cerium (IV) ammonium nitrate, Oxone ($KHSO_5$), NaOCl, are the most commonly used in chemical water oxidation The use of these oxidants is advantageous because it enables the study of oxidative intermediates in solution. They also aid in the production of relatively large amounts of oxygen, thereby making the screening of catalytic parameters for potential catalysts rapid and cost effective. The main disadvantage of their use is that they do not perfectly mimic the conditions that will be experienced by a catalyst and hence are considered preliminary at best.

B) **Electrocatalytic Water Oxidation:** In this method, the oxidation of water is achieved at the surface of an electrode when an electrochemical potential is applied to a solution containing an electrocatalyst.

C) **Photocatalytic Water Oxidation:** This process involves the use of a photosensitizer, a catalyst, and a sacrificial electron acceptor. The photosensitizer absorbs radiation of an appropriate wavelength and transitions to an excited state where the transfer of electron/s to the sacrificial acceptor takes place. The catalyst then transfers its electrons unto the photosensitizer by sequential oxidations until a high-valent electrophilic oxidation state is attained. Water then attacks and produces oxygen.

www.manaraa.com

1.3. Important Parameters for Electrocatalytic Water Splitting

A water-splitting catalyst must meet and be benchmarked against certain parameters that are relevant water splitting electrocatalysis.

Those parameters are:

Turnover number (TON): The number of moles of hydrogen generated per mole of catalyst used

TON = number of moles of hydrogen/number of moles of catalyst

Turnover frequency (TOF): The turnover number per unit time. This parameter describes the rate of efficiency of a catalyst.

TOF = TON/time

Faradaic efficiency (FE): The ratio of the number of moles of hydrogen generated (n_{H2}) to half of the moles of the number of electrons passed during the electrocatalytic experiment ($n_e/2$).

FE = $n_{H2}/(n_e/2)$

An efficient molecular electrocatalyst should operate at a Faradaic efficiency of 80 – 100%.

1.4. Mechanistic Pathways for Catalytic Water/Proton Reduction

The production of H_2 from Co^{III}-H follows either heterolytic or homolytic pathways shown in **Figure 1.1**.[46,16,47] The former mechanism relies on a single $Co^{III}–H^-$ reacting with another H^+, while homolytic mechanisms involve two independent $Co^{III}–H^-$moieties.[48]

The reliance on a particular mechanism is governed by factors such as the concentration of acid used,[49] catalyst design, applied potential,[50] the rate constants for hydride formation,[51] and whether H_2 is evolved by hydride protonation or dimerization.[52] Weak organic acids such as trifluoroacetic acid (TFA),[53-55] acetic acid, and triethyl ammonium chloride, have been used as proton source in electrocatalytic hydrogen production but are susceptible to concentration degradation, and organic waste produced during the production of dihydrogen.[56] The susceptibility

www.manaraa.com

to degradation can limit the wide use of weak acids as suitable proton sources, therefore a more benign source is desirable.

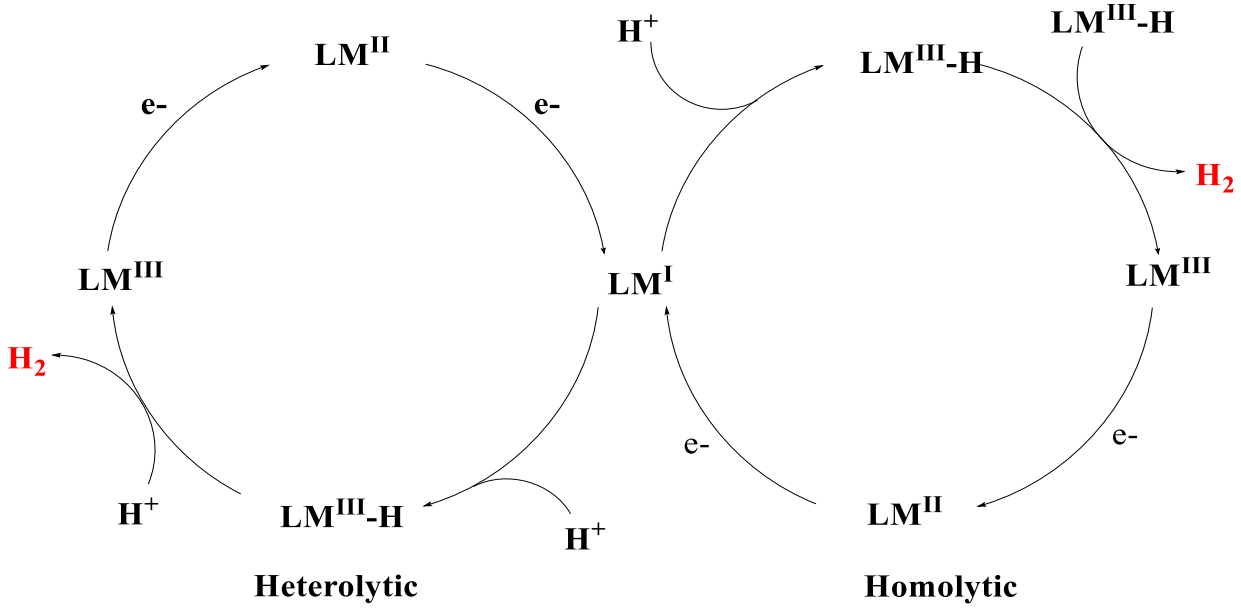

Figure 1.1. Generalized Catalytic mechanisms of H_2 generation.

1.5. Homogeneous Molecular Catalysts for Water/Proton Reduction

The efficient reduction of protons or water to form dihydrogen as shown in Equation 3 above is crucial to the use of hydrogen as the fuel for the future. Therefore Earth-abundant molecular proton/water reduction catalysts have been of immense scientific importance in the past three decades. Ideally, a transition metal-complex should be reduced to its monovalent state and be sufficiently nucleophilic when it accepts an electron. This nucleophilic monovalent species should then attract protons, reduce them to hydrogen and get oxidized to its original oxidation state. The most efficient proton reducing electrocatalysts are based on platinum complexes.[57,58] platinum catalysts are however expensive and rare. First-row transition metals such as manganese, iron,[29-30, 59-60] nickel,[23-25, 61-64] and cobalt[62, 65-67] have been explored as affordable replacements for the platinum catalysts.

www.manaraa.com

1.5.1 Molecular Water/Proton Reduction Catalysts based on Cobalt

1.5.1.1. Molecular Cobalt Oximes

Schrauzer and Holland[68] observed hydrogen evolved hydridocobaloximes when working on model analogs of Vitamin B12 **(Figure 1.2a)**. This discovery led to the exploration of the field of hydrogen generation led by Espenson and Connelly in 1986.[14] During their work on an analog of Schrauzer's cobaloxime **(Figure 1.2b)**, they found out that upon treatment of the complex with Cr^{2+} reductants under acidic conditions, hydrogen gas could be formed.

Peters *et al*,[53] and, Artero *et al*[50, 69] have studied cobalt-based oximes **(Figures 1.2c,d)** extensively and found that they are excellent catalysts for proton reduction in organic media with weak organic acids. These compounds require low overpotentials to generate hydrogen from acids. Verani[54] and coworkers performed an extensive study on cobalt oximes bearing hetero-axial ligands **(Figure 1.3)** to evaluate the effect of coordination preferences on their mechanistic pathways.

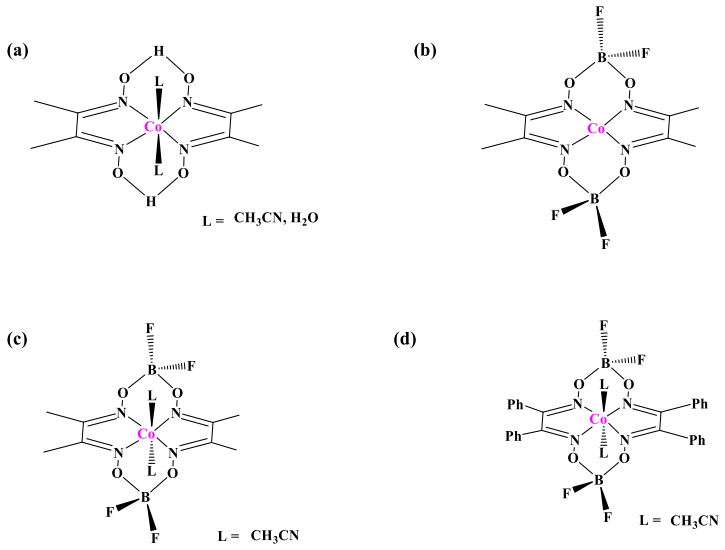

Figure 1.2. Selected cobalt-based oximes for proton reduction.

www.manaraa.com

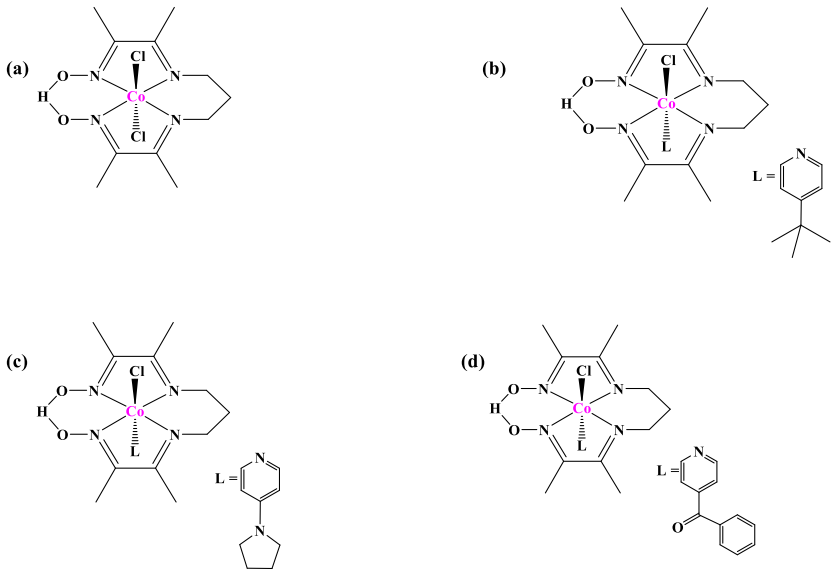

Figure 1.3. Selected heteroaxial cobalt oximes for proton reduction by the Verani *et al*.[54]

The variation of axial ligands has a significant effect on both the overpotential and TONs of the catalysts, except in the case of pyridine substitution where TONs are affected but overpotentials remain unchanged. The study provided experimental evidence for a five-coordinate environment for the catalytically active $3d^8$ Co^I species.

A catalytic pathway was proposed for H_2 production by the complex in **(Figure 1.3b)** in the presence of TFA in CH_3CN, where the catalytically Co^{III}–H^+ intermediate undergoes either a heterolytic or a homolytic pathway, with the latter mechanism more likely under low acidic conditions **(Figure 1.4)**.

The main drawback associated with cobalt oxime catalysts is ligand stability under harsh acidic conditions;[66] therefore, pyridine ligands were introduced to provide some steric bulk and robustness. Pyridines are aromatic and have strong bonds, hence tend to be hydrolysis resistant. They are strong σ-donors and are capable of π back-bonding as well, hence are capable of stabilizing monovalent cobalt species.

www.manaraa.com

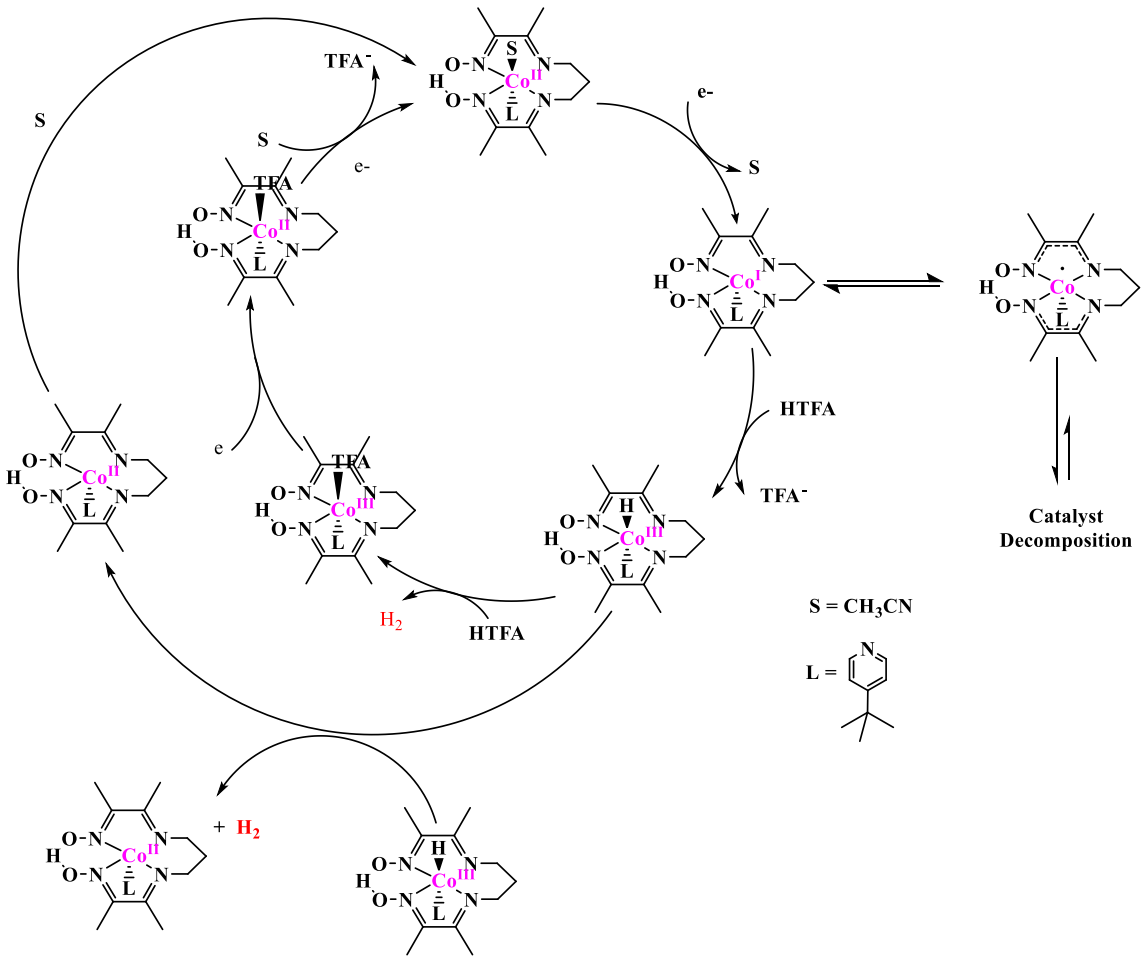

Figure 1.4. Proposed proton reduction catalytic mechanism of H_2 generation by Verani *et. al.*[54]

1.5.1.2. Molecular Cobalt Polypyridyl Systems

Chang[70] and coworkers studied the proton/water reduction catalysis of a $[Co(Py_4)CH_3CN]$ complex **(Figure 1.5a)** (Py_4 = 2-bis(2-pyridyl)(methoxy)methyl-6-pyridylpyridine). The pyridine ligands gave an added advantage of solubility in water which improved the catalytic activity during proton reduction with 99% Faradaic yields in organic solvent, and CH_3CN : water (50 : 50). However, the authors did not report any TONs, choosing instead to do a qualitative study. Zhao *et. al.* [71] studied the electro- and photocatalytic activity of a mononuclear Co complex, [Co(DPA-Bpy)Cl]Cl and its Aqua analog $[Co(DPA\text{-}Bpy)(H_2O)](PF_6)_3$ (**1.5b**), [DPA-Bpy = *N*,*N*-bis(2-pyridinylmethyl)-2,2′-bipyridine-6-methanamine] and observed that the aqua complex catalyzed

www.manaraa.com

H_2 production from H^+ efficiently with an overpotential of 0.6 V in water. Seeking to investigate the electronic effects of replacing the pyridines with a more basic isoquinoline ligand on catalytic efficiency of the catalyst, the authors replaced the ligand moiety to yield [Co(DIQ-Bpy)Cl]Cl and [Co(DIQ-Bpy)(H_2O)](PF_6)$_3$ (**1.5c**), [DIQ-Bpy = *N*,*N*-bis((isoquinolin-1-yl)methyl)(6-(pyridin-2-yl)pyridin-2-yl)methanamine]. When a more basic and conjugated ligand moiety replaces pyridines for their cobalt catalyst, the water reduction catalytic efficiency increased dramatically with lower overpotential, improved TON and TOF, and a more robust and stable catalyst overall.

A detailed mechanistic study was undertaken by Muckerman, Fujita, and Polyansky,[72] using Zhao's 1st generation catalyst **(Figure 1.5b).** They relied on an array of experimental and theoretical techniques such as cyclic voltammetry, bulk electrolysis, mass spectrometry, pulse radiolysis, laser flash photolysis, and density functional theory (DFT), to track, and characterize the relevant intermediates proposed in the catalytic cycle.

The results of their study indicated that the aqua axial ligand is strongly bound to the trivalent cobalt center in an octahedral geometry. Upon one-electron reduction, the Co – O bond weakens making the $3d^7$ $[Co^{II}–OH]^+$ species relatively stable. Upon a second one-electron reduction of the $[Co^{II}–OH]^+$ yields a $3d^8$ Co^I species in which the Co-O bond further weakens and eventually breaks to form a five-coordinate $[Co^I–VS]^+$ species (VS = vacant site). Interestingly, they observed that there was a transient rearranged $[Co^I(\kappa^4\text{-L})(OH_2)]^+$ intermediate species where water is still bound and one pyridine is detached from the Co center instead. The results of this study benchmarked the now widely accepted conclusion that the $3d^8$ Co^I species undergoes some structural reorientation to form a preferred five-coordinate geometry prior to attracting a proton, to form a cobalt hydride. This structural reorganization or transformation is considered the rate-

www.manaraa.com

determining step (RDS). Pentadentate ligand platforms have been designed for cobalt catalysts after the study described to ensure a more efficient catalysis

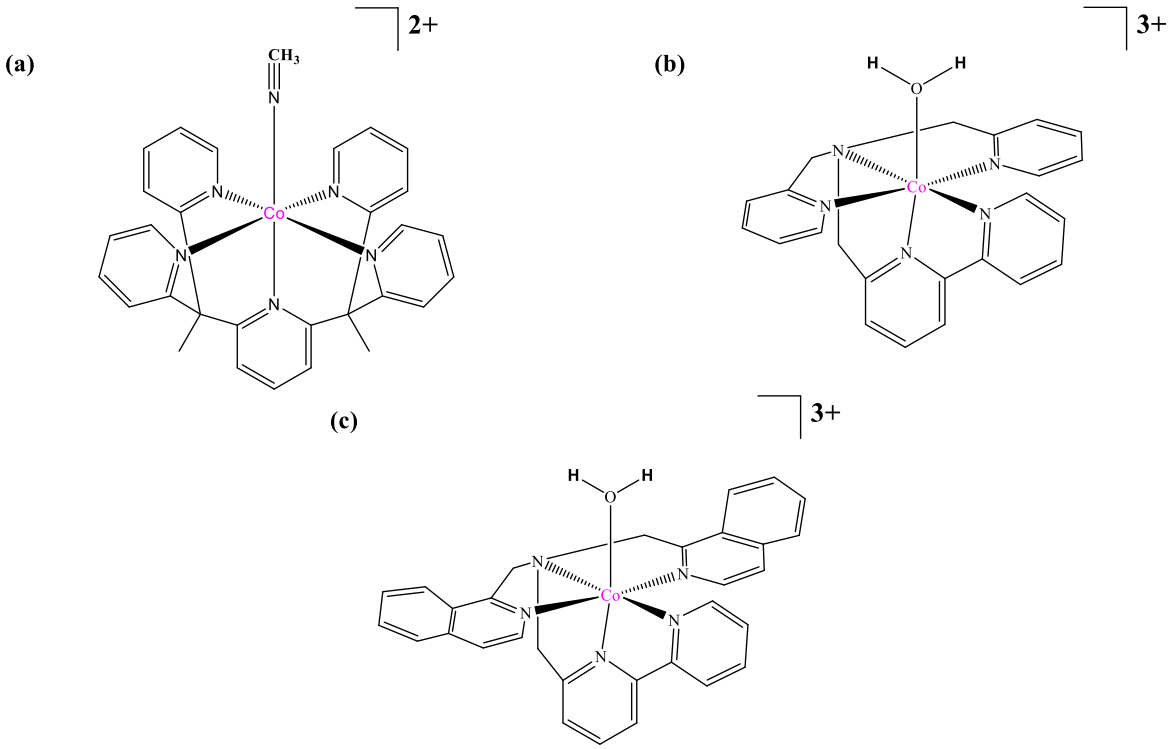

Figure 1.5. Selected cobalt-based polypyridyl catalysts for water reduction.

The Verani group recently published a series of water-reduction catalysts **(Figure 1.6)** based on pentadentate pyridine-rich ligand platforms of iminopyridine **(Figure 1.6a)**, amidopyridine **(Figure 1.6b)**, methoxy-substituted **(Figure 1.6c)**, and *N*-methyl substituted pyridine **(Figure 1.6d)**.[73]

The methoxy and amido catalysts resulted from the transformation of ligand scaffold in imine complex by adventitious methanol and water solvents, respectively. The *N*-methylated ligand analog prevented the transformation but increased the overpotential required for catalytic water reduction because the ligand has lost its redox activity.

www.manaraa.com

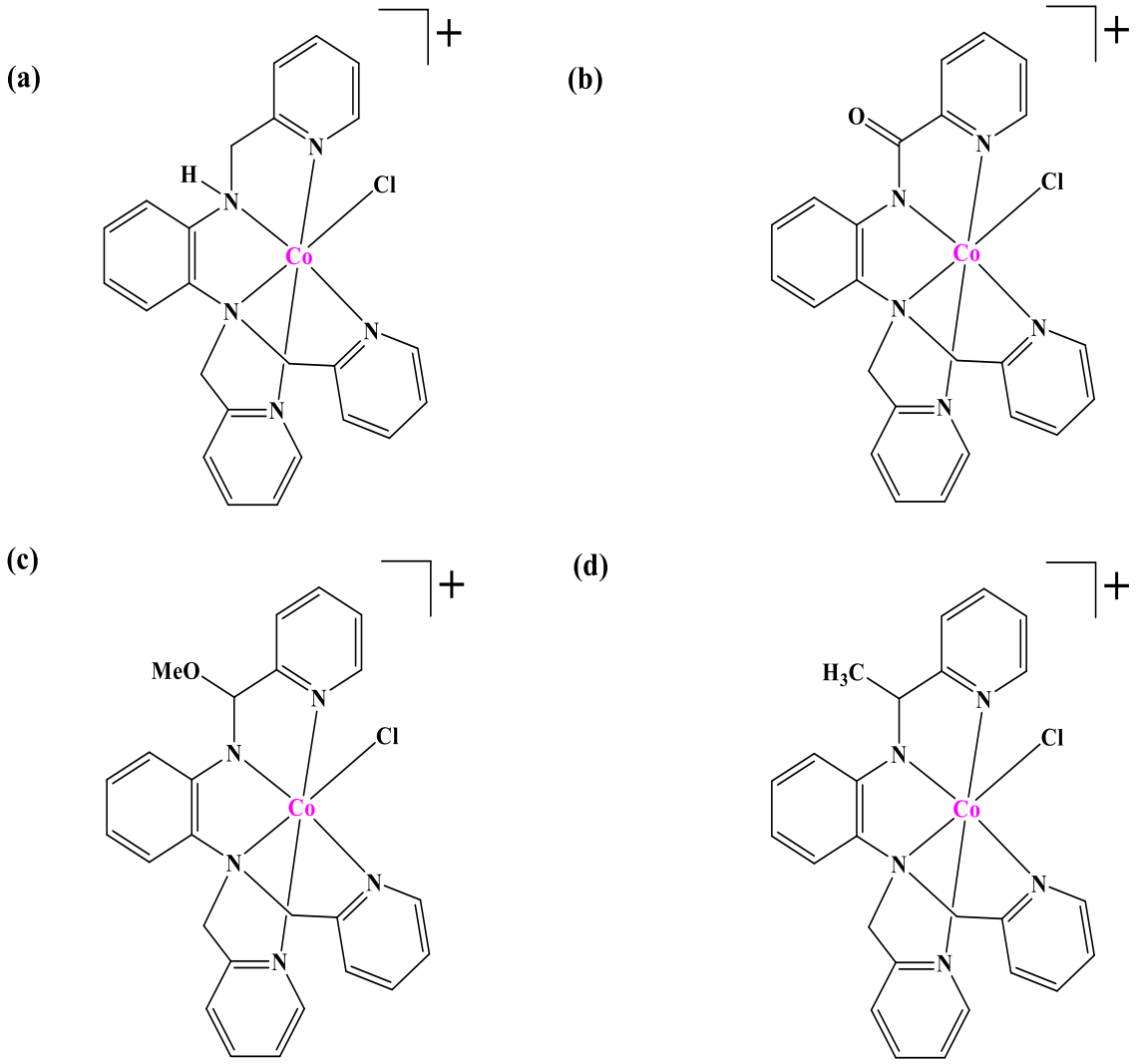

Figure 1.6. Pentadentate cobalt-based polypyridyl catalysts by Verani *et. al.*[73]

The two catalysts, **1.6b and 1.6d**, showed excellent water reduction activity with $TONs_{18h}$ of 7000 and 6000 respectively, placing them among the most efficient molecular cobalt catalysts for hydrogen production. Based on experimental and DFT results, a detailed mechanism was proposed **(Figure 1.7),** in which a nucleophilic five-coordinate $3d^8$ Co^I attracts a proton to form a Co^{III}-H, which undergoes further reduction to a Co^{II}-H state before attracting another proton to give hydrogen.

www.manaraa.com

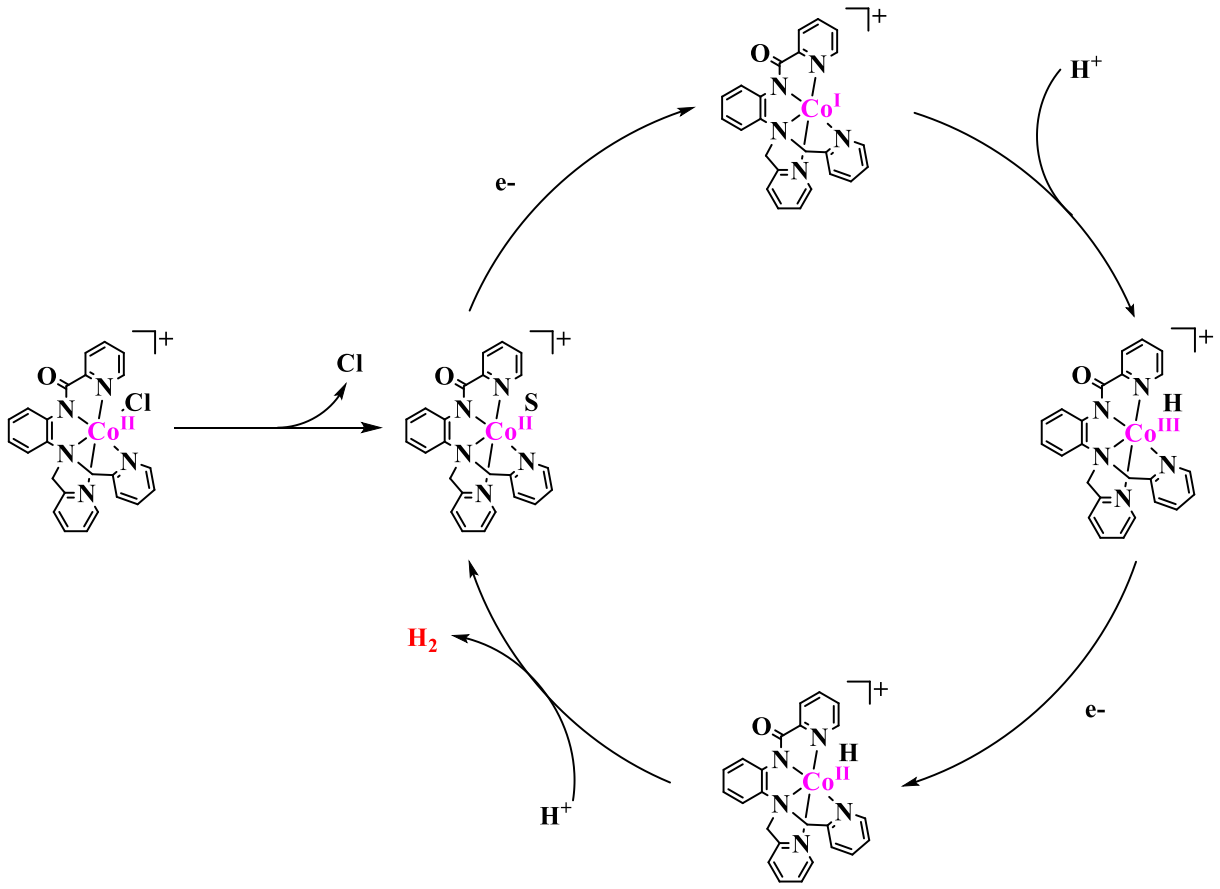

Figure 1.7. Catalytic pathway for H_2O reduction with cobalt amidopyridine by Verani *et al.*[73]

1.5.1.3. Molecular Bimetallic Cobalt Systems

Over the past 5 years, attempts were made to design and study the catalytic activity of bimetallic cobalt proton reduction catalyst with the expectation of enhanced performance. The idea of bimetallic catalysts being twice as efficient as their monometallic counterparts has led to the design of bimetallic cobalt complexes **(Figure 1.8).** Peters[74] and his group synthesized a dinuclear $Co_2(dmgBF_2)_2L_2$ complex based on a bridging pyridazine backbone **(Figure 1.8a).** This complex did not catalyze the production of hydrogen from protons but served to be a model for rich redox chemistry of bimetallic cobalt complexes.

Fukuzumi[48] and coworkers designed a bimetallic Co complex with bis(pyridyl)-pyrazolato (bpp) and terpyridine (terpy) ligand platforms **(Figure 1.8b)** and studied its catalytic activity

www.manaraa.com

towards proton reduction by a combination of chemical and electrochemical techniques designed to track the kinetics of the catalytic process. The parent [$Co^{III}Co^{III}$] undergoes a three- or four-electron reduction by cobaltocene in acetonitrile to produce [$Co^{II}Co^{I}$] or [$Co^{I}Co^{I}$], respectively, which they observed was in the protonation equilibrium with [$Co^{II}Co^{III}$–H] intermediate. The hydride was further protonated by trifluoroacetic acid (TFA) to produce hydrogen. The authors, however, did not see a cooperative mechanism suggested by Gray[75] and coworkers. The catalyst operates at an overpotential of 0.6 V. A heterolytic mechanistic pathway was proposed where either cobalt center forms the hydride and produces hydrogen independent of the other.

Gray[76] and his group investigated the proton reduction catalysis of two bimetallic $Co(dmgBF_2)_2$ type catalysts; one with an eight-carbon (8C) chain bridge **(Figure 1.8c)**, and the other with a boron bridge **(Figure 1.8d)**. When the catalytic activity of the long chain complex was compared with a monometallic model, there was no improvement in catalysis, which suggests that the long chain complex undergoes catalysis through a bimolecular heterolytic pathway. The boron-bridged analog performed less efficiently than its monometallic analog operating at an overpotential of 1 V). Dinolfo[77] and his group studied the proton reduction catalytic activity of two dicobalt tetrakis-Schiff base catalysts, [Co_2LAc^+] and [Co_2L^{2+}] (Figure 1.12e), in CH_3CN using with TFA and CH_3COOH as proton sources, [L = N_6O_2 Schiff base macrocycle; Ac = acetate bridge].

Results of the study indicate that Co_2L^{2+} operates at an average Faradaic efficiency of 90% in the presence of CH_3COOH but requires a relatively high overpotential for catalysis. Hydrogen production may be initiated by a bimetallic catalytic mechanism involving adjacent [Co^{III}–H]$_2$ or a heterolytic attack of an incoming proton on a [$Co^{II}Co^{II}$-H] due to the close proximity of the two

www.manaraa.com

Co ions in both complexes (3.2 Å), but no evidence was provided by the authors to support the proposed mechanism.

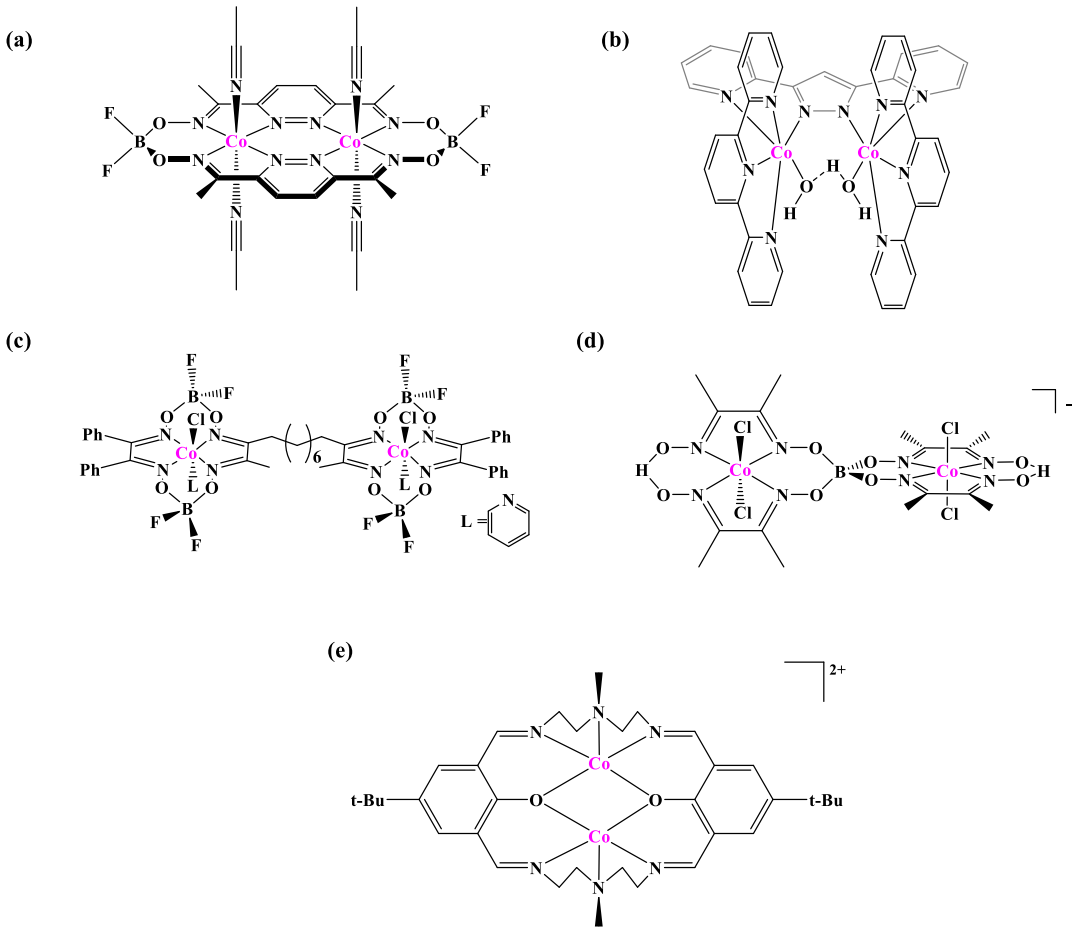

Figure 1.8. Selected bimetallic cobalt-based catalysts for proton reduction.

1.6. Homogeneous Molecular Catalysts for Water Oxidation

Over the decades, scientists have tried to mimic the functions of the oxygen-evolving complex (OEC) in Photosystem II, thereby designing not only functional mimics but also structural mimics for water oxidation. An efficient water oxidation catalyst is expected to allow the transfer of four electrons at potentials greater than the thermodynamic potential of +1.23 V in one-electron oxidation processes. The design of such a catalyst requires identifying and characterizing key intermediates and the understanding of mechanistic pathways. The catalyst will have to stabilize

www.manaraa.com

various intermediates required to oxidize water to oxygen in order to lower the kinetic energy barrier and hence result in quicker turnovers of oxygen from water. Many transition-metal complexes have been developed as catalysts for water oxidation. These include but are not limited to manganese, ruthenium, cobalt, iron, and iridium. Each of these elements has shown catalytic efficiency with ligand platforms such as terpyridines,[7, 78] phenolates,[79, 80] and pyridines.[41, 81] The search for an efficient artificial catalytic water oxidation catalyst was started by Calvin[82] and coworkers in the mid-1970s where, they performed photochemical evaluations on a dinuclear -μ-oxo bridged mixed-valent manganese polypyridine complex. However, their results were inconclusive, as they later observed that the oxygen detected may have percolated through their experimental set up from the atmosphere.

1.6.1 Molecular Water Oxidation Catalysts based on Ruthenium Complexes

Several studies based on ruthenium have been undertaken since that time **(Figure 1.9)** Meyer[83] and coworkers are known to have developed the first 'true' homogeneous water oxidation catalyst $[(bpy)_2Ru^{III}(\mu\text{-}O\text{-})\ Ru^{III}(bpy)_2]^{4+}$, called the "Blue Dimer" **(Figure 1.9a)**, utilizing a bipyridine ligand platform and ruthenium.

The choice of ruthenium afforded the observation of key intermediates due to relatively slower ligand exchange rates in ruthenium complexes. They observed the rapid evolution of oxygen upon addition of four or more equiv of a one-electron chemical oxidant, ceric ammonium nitrate (Ce^{IV}), suggesting that the catalytic-active species is a four-electron oxidized intermediate. The authors, therefore, proposed a mechanism involving an initial four-electron oxidation to give a pentavalent dimeric rutenyl intermediate, which in turn gives O_2 in a concerted four-electron step. Llobet *et. al.* [84] reported on a bimetallic Ru catalyst bearing a Hbpp type bridging ligand **(Figure 1.9b).** This terpy-Ru-bpp dimer $[Ru_2^{II}(bpp)(terpy)_2(H_2O)_2]^{3+}$ (Hbpp = 2,2′-(1H-pyrazole-

www.manaraa.com

3,5-diyl)bis(pyridine), which had the two ruthenium ions in close proximity thus avoiding the Ru-O-Ru bridge that was present in the blue dimer.

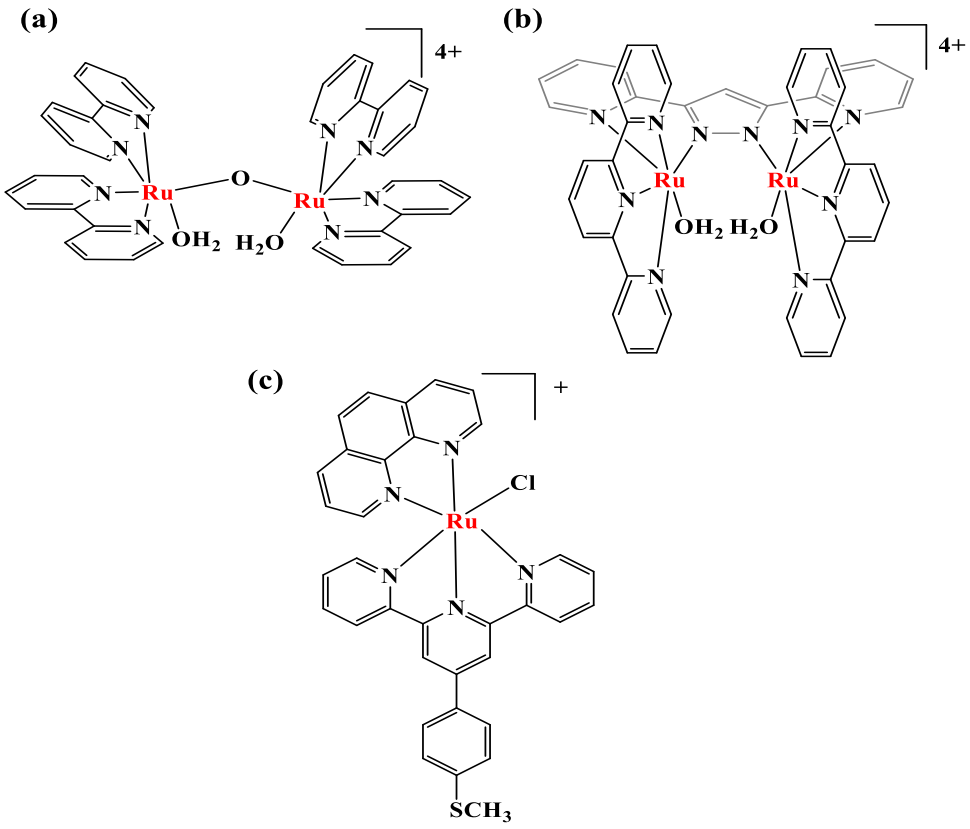

Figure 1.9. Selected homogeneous ruthenium-based catalysts for water oxidation.

The unique modification of the µ-oxo bridge in the terpy-Ru-bpp dimer enhanced the activity of the catalyst for homogeneous oxygen evolution and avoided decomposition. Thummel[35,85,86] and coworkers introduced a new type of binuclear and a variety of single site ruthenium derived water oxidation complexes They proposed a mechanism involving a seven-coordinate Ru^{IV} species which suggested the O – O bond formation occurs at an electrophilic Ru^{VI}=O bond. However, a detailed and critical evaluation of the mechanistic pathways for these catalysts is either lacking or are solely based on DFT computations. Verani[12] and coworkers studied substituent effect on water oxidation for a series of $[Ru^{II}(terpy)(phen)Cl]^{+}$ catalysts

www.manaraa.com

(Figure 1.9c). When the authors compared the effects of substituted phenanthroline with electron-donating and electron-withdrawing groups on the catalytic activities of their catalysts, they concluded that catalytic activity was enhanced by the presence of electron-donating groups on the phenanthroline moiety, while the presence of electron-withdrawing substituents impedes the catalytic activity. They also observed an induction period for catalysis and ruled out a ligand-exchange mechanism. Based on their findings, they proposed a mechanism of water oxidation involving a seven-coordinate ruthenyl (Ru^{IV}=O) similar to the mechanism proposed by Thummel, supported by experimental evidence.

1.6.2 Molecular Water Oxidation Catalysts based on Manganese Complexes

Manganese-based water oxidation catalysts **(Figure 1.10)** have unique relevance because this ion has a broad range of oxidation states and is abundant in the Earth's crust.[87] Manganese is also the main transition element that constitutes the OEC in Photosystem II, and therefore, has been used extensively.

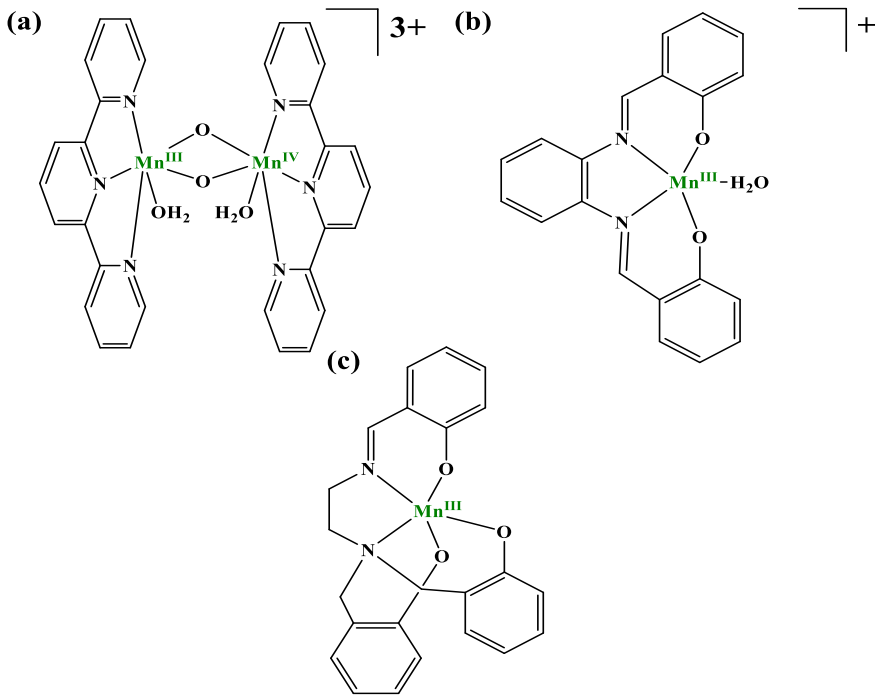

Figure 1.10. Selected homogeneous manganese-based catalysts for water oxidation.

www.manaraa.com

Brudvig[88] and coworkers, reported the so-called "terpy-dimer" **(Figure 1.10a),** a di-terpyridine di-manganese complex, $[(terpy)(H_2O)Mn(\mu\text{-}O)_2Mn(terpy)\ (H_2O)]^{3+}$, in 1997 with a $3d^4$ Mn^{III} as one of the metal centers and a $3d^3$ Mn^{IV} as occupying the other center. The oxygen evolution activity of this catalyst in the presence of sodium hypochlorite was studied, utilizing ceric ammonium nitrate (Ce^{IV}), and observed a low (TON) of 4 after six hours of catalysis. This was due to the decomposition of the Mn dimer to form permanganate ions in solution.[88]

However, when Oxone (HSO_5^-) was used as the chemical oxidant, continuous water oxidation activity was observed. They proposed a mechanism **(Figure 1.11)** where Oxone first binds to the Mn(III, IV) dimer

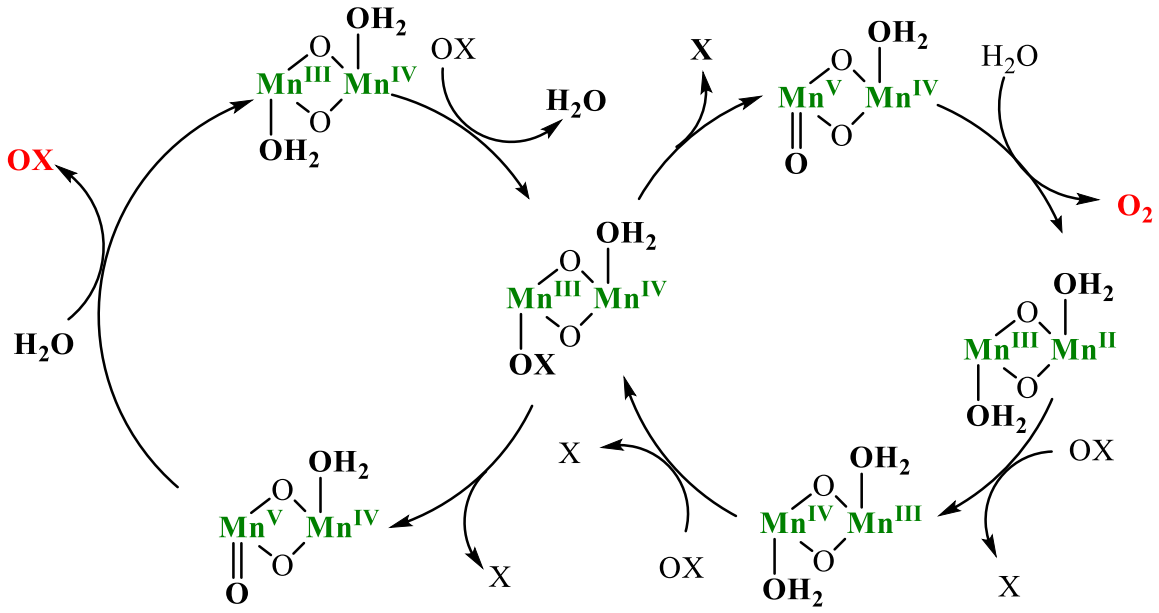

Figure 1.11. Proposed mechanism by Brudvig *et al* for the reaction between $[(terpy)(H_2O)Mn(\mu\text{-}O)_2Mn(terpy)\ (H_2O)]^{3+}$ and chemical oxidants XO (XO = NaOCl or $KHSO_5$).

After binding there are two mechanistic pathways possible due to the presence of two manganese centers, one in which no oxidation occurs when (HSO_5^-) binds to Mn(IV), because a two-electron oxidation would give a Mn(VI) which is inaccessible in that ligand environment. The second pathway involves the (HSO_5^-) binding to the Mn(III) and produces oxygen. The bound

www.manaraa.com

sulfate (SO_4^{2-}) from the (HSO_5^-) is released, resulting in a two-electron oxidation of the manganese(III) to form the key high–valent manganese(V) necessary for the formation of the O–O bond. The highly reactive manganese(V)–oxo or manganese(IV)–oxyl intermediate involve in these pathways could be due to trans influence. The Collomb[89] group tried unsuccessfully to perform electrochemical water oxidation of the same Mn-terpy dimer because the complex transforms into an inactive tetranuclear analog.

It has been proposed by various reports that the incorporation of phenolate moieties into manganese species could lead to enhanced catalytic activity.[90,91,92] Akermark[93-94] and coworkers has shown impressive progress in this design, incorporating bimetallic [Mn_2] and multimetallic [RuMn][95] and studying charge, and electron transfer rates between photosensitizer and electron donor moieties. The study of electron-transfer rates in the [RuMn] triads, for instance, were conducted in an effort to mimic the photosynthetic process. The study revealed that the manganese ion has intrinsic properties that are favorable for creating and maintaining a long-lived charge separated state for electron transfer to occur from the Mn electron donor to the Ru ion. A similar approach based on modifications of the triazacyclononane ligand was undertaken by Wieghardt[96] and collaborators who found out that Mn^{II}, Mn^{III}, and Mn^{IV} redox states in their complexes were accessible and Ru(II) centers could be reversibly oxidized to Ru^{III}. Interestingly enough, it was also observed that the coordinated phenolate ligand could be oxidized to a phenoxyl radical. Fujii[79, 97-98] *et al.* have also studied examples of Mn^{IV} stabilization using [N_2O_2] salen platforms **(Figure 1.10b).** These systems build on an equilibrium between [Mn^{III}/phenoxyl] and [Mn^{IV}/phenolate] species relying on the energy of their frontier orbitals. It was initially suggested by Åkermark *et al*[99] that formation of Mn^{IV} leads to a Mn^{III}/phenoxyl species where radical decay is prevented by coordination to the metal center **(Figure 1.10c)**, but Fujii[100] proposes that the [Mn^{III}/phenoxyl]

www.manaraa.com

state is favored upon coordination with water and the metal-centered high oxidation is only achieved by water deprotonation or formation of a Mn^{IV}=O moiety. A study from Anxolabéhère-Mallart *et al.*[80] proposed that an alternative and milder mechanism for water oxidation might involve the formation of Mn^{III}-oxyl species in pentadentate ligands similar to those developed by the groups of Pecoraro[101] and Åkermark.[99]

1.6.3 Molecular Water Oxidation Catalysts based on Cobalt Complexes

Though the cobalt ion plays no significant role in photosystem II to aid water oxidation, it has become a reliable water oxidation catalyst over the past decade because it can effectively stabilize multiple oxidation states, from $3d^8$ Co^I through $3d^5$ Co^{IV}. Whilst several heterogeneous cobalt oxide water oxidation catalysts have been reported in the literature, only a few molecular cobalt-based water oxidation catalysts have been reported **(Figure 1.12)**. Berlinguette[21] and his group, in 2010, reported on the electrocatalytic water oxidation of a homogeneous cobalt catalyst, ($[Co(Py_5)(OH_2)]^{2+}$) in basic medium (pH 9.2) with an overpotential of 0.5 V [Py_5 = 2,6-(bis(bis-2-pyridyl)-methoxymethane)pyridine)] **(Figure 1.12a).** They observed that their catalyst undergoes a series of (PCET) steps during catalysis to yield a $3d^5$ Co^{IV} intermediate, which is then attacked by a molecule of water under basic conditions producing oxygen. The catalyst remains stable at neutral through mildly basic pH conditions of 7-10. Under strong alkaline conditions, however, it was observed that there was deposition of CoO_x on the surface of the electrode. The authors concluded that whilst the catalyst is a molecular catalyst under mildly basic conditions, the catalyst transforms to nano-particulate cobalt oxide under harsh basic conditions. This phenomenon was attributed to the possibility of the metal–ligand bond *trans* to the M–O bond being "compromised at higher redox levels"[21] hence the decomposition of the molecular catalyst. Nam[102] and coworkers observed similar results when they studied $[Co^{II}(Me_6tren)(OH_2)]^{2+}$ and

www.manaraa.com

$[Co^{III}(Cp^*)(bpy)(OH_2)]^{2+}$ [Me_6tren = tris(N,N′,N″-dimethyl aminoethyl) amine, Cp* = η^5-pentamethylcyclopentadienyl] in water over the 6–10 pH range.

Llobet[84] modified a known Ru-bpp water oxidation catalyst shown in **Figure 1.9b**, with cobalt and studied its catalytic activity towards water oxidation.[103] Several attempts to just replace the metal center and maintain the aqua axial ligands proved unsuccessful, producing an end-on peroxo bridge between the two cobalt centers **(Figure 1.12b)**, which remained stable in aqueous 0.1 M, pH 2.1 phosphate buffer over a period of several hours with no signs of degradation or decomposition. Its redox behavior during catalysis suggests that the $Co^{III}Co^{III}$ dimer undergoes a 2-electron oxidation before catalytic current enhancement is observed.

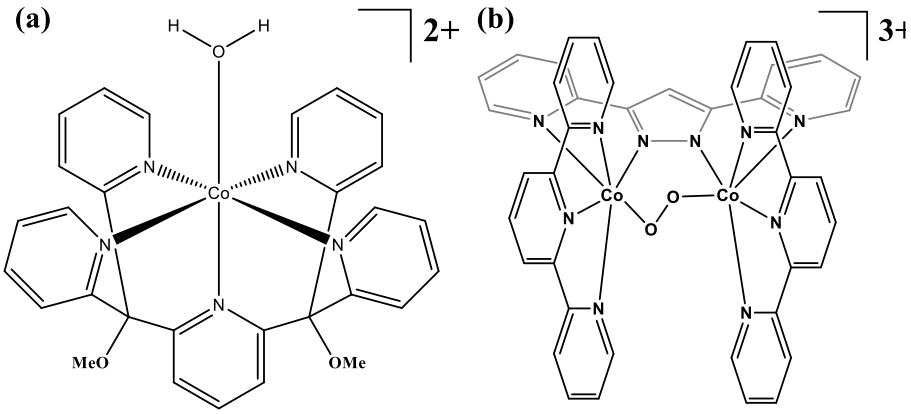

Figure 1.12. Selected homogeneous cobalt-based catalysts for water oxidation.

A mechanistic pathway was proposed by the authors in which the $Co^{III}Co^{III}$ parent dimer undergoes a one-electron oxidation to form a peroxo-bridged $Co^{III}Co^{IV}$ species which then follows two PCET steps to yield a dioxo-$Co^{IV}Co^{IV}$ intermediate, attacked by water, followed by the formation of an O–O bond to yield oxygen and regenerates the peroxo-bridged $Co^{III}Co^{III}$ complex, suggesting that both bpp-ligated Co and Ru complexes appear to catalyze water oxidation by "similar mechanisms".

www.manaraa.com

1.7. Outlook and Prospects

Efficient water splitting using energy from the sun is central to efforts toward a future based on a renewable and sustainable energy supply. For the development of a system that can harvest the energy of the sun and use it to split water, there must be a systematic effort targeted at the design and evaluation of catalytic systems which can utilize the photons to mediate the multi electronic processes involved in water splitting. Whilst significant progress has been made, questions persist as to how to identify and characterize key intermediates, as well as optimize the efficiency of these catalysts in order to utilize energy from the sun to split water. The prospect of designing a *bonafide* molecular catalyst that can efficiently use energy from the sun to split water remains the ultimate goal of achieving a sustainable hydrogen economy for the future. The Verani group at Wayne State University has focused its research interests towards achieving that goal. The results discussed in this dissertation constitute part of the research efforts.

1.8. Research Statements and Objectives

It is essential to understand the mechanistic processes governing water oxidation and water/proton reduction to achieve efficient electro- or photocatalysis. In the Verani group, we design ligands containing redox-active frameworks for the formation of metal complexes capable of water reduction and water oxidation. Cobalt and manganese complexes are important as water-splitting catalysts to generate dioxygen and dihydrogen stabilizing highly nucleophilic reduced species, and high-valent oxidative species respectively.

The focus of this dissertation was to design, and evaluate the redox, electronic, catalytic, and mechanistic properties of cobalt, and manganese complexes in various redox-active ligand frameworks towards efficient electrocatalytic water oxidation and reduction. These systematic studies are geared towards the eventual design of excellent photocatalysts based on affordable

www.manaraa.com

Earth-abundant metal complexes. To obtain this objective, the following specific goals have been pursued.

- **Goal # 1:** ***Probing the Versatility of a Quinoline-based Pentadentate Co(II) Complex for Electrocatalytic Water Splitting.*** The primary focus was to synthesize, characterize and evaluate the stability and robustness of the cobalt(II) complex of a pentadentate quinoline-based polypyridine ligand towards water splitting. I hypothesized that modifying the ligand architecture by incorporating a more rigid quinoline ligand, which has increased aromaticity, stabilized by mesomeric and inductive effects, yielded a robust catalyst capable of efficient catalysis. The results of this goal are addressed in **Chapter 3** of my dissertation.

- **Goal # 2:** ***Evaluating Electronic Communication and Cooperativity in a Dicobalt Complex for Proton Reduction.*** The principal objective is to study whether distance and topology enhance the electronic communication and thereby cooperativity between two cobalt centers in a dicobalt complex towards efficient proton reduction. I hypothesized that cooperativity will be dependent on (i) the distance between the Co centers, (ii) the relative topology of the coordination environments, and (iii) the degree of orientation and overlap between redox-active orbitals. **Chapter 4** of my dissertation discusses the results.

- **Goal # 3:** ***Investigating Valence Tautomerism on Coordination Preferences in Manganese Complexes for Water Oxidation.*** The principal objective is to investigate whether the coordination environments around a manganese center can determine high-valent states relevant for electrocatalytic water oxidation. The hypothesis is that, by incorporating redox-active ligands such as phenolates and a redox-active metal ion such as Mn, valence tautomeric transitions can occur through intramolecular electron transfer,

www.manaraa.com

yielding two different valence tautomers or redox isomers. This valence tautomerism can lead to the formation of Mn(IV) species, and support catalytic water oxidation. The results of this project constitute **Chapter 5** of my dissertation.

www.manaraa.com

CHAPTER 2:

MATERIALS, METHODS AND INSTRUMENTATION

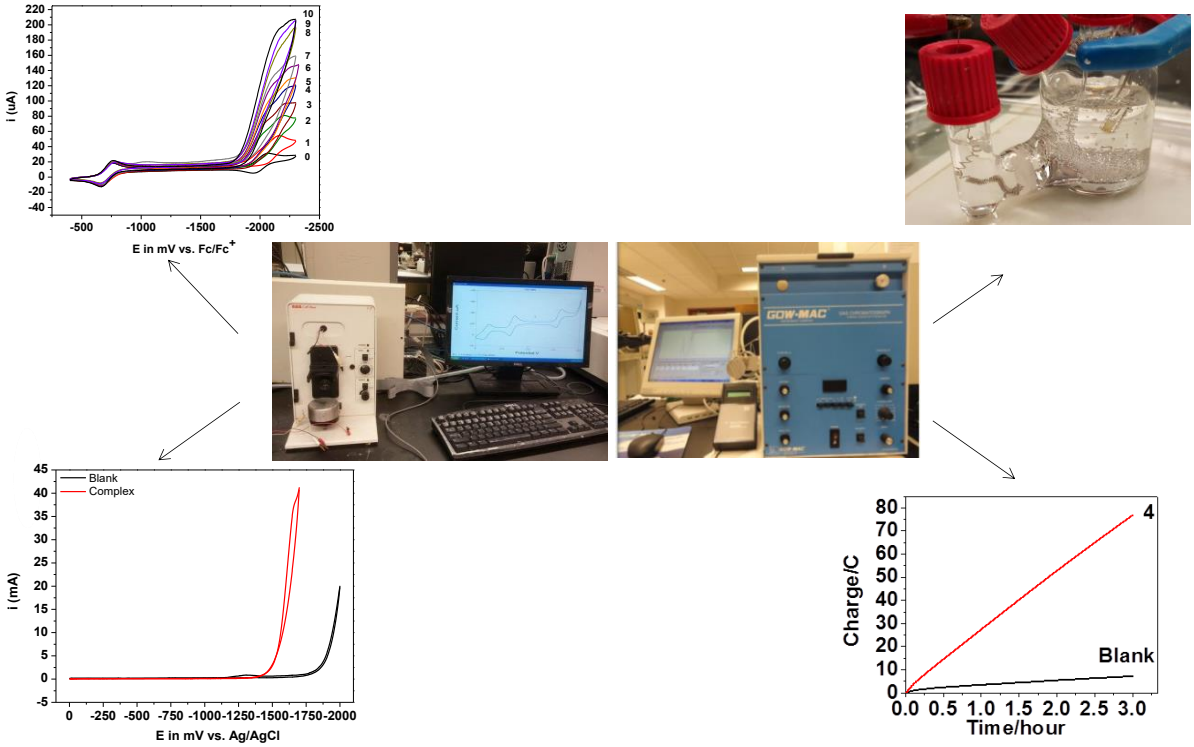

www.manaraa.com

CHAPTER 2: MATERIALS, METHODS, AND INSTRUMENTATION

2.1. Materials

The research described in this dissertation consisted of the organic synthesis of ligand precursors, ligands, inorganic transition metal complexes, and where possible their intermediates. Chemical reagents were purchased from various commercial sources such as Sigma-Aldrich, Oakwood Chemicals, and Alfa Aesar. Safe and appropriate reaction protocols were strictly followed to obtain ligands and their complexes. Solvents and reagents were received and used from commercial sources without further purification unless otherwise stated.

2.2 Methods and Instrumentation

All the ligands and complexes used in the dissertation described in this dissertation were synthesized and characterized using a variety of synthetic, spectroscopic, and spectrometric methods and techniques to study the composition, electronic structure, redox properties, catalytic behavior, and mechanistic pathways.

These methods and techniques include, but are not limited to, proton nuclear magnetic resonance spectroscopy (1H-NMR), Fourier transform infrared spectroscopy (FTIR), electrospray ionization mass spectrometry (ESI-MS), elemental analysis, UV-visible spectroscopy, cyclic voltammetry, electron paramagnetic resonance spectroscopy (EPR), gas chromatography (GC), scanning electron microscopy (SEM), single crystal x-ray diffraction analysis (SC-XRD), and energy-dispersive electron microscopy (EDS).

2.2.1 Nuclear Magnetic Resonance Spectroscopy (NMR)

NMR is a widely used method of characterization in organic compounds, because it affords a versatile way to determine the structure of the organic compound. It has gradually become an effective technique in inorganic chemistry for providing valuable structural information about

www.manaraa.com

diamagnetic metal complexes. The nuclei of various atomic isotopes each possess a unique spin (I), which in turn is associated with nuclear magnetic resonance. Some of these spins are fractional, such as I = 1/2, 3/2, 5/2. Isotopes such as ^{1}H, ^{13}C, ^{19}F and ^{31}P all have I = ½ and hence magnetic moment. They act as subatomic magnets and therefore can be analyzed by NMR spectroscopy. The resonance produced when these isotopic nuclei are placed in an external magnetic field can be detected and converted into an NMR spectrum. Generally, the peak positions in an NMR spectrum are reported relative to a standard signal, like that of tetramethylsilane (TMS). This ensures uniformity in signal output. The position and multiplicity of an NMR peak is dependent on the local chemical environment of the isotope. Peak integration is used to determine the number of isotopes (i.e. protons) present in a particular compound. In this dissertation, ^{1}H-NMR was used predominantly to identify organic ligands, ligand precursors, and metal complexes when appropriate, such as $3d^6$ $^{LS}Co^{III}$ and $4d^6$ $^{LS}Ru^{II}$ due to their diamagnetic nature**.** ^{1}H NMR spectra were obtained in deuterated solvents such as $CDCl_3$, CD_3CN, and DMSO-d6 at room temperature**,** using a Varian 400 MHz instrument.

2.2.2 Fourier Transform Infrared Spectroscopy (FTIR)

FTIR is an important technique used in identifying functional groups in organic compounds and in some cases inorganic complexes. This technique relies on the principle of infrared transmittance. For instance, when a sample is placed in an IR beam, some radiation is absorbed by the sample and some of it is transmitted. The detected signal is converted into a spectrum from which functional groups can be identified as well as the unique 'fingerprint' region of the sample. The utility of infrared spectroscopy is derived from different molecules' different FTIR fingerprints.[104] FTIR samples are prepared liquids or as potassium bromide (KBr) pellets for analysis by the spectrophotometer. In this dissertation, FTIR was used to confirm the presence of

www.manaraa.com

the following major functional groups; C=N, C=O, C=C, and inorganic counter ions such as the perchlorate (ClO_4^-), and the hexafluorophosphate (PF_6^-). The FTIR data was measured from 4000 to 400 cm^{-1} as KBr pellets on a Bruker Tensor FTIR spectrophotometer, with spectra plotted as percent transmittance (% T) of IR radiation against centimeter wave numbers (cm^{-1}).

2.2.3 Electrospray Ionization Mass Spectrometry (ESI-MS)

Electrospray mass spectrometry (ESI-MS) is an essential analytical tool used to quantify known compounds, but also to elucidate structural and chemical properties of unknown compounds within a sample. The principle of MS includes the ionization of a sample into gaseous ions. These ions are then categorized according to their mass to charge ratios (m/z) and relative abundances.[105] Since ESI ionization techniques preclude the fragmentation of gaseous ions, this method is useful in identifying molecular ion peaks of organic ligands and inorganic complexes. ESI-MS was used extensively in this dissertation to ascertain the identity of ligands, inorganic metal complexes, post-catalytic species, or transformed catalytic intermediates. A typical sample for ESI-MS analysis is dissolved in polar solvents such as acetonitrile or methanol. The sample is then bombarded with high-energetic electrons to produce charged species. Low-resolution modes are convenient for organic compounds, whereas for inorganic metal complexes, the high resolution modes with isotopic distribution capabilities are more useful. Low resolution ESI-MS data was obtained on a Nexera X2 LC system with a LC-MS 8040 triple quadrupole mass spectrometer, and high resolution data on a Waters Micromass LCT Premier TOF (time of flight) instrument with a Waters HPLC 2695 Alliance LC system. These analyses were performed with the help of Drs. Lew Hryhorczuk, from 2012- 2013, Yuri Danylyuk, from 2013-2014, and Nicole Lenca 2014-2017 at the Lumigen instrument center (LIC) of the Department of Chemistry at Wayne State University.

www.manaraa.com

2.2.4 Electron Paramagnetic Resonance Spectroscopy (EPR)

Electron paramagnetic resonance (EPR), is a spectroscopic tool which employs microwave radiation to analyze species with an odd number of electrons, such as organic radicals, radical cations, and metal cations such as $3d^9$ Cu^{II} , $3d^7$ Co^{II}, $3d^5$ Co^{IV}, $3d^5$ Fe^{III} in an applied external magnetic field.[106] The basic principles of this technique are analogous to the NMR technique described in section 2.2.1. Electrochemically generated catalytic intermediates during the research described in this dissertation, were characterized using the EPR technique. EPR samples are usually prepared under inert conditions depending on the nature of the species under study. A 10^{-3} M aliquot of the sample is then put in suprasil quartz capillary EPR tubes which are then frozen in liquid N_2. Continuous wave (CW) X-band (9-10 GHz) EPR experiments are then performed on a Bruker ELEXSYS E580 EPR spectrometer (Bruker Biospin, Rheinstetten, Germany), equipped with a Bruker ER 4102ST resonator or a Bruker ER 4122SHQ resonator. A temperature-controlled device equipped with a helium gas-flow cryostat (ICE Oxford, UK) and an ITC (Oxford Instruments, UK) helps keep the samples at low temperature. Data is processed on Xepr (Bruker BioSpin, Rheinstetten) and Matlab 7.11.2 (The MathWorks, Inc., Natick) software. Simulated spectra are generated using the EasySpin software package (version 4.5.5).[107] These analyses were done in collaboration with Dr. Oleg Poluektov and Dr. Jens Niklas of Argonne National Laboratory (ANL).

2.2.5. Ultraviolet-visible Spectroscopy (UV-visible)

UV-visible spectroscopy is a technique used to analyze the electronic transitions of complexes absorbing radiation. The absorption of UV or visible radiation is associated with the excitation of valence electrons. There are three main types of electronic transition: (i) transitions relating to π, σ, and n electrons; (ii) charge-transfer transitions – the transfer of an electron from

www.manaraa.com

the orbital of an electron donor moiety to an orbital associated with an electron acceptor; (iii) *d-d* transitions – electron transfer from d-orbital in a metal complex to another d-orbital of higher energy. When a compound absorbs radiation, valence electrons get excited and are promoted from the ground state energy level to an excited state energy level. These transitions can be spin and Laporte allowed, or forbidden, depending on selection rules. Transition metal complexes typically exhibit electronic transitions such as intraligand-charge transfers (ILCT), ligand-to-ligand charge transfers (LLCT), metal-to-ligand charge transfers (MLCT), ligand-to-metal charge transfers (LMCT), and *d-d* transitions. The ligand-based transitions usually occur in the ultraviolet region, at low wavelengths with intense molar absorptivities ($\varepsilon \sim 20000 - 60000$), whereas the charges transfer transitions occur in the mid-visible region with medium molar absorptivities ($\varepsilon \sim 5000 - 20000$). The *d-d* transitions are usually weak as they are forbidden transitions according to the selection rules described, and hence have notably low absorptivities ($\varepsilon \sim 50 - 1000$). In this dissertation, UV–visible spectroscopy was used to track the electronic behavior of ligands and metal complexes. UV-visible spectra were typically obtained at room temperature using a Shimadzu 3600 UV-visible-NIR spectrophotometer operating in the range of 190 to 3600 nm with samples prepared in quartz cells as methanolic solutions. Other solvents used are dichloromethane, acetonitrile, and dimethyl formamide as needed. Spectral data is plotted as absorbance, or molar absorptivity (ε) in M^{-1} cm^{-1} when concentration is known, versus wavelength in nanometers.

2.2.6. Elemental Analyses (EA)

The technique of elemental analysis operates on the principle that during combustion, at elevated temperatures, all available carbon will easily decompose to become carbon dioxide, all hydrogen will decompose to become water and all nitrogen will decompose to nitric oxides. This will enable the determination of any compound's relative percent of carbon, hydrogen, and

www.manaraa.com

nitrogen. These elemental analyses (C, H, and N) for metal complexes used during this dissertation were performed on an Exeter Analytical 440 elemental CHN analyzer by Midwest Microlab: Indianapolis, Indiana. Elemental analysis values are presented as percentages. A CHN elemental analysis sample calculation is shown:

Anal. Calc. for [$\mathbf{C_{30}H_{31}}CoCl\mathbf{N_6}O_5$]: C, 50.22; H, 4.36; N, 11.71%. Found: C, 50.37; H, 4.32; N, 11.57%.

C	**H**	**N**
50.37 g/12.00 $gmol^{-1}$	4.32 g/ 1.00 $gmol^{-1}$	11.57 g/ 14.00 $gmol^{-1}$
= 4.19 moles	= 4.32 moles	= 0.83 moles

Now dividing through by the lowest number of moles;

4.19/0.83	4.32/0.83	0.83/0.83
= 5.04	= 5.2	= 1

Now multiply by 6 (number of nitrogen atoms in the formula above)

= 30.24	= 31.20	= 6

Hence the CHN formula is $\mathbf{C_{30}H_{31}N_6}$.

In order to get a good elemental analysis result, purity is important. All samples must be pure and thoroughly dried. The following are sources of impurities and must be avoided at all cost.

1. Inorganic salts
2. Water of hydration

2.2.7. Single Crystal X-Ray Crystallography (SC-XRD)

Single crystal X-ray diffraction (SC-XRD) is one of the most authoritative techniques for obtaining detailed insight into the structure-to-function relationship of transition metal complexes in the solid state.[108] In the research reported in my dissertation, the single crystal X-ray structures

www.manaraa.com

of inorganic complexes were obtained whenever possible. X-ray quality crystals were grown by either vapor diffusion, slow evaporation, or solvent layering when applicable. Diffraction patterns were measured on a Bruker X8 APEX-II[109] kappa geometry diffractometer with Mo radiation and a graphite monochromator SAINT[110] collection suite. The OLEX2[111] structure solution suite was used to solve various structures with refinements and absorption correction techniques utilized using SHELX[112] and SADABS[113] software. Dr. Mary J. Heeg, and Kenneth K. Kpogo solved all the crystal structures.

2.2.8. Cyclic Voltammetry (CV)

Cyclic voltammetry was extensively used in the course of my dissertation. It has become an indispensable analytical tool in studying electron transfer phenomena. In the context of this dissertation, cyclic voltammetry was used predominantly to evaluate the effects of ligand design on metal-centered redox potentials as well as probe the mechanistic details of electrocatalytic water splitting. In a typical CV experiment, the potential at a working electrode immersed in a solution containing a sample and a supporting electrolyte is scanned linearly with time; the current is monitored and plotted as a function of either time or potential. The use of CV as a successful technique depends on a few parameters such as choice of solvent, supporting electrolyte, choice of working electrode, reference electrode, and choice of standard reference material. CV experiments were conducted using a three-electrode setup comprised of a glassy carbon working electrode (W.E.), a saturated Ag/AgCl as reference electrode (R.E.), and a Pt wire as an auxiliary electrode (A.E.) on a BASi 50W potentiostat. Typical organic solvents used to obtain cyclic voltammograms were dichloromethane (CH_2Cl_2), acetonitrile (CH_3CN), and *N*,*N*'-dimethylformamide (DMF) when possible. Supporting electrolytes such as 0.1 M of *n*-Bu_4NPF_6 or *n*-Bu_4NBF_4 were used. CV experiments were conducted under an inert atmosphere at room

www.manaraa.com

temperature. The ferrocene/ferrocenium (Fc/Fc^+) couple (E^o = 400 mV *vs* NHE)[114] was used as a standard reference material (SRM) and added as an internal standard. Usually, $E_{1/2} = (Epc + Epa)/2$ are reported for reversible redox couples, whereas Epc (cathodic peak potential) and Epa (cathodic peak potential) are used to designate irreversible process. Peak-to-peak redox potential separations ($\Delta Ep = |Epc - Epa|$) and |ipa / ipc| values are often measured to assess reversibility of redox processes [ipa = anodic peak current; ipc = cathodic peak current].

2.2.9 Spectroelectrochemistry (SEC)

Spectroelectrochemistry is an electroanalytical technique which combines electrochemical reactions with species-focused spectroscopy. Spectroelectrochemistry (SEC) gives a more detailed analysis of single and multiple electron-transfer processes during an electrochemical experiment. Spectroelectrochemical experiments were conducted in an optically transparent cuvette (*ca.* 0.1 mm) using a procedure described as follows:[115] a flat platinum wire (W.E.) in a "U" shape is sandwiched between two indium-tin oxide (ITO) (8-12 Ω/sq) coated glass slides. Redox potentials were measured vs. Ag/AgCl (R.E) and a second platinum wire (A.E.). Potentials were applied using a BASi 50W potentiostat, and the accompanying UV-visible spectra collected on a Varian Cary 50 spectrophotometer at 25 °C, over a period of time.

2.2.10. Bulk Electrolysis (BE)

Controlled potential electrolysis or bulk electrolysis is a technique where either a constant current or constant potential is applied to an electrochemical cell in order to assess significant changes in oxidation states or evaluate electrochemical robustness of a redox-active sample.[116] The total charge consumed by the system during electrolysis is obtained by plotting the current versus time.[116] Products of catalytic bulk electrolysis experiments are typically identified and quantified by gas chromatography. Other methods such as EPR, NMR, and sometimes ESI-MS, are used in

www.manaraa.com

the case of complete or partially oxidized/reduced species. Bulk electrolysis was done based on a modified method[73, 117] in a custom-made airtight H-type cell with two chambers separated by a frit. A mercury-pool (Hg-pool) W.E. and Ag/AgCl R.E. were placed in the larger, major chamber, while a Pt wire A.E. was placed in the minor auxiliary chamber. Tetrabutylammonium hexafluorophosphate ($TBAPF_6$) was used as a supporting electrolyte. The major chamber was filled with the electrolyte solution and the sample. The auxiliary chamber contained only electrolyte solution.

In a typical experiment, the cell is evacuated with N_2 gas for approximately 15 minutes, after which the headspace is sampled with gas chromatography (GC) to ensure an O_2 free environment before applying a potential. A blank solution containing only supporting electrolyte was then electrolyzed over a period of time, at an appropriately applied potential (i.e. -1.7 V vs. Ag/AgCl). After electrolysis, the headspace gas was again sampled to measure the amount of dihydrogen generated. The cell was subsequently degassed with N_2 gas for another 15 minutes and the experiment repeated, this time containing the catalytic sample.

2.2.11 Gas Chromatography (GC)

Gas chromatography (GC) is an analytical technique which analyses the content of a gaseous compound. In a typical experiment, a sample is injected into a gas chromatograph, then enters a gas stream which transfers the sample into a column. A carrier gas (helium or nitrogen) aids this transfer. Separated components in the column are detected and quantified. To analyze an unknown sample, standard samples are injected, and their peak retention times and areas are compared to the unknown sample to determine its concentration. Gas chromatography was used to analyze and quantify electrocatalytic products of water splitting such as hydrogen (H_2), and O_2. A Gow-Mac 400 equipped with a thermal detector and an 8’ x 1/8” long 5Å molecular sieve

www.manaraa.com

column working at 60°C was used, with N_2 as the carrier gas for hydrogen, whilst He was used as carrier gas for O_2.

2.2.12. Scanning Electron Microscopy and Energy Dispersive Spectroscopy (SEM-EDS)

Scanning electron microscopy (SEM) is one of the most versatile techniques available for analyzing the morphology of surface materials.[118] Images are formed from signals generated when the surface of a sample is scanned with a focused electron beam.[118] The electron beam and specimen interactions produce many signals that are processed to obtain useful information about the surface topography and composition of the sample.[119] Energy dispersive spectroscopy (EDS) supplements SEM by identifying particular elements in a scanning electron micrograph and determining their relative proportions.[120] EDS analysis involves the generation of X-ray spectra from the scanned SEM and plotted as number of X-rays processed by the detector *vs* the energy level of the X-rays.[121] SEM and EDS were used to characterize the nature and composition of post-catalytic electrodes in this dissertation to determine if catalyst deposition has occurred. Data was taken on a JSM-7600 FE SEM instrument, equipped with a Pegasus Apex 2 integrated EDS and EBSD system.

2.2.13. Density Functional Theory Calculations (DFT)

Density functional theory (DFT) finds utility in almost every aspect of science.[122] DFT effectively complements experimental studies and provides a theoretical approach to determining electronic structures of molecules. DFT can also provide insight into a great variety of molecular properties such as relative energies of molecular orbitals, reaction pathways, and reaction dynamics as a support for experimental reactions and design. DFT computations were used to predict the nature of catalytic intermediates that are often difficult to isolate experimentally, as well as predict energetically favorable reaction pathways. Calculations ultimately aimed to

www.manaraa.com

elucidate plausible mechanistic pathways based on experimental observations. DFT calculations were performed in collaboration with the Schlegel group at Wayne State University, using the Gaussian suite with revisions H.31,[123] using B3LYP/6-31G(d,p)[124-125], and the BPW91[125] functional with SDD,[126,127] and the 6-31G(d,p)[128] basis set by Dr. Shivnath Mazumder, and Dr. Bishnu Thapa, for different projects described in my dissertation.

www.manaraa.com

CHAPTER 3:
VERSATILITY OF A QUINOLINE-BASED PENTADENTATE Co(II) COMPLEX FOR ELECTROCATALYTIC WATER SPLITTING

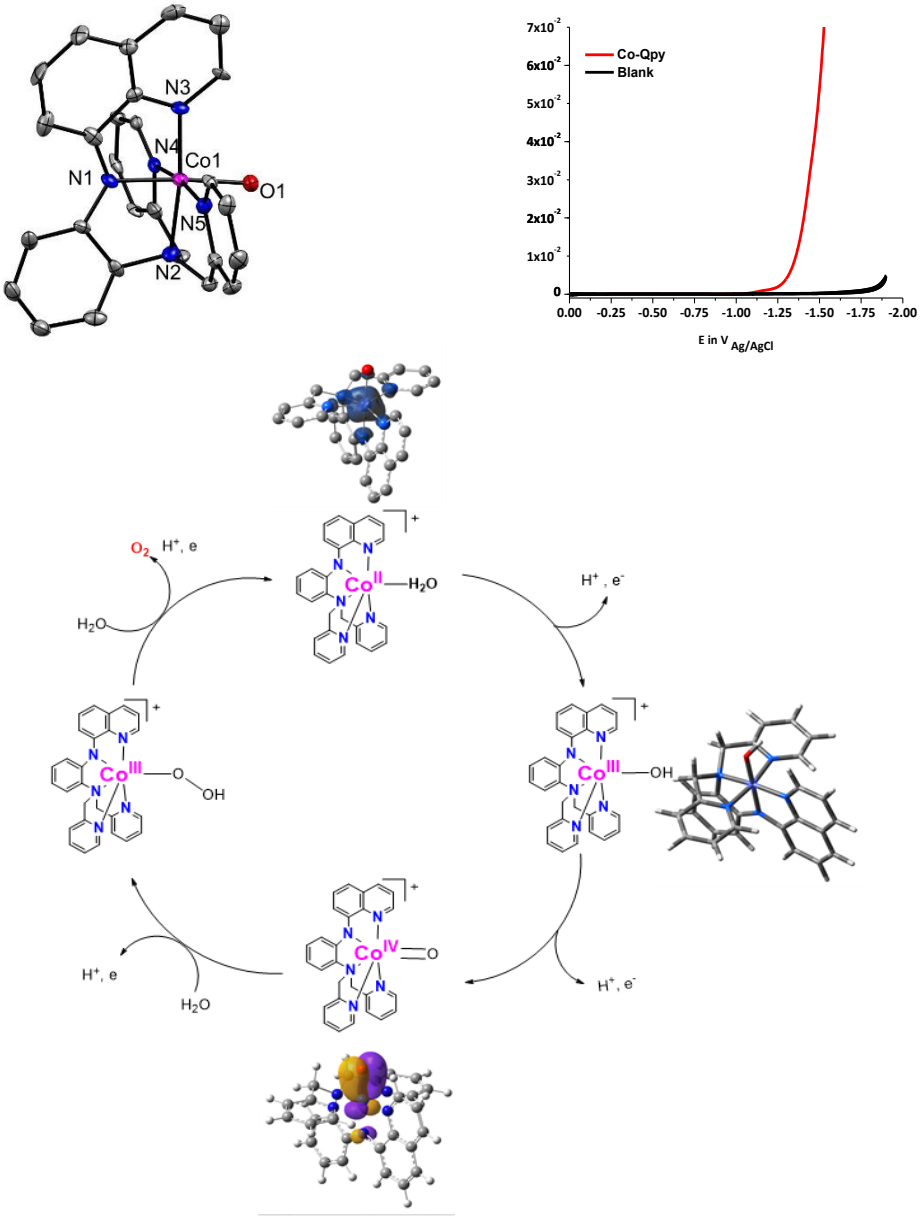

www.manaraa.com

CHAPTER 3: VERSATILITY OF A QUINOLINE-BASED PENTADENTATE Co(II) COMPLEX FOR ELECTROCATALYTIC WATER SPLITTING

3.1. Introduction

Earth-abundant transition metals like cobalt, nickel, and iron have attracted attention due to their ability to generate H_2 and O_2 from water.[129,17,59,130] Among these, cobalt is particularly relevant because it can effectively stabilize the catalytically active species $3d^8$ Co^I and the cobalt/hydride intermediate Co^{III}–H^- which is pivotal for H^+ reduction to H_2.[14,131,46,132,133] The production of H_2 from Co^{III}-H follows either heterolytic or homolytic pathways shown in **Figure 3.1**.[46,16,47] The former mechanism relies on a single Co^{III}–H^- reacting with another H^+, while homolytic mechanisms involve two independent Co^{III}–H^-moieties.[48]

The reliance on a particular mechanism is governed by factors such as the concentration of acid used,[49] catalyst design, applied potential,[50] the rate constants for hydride formation,[51] and whether H_2 is evolved by hydride protonation or dimerization.[52]

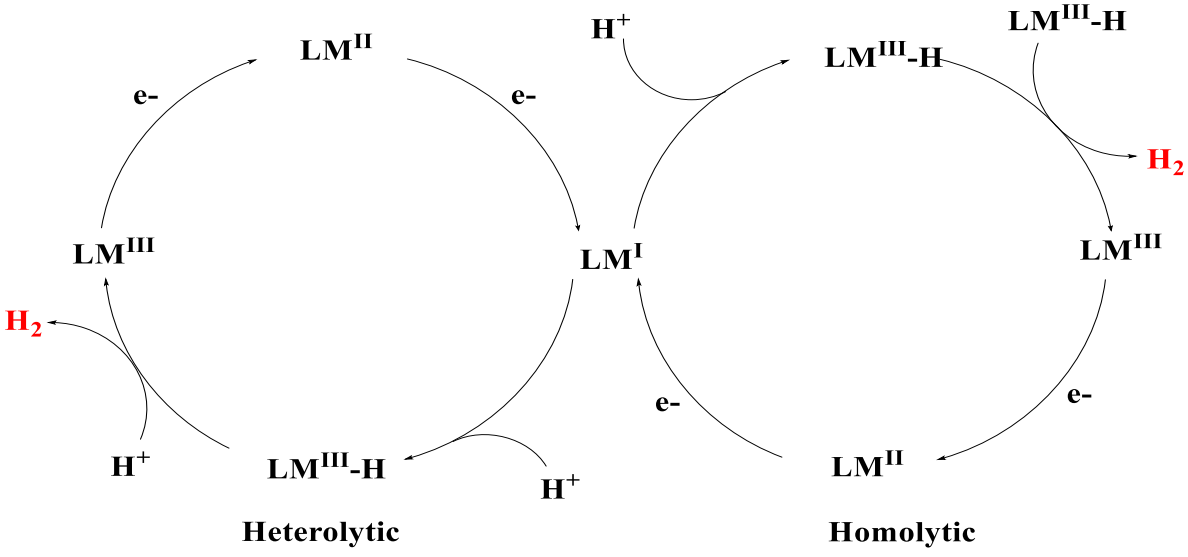

Figure 3.1. Generalized Catalytic mechanisms of H_2 generation.

www.manaraa.com

Cobalt-based catalysts are also expected to oxidize water to dioxygen in basic media undergoing a well-defined PCET steps **(Figure 3.2)** to a tetravalent intermediate which is electrophilic enough to be attacked by a nucleophilic water molecule.

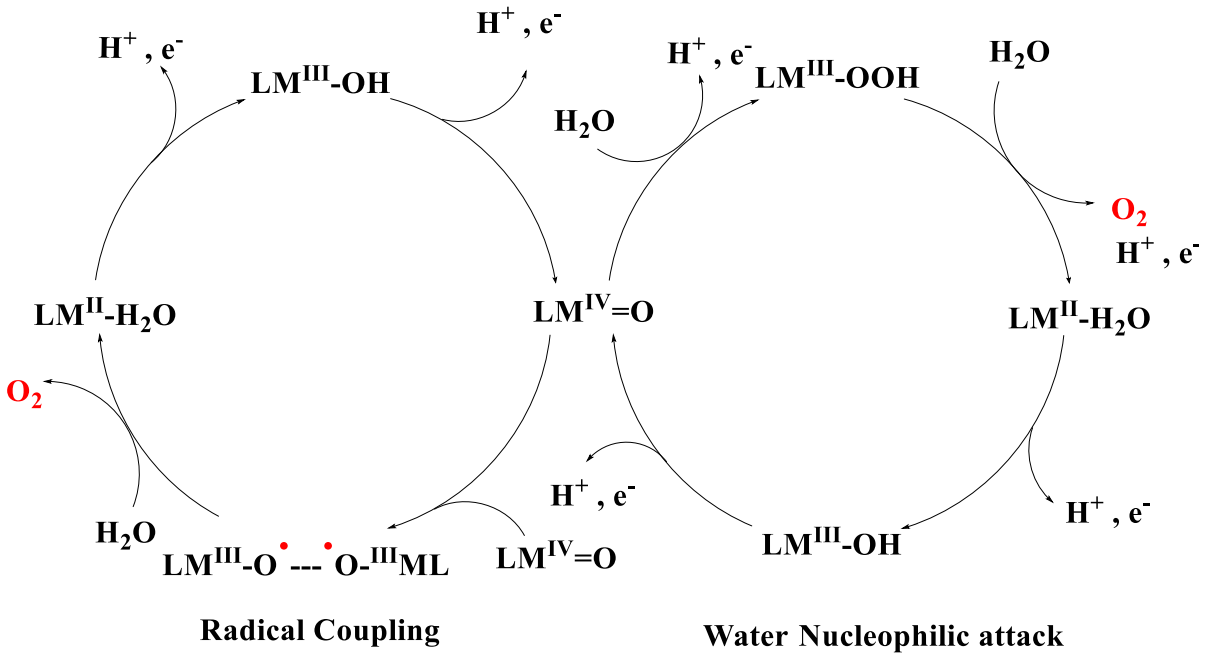

Figure 3.2. Generalized Catalytic mechanisms of O_2 generation.

For this step, two main mechanisms have been generally reported: (i) The water nucleophilic attack (WNA) pathway, where water attacks an oxo ligand bound to a high valent species,[134,135,21,136,137] and (ii) The radical homo-coupling (RC) pathway, where two metal–oxo species having radical character predominantly on the oxo group.[138]

Other mechanisms have been proposed, such as the expanded coordination sphere (seven-coordinate Ru).[86,12] The ability to isolate, identify and track key intermediate species during catalysis using analytical and spectroscopic techniques such as EPR and UV-visible spectrophotometry enables a systematic study of the various interactions that occur during catalysis and guide the design of better catalysts.

www.manaraa.com

Finally, photocatalytic water splitting is viewed as the ultimate goal of developing a sustainable hydrogen economy. The ability of a well-studied electrocatalyst to work in tandem with a requisite photosensitizer to produce hydrogen from water, using solar energy is therefore highly desired.

In a recently published report on cobalt catalysts with pentadentate pyridine-rich ligands catalysts for proton and water reduction, The Verani group discussed how ligand architecture influences catalytic activity.[73] In that report we observed that one of the aminopyridine ligands transformed into an amido derivative through a hydroxy intermediate formed from addition of adventitious aqueous solvent to the imine moiety.[73] I therefore hypothesize that modifying the ligand architecture by incorporating a more rigid ligand, which has increased aromaticity, stabilized by mesomeric and inductive effects, will yield a robust second generation catalyst capable of efficient catalysis.

3.2 Experimental

3.2.1 Synthesis of N,N′-Mono(8-quinolyl) bispyridine-phenylenediamine (HL^{Qpy})

The synthesis of the pentadentate quinolyl-bispyridine ligand, $\mathbf{HL^{Qpy}}$, with a phenylenediamine backbone was adapted from the literature[139] and modified by treating one equivalent of 8-hydroxyquinoline with an equivalent of *ortho*-phenylenediamine in the presence of sodium metabisulfite ($Na_2S_2O_5$), triethylamine, and water under reflux for 7 days. The resulting orange solution was extracted with dichloromethane.

The pale yellow crystalline solid obtained was reacted with an aqueous solution of 2-(chloromethyl) pyridinium chloride (two equivalents) in the presence of sodium hydroxide and catalytic amounts of hexadecyltrimethyl ammonium chloride under inert conditions for 24 hours. Yield: 56%. ESI (m/z+) in CH_3OH for $[\mathbf{HL^{Qpy}} + H^+]^+$ = 418, ^1H NMR ($CDCl_3$): δ 8.90 (d, 1H,

www.manaraa.com

QnH), 8.46 (d, 2H, 2-ArH), 8.17 (d, 1H, QnH) 7.78 (d, 2H, ArH), 7.62 (m, 4H, QnH), 7.41 (m, 4H, Ar H), 7.15 (m, 3H, ArH), 6.88 (m, 1H, Ar H), 4.53 (s, 4H, CH_2), 1.24 (s, 1H, sec-amine), IR (KBr, cm^{-1}) 3350(ν_{N-H}), 1610 ($\nu_{C=C}$, aromatic), 1580 (ν_{N-H},) 1589 ($\nu_{C=N}$), 1342 (ν_{C-N} aromatic), 750 (ν_{C-H}).

3.2.2 Synthesis of $[Co^{II}(L^{Qpy})H_2O]ClO_4$

A water-soluble Co(II) complex was prepared from the pentadentate $\mathbf{HL^{Qpy}}$ ligand. The complex was obtained by treating one equivalent of $\mathbf{HL^{Qpy}}$ with one equivalent of $Co(ClO_4)_2 \cdot 6H_2O$ in the presence of triethylamine in methanol under inert conditions for three hours at room temperature. Yield: 49%. ESI (m/z+) in CH_3OH for $\mathbf{[Co^{II}(L^{Qpy})H_2O]ClO_4]H^+}$ = 476 (100%), Anal. Calc. for $[C_{30}H_{31}CoClN_6O_5]$: C, 50.22; H, 4.36; N, 11.71%. Found: C, 50.37; H, 4.32; N, 11.57%. IR (KBr, cm^{-1}) 1610 ($\nu_{C=C}$, aromatic), 1580 (ν_{N-H},) 1589 ($\nu_{C=N}$), 1342 (ν_{C-N} aromatic), 1090 (ν_{ClO4}), 665($\nu_{C=C}$, aromatic).

3.2.3 X-Ray Structural Determinations

Yellow colored hexagonal X-ray quality crystals of $\mathbf{(HL^{Qpy})}$ precursor were grown by vapor diffusion of the complex dissolved in a 1 : 1 dichloromethane : pentane solvent mixture. A suitable crystal was selected and mounted on a mitogen loop, and diffraction data was collected on a Bruker X8 SMART APEX II CCD[140] diffractometer using a monochromatic graphite-Mo Kα radiation source (0.7107 Å) and SMART/SAINT[108] software. The crystal was kept at 100.1 K during data collection and a total of 87619 reflections were measured, with 4402 unique reflections. Using the Olex2 structure solution suite,[111] the structure was solved with the ShelXT[112] structure solution program using Intrinsic Phasing and refined with the ShelXL[112] refinement package using Least Squares minimization.[112] Hydrogen atoms were calculated using the riding model.

www.manaraa.com

For the **2[Co^{II}(L^{Qpy})H$_2$O]ClO$_4$** complex, pink colored oblong X-ray quality crystals of were grown by vapor diffusion of the complex dissolved in a 1 : 1 methanol : isopropanol solvent mixture. A suitable crystal was selected and mounted on a mitogen loop, and diffraction data were collected as described above. The crystal was kept at 100.1 K during data collection and a total of 83673 reflections were measured, with 23563 unique reflections.

Using the Olex2 structure solution suite,[111] the structure was solved with the ShelXT[112] structure solution program using Intrinsic Phasing and refined with the olex2.refine refinement package using Gauss-Newton minimization.[111] Hydrogen atoms were placed in calculated positions. There are two independent dimeric octahedral complexes in the asymmetric unit. Each dimer has a trans-peroxo bridge connecting the monomeric units through the axial position.

Each of the dimers has two perchlorate anions consistent with the solid state oxidation of +2 for the cobalt center in each of the monomeric units. Selected crystallographic data for both the precursor and complex are shown in **Table 3.1.**

Table 3.1. **Summary of Crystallographic Data for** (HL^{Qpy}) **and** 2[Co^{II}(L^{Qpy})H$_2$O]ClO$_4$**.**

	(HL^{Qpy})	**4[Co^{II}(L^{Qpy})O]ClO$_4$**
Formula	$C_{15}H_{13}N_3$	$C_{113}H_{88}Cl_4Co_4N_{19}O_{20}$
M	235.28	2409.62
Temperature/K	100.1	100.1
Crystal system	Orthorhombic	Monoclinic
Space group	*Pca2$_1$*	*P*2$_1$
a/Å	10.6800(5)	13.5658(14)
b/Å	11.0757(5)	30.847(3)
c/Å	10.0873(5)	13.6410(13)
α/°	90	90

www.manaraa.com

β/°	90	90.009(7)
γ/°	90	90
Volume/Å^3	1193.21(10)	5708.3(10)
Z	4	2
D_{calc} / g cm^{-3}	1.310	1.4018
μ/ mm^{-1}	0.080	0.740
R(F) (%)	3.68	8.28
Rw(F) (%)	10.38	18.99

[a] $R(F) = \sum \| F_o | - | F_c \| / \sum | F_o |$; $Rw(F) = [\sum w(F_o^2 - F_c^2)^2 / \sum w(F_o^2)^2]^{1/2}$ for $I > 2\sigma(I)$

3.2.4 Computational Details

The electronic structure calculations were performed in collaboration with the Schlegel group at WSU, by Dr. Bishnu Thapa, using the BP86 density functional[141-142] implemented in the Gaussian 09 (revision E.01) suit of package.[143] SDD basis set and an effective core potential (ECP)[144-145] was used for cobalt atom, and 6-31+G(d,p) basis set[146-150] was used for all the other atoms. All the structures were optimized in aqueous environment, modeled by using SMD implicit solvation.[151] The optimized structures were confirmed to be the minima on the potential energy surface by performing harmonic frequency calculations and had no imaginary normal mode frequency. Wave functions were tested for their stability. GaussView[152] was used to visualize the isodensity plot of canonical and biorthogonal orbitals, and spin density.

3.2.5. Electrocatalytic Studies

Electrocatalytic water reduction was performed in the previously described custom-made air-tight H-type cell **(Chapter 2)** under inert conditions,[73, 117, 130] where one side of the frit the working (mercury pool) and reference electrodes (Ag/AgCl) were placed, while the auxiliary electrode (coiled 12 inch Pt wire) was placed on the other side. During electrocatalysis the cell was

www.manaraa.com

purged with N_2 gas for 10-15 minutes followed by sampling of the head space gas (100 μL) to ensure an O_2 free environment in the gas chromatograph.

The amount of hydrogen generated was determined in a Gow-Mac 400 gas chromatograph (GC) equipped with a thermal conductivity detector, and an 8 ft. x 1⁄8 in., 5 Å molecular sieve column operating at a temperature of 60 ℃. Nitrogen was used as a carrier gas at a flow rate of 30 mL/min. The amount of H_2 produced was quantified using a calibration curve of moles of hydrogen versus peak area. Turnover numbers and the Faradaic efficiency of the metal complex were calculated from the amount of H_2 released and the charge consumed.

For water reduction, a 1.0 M phosphate buffer was prepared by mixing NaH_2PO_4 (0.454 mol, 27.24 g) and Na_2HPO_4 (0.545 mol, 38.695 g) in ultrapure water. Then, the pH was adjusted to 7 by adding suitable amounts of NaOH or HCl. For the bulk electrolysis experiment, the main chamber was filled with 20 mL of phosphate buffer solution and mercury-pool electrode (working electrode) whereas the glass-fitted chamber was filled with 5 mL of solution. Bulk electrolysis was performed with an appropriate potential (i.e. -1.7 $V_{Ag/AgCl}$) applied in the presence of the same set of electrodes to generate H_2.

Electrocatalytic water oxidation was performed under similar conditions as described for water reduction, but in borate buffer (0.1 mol•L^{-1}, pH 8) using a fluorine-doped tin oxide (1.27 cm^2) glass working electrode, a Pt wire as the auxiliary electrode and Ag/AgCl as the reference electrode.

3.2.6. Photocatalytic Studies

Samples for photocatalytic water reduction were prepared in 15 mL clear cylindrical vials with gas tight screw caps fitted with septa. All the samples were filled with a 10 mL aliquot of 0.1 M pH 4 acetate buffer containing the $[Ru(bpy)_3]^{2+}$ photosensitizer (5.0×10^{-4} M), ascorbic acid

www.manaraa.com

(1.1 M) and catalyst **$[Co^{II}(L^{Qpy})H_2O]ClO_4$** (1.0 10^{-4}M). The vials and their contents were then thoroughly degassed with nitrogen gas, and verified by GC prior to light irradiation. The vials were then placed in a water-jacketed beaker with a constant temperature of 20 °C.[153] The contents of the vials were irradiated by an 18 module blue LED strip (λ_{max} = 460 nm) wrapped around the beaker and connected to a 12 V power controller.

The headspace gas was analyzed in triplicates at 30 minute intervals over 4 hours by a GOW MAC GC with a TCD detector to determine the amount of hydrogen produced over time. Nitrogen was used as the carrier gas at a flow rate of 30 mL/min. The amount of H_2 produced was quantified using a calibration curve of moles of hydrogen versus peak area.

3.2.7. Electron paramagnetic resonance (EPR) studies

All samples were prepared under inert conditions atmosphere. A 10^{-3} M solution of the ($^{HS}Co^{II}$, d^7 S = 3/2) parent **$[Co^{II}(L^{Qpy})H_2O]ClO_4$** complex was transferred into a suprasil-quartz EPR capillary tube having a 4 mm outer diameter and frozen in liquid nitrogen. A series of one-electron and 2-electron electrochemical oxidation experiments were conducted to generate ($^{LS}Co^{III}$, d^6 S = 0) and ($^{HS}Co^{IV}$, d^5 S = 5/2) species, respectively.

Continuous wave (CW) X-band (9.48 GHz) EPR experiments were carried out by Drs. Oleg Poluektov and Jens Niklas at Argonne National Laboratories, with a Bruker ELEXSYS E580 EPR spectrometer (Bruker Biospin, Rheinstetten, Germany), equipped with a Bruker ER 4102ST resonator or a Bruker ER 4122SHQ resonator. The temperature was controlled using a helium gas-flow cryostat (ICE Oxford, UK) and an ITC (Oxford Instruments, UK). Data processing was done using Xepr (Bruker BioSpin, Rheinstetten) and Matlab 7.11.2 (The MathWorks, Inc., Natick) environment.

www.manaraa.com

3.3 Results and Discussion

3.3.1 Synthesis and Characterization

An asymmetric, pentadentate quinolyl-bispyridine ligand, **HL^{Qpy}**, with a phenylenediamine backbone was synthesized and characterized by spectroscopic and spectrometric techniques (**Scheme 3.1)**. The ligand synthesis was adapted from the literature[139] and modified by treating one equivalent of 8-hydroxyquinoline with an equivalent of *o*-phenylenediamine in the presence of sodium metabisulfite, triethylamine (TEA) and water under reflux for 7 days. The resulting solution was extracted with dichloromethane yielding a pale-yellow crystalline precursor.

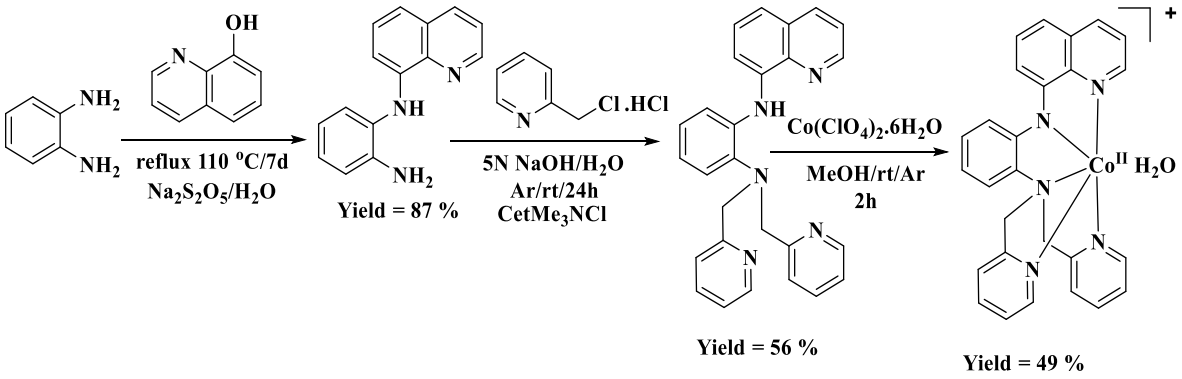

Scheme 3.1. Synthesis of the complex $[Co^{II}(L^{Qpy})H_2O]ClO_4$.

The pale yellow crystalline solid was reacted with an aqueous solution of 2-(chloromethyl) pyridinium chloride in the presence of NaOH and catalytic amounts of hexadecyltrimethyl ammonium chloride under inert conditions for 24 h to generate the crude ligand. The pure ligand was obtained by column chromatography on silica using a 3 : 1 EtOAc : hexanes solvent mixture. The ^{1}H-NMR spectrum of the ligand recorded in deuterated chloroform is shown in **Figure 3.3**, and the proton assignments detailed in **section 3.2.1** above.

www.manaraa.com

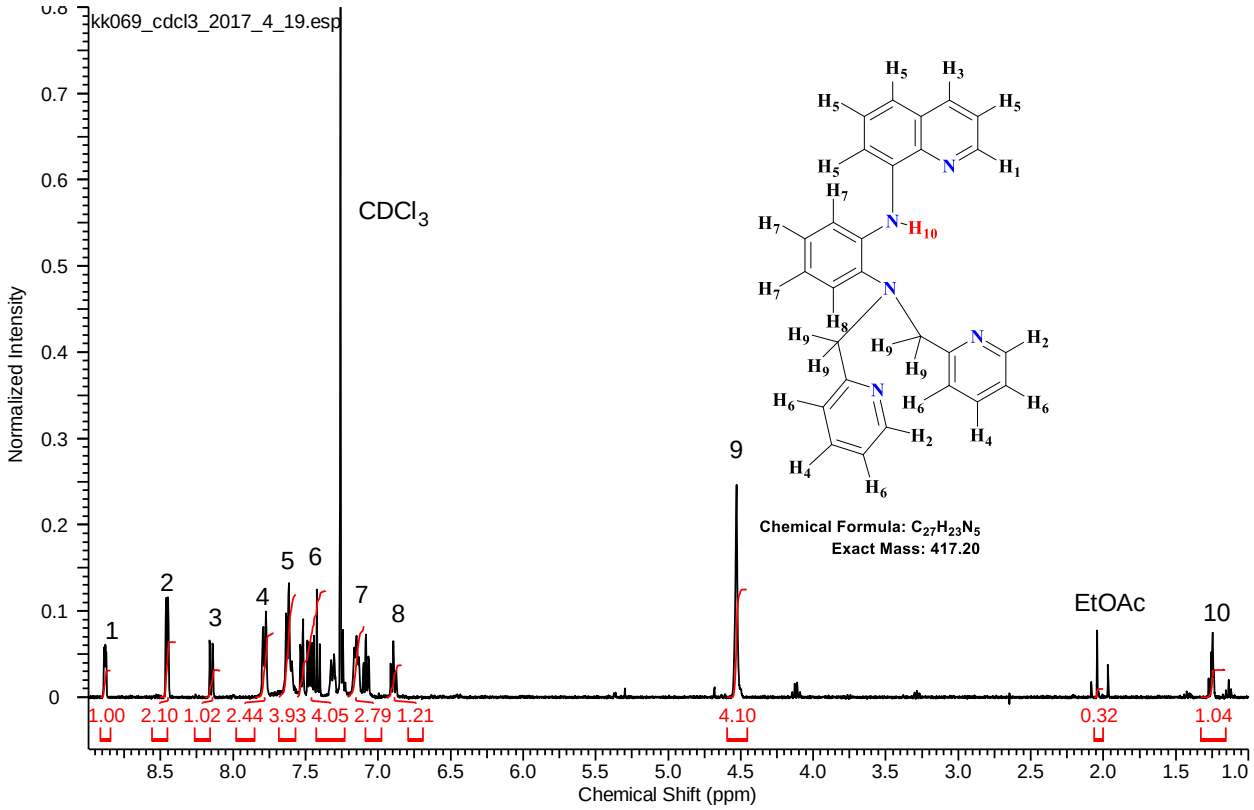

Figure 3.3. ^{1}H-NMR of **HL^{Qpy}** showing proton peaks with integration.

The water-soluble 3d^{7} ^{HS}Co^{II} complex was obtained by treating one equivalent of the pentadentate L^{Qpy} ligand with one equivalent of $Co(ClO_4)_2$ salt in presence of triethylamine (TEA) in methanol under inert conditions for 3 h. The ^{HS}Co^{II} aqua complex was characterized by FT-IR, ESI-MS, and elemental analyses. The disappearance of the N-H peak at 3350 cm $^{-1}$ in the FT-IR spectrum indicates the deprotonation of the secondary amine proton in the ligand from coordination to cobalt **Figure 3.4**. A sharp peak near 600 cm^{-1} and a very strong, and broad band at 1100 cm^{-1} both show the presence of a perchlorate counterion.

www.manaraa.com

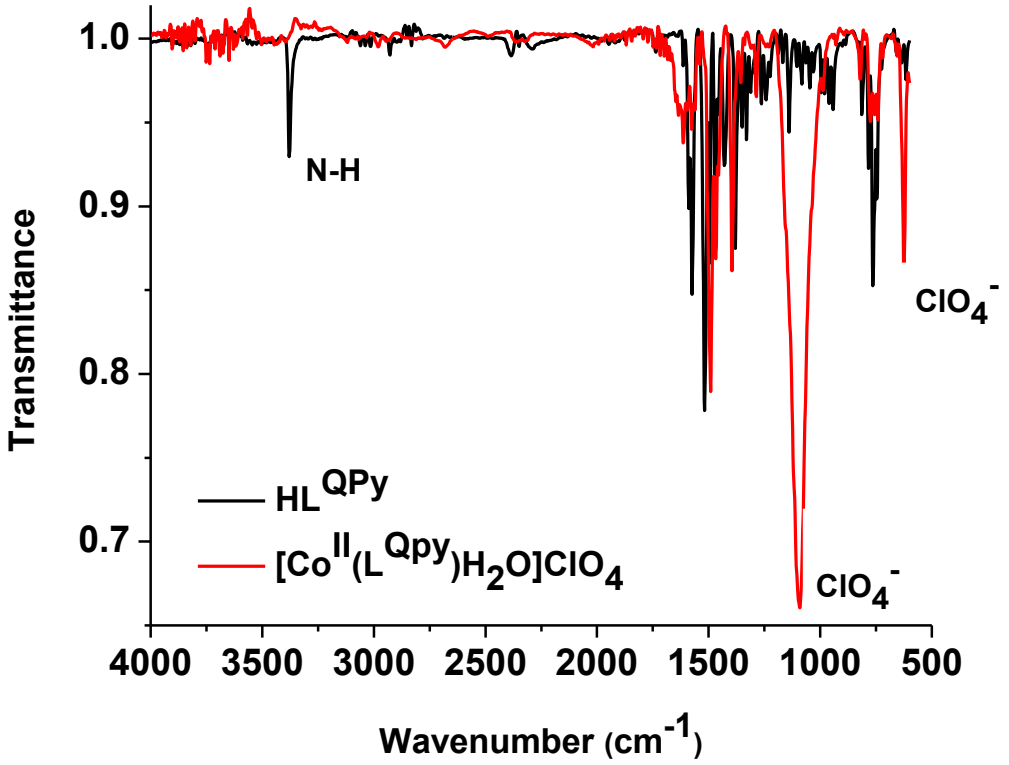

Figure 3.4. FTIR of **HL^{Qpy}** and **[Co^{II}(L^{Qpy})H$_2$O]ClO$_4$** showing relevant functional groups.

3.3.2 Geometric and Electronic Structures

The molecular structures of **HL^{Qpy}** and [Co^{II}(L^{Qpy})H$_2$O]ClO$_4$ were both determined by single crystal X-ray crystallography. Yellow colored hexagonal X-ray quality crystals of **(L^{Qpy})** precursor were grown by vapor diffusion of the complex dissolved in a 1 : 1 dichloromethane pentane solvent mixture for the structural determination (**Figure 3.5**). For **[Co^{II}(L^{Qpy})H$_2$O]ClO$_4$**, X-ray quality crystals grown by slow evaporation from 1 : 1 methanol : isopropanol were used for the structural determination. However it is important to state that, the crystal structure obtained from the diffraction studies indicate a dimeric form of the complex with an end-on transperoxo bridge. The formation of this dimer could be the oxidation of the complex dring the crystalization

www.manaraa.com

process. The dimeric structure is shown in the Oak Ridge Thermal-Ellipsoid Plot (ORTEP)[154] representations at 50% probability in (**Figure 3.6**).

The **HL^{Qpy}** crystalized in an orthorhombic lattice with a *pca*2$_1$ space group. The asymmetric unit cell has one neutral molecule of a phenyldiamino-quinoline. Selected bond lengths for both crystal structures are shown in **Table 3.2.** The C-N bond lengths fall within the range of 1.323(1) Å and 1.421(1) Å consistent with reported C-N bonds for similar systems.[73,155]

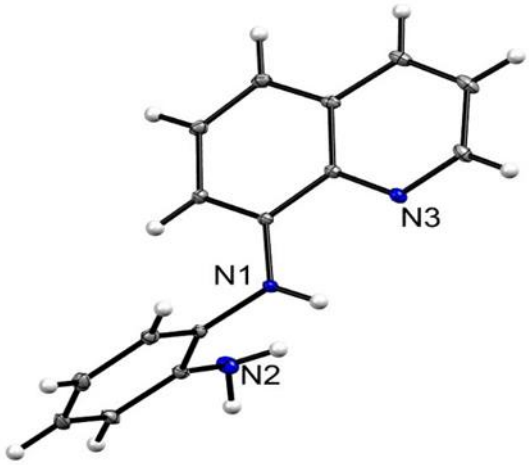

Figure 3.5. ORTEP[154] representations of **HL^{Qpy}** precursor at 50% probability. H atoms are shown for emphasis.

The structure is consistent with the presence of the characteristic secondary amine hydrogen (N-H) bonded to the nitrogen linking the phenylenediamine backbone and the quinoline moiety observed in FT-IR. The primary amine on the benzene ring does not form hydrogen bonds with the quinoline nitrogen in the solid state.

The **2[Co^{II}(L^{Qpy})O]ClO$_4$** complex crystallized with a *trans*-μ-peroxo bridge between the two cobalt centers, each of which adopts a distorted octahedral geometry with the ligand.

www.manaraa.com

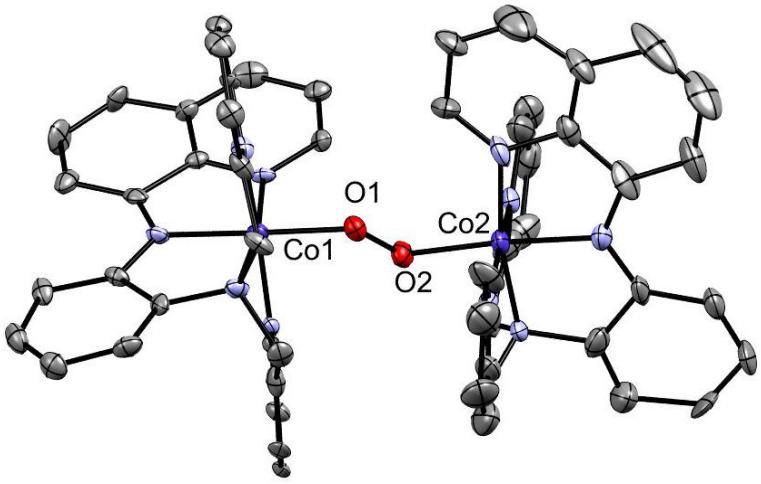

Figure 3.6. ORTEP[154] representations of dimeric form of **2[Co^{II}(L^{Qpy})O]ClO$_4$** at 50% probability H atoms are omitted for clarity.

The asymmetric unit cell consists of two dimeric cationic complexes with two perchlorate anionic moieties per each dimeric unit. The Co–N bond lengths fall in the range of the expected values of 1.88-1.95 Å.[156,73,155-159] The Co–O bond lengths range from 1.862(5) to 1.87(5) Å, which are similar to those reported.[70, 160-161] The O−O bond length of 1.422(8) Å, is typical for dinuclear Co−peroxo complexes.[103,162,155]

Table 3.2. Selected bond lengths (Å) and angles (º) from crystal data for (**HL^{Qpy}**) and **2[Co^{II}(L^{Qpy})O]ClO$_4$**

(L^{Qpy})			2[Co^{II}(L^{Qpy})O]ClO$_4$		
N3	C8	1.364(1)			
N3	C12	1.323(1)	Co1	O1	1.862(5)
N1	H1	0.880(1)	Co1	N1	1.885(6)
N1	C3	1.381(1)	Co1	N2	1.945(6)
N1	C7	1.421(1)	Co1	N3	1.900(6)

www.manaraa.com

C3	C8	1.432(1)	Co1	N4	1.953(6)
C3	C11	1.384(1)	Co1	N5	1.928(6)
C4	C5	1.417(1)	Co2	O2	1.875(5)
C4	C8	1.421(1)	Co2	N6	1.896(6)
C4	C10	1.415(1)	Co2	N7	1.928(9)
			Co2	N8	1.943(9)
			Co2	N9	1.908(7)
			Co2	N10	1.939(9)

3.3.3 Electronic Spectroscopy

To probe metallation and gain insight into the electronic behavior of the complex before catalytic evaluation, a UV-visible spectrum was recorded in methanol and compared with that of the ligand (**Figure 3.7**). The ligand displays two bands at *ca.* 290 nm (ε = 38,500 L•mol^{-1}•cm^{-1}) and 380 nm (ε = 10,000 L•mol^{-1}•cm^{-1}) which are associated with $\pi \rightarrow \pi^*$ ILCT. The complex retained the band at 290 nm (ε = 22,000 L•mol^{-1}•cm^{-1}) associated with $\pi \rightarrow \pi^*$ ILCT, albeit with reduced intensity of the molar absorptivity due to coordination of the cobalt metal to the ligand. A new LMCT appears band at 330 nm (ε = 24,800 L•mol^{-1}•cm^{-1}) is assigned as quinoline $\pi \rightarrow {}^{HS}Co^{II}$–*d*$\sigma^*$.[163] The third band at 527 nm (ε = 6,650 L•mol^{-1}•cm^{-1}) is associated with a MLCT. The MLCT involves the promotion of an electron from the metal's d-orbital to the π^*-orbital of the ligand. A more rigid and planar ligand results in greater π-delocalization, producing the longest wavelength absorption.[164] These attributions are in agreement with similar published reports in the literature.[139, 164]

www.manaraa.com

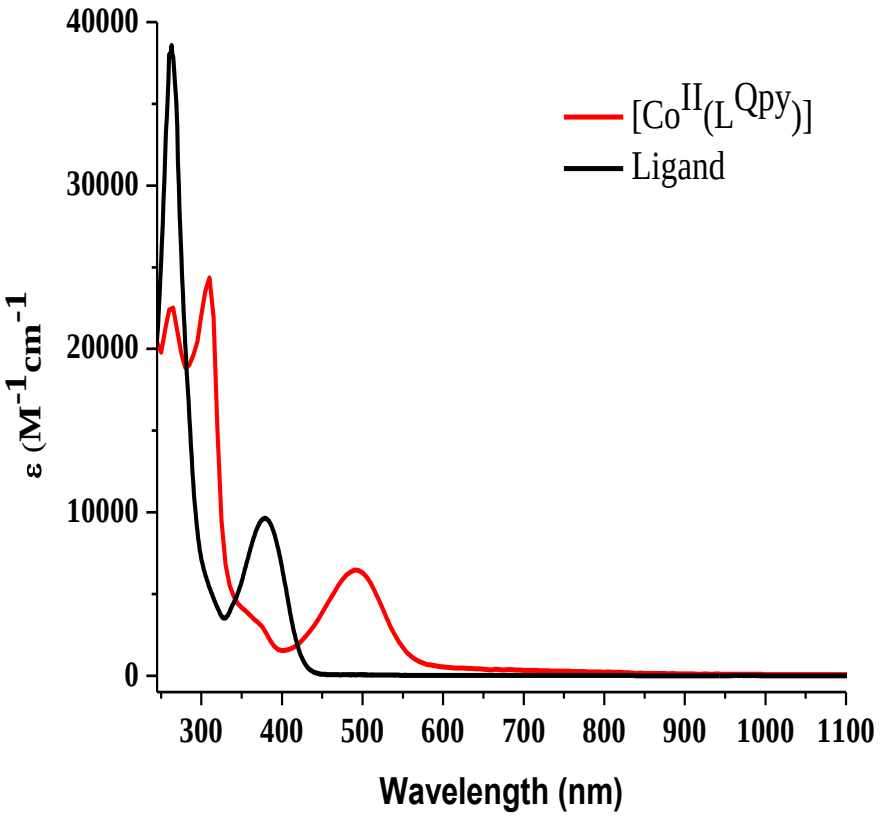

Figure 3.7. Electronic behavior of **HL^{Qpy}** and **[Co^{II}(L^{Qpy})H$_2$O]ClO$_4$** in 1.0 × 10^{-4} mol•L^{-1} methanol solution.

3.3.4 Electrochemical Properties

To probe the redox behavior of the metal complex, cyclic voltammograms were measured in 1.0 × 10^{-3} mol•L^{-1} acetonitrile solution using $TBAPF_6$ as the electrolyte (**Figure 3.8**). Redox potentials are reported versus Fc^+/Fc and are summarized in **Table 3.3**. The CV of **[Co^{II}(L^{Qpy})]** showed one quasi-reversible reduction event at -1.15 $V_{Fc+/Fc}$ attributed to a metal-based Co^{II}/Co^{I} reduction, with a second irreversible reduction peak arising at -2.2 $V_{Fc+/Fc}$ likely associated with ligand reduction. A quasi-reversible oxidation process observed at 0.60 $V_{Fc+/Fc}$ is assigned to a Co^{II}/Co^{III} oxidation event. [67,165]

www.manaraa.com

Table 3.3. Electrochemical parameters for $[Co^{II}(L^{Qpy})H_2O]ClO_4$.

Redox Couples	E (V) vs. Fc/Fc^+	ΔE_p (V)	i_{pa} / i_{pc}
Co^{III}/Co^{II}	0.54	0.11	1.85
Co^{II}/Co^{I}	-1.16	0.09	1.42
L/L^-	-2.25	0.15	-

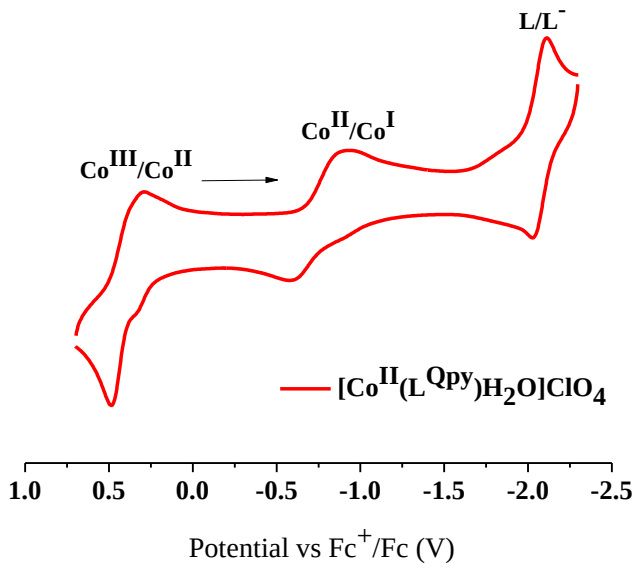

Figure 3.8. CV of **$[Co^{II}(L^{Qpy})H_2O]ClO_4$** in 1.0×10^{-3} mol•L^{-1} acetonitrile solution.

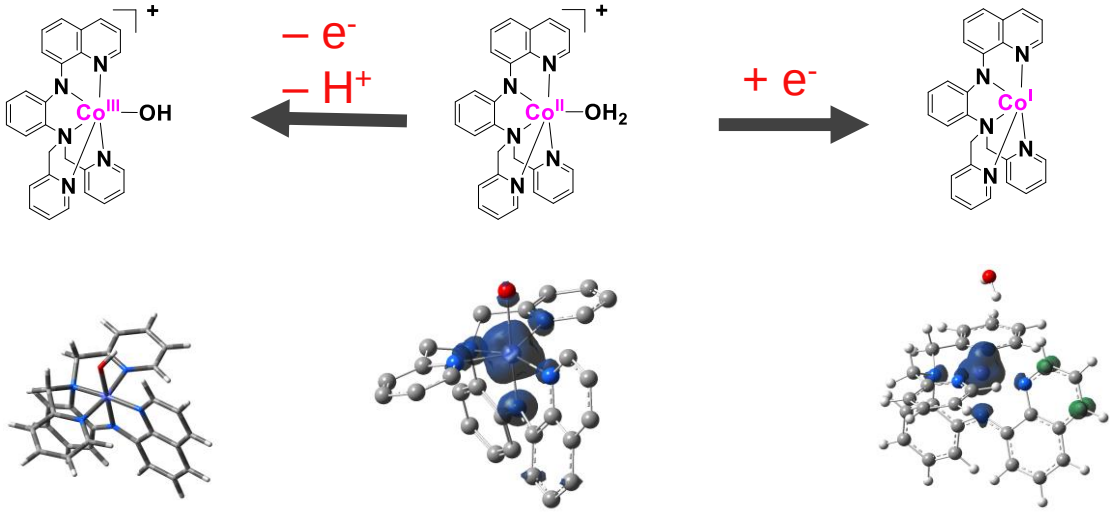

Figure 3.9. Spin density plots (isosurface value of 0.004 a.u.) of the redox-intermediate species generated during the electrochemical reduction, and oxidation of the complex.

www.manaraa.com

The one-electron reduction potential of -1.15 $V_{Fc+/Fc}$ is affordable for water reduction based on,[133,71] and hence theoretical calculations were computed for an electronic comparison **(Figure 3.9).** Mulliken spin density plots show that the parent $3d^7$ Co^{II} is high spin.

Upon a one-electron reduction, a five-coordinate, $3d^{8\ LS}Co^{I}$ was found to be more favorable than a six-coordinate $3d^{7\ LS}Co^{II}$-$L^{\bullet}$ intermediate species by 10 kcal/mol. The one-electron oxidation of the parent $3d^{7\ HS}Co^{II}$ yielded a closed shell $3d^{6\ LS}Co^{III}$ which was favorable by 21.1 kcal/mol.

3.3.5 Electrocatalytic Studies

3.3.5.1. Water Reduction Electrocatalysis

The complex was evaluated for dihydrogen production in aqueous media by conducting cyclic voltammetry experiments in aqueous pH 7 phosphate buffer (0.1 mol•L^{-1}) using a three-electrode setup: Ag/AgCl as the reference electrode, a platinum wire auxiliary electrode, and Hg-pool as the working electrode due to its low affinity for water reduction and large reductive window[165]. A CV sweep was done for the blank buffer without the catalyst, with no catalytic current enhancement observed until -1.85 $V_{Ag/AgCl}$ **(Figure 3.10).**

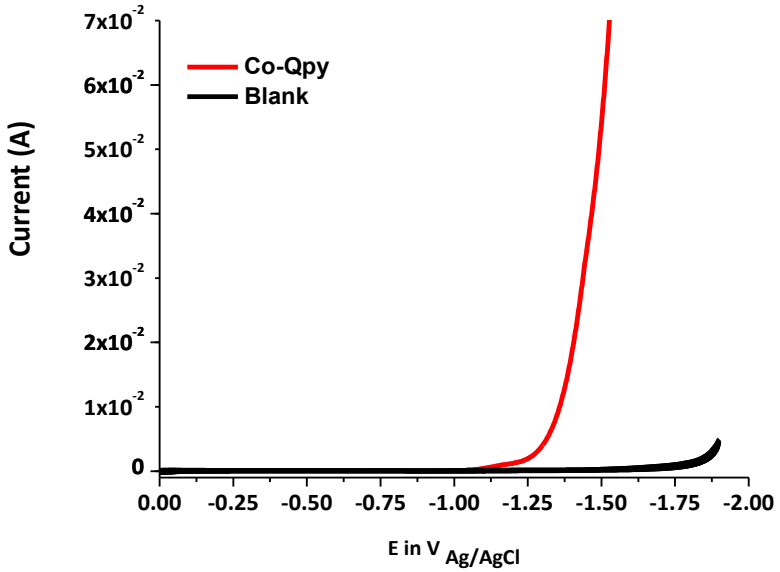

Figure 3.10. Catalytic water reduction CV of **$[Co^{II}(L^{Qpy})H_2O]ClO_4$** in 0.1 mol•$L^{-1}$ phosphate buffer at neutral pH.

www.manaraa.com

In the presence of the catalyst, however, a current enhancement was observed at -1.15 $V_{Ag/AgCl}$ accompanied by evolution of bubbles. The identity of the bubbles was confirmed as hydrogen by gas chromatography.

An onset potential for catalysis of –1.20 $V_{Ag/AgCl}$ was observed, yielding an overpotential of 0.65 V. The identity of the gas was determined to be H_2 by injecting the headspace into a gas chromatograph. To ascertain the efficiency of the catalyst for H_2 production and quantify the amount of H_2 produced, a 3 h bulk electrolysis was performed to determine the (TON) and (%FE) at an applied potential of -1.7 $V_{Ag/AgCl}$ **(Figure 3.11)**.

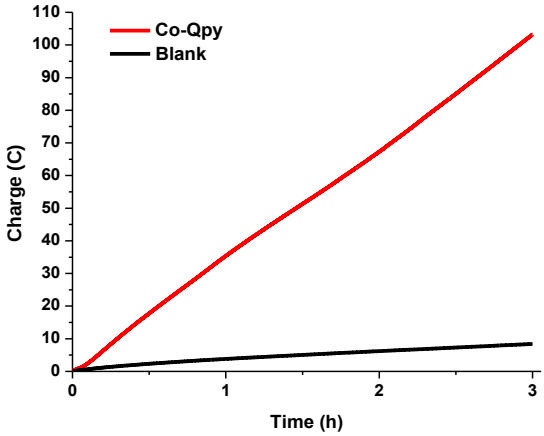

Figure **3.11.** Charge consumption vs. time during BE (0.2 umol•L^{-1}) of **$[Co^{II}(L^{Qpy})H_2O]ClO_4$** in 0.1 mol•$L^{-1}$ phosphate buffer at pH 7 at –1.7 $V_{Ag/AgCl}$ for 3 hours.

After 3 h, the catalyst operated at 98% Faradaic efficiency with a TON of 2900, with no apparent loss in activity. The high Faradaic efficiency indicates that every electron transferred is utilized in the production of H_2.[165] The TON and high (%FE) are higher than those reported for cobalt catalysts with similar ligand architectures, and under similar experimental conditions by Chang *et al*,[18] Zhao *et al.*[166] and show a remarkable improvement on the TON reported by 1st-generation cobalt pyridine catalyst by Verani *et al.*[73]

www.manaraa.com

To determine the robustness of the catalyst, bulk electrolysis was conducted under the same conditions for 18 h **(Figure 3.12)**. The 18-hour catalysis by **[$Co^{II}(L^{Qpy})$]** gave a TON of 12,100, with a (%FE) of 97, with negligible loss in activity by the charge versus time plot, suggesting a stable and robust catalyst.

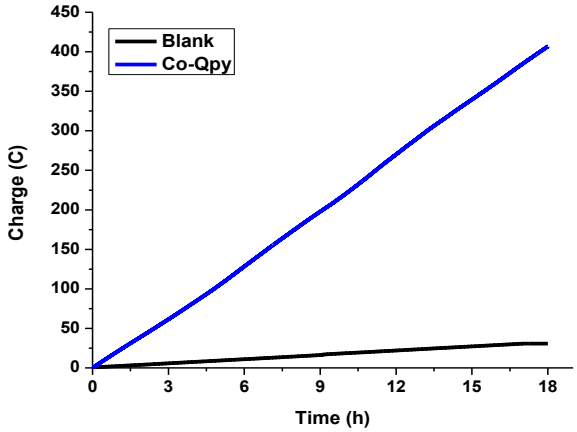

Figure 3.12. Charge versus time plot during controlled potential electrolysis of **[$Co^{II}(L^{Qpy})H_2O$]ClO_4** for 18 hours.

Post–catalytic analysis is often performed on molecular water-splitting catalysts to determine whether the catalyst has retained its molecular identity or it has been transformed to different species. Several techniques are employed for this analysis, including UV-visible spectroscopy, SEM and EDS. For the **[$Co^{II}(L^{Qpy})H_2O$]ClO_4** catalyst**,** UV-visible spectral analysis was performed in neutral water (pH 7.0, 1.0 M phosphate buffer) before and after bulk electrolysis to determine the fate of the catalyst **(Figure 3.13)**.

The post-catalysis spectrum remains practically the same as the spectrum before catalysis with only a slight increase of ~4% in the band around 300 nm and ~2% increase in 450 nm band. A plausible hypothesis for this slight increment in the spectral profile is the possibility of solvent percolation from the catalytic chamber to the auxiliary chamber through the semi-permeable frit.

www.manaraa.com

To further confirm the molecular nature of the **[Co^{II}(L^{Qpy})H$_2$O]ClO$_4$** catalyst by SEM and EDS analyses, we performed BE experiments under identical experimental conditions but using a conductive grafoil sheet as the working electrode instead of the liquid Hg-pool electrode used for catalysis. The scanning electron microscope (SEM) images (**Figure 3.14**) show some formation of particulate species which were then analyzed by EDS to determine their composition.

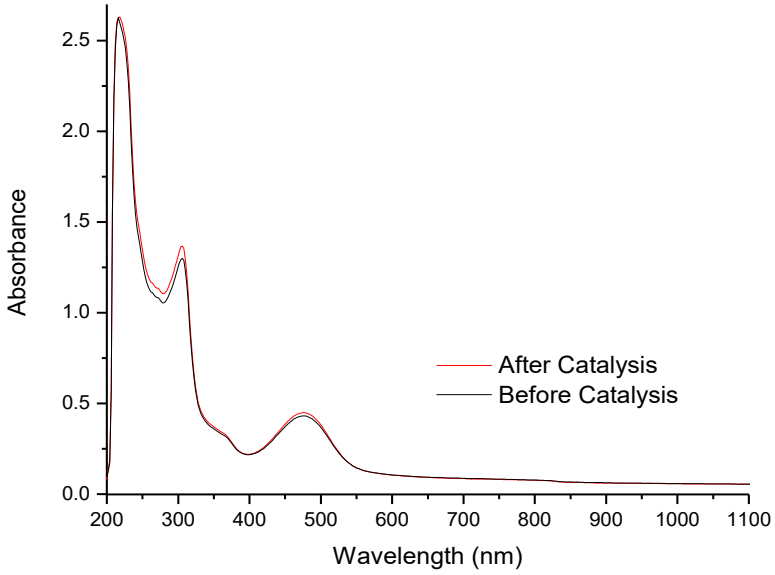

Figure 3.13. Spectral profile of **[Co^{II}(L^{Qpy})H$_2$O]ClO$_4$** before and after bulk electrolysis.

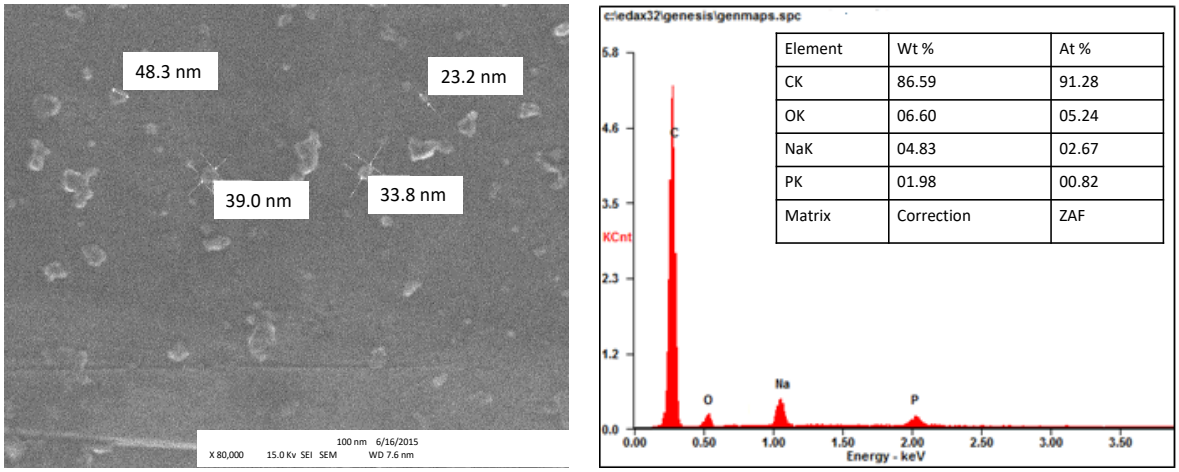

Figure 3.14. Post-catalytic SEM and EDX analysis of grafoil electrode surface.

www.manaraa.com

The (EDS) analysis results indicate that the particulate species were composed of carbon and sodium phosphate, which are likely from the grafoil electrode and the phosphate buffer used for the catalysis. Cobalt nanoparticles were however not detected; thus ruling out catalyst transformation and suggesting the molecular nature of the catalyst.

3.3.5.2. Water Oxidation Electrocatalysis

To assess the capability of **$[Co^{II}(L^{Qpy})H_2O]ClO_4$** to catalyze water oxidation, a CV sweep was performed in borate buffer (0.1 mol•L^{-1}, pH 8.0) using a fluorine-doped tin oxide (FTO) glass working electrode, a Pt wire as the auxiliary electrode and Ag/AgCl as the reference electrode **(Figure 3.15)**. Upon scanning the borate buffer without the catalyst, a current enhancement peak of -0.5 mA was observed starting from 1.8 $V_{Ag/AgCl}$ to 2.0 $V_{Ag/AgCl}$. Upon the addition of the catalyst, two peaks were observed. An oxidation peak is observed at 1.25 $V_{Ag/AgCl}$ and is followed by a catalytic wave for water oxidation.

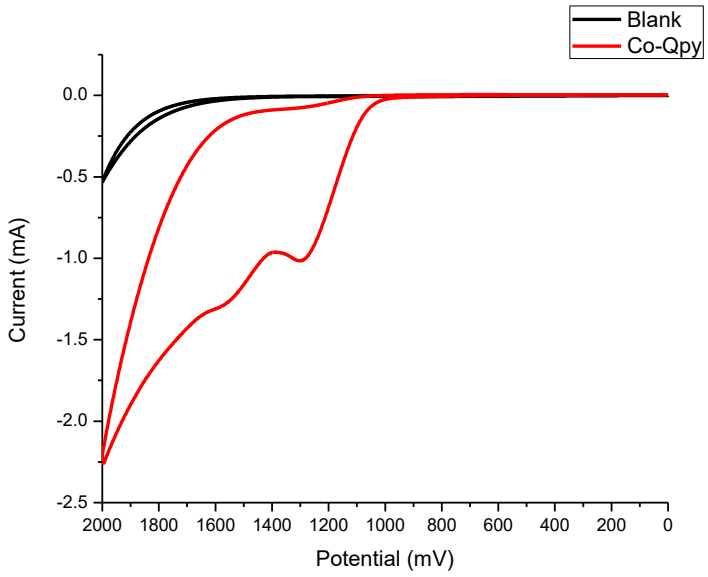

Figure 3.15. Catalytic water oxidation CV of **$[Co^{II}(L^{Qpy})H_2O]ClO_4$** in 0.1 mol•$L^{-1}$ borate buffer at pH 8.

www.manaraa.com

Bulk electrolysis was performed under the same conditions **(Figure 3.16)**, using a 0.2 μ mol•L^{-1} concentration of the catalyst and 1.27 cm^2 FTO as working electrode, with an applied potential of 1.5 $V_{Ag/AgCl}$ for 3 h to quantify the oxidative catalytic product. After 3 h the catalyst gives a linear charge versus time consumption plot of 18 C/h, with no substantial loss in activity, and operates at 91% (F.E.) with a TON of 97. It is important to note that only a few reports exist on the catalytic activity of single-site molecular cobalt-based electrocatalysts for water oxidation,[167-169] and out of those, only a handful try to quantify the amount of oxygen produced during catalysis due to harsh oxidative conditions needed to perform water oxidation.[170-171] The TON of these catalysts range between 0 and 70 turnovers, with faradaic efficiencies ranging from 75% to 95%. Thus the high catalytic activity of this **$[Co^{II}(L^{Qpy})H_2O]ClO_4$** establishes it as one of the very few catalysts with TONs around 100 in 3 hours.

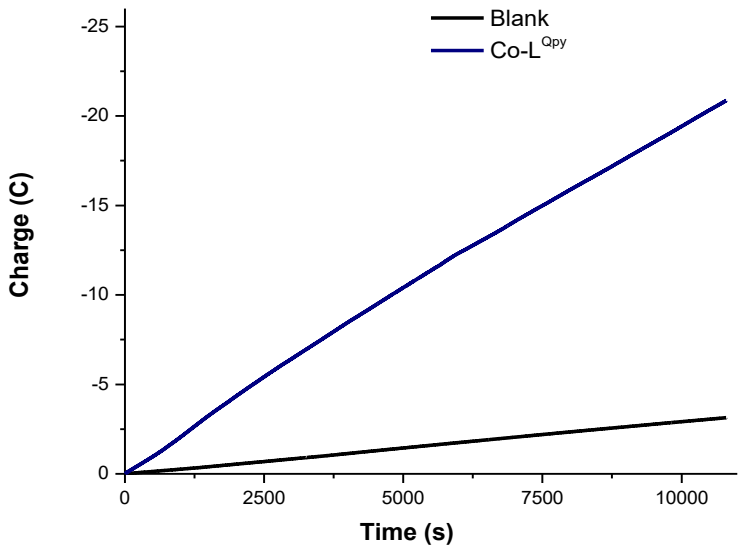

Figure 3.16. Charge versus time plot during bulk electrolysis of **$[Co^{II}(L^{Qpy})H_2O]ClO_4$** in 0.1 mol•$L^{-1}$ borate buffer at pH 8.

www.manaraa.com

A BE experiment was performed again in borate buffer (0.1 mol•L^{-1}, pH 8.0) using an FTO electrode as the working electrode which was analyzed by SEM and EDS techniqes to ascertain whether the catalyst retained its molecular nature of during water oxidation because ligand transformations and catalyst degradation remain a challenge for most water oxidation electrocatlysts reported in the literature.

The SEM analysis results show no evidence of nanoparticles, with EDS analysis indicating only elements that constitute the FTO-glass electrode with no cobalt particles deposited on the electrode **(Figure 3.17)**. This lack of detectable nanoparticles suggests that the catalyst remains molecular during electrocatalysis.

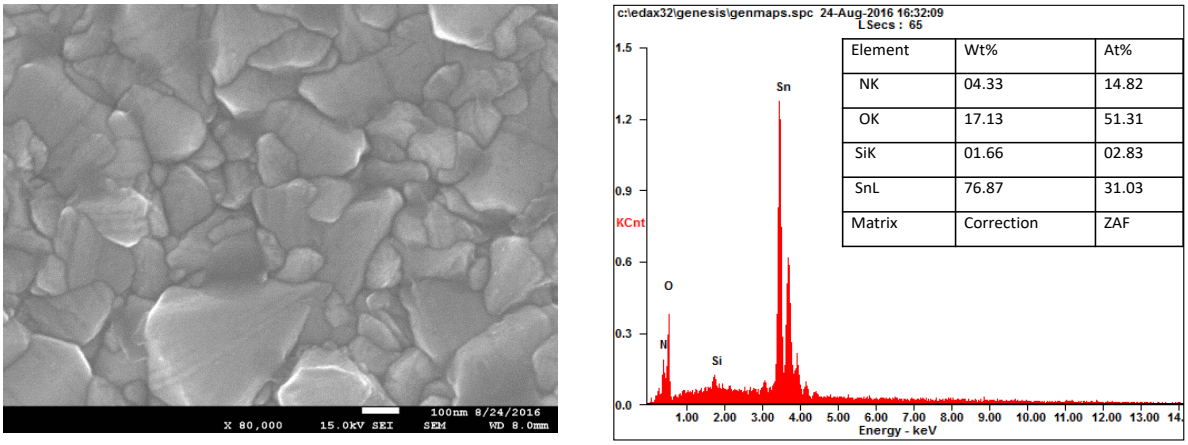

Figure 3.17. Post-catalytic SEM and EDX analysis of FTO electrode surface.

3.3.6 Characterization of Catalytic Oxidative Intermediates

Cobalt-based catalysts are expected to oxidize water to dioxygen in basic media undergoing well-defined PCET steps **(Figure 3.2)** to a tetravalent intermediate which is electrophilic enough to be attacked by a nucleophilic water molecule. The results from the redox behavior, and the electrocatalytic water oxidation of **$[Co^{II}(L^{Qpy})H_2O]ClO_4$**, shows that the $3d^7$ $^{HS}Co^{II}$ parent species complex undergoes a first one-electron oxidation event to yield a $3d^6$ [$^{LS}Co^{III}$-OH] species, and subsequently undergoes a second oxidation event after which a catalytic current

www.manaraa.com

enhancement is observed. According to mechanisms reported by Berlinguette,[21, 81, 172] Nocera,[173] and Thapper,[170] the catalytic-active intermediate required for the crucial O – O bond formation in single-site cobalt catalyst for water oxidation is a $3d^5$ [Co^{IV}=O] species. To determine if the high-valent $3d^5$ [Co^{IV}=O] is involved in the catalytic pathway of the **[$Co^{II}(L^{Qpy})H_2O$]ClO_4** as well, I performed a series of independent one-electron, and 2-electron electrochemical oxidation experiments and used EPR to characterize the intermediate products (**Figure 3.18)**.

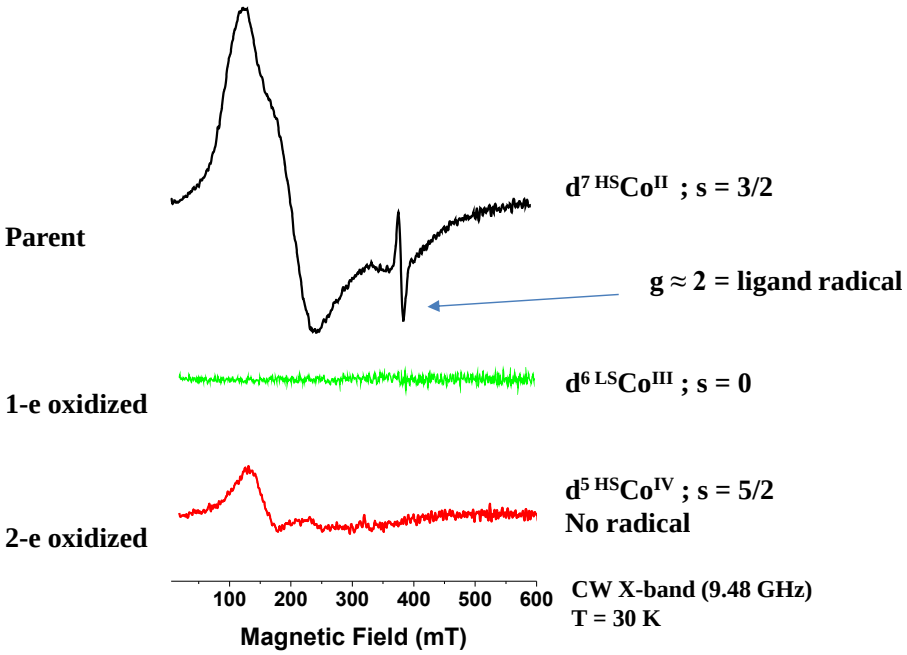

Figure 3.18. EPR spectra of catalytic oxidative **[$Co^{II}(L^{Qpy})H_2O$]ClO_4** intermediates.

The samples for EPR were prepared in CH_3CN under inert conditions and measured at the Argonne National Laboratory for analysis by Drs. Oleg Poluektov and Jens Niklas. The CW X-band (9.48 GHz) EPR analysis were performed at 30 Kelvin. The EPR data shows that, the main EPR signal for the parent complex (black trace) is from a $3d^7$ $^{HS}Co^{II}$ (S = 3/2) species with no sign of $^{LS}Co^{II}$ species. The narrow signal (line width peak-peak around 7 mT) close to g≈2 could be traces of ligand radical character. The one-electron oxidized sample gave no EPR signal suggesting

www.manaraa.com

a closed shell $3d^6$ $^{LS}Co^{III}$ ($S = 0$) diamagnetic species. The 2-electron oxidized sample gives a signal characteristic of a $3d^5$ $^{HS}Co^{IV}$ ($S = 5/2$) species with no radical species visible.

The absence of a radical species suggests the presence of only the $^{HS}Co^{IV}$ species, thereby eliminating the possibility of the intermediate being a radical-bearing "[Co^{III}-L•]" species. These results constitute one of the few reports in the literature[174-175] that track, isolate and characterize experimentally, the oxidative intermediates for catalytic water oxidation.

3.3.7 Mechanism of Catalytic Water Oxidation

Based on the results from the water oxidation bulk electrolysis, the characterization of intermediate catalytic products, and DFT computations, we propose a 'water nucleophilic-attack' (WNA) mechanism of water oxidation for the **$[Co^{II}(L^{Qpy})H_2O]ClO_4$** complex **(Figure 3.19).** We propose that the parent $3d^7$ [$^{HS}Co^{II}$–OH_2] undergoes an oxidative one-electron, proton-coupled electron-transfer (PCET) step to yield $3d^6$ [$^{LS}Co^{III}$–OH] species.

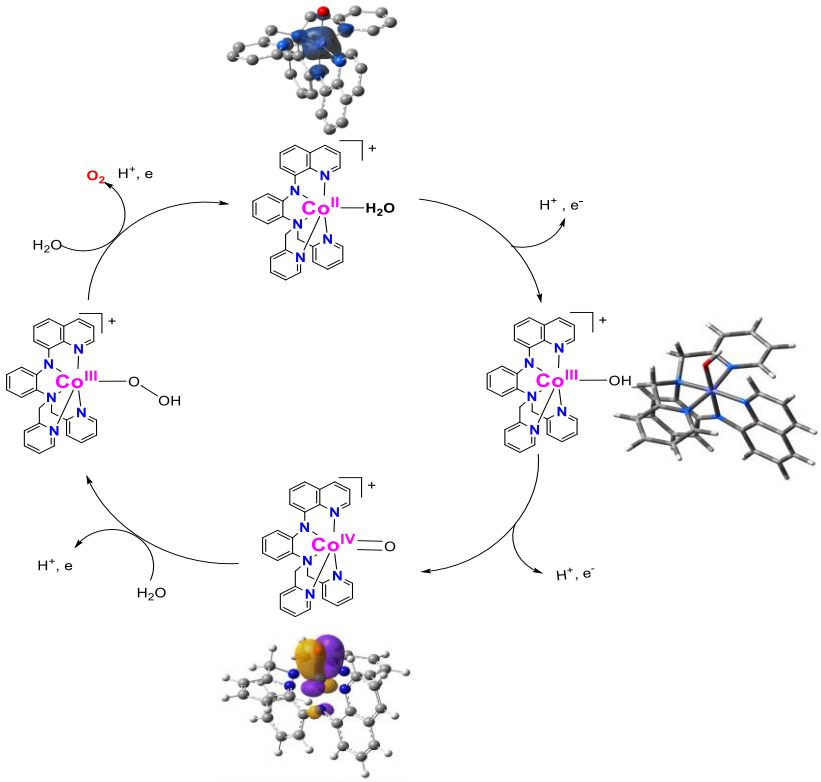

Figure 3.19. Proposed catalytic mechanism of O_2 generation by **$[Co^{II}(L^{Qpy})H_2O]ClO_4$.**

www.manaraa.com

This intermediate further undergoes another one-electron oxidative process to yield the key $3d^5$ [$^{HS}Co^{IV}$=O], which is sufficiently electrophilic and very reactive. This intermediate is then attacked by a water molecule thus forming the essential O – O bond and releasing dioxygen in the process and yields he parent $3d^7$ [$^{HS}Co^{II}$–OH_2] catalyst.

The nucleophilic attack by the water molecule could be made possible by the interaction between the highest-occupied molecular orbital (HOMO) of water (σ symmetry) and (LUMO) of the pseudo-octahedral [$^{HS}Co^{IV}$=O] complex (dπ* character), accompanied by the breaking of the Co–O π bond and thus the two-electron reduction of the cobalt to yield the parent species.[174, 176-178] The non-detection of any radical character in the EPR spectrum of the $3d^5$ [$^{HS}Co^{IV}$=O] suggests that the catalysts does not undergo the oxidative mechanism, radical homo-coupling.

3.3.8 Photocatalytic Studies

To determine if **[$Co^{II}(L^{Qpy})H_2O$]ClO_4** could be an ideal candidate for eventual photocatalysis, preliminary photocatalytic activity was studied in acetate buffer (pH 4), using 1.0 $^{-4}$ of the catalyst, and [Ru(bpy)$_3$] $^{2+}$ (5.0 $^{-4}$ mol•L $^{-1}$) as the photosensitizer (P.S.) in the presence of ascorbic acid (1.1 mol•L $^{-1}$) as the sacrificial electron donor.[179] For an experiment, a series of 15 mL clear cylindrical vials with gas tight screw caps and septa were filled with a 10 mL aliquot of 0.1 mol•L $^{-1}$ pH 4 acetate buffer containing the P.S., ascorbic acid, and **[$Co^{II}(L^{Qpy})H_2O$]ClO_4**. The vials and their contents were then degassed with nitrogen. The absence of oxygen was verified by GC prior to light irradiation. The vials were then placed in a water-jacketed beaker with a constant temperature of 20 °C.[153] The contents of the vials were irradiated by an 18 module blue LED strip (λ_{max} = 460 nm) wrapped around the beaker and connected to a 12 V power controller.[180]

The headspace gas was analyzed in triplicate over in 30 m, intervals over 6 h by a GOW-MAC GC with a thermal conductivity detector (TCD) to determine the amount of hydrogen

www.manaraa.com

produced over time using nitrogen gas as the carrier gas at a flow rate of 30 mL min^{-1} **(Figure 3.20).** The amount of H_2 produced was calculated using a calibration curve of moles of hydrogen versus peak area. A TON of 294.40 was achieved with TOF of 50.00/h. Even though the preliminary TON is modest, it is comparable to those reported by Wang,[181] and Blackman,[179] using identical experimental conditions for the same period of time. A blank experiment was conducted under the same conditions without the catalyst as control and the negligible hydrogen produced was duly subtracted before calculating the TON.

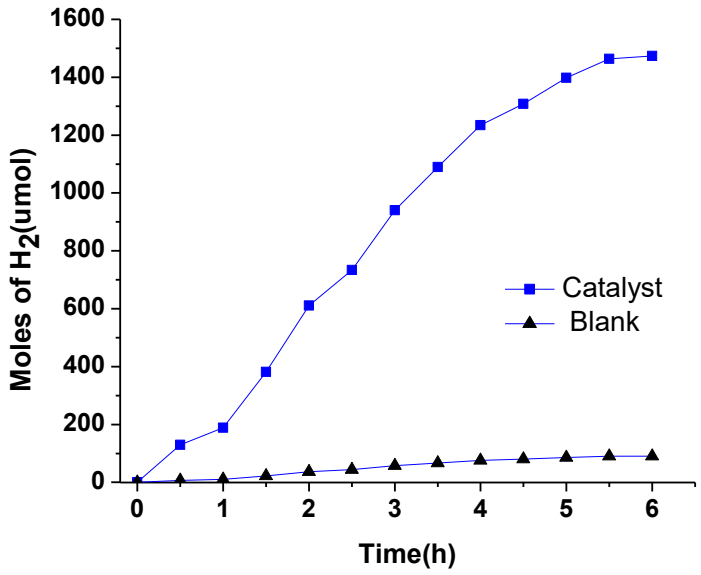

Figure 3.20. Plot of amount of H_2 produced over time during photocatalysis by **$[Co^{II}(L^{Qpy})H_2O]ClO_4$**.

To test whether the catalyst remains molecular during the photocatalytic experiment, a mercury-poison test was conducted on the samples to ensure that cobalt oxides or nanoparticles are not responsible for the photocatalytic activity **(Figure 3.21)**.[179, 182-183] Mercury was added to each sample after which the experiment was conducted under the same conditions. At the end of

www.manaraa.com

the catalysis, the catalytic efficiency remained unchanged suggesting that the catalyst did not transform to cobalt oxides nor nanoparticles during the catalysis.

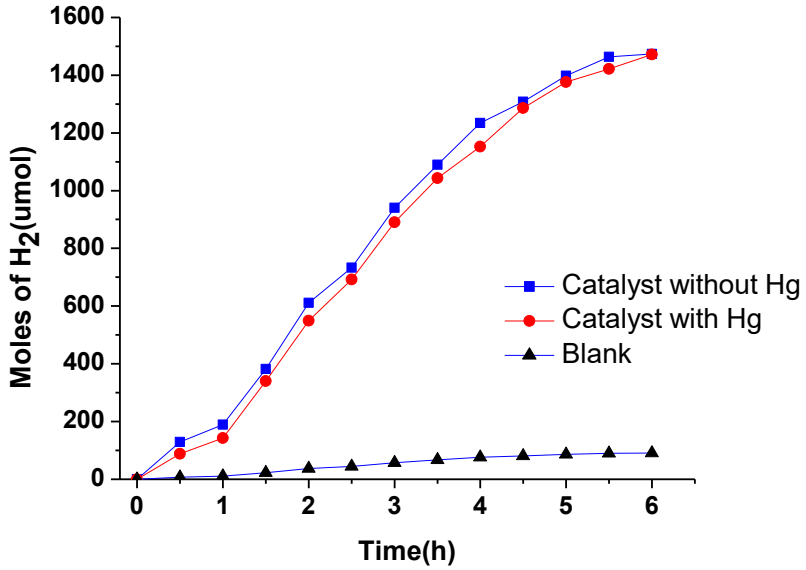

Figure 3.21. Plot of amount of H_2 produced by **[Co^{II}(L^{Qpy})H$_2$O]ClO$_4$** in the presence of Hg and without Hg over time.

3.4 Conclusions

In conclusion, I investigated an asymmetric, pentadentate quinolyl-bispyridine ligand **L^{Qpy}** with a phenylenediamine backbone and its water-soluble Co(II) complex **[Co^{II}(L^{Qpy})H$_2$O]ClO$_4$** that has been synthesized and characterized. This complex is active as an electrocatalyst as well as a photocatalyst. **[Co^{II}(L^{Qpy})H$_2$O]ClO$_4$** is catalytic towards H_2O reduction at a low overpotential of 0.63 V, giving a TON of 2900 with a Faradaic efficiency of 98%. An 18 h catalytic TON of 12,100 suggests a highly robust and stable catalyst. **[Co^{II}(L^{Qpy})H$_2$O]ClO$_4$** serves as a robust water oxidation catalyst as well, with a TON of 97 at 91% FE. By using a series of experimental and DFT techniques, I was able to isolate and characterize the catalytic oxidative intermediates for **[Co^{II}(L^{Qpy})H$_2$O]ClO$_4$**, and proposed a 'water nucleophilic-attack' (WNA) mechanism of water oxidation, where the highly electrophilic $3d^5$ [^{HS}Co^{IV}=O] intermediate is attacked by a nucleophilic

www.manaraa.com

water molecule thus forming an O-O bond and releasing dioxygen. Finally, the photocatalytic activity of **$[Co^{II}(L^{Qpy})H_2O]ClO_4$** in the presence of $[Ru(bpy)_3]^{2+}$, and ascorbic acid in an acetate buffer (pH 4) gave a TON of 295 with a TOF of 50/h.

www.manaraa.com

CHAPTER 4

ELECTRONIC COMMUNICATION AND COOPERATIVITY IN A DICOBALT COMPLEX FOR PROTON REDUCTION

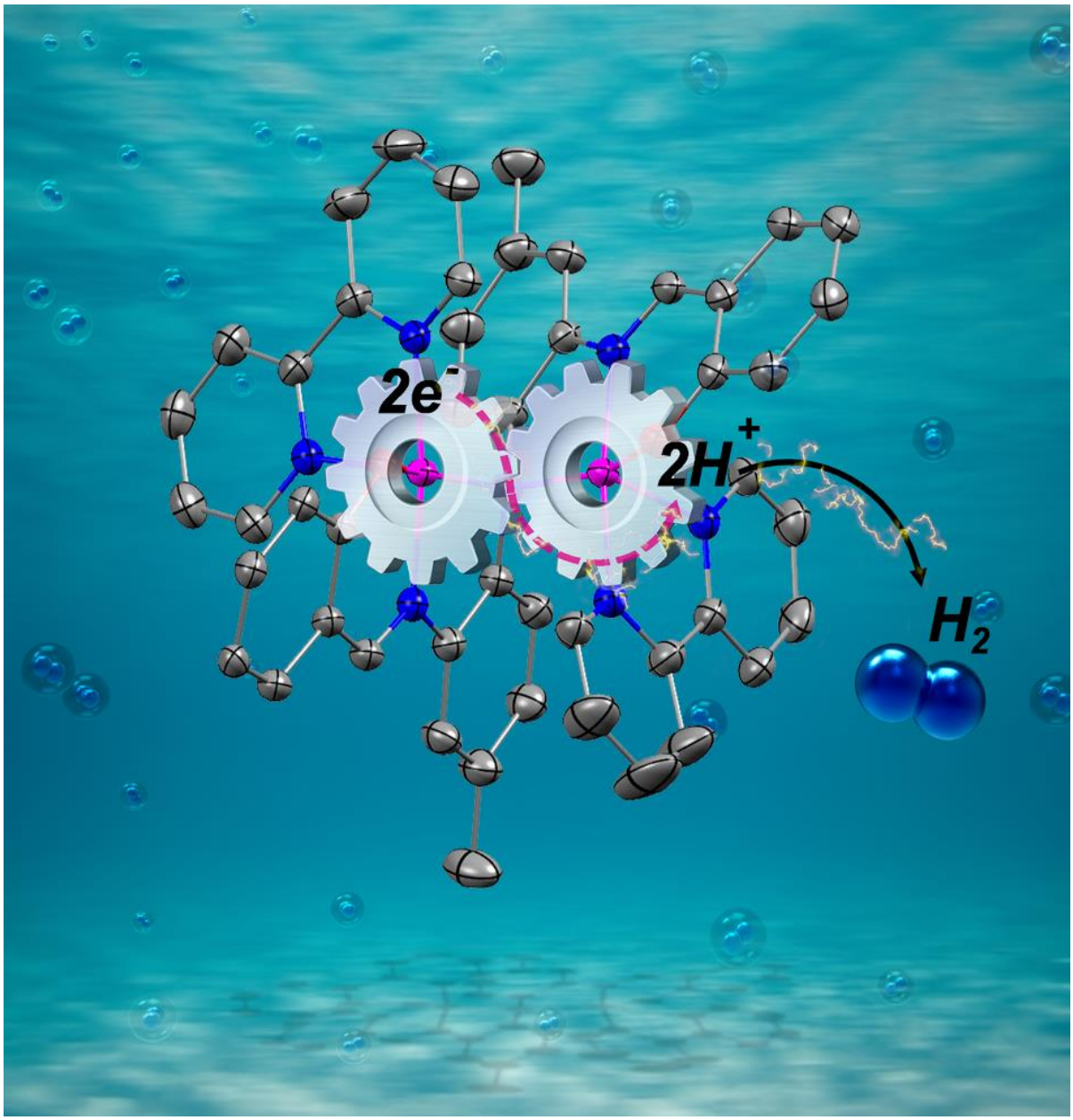

www.manaraa.com

CHAPTER 4: ELECTRONIC COMMUNICATION AND COOPERATIVITY IN A DICOBALT COMPLEX FOR PROTON REDUCTION

Portions of the text in this chapter were reprinted or adapted with permission from:

Kpogo, K. K.; Mazumder, S.; Wang, D.; Schlegel, H. B.; Fiedler, A. T.; Verani, C. N.; *Chemistry-A European Journal* ***2017,*** *23,* 9272. All rights to the work are retained by the authors and any reuse requires permission of the authors.

4.1. Introduction

The widespread dependence of our society on fossil fuels and the impending depletion of carbon-based reserves have triggered the search for renewable and clean H-based energy.[184,1] Earth-abundant transition metals like cobalt, nickel, and iron have attracted attention due to their ability to generate H_2.[129,17,59,180] Among these metals, cobalt is particularly relevant because of its affordable redox potentials between the $3d^6$ Co^{III}, $3d^7$ Co^{II} and $3d^8$ Co^{I} states. The catalytically active monovalent species can be stabilized and yield the doubly-oxidized cobalt/hydride intermediate Co^{III}–H^-, which is pivotal for H^+ reduction to H_2 after reduction to more reactive Co^{II}–H^-.[14,131,46,132,133] Known cobalt catalysts follow either a heterolytic or a homolytic pathway.[46,16,47] The former mechanism relies on a single Co^{III}–H^- or a Co^{II}–H^- [51,185] reacting with another H^+ and is favored when the concentration of protons is not limiting. The latter involves the collision of two Co^{III}–H^- moieties from independent molecules.[48]

Enhanced activity is expected from some binuclear analogs of monometallic catalysts in which close proximity between two cobalt centers triggers cooperativity either by facilitating homolytic pathways[74] or by enabling electron transfer between the metal centers, thus avoiding the formation of a Co^{III}–H^- species.

www.manaraa.com

Cooperative effects have been proposed by Dinolfo *et al.* [77] for a binuclear Co^{II} catalyst in a bicompartmental Robson/Okawa-type [N_6O_2] macrocycle[186-187] with a Co-Co distance of 3.22 Å, while Gray *et al.* [75,188] evaluated oxime-based Co^{III} catalysts with both flexible hydrocarbon and rigid BO_4 bridges that revealed no significant catalytic enhancement. Similarly, the lack of cooperativity observed in dicobalt complexes featuring pyrazolato bridges[48,189] was attributed either to the large distance of 3.95 Å between the Co centers or to the flexibility of the ligand. To date, it is unclear what factors control metal cooperativity in proton reduction and this lack of understanding prevents a more rational design of Co_2 catalysts.

The Verani group has a long-standing interest in the mechanisms of H_2 generation by Co catalysts,[115,73,190,54] and continuing with that research focus, we collaborated with the Fiedler group from the University of Marquette who previously published the **$[Co^{II}_2(L^{1'})(bpy)_2]ClO_4$** complex **(Figure 4.1).** We hypothesized that cooperativity will be dependent on (i) the distance between the Co centers, (ii) the relative topology of the coordination environments, and (iii) the degree of orientation and overlap between redox-active orbitals. To evaluate this hypothesis, we analyzed the catalytic potential of the bimetallic complex **$[Co^{II}_2(L^{1'})(bpy)_2]ClO_4$**,[191] where $(L^{1'})^{3-}$ is the triply deprotonated ligand shown in **Figure 4.1**, by means of electrochemical, spectroscopic, and computational methods.

The complex **$[Co^{II}_2(L^{1'})(bpy)_2]ClO_4$** is a unique bimetallic species singularly suited for this study because of the short distance between the two vicinal Co centers along with the presence of a Co-$N_{arylamido}$-Co unit that may foster the proper orientation of Co orbitals involved in catalysis. Our results indicate that the two cobalt centers of $[Co^{II}_2(L^1)(bpy)_2]ClO_4$ function cooperatively in the electrocatalytic reduction of H^+, thus offering a viable mechanistic alternative to homolytic and heterolytic pathways employed by mononuclear cobalt catalysts.

www.manaraa.com

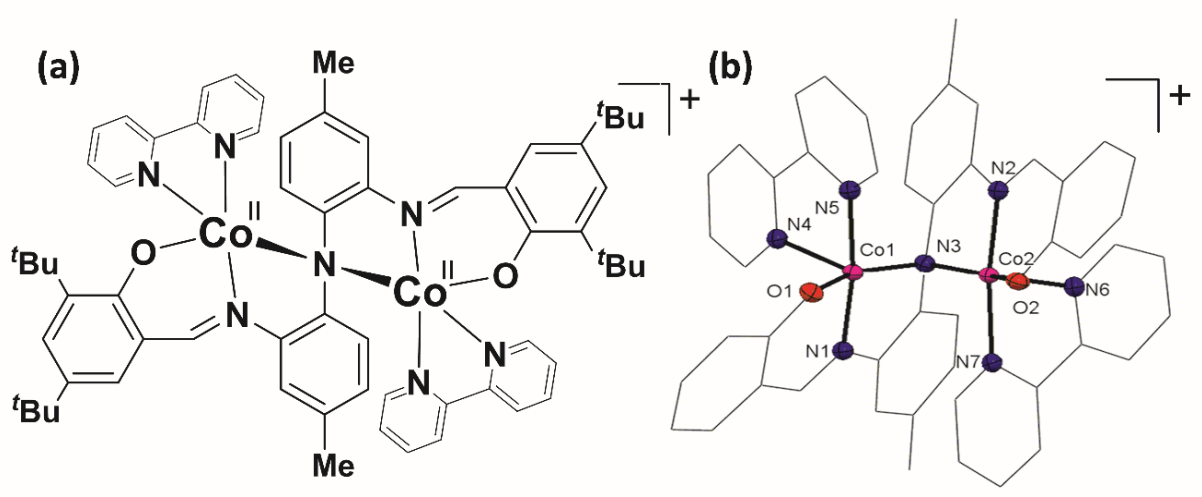

Figure 4.1. The complex **$[Co^{II}_2(L^{1'})(bpy)_2]ClO_4$ (1)**: (a) Drawing and (b) ORTEP of the core showing a Co1-N3-Co2 angle of 86.9° expected to facilitate cooperativity.

4.2 Experimental

4.2.1 Materials and Methods

All reagents were used without further purification as purchased from commercial sources. **$[Co^{II}_2(L^{1'})(bpy)_2]ClO_4$** was obtained by dissolving the ligand H_3L^1 (0.066 g, 0.10 mmol), 2,2'-bipyridine (bpy, 0.032 g, 0.20 mmol), and $Co(ClO_4)_2 \cdot 6H_2O$ (0.073 g, 0.20 mmol) in a 1:1 mixture of CH_3CN and CH_2Cl_2 (10 mL). A detailed synthetic protocol and characterizations have been described recently.[191] ^1H NMR spectra were measured using a Varian 400 MHz instrument. Elemental analyses were performed by Midwest Microlab (Indianapolis, Indiana) in an Exeter-CE440 CHN analyzer. UV-visible spectra of 1.0×10^{-4} M and 1.0×10^{-5} M CH_2Cl_2 solutions were measured using a Shimadzu 3600 spectrophotometer in the range 190-1600 nm.

4.2.2 Redox Studies

The electrochemical behavior of **$[Co^{II}_2(L^{1'})(bpy)_2]ClO_4$** was investigated with a BASi 50W potentiostat/galvanostat. Cyclic voltammograms (CV) were obtained at room temperature in CH_3CN containing 0.1 M of tetrabutylammonium hexafluorophosphate ($TBAPF_6$) as the

www.manaraa.com

supporting electrolyte under argon atmosphere. The electrochemical cell employed three electrodes: glassy-carbon (working), platinum wire (auxiliary) and Ag/AgCl (reference). The ferrocene/ferrocenium (Fc/Fc^+) redox couple (E^o = 401 mV_{NHE}) was used as internal standard.

Bulk electrolysis (BE) was performed in a custom-made air-tight H-type cell under inert conditions according to the procedure reported by Basu *et al.*[73] The cell was comprised of two compartments separated by a frit. On one side of the frit was placed the Hg-pool working and Ag/AgCl reference electrodes, while a coiled 12-inch Pt wire serving as the auxiliary electrode was placed in the other compartment. BE experiments were performed in acetonitrile (20 mL) with $TBAPF_6$ as the supporting electrolyte until the calculated final charges were reached. All potentials were measured vs. Ag/AgCl. During BE, potentials were controlled with a BASi 50W potentiometer and UV-visible spectra were collected on a Shimadzu UV-3600 UV-visible-NIR spectrophotometer at room temperature.

4.2.3 Computational Studies

Electronic structure calculations were carried out by Dr. Shivnath Mazumder, using the BPW91 density functional[124,192] as implemented in a development version of Gaussian.[123] The SDD basis set and effective core potential[128] were used for Co atom and the 6-31G(d,p) basis set[126,127] was used for the other atoms. To streamline calculations, a slightly modified model was used where the *tert*-butyl substituents of $[Co^{II}_2(L^1)(bpy)_2]ClO_4$ were replaced by methyl groups. Geometry optimization was performed in the gas phase and all of the optimized structures were confirmed as minima by harmonic vibrational frequency calculations. The energies of the optimized structures were reevaluated by additional single point calculations on each optimized geometry in acetonitrile using the implicit SMD solvation model.[193] The converged wave functions in solvent were tested for SCF stability. The free energy in solution phase G(sol) was calculated

www.manaraa.com

as follows: G(sol) = E_{SCF}(sol) + [zero-point energy(ZPE) + thermal correction – TS] (gas). E_{SCF} was calculated in the solvent while ZPE, thermal correction, and entropic contributions were calculated in the gas phase. The standard states of 1 M concentration were considered for all the reactants and products for calculating the free energies of reactions (ΔG(sol)). The spin density plots (isovalue = 0.004 au) and corresponding orbitals[194] (isovalue = 0.05 au) of the calculated structures were visualized using GaussView.[195] The literature value[196] of -264.6 kcal/mol was used for the free energy of proton in acetonitrile. The calculation of the reduction potentials (*E*, V in volts) of the complexes included ZPE, thermal correction, and entropic contribution. The standard thermodynamic equation ΔG(sol) = -nFE was used. The calculated potentials were referenced to a value of $E_{1/2}$ = 4.38 V for the ferrocene/ferrocenium couple calculated under our level of theory.

4.2.4 Catalytic Studies

Electrocatalytic experiments to determine the amount of H produced by the catalyst, turnover numbers, and Faradaic efficiencies was performed as previously described[73] in an H-type cell (Hg-pool; Ag/AgCl | Pt-coil). The main chamber was filled with $[Co^{II}_2(L^1)(bpy)_2]ClO_4$ (0.005 g; $4x10^{-6}$ moles), the $TBAPF_6$ electrolyte (1.56 g) and acetic acid (0.024 g; $4x10^{-4}$ moles; 100 equiv) were dissolved in 20 mL CH_3CN. The small chamber housing the auxiliary electrode was filled with 0.390 g $TBAPF_6$ in 5 mL ACN. In a typical run, the cell is purged for 20 minutes followed by sampling the head space gas with a Gow-Mac 400 gas chromatograph equipped with a thermal conductivity detector, and a 8 ft. x 1⁄8 in., 5 Å molecular sieve column operating at a temperature of 60 °C. The amount of H_2 produced is determined *via* GC with a calibration curve obtained with known volumes of 99.999+ %H_2 gas. (**Figure 4.2 and Table 4.1**). A catalyst-free solution is electrolyzed for 3 h and analyzed by GC as a blank. The cell is then purged again and

www.manaraa.com

the catalyst is added. Electrolysis ensues for 3 h and the headspace is analyzed by GC to determine the H_2 gas produced.

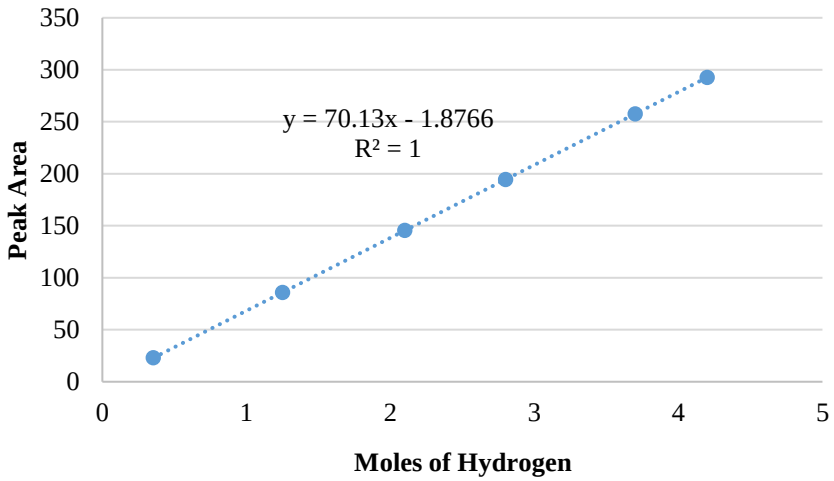

Figure 4.2. Calibration curve used for the determination of the amount of hydrogen.

The turnover number is then calculated after background subtraction as the ratio between moles of dihydrogen produced per mole of catalyst. Faradaic efficiency is calculated from the GC measurements.

Table 4.1. Sample Calculations:

Blank Peak Area	Catalyst Peak Area	Volume of the Cell (mL)	Volume of Solution (mL)	Volume injected into GC (µL)	Number of moles of catalyst (µmol)
8.0	34.7	46.2	27.4	100	4

$V_{headspace}$ = 46.2 - 27.4 = 18.8 mL

Number of moles of hydrogen in 100 µL of headspace for both blank ($n_{blank\ (100)}$) and catalyst ($n_{catalyst\ (100)}$):

$n_{blank\ (100)}$ (8.00 + 1.88)/70.13 = 0.14 µmol

$n_{catalyst\ (100)}$ (34.68 + 1.88)/ 70.13 = 0.52 µmol

www.manaraa.com

The net amount of hydrogen produced by the catalyst in 100 µL of headspace $n_{net\ (100)}$, is equal to the difference between $n_{blank\ (100)}$ and $n_{catalyst\ (100)}$

$n_{net\ (100)} = n_{catalyst\ (100)} - n_{blank\ (100)} = 0.52 - 0.14 = 0.38$ µmol

The total net amount of hydrogen that was produced $n_{net\ (total)}$ is obtained by adjusting the injection volume to that of the total headspace volume

$$n_{net\ (total)} = \frac{n_{net\ (100)} \times V_{headspace}}{V_{injected}} = 71.56\ \mu mol$$

$$TON = \frac{n_{net\ (total)}}{n_{catalyst}} = 71.56/4 = 17.89$$

4.3 Results and Discussion

4.3.1 Synthesis and Characterization

The bimetallic **$[Co^{II}_2(L^{1'})(bpy)_2]ClO_4$** was prepared by treatment of 1 equiv of H_3L^1 with 2 equiv of $Co(ClO_4)_2 \cdot 6H_2O$ and pyridine in presence of Et_3N as the base. A detailed description of the synthesis of **$[Co^{II}_2(L^{1'})(bpy)_2]ClO_4$**, along with its thorough characterization and molecular structure, was recently reported by the Fiedler group.[191] **Figure 4.3** shows that the $(L^1)^{3-}$ ligand loses two phenolic and one amidic protons to support a dicobalt(II) core in which the metal centers lie at a short distance of 2.70 Å from each other, and bridged by the N3 atom of a diaryl amido unit with a Co1-N3-Co2 angle of 86.9°. Each of the five-coordinate Co^{II} centers is bonded to the N atom of an azomethine (N1 or N2) and the O atom of a phenolate (O1 or O2), with a bidentate bipyridine (bpy) completing the coordination sphere. This mono-cationic unit is neutralized by a single ClO_4^- counterion.

The low-spin (S = 1/2) nature of both Co^{II} centers is indicated by relatively short metal–ligand bond distances, ranging between 1.89 and 2.06 Å (the average Co–N/O bond length is 1.95 Å). The Co(II) centers are antiferromagnetically coupled, which was discovered by the sharpness of the ^1H NMR features.[191] The UV-visible spectrum of **$[Co^{II}_2(L^{1'})(bpy)_2]ClO_4$** was recorded in acetonitrile (**Figure 4.4**). The catalyst presents a yellowish brown color due to the presence of

www.manaraa.com

tense intraligand charge transfers. The initial spectrum shows bands below 320 nm tentatively attributed to σ* ← σ and π* ← σ ILCT processes, while the shoulders around 343 and 452 nm are attributed to low-intensity π–π* transitions typical of distorted environments.[191]

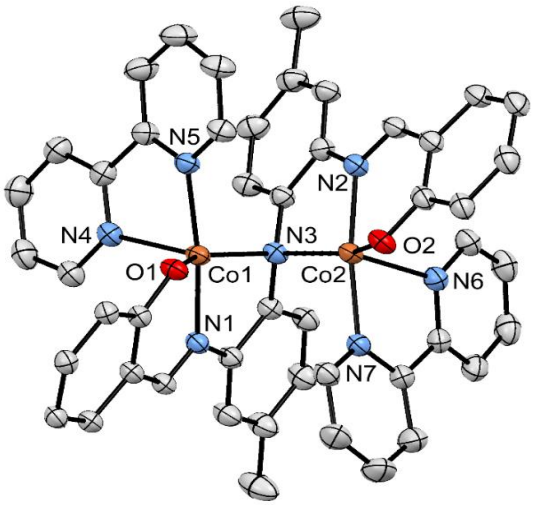

Figure 4.3. ORTEP of the complex **[$Co^{II}_2(L^{1'})(bpy)_2$]ClO_4** with ellipsoids at 30% probability. Hydrogen atoms and *tert*-butyl groups removed for clarity. Used with permission from reference 28.

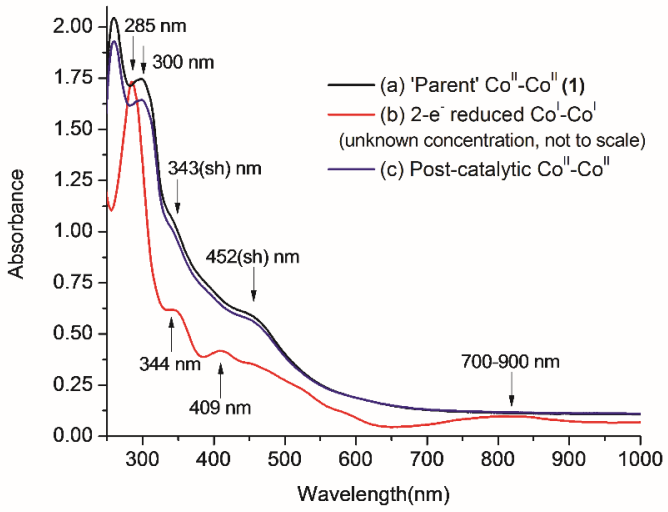

Figure 4.4. UV-visible spectra of **[$Co^{II}_2(L^{1'})(bpy)_2$]ClO_4**: (a) Pre-catalytic [$Co^{II}Co^{II}$] at 1x10^{-3} M, (b) chemically reduced [$Co^{I}Co^{I}$], unknown concentration, (c) Post-catalysis.

www.manaraa.com

4.3.2 Electrocatalytic H^+ Reduction

To study the possibility of **$[Co^{II}_2(L^{1'})(bpy)_2]ClO_4$** as a catalyst for the reduction of H^+ to H_2, we investigated the electrochemical response of **$[Co^{II}_2(L^{1'})(bpy)_2]ClO_4$** in anhydrous acetonitrile (CH_3CN) using a glassy carbon working electrode with increasing concentrations of acetic acid (HOAc, pK_a = 22.3 in CH_3CN) as the proton source.[24]

The standard reduction potential of H^+ in CH_3CN, $E^{\circ(H+/H2)}$ was determined via open circuit potential measurements as -0.028 ± 0.008 $V_{Fc+/Fc}$. [49] Under standard conditions, $E^{\circ(AH/A-;H2)}$ would be -1.35 $V_{Fc+/Fc}$ for HOAc; however, high concentrations can afford homoconjugation, leading to an incremental acidity and increasing the standard reduction potential.[197] As shown in **Figure 4.5**, a cyclic voltammogram of **$[Co^{II}_2(L^{1'})(bpy)_2]ClO_4$** shows three cathodic events.

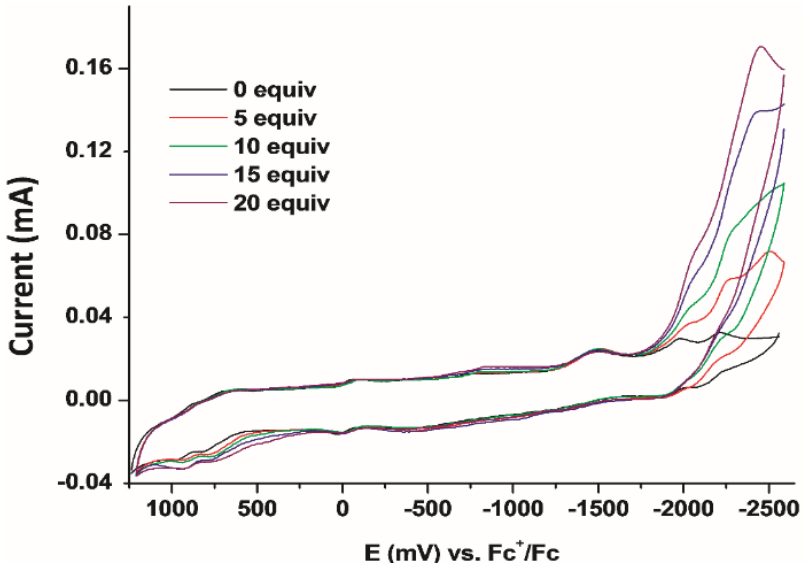

Figure 4.5. Cyclic voltammograms (CVs) of **$[Co^{II}_2(L^{1'})(bpy)_2]ClO_4$** (2.0 mM) measured vs. Ag/AgCl and plotted vs. Fc^+/Fc in the presence of increasing concentrations of HOAc. The CH_3CN solvent contained 0.1 M NBu_4PF_6 as the supporting electrolyte and a glassy carbon working electrode was employed.

Upon addition of HOAc (2.0 mM), an irreversible wave near -1.51 $V_{Fc+/Fc}$ (-0.99 $V_{Ag/AgCl}$) was observed and has been assigned to the reduction of the dicobalt(II) core [$Co^{II}Co^{II}$] to the formal

www.manaraa.com

[$Co^{I}Co^{II}$] state. This [$Co^{I}Co^{II}$] state does not seem able to afford catalysis, which is observed at a potential of −1.86 $V_{Fc+/Fc}$ (–1.34 $V_{Ag/AgCl}$), thus requiring a [$Co^{I}Co^{I}$] state.

Upon increase of the HOAc concentration, this electrocatalytic current enhancement becomes evident and reaches its maximum at −2.08 $V_{Fc+/Fc}$ (–1.56 $V_{Ag/AgCl}$) with the addition of 20 equiv of acid. Control experiments where HOAc is added to CH_3CN in absence of **[$Co^{II}_2(L^{1'})(bpy)_2$]ClO_4** show negligible increase in current, even when more negative potentials are applied. These results validate the catalytic role of **[$Co^{II}_2(L^{1'})(bpy)_2$]ClO_4** and support our hypothesis of homogeneous H^+ reduction using **[$Co^{II}_2(L^{1'})(bpy)_2$]ClO_4** as an electrocatalyst. The experimentally determined redox events were further studied using DFT calculations in model compounds. **[$Co^{II}_2(L^{1'})(bpy)_2$]ClO_4** was modeled with two low-spin Co^{II} centers in agreement with NMR data.[191] Each center contained one unpaired electron and the [$Co^{II}Co^{II}$] core was antiferromagnetically coupled to provide a singlet (S = 0) ground state.[191] For simplicity, the *t*-Bu groups on the phenolates were replaced by methyl groups.[122] The results for relevant species are shown in **Figure 4.6** as calculated spin density plots with Mulliken spin density values.

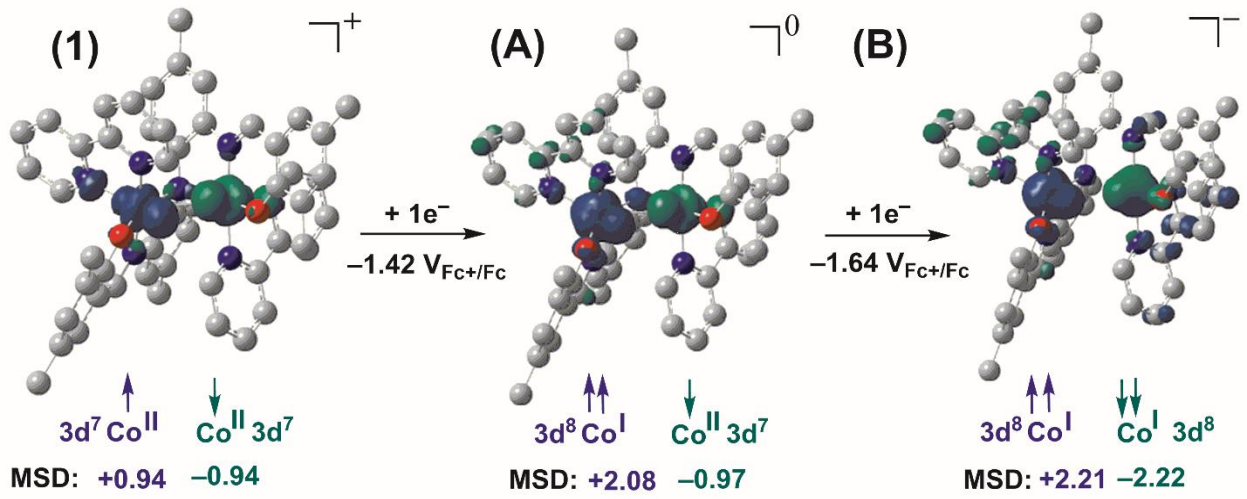

Figure 4.6. DFT-calculated spin density plots (isodensity 0.004 au), reduction potentials, and the Mulliken spin density (MSD) values showing reduction of [$Co^{II}Co^{II}$] **[$Co^{II}_2(L^{1'})(bpy)_2$]ClO_4** to [$Co^{I}Co^{II}$] (**A**) to [$Co^{I}Co^{I}$] (**B**). H atoms are omitted for clarity.

www.manaraa.com

The initial singlet $[Co^{II}Co^{II}]$ $^{LS}3d^7$–$^{LS}3d^7$ core in **$[Co^{II}_2(L^{1'})(bpy)_2]ClO_4$** is reduced to the doublet $[Co^{I}Co^{II}]$ $^{HS}3d^8$–$^{LS}3d^7$ core in **A**. Species **A**, therefore, contains a high-spin $3d^8$ Co^I with two unpaired electrons and can be further reduced to the singlet $[Co^{I}Co^{I}]$ **B** with a $^{HS}3d^8$–$^{HS}3d^8$ core at a calculated potential of –1.64 $V_{Fc+/Fc}$. The presence of the monovalent species **B** was confirmed experimentally via UV-visible spectroscopy by reducing chemically a sample of $[Co^{II}Co^{II}]$ **(1)** with 2 equivalents of KC_8 under inert atmosphere. The resulting spectrum is shown in **Figure 4.4b** and displays bands typical of previously reported Co^I species; based on similarities to the spectrum of the Co^{II}-containing species, the band at 285 nm is attributed to ILCT processes. Bands at 344, 409, and 700-900 nm are comparable to those observed for a Co^I tetraaza-macrocyclic catalyst[183] and associated with d-d bands. In an octahedral Co^I bis(pyridine-2,6-diimine) complex these broad bands were attributed to d-π* CT processes,[198] and several shoulders in the 500-600 nm range were diagnostic of the presence of radical species. Similar shoulders were observed for **B** between 450-650 nm, thus suggesting that ligand reduction may have taken place to some extent.

To ascertain experimentally the overpotential at which **$[Co^{II}_2(L^{1'})(bpy)_2]ClO_4$** shows electrocatalytic activity, a series of 2-minute bulk electrolyses (BE) were run at applied potentials ranging between –0.7 and –1.6 $V_{Ag/AgCl}$ **(Figure 4.7).** The experiment was performed in an airtight H-type cell using a Hg-pool working electrode, Ag/AgCl as reference and a Pt-coil auxiliary electrode placed in an adjacent compartment separated by a frit. The main chamber was filled with **$[Co^{II}_2(L^{1'})(bpy)_2]ClO_4$**, $TBAPF_6$ electrolyte solution and HOAc in 20 mL CH_3CN. The auxiliary chamber was filled with the electrolyte solution only.

www.manaraa.com

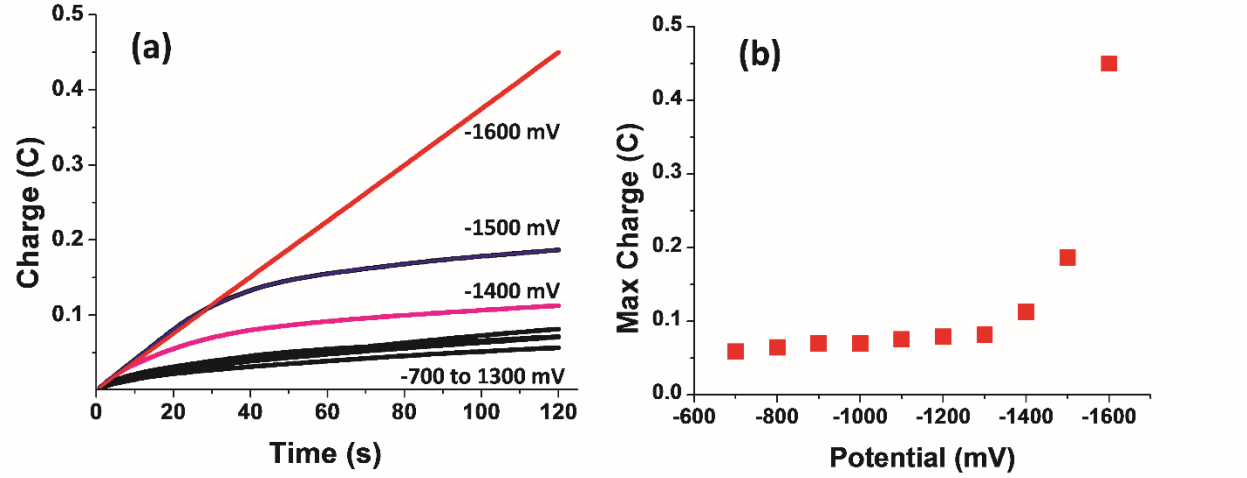

Figure 4.7. (a) Charge consumed at variable potentials (vs. Ag/AgCl) with 2 min. BE; (b) Maximum charge consumed vs. potential (vs. Ag/AgCl).

Figure 4.7a illustrates the total charge consumed by **$[Co^{II}_2(L^{1'})(bpy)_2]ClO_4$** in the presence of acid during BE; charge consumption remained constant up to –1.4 $V_{Ag/AgCl}$, after which it increased significantly until –1.6 $V_{Ag/AgCl}$, concomitant with evolution of H_2 gas, as confirmed by gas chromatography (GC). **Figure 4.7b** shows a plot of charge consumed vs. applied potential. The graph indicates that the onset potential for catalysis is –1.4 $V_{Ag/AgCl}$. This overpotential is comparable to that of the mononuclear cobalt polypyridyl catalyst recently published by the Verani group[73] and investigated under similar conditions that enable comparison. The plot of current vs. concentration of HOAc at a potential of –2.08 $V_{Fc+/Fc}$ is provided in **Figure 4.8**. The measured current increases linearly with concentration of HOAc, whereas negligible current increase was observed in absence of **$[Co^{II}_2(L^{1'})(bpy)_2]ClO_4$**. An apparent overpotential of 0.63 V has been calculated assuming homoconjugation (E_{Fc/Fc^+} AcOH in CH_3CN = -1.23 V), and a rate of H_2 generation[197] (k_{obs}) of 6.33 s^{-1}results.

www.manaraa.com

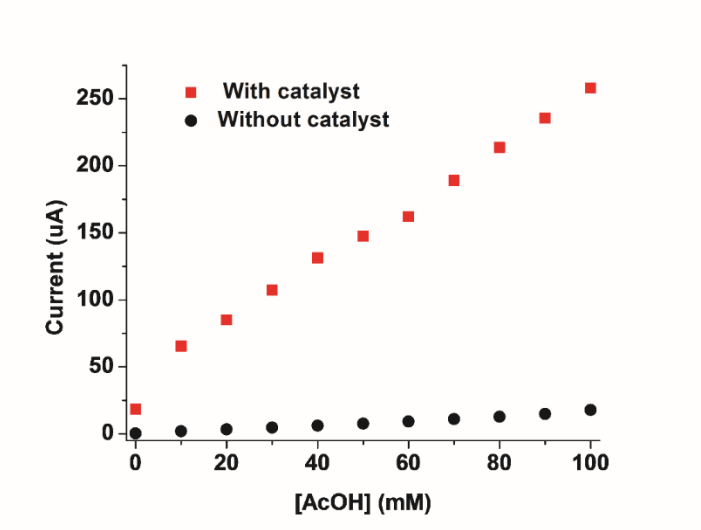

Figure 4.8. *Squares*: CV current at –2.08 $V_{Fc+/Fc}$ as a function of HOAc concentration for solutions of **[$Co^{II}_2(L^{1'})(bpy)_2$]ClO_4** (2.0 mM) in CH_3CN. *Circles*: corresponding data measured under identical conditions but in the absence of **[$Co^{II}_2(L^{1'})(bpy)_2$]ClO_4**.

A charge consumption plot over 3 h is shown in **Figure 4.9.** The slight curvature observed within the first 10 minutes is typical for proton reduction and tentatively associated with solvent dissociation.[190] The amount of H_2 produced over the same period of time was determined by BE as already discussed, using 100 equiv of acid at an applied potential of –1.6 $V_{Ag/AgCl}$.

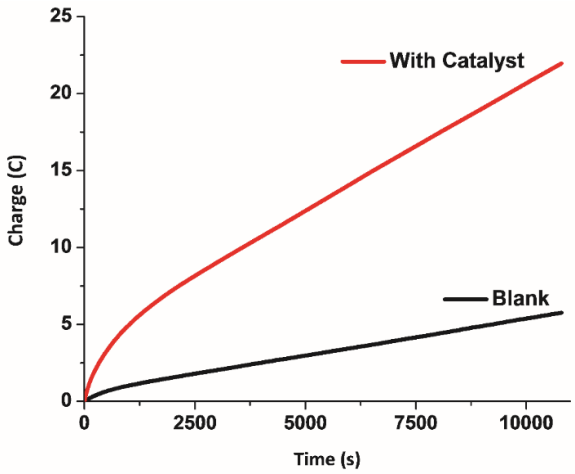

Figure 4.9. Charge consumption versus time during BE by **[$Co^{II}_2(L^{1'})(bpy)_2$]ClO_4** with ($TBAPF_6$: 1.560 g, HOAc: 0.024 g [0.400 mmol], **1:** 0.0047 g [0.0040 mmol], 20 mL CH_3CN) at –1.6 $V_{Ag/AgCl}$.

www.manaraa.com

A sample of 100 μL of the headspace gas was injected into a GC to quantify the amount of H_2 produced and repeated in triplicate. A calibration curve (Figure 4.2) was used to standardize the calculations.

An average amount of 0.072 mmol of H_2 was calculated after background correction which is associated with a turnover number (TON) of 18, equivalent to ca. 40% conversion rate. Faradaic efficiency (FE) was calculated at 94% from the maximum charge consumed. BE experiments were performed under similar conditions as described above using an incremental concentration of acid leading to an increase in the calculated TONs. Accordingly, the use of 200 equiv of acid led to TON of 75, (Figure 4.10) whereas 300 equiv led to TON of 97. In both cases, the Faradaic efficiency remained consistent at > 90%.

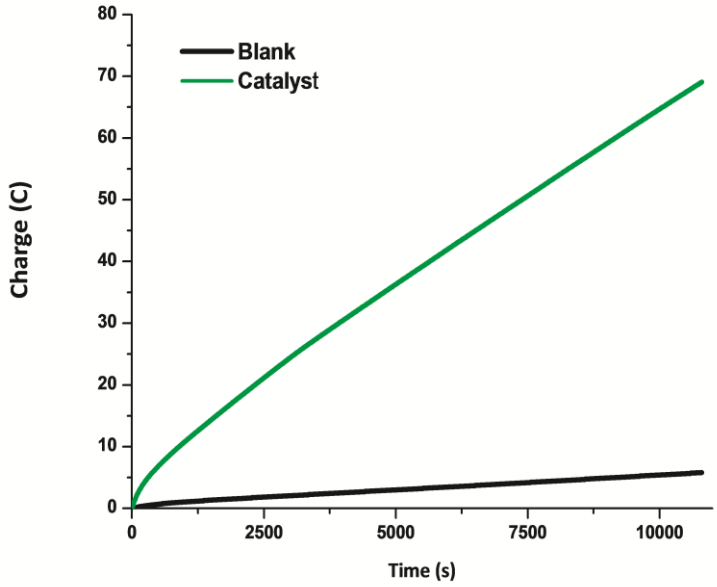

Figure 4.10. Charge consumption versus time by **$[Co^{II}_2(L^{1'})(bpy)_2]ClO_4$** during BE with 200 equivalents of HOAc.

www.manaraa.com

As expected, high yields were observed when the concentration of acid was not a limiting factor, and the use of 400 equiv of acid led to the highest TON of 120 with an associated drop in %FE to *ca.* 85%. The charge vs. time plots for the 300 and 400 equiv experiments are shown in **Figures 4.11 and 4.12**. The initial lagging observed in **Figure 4.9** is almost a linear charge consumption behavior in the 200 and 300 equiv graphs. The plot with 400 equiv shows slightly increased activity after the first 10 minutes followed by a decrease after *ca.* 2.5 h, likely related to slow degradation of the catalyst under such acidic conditions.

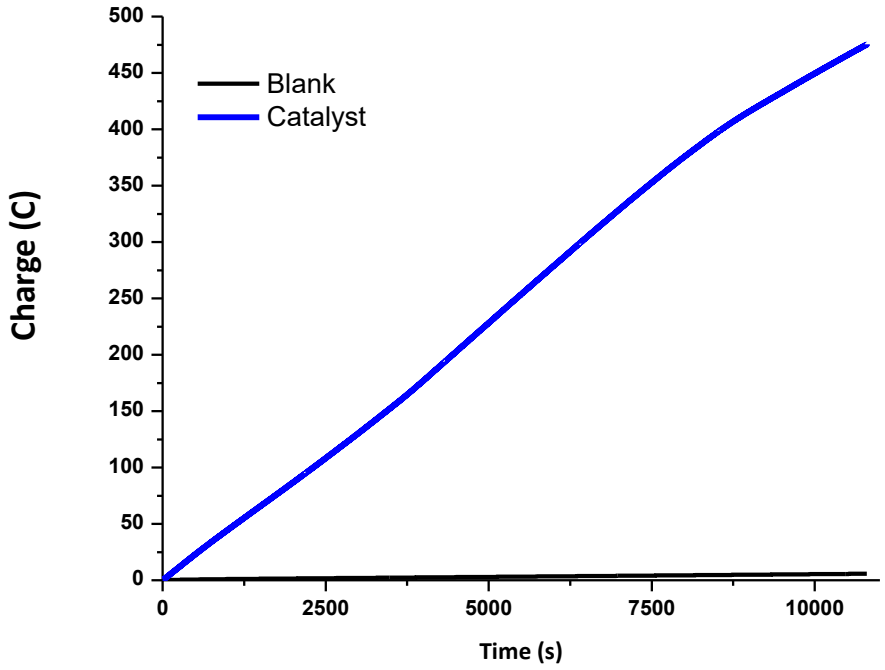

Figure 4.11. Charge consumption versus time by [CoII2(L1')(bpy)2]ClO4 with 300 equivalents of HOAc.

Considering the near-linearity of the graph in **Figure 4.10** the system seems optimized in the presence of 200 equiv of acid. Comparison of activity with other reported bimetallic species [48,77,75,161] is hampered by the lack of information on directly measured TONs by those reports. However, simple assessment of this system (without considering variables such as proton source

www.manaraa.com

and applied potential) reveal that the TON, rate of conversion, and Faradaic efficiency values compare favorably with mono cobalt catalysts. [115,73]

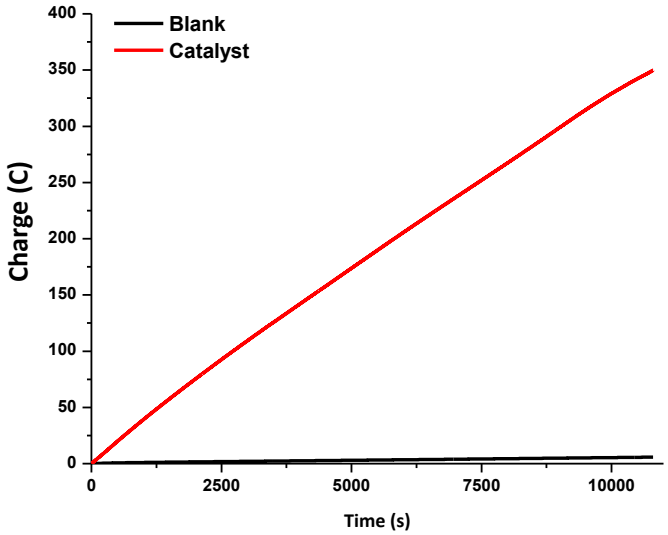

Figure 4.12. Charge consumption versus time by **[$Co^{II}_2(L^{1'})(bpy)_2$]ClO_4** with 400 equivalents of HOAc.

4.3.3 Mechanism of H^+ Reduction

A catalytic mechanism of H^+ reduction (**Figure 4.14)** was proposed based on the results from the redox studies, electrocatalytic studies and the electronic structure calculations carried out using the BPW91 density functional.[124,192] Orbital plots (isovalue = 0.05 au) of the singly occupied molecular orbitals (SOMOs) of complexes **1**, **A**, **B**, and **C** are shown in **Figure 4.13**. Each $^{LS}3d^7$ ion in **[$Co^{II}_2(L^{1'})(bpy)_2$]ClO_4** displays one unpaired electron in the d_{z2}-based singly occupied MO (SOMO) yielding an antiferromagnetically coupled singlet (S = 0). The reduction of **[$Co^{II}_2(L^{1'})(bpy)_2$]ClO_4** generates [$Co^{I}Co^{II}$] (**A**) with a Co^{I} ($^{HS}3d^8$) and a Co^{II} ($^{LS}3d^7$). The Co^{I}-based d_{x2-y2} orbital is now occupied by an electron leading to an overall doublet (S = 1/2) ground state. On further reduction the second Co^{II} center in **A** accepts an electron to its empty d_{x2-y2} orbital and is transformed into a second $^{HS}3d^8$ ion in [$Co^{I}Co^{I}$] (**B**).

www.manaraa.com

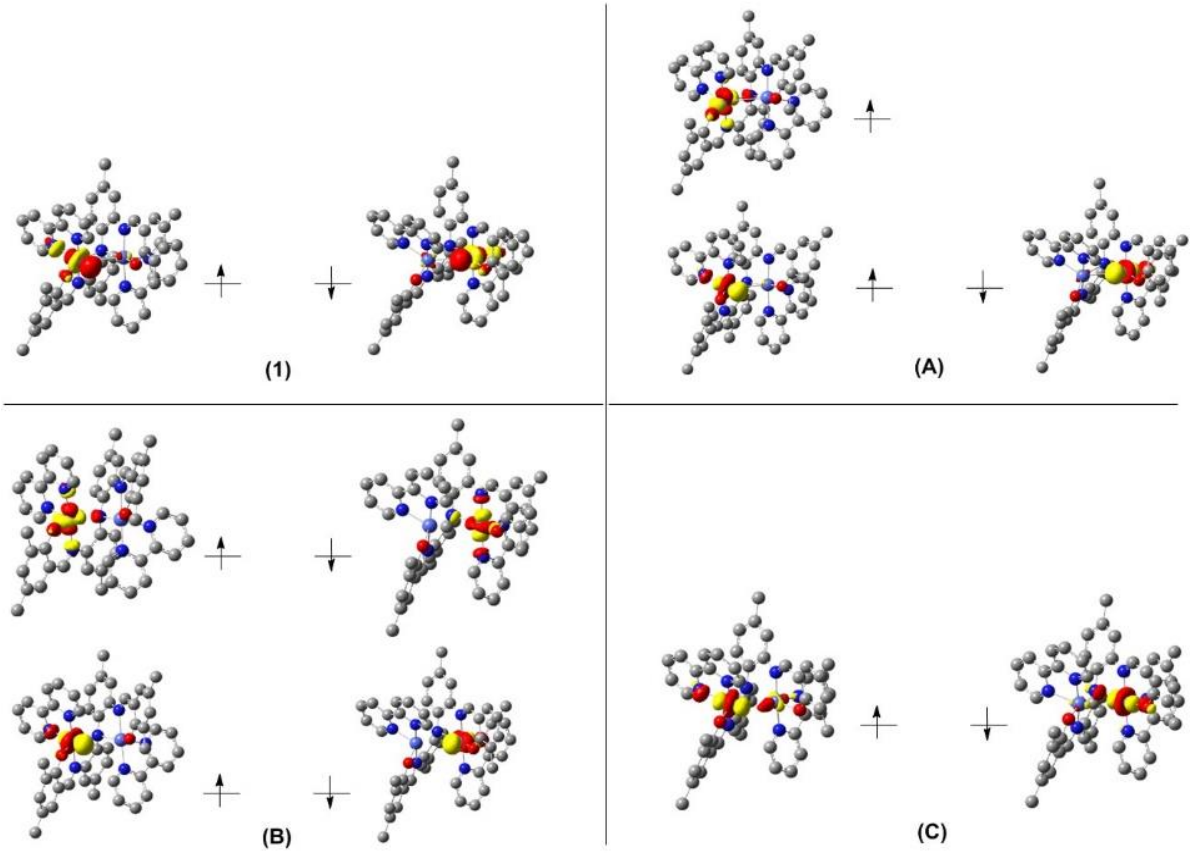

Figure 4.13. The corresponding orbital plots (isovalue= 0.05 au) of the SOMOs (singly occupied molecular orbitals) of **$[Co^{II}_2(L^{1\cdot})(bpy)_2]ClO_4$**, and species **A**, **B**, and **C.**

This is the proposed catalytically active species. The two adjacent d_{x2-y2} SOMOs in **B** do not overlap spatially and therefore are not coupled with each other. As a consequence, each of these electrons can be transferred onto an incoming H^+ to reduce it to a hydride (H^-). As a result, protonation of **B** is favorable by 28 kcal/mol (ΔG). Each of the two $^{HS}Co^{I}$ centers transfers one electron from its d_{x2-y2} SOMO and the resulting complex is described as the species $[Co^{II}Co^{II}(H^-)]$ (**C**). The hydride moiety is bound more tightly to one of the Co^{II} ions, rather than symmetrically bridged between the two centers. The shortest Co^{II}–H^- distance is calculated at 1.54 Å, while the other distance has a computed value of 1.85 Å. It is noteworthy that the cooperativity between both centers in species **B** leads to **C**, $[Co^{II}Co^{II}(H^-)]$, thereby precluding formation of a $[Co^{I}Co^{III}(H^-)]$ intermediate.

www.manaraa.com

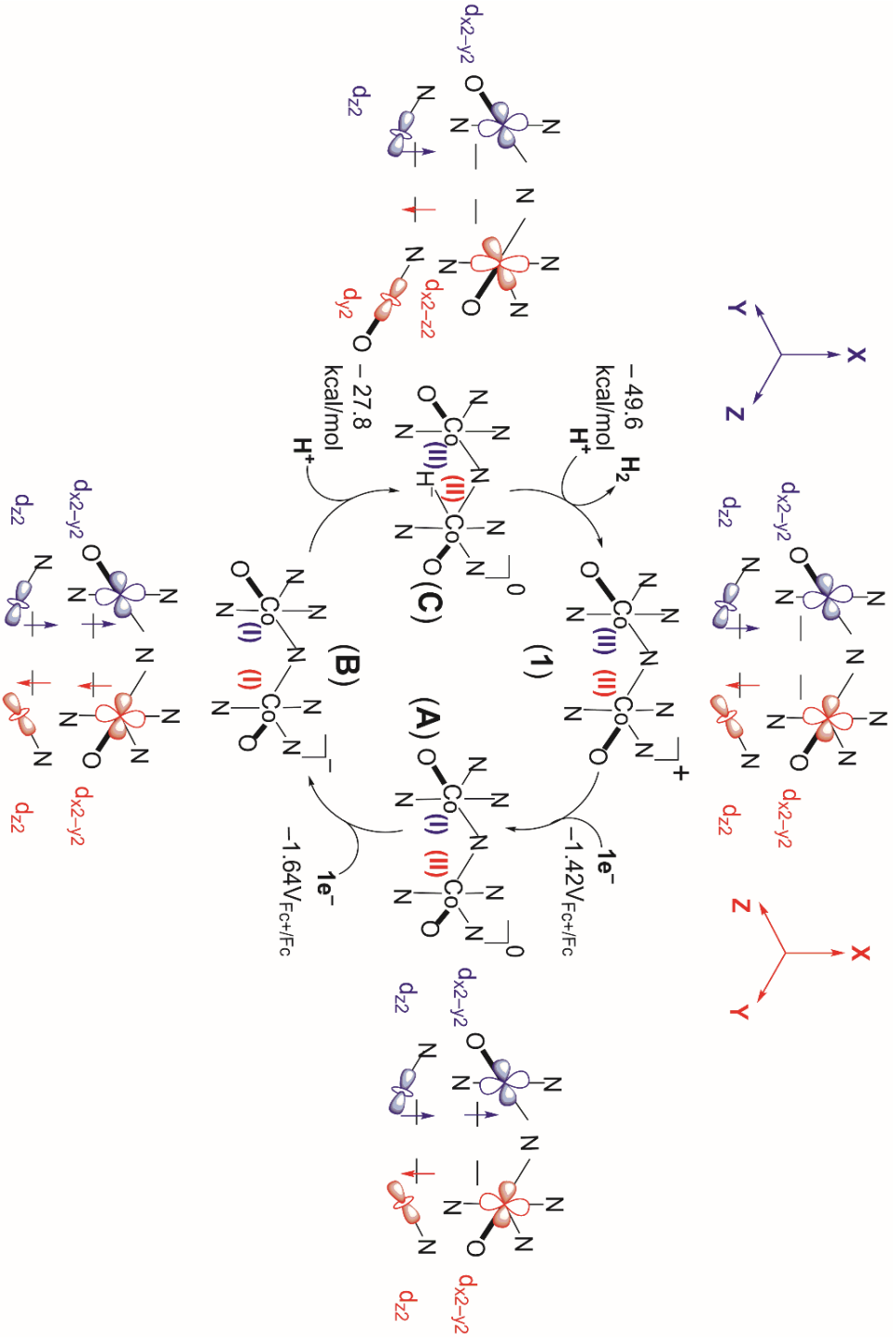

Figure 4.14. Catalytic mechanism of H_2 generation by **$[Co^{II}_2(L^{1'})(bpy)_2]ClO_4$** in CH_3CN. Protonation of the [CoICoI] intermediate B causes each CoI center to donate 1e– to H+, resulting in the formation of the [CoIICoII]-hydride complex C. Free energies (kcal/mol)199 and potentials (volt) calculated at the BPW91/SDD/6-31G(d,p) level of theory.[200]

www.manaraa.com

The latter species, containing the trivalent $3d^6$ Co^{III} ion, can only be invoked if there is no cooperativity and the two metal centers function independently. Succinctly, protonation of one of the Co^{I} centers in **B** prompts a $2e^-$ transfer where each of the two Co^{I} centers donates an electron to the H^+. As a result, the more reactive $Co^{II}(H^-)$ unit is achieved without prior or concurrent formation of the $Co^{III}(H^-)$ moiety.

4.3.4 Fate of $[Co^{II}_2(L^{1'})(bpy)_2]ClO_4$ after Catalysis

The post-catalysis spectrum shown in **Figure 4.3c** displays the similar features observed in the $[Co^{II}Co^{II}]$ state, (**Figure 4.3a**) thus attesting to the catalytic nature of **$[Co^{II}_2(L^{1'})(bpy)_2]ClO_4$** along with a decrease of *ca.* 10% in the UV bands and of 2% in the 450 nm band. This small discrepancy is explained by slow percolation of solution between the chambers and through the frit of the electrochemical cell. Alternatively, a fraction of the catalyst may be deactivated and evaluation of a grafoil sheet electrode was performed by SEM and EDS to assess the possibility of nanoparticle formation **(Figure 4.15)**.

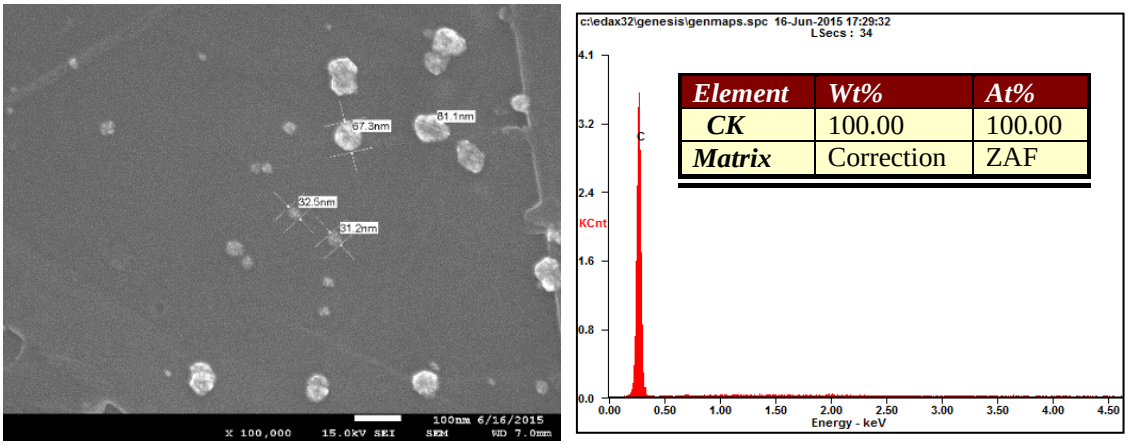

Figure 4.15. Micrograph of post-catalytic grafoil sheet electrode by SEM and EDS of **$[Co^{II}_2(L^{1'})(bpy)_2]ClO_4$**.

Notwithstanding evidence for formation of organic nanoparticles, no Co was detected on the surface of the electrode. Thus, UV-visible, SEM, and EDX analyses support the presence of a catalyst that is molecular in nature.

www.manaraa.com

4.4 Conclusions

In conclusion, we have investigated both experimentally and theoretically the bimetallic complex **$[Co^{II}_2(L^{1'})(bpy)_2]ClO_4$**. This species supports the catalytic H^+ reduction to H_2 in CH_3CN when in the presence of a weak acid such as HOAc at an overpotential of 0.63 V. This catalytic activity relies on a $2e^-$ reduction of the parent species $[Co^{II}Co^{II}]$ to form a $[Co^{I}Co^{I}]$ complex. Each of these Co^{I} centers contributes with the donation of one electron to a single incoming H^+, thus forming a reactive Co(II)-hydride. The novel bimetallic cooperativity exhibited by this system arises from the close proximity of the cobalt centers and an appropriate orbital topology that avoids the formation of the Co^{III}–H^- moiety required for proton reduction in monometallic catalysts. The second Co^{I} center plays a pivotal role in the catalytic reduction of H^+, acting as an electron reservoir to donate the second electron necessary for formation of the Co^{II}–H^- unit that favorably accepts another H^+ and releases H_2. Post-catalytic SEM and EDX analyses support the molecular nature of the catalyst. Therefore, the observations resulting from this work lead to considerations on how to optimize topology and orbital overlap to promote the use of a neighboring metal center as electron reservoir. These factors will become pivotal in the development of new and improved bimetallic catalysts.

www.manaraa.com

CHAPTER 5:

EFFECT OF VALENCE TAUTOMERISM ON COORDINATION PREFERENCES IN MANGANESE COMPLEXES WITH [N_2O_3] LIGANDS FOR WATER OXIDATION

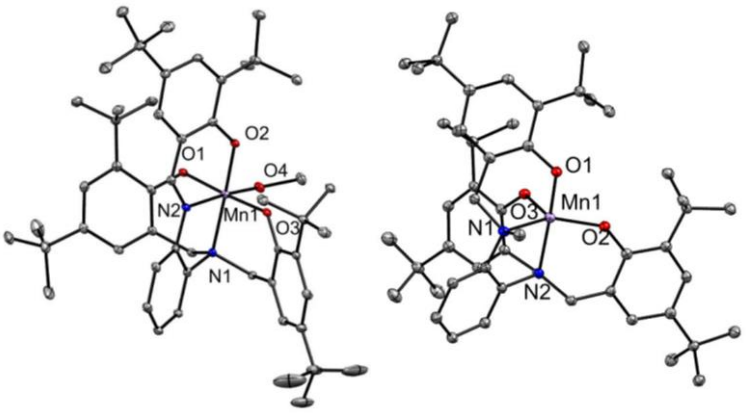

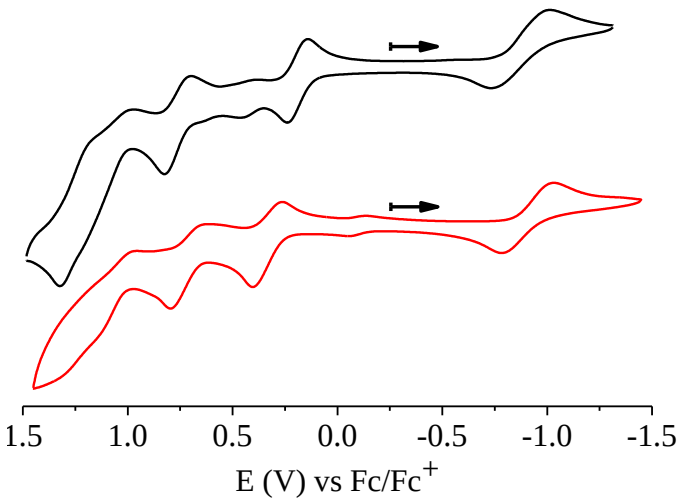

www.manaraa.com

CHAPTER 5: EFFECT OF VALENCE TAUTOMERISM ON COORDINATION PREFERENCES IN MANGANESE COMPLEXES WITH [N_2O_3] LIGANDS FOR WATER OXIDATION

Portions of the text in this chapter were reprinted or adapted from a manuscript under preparation. Dr. Rajendra Shakya is acknowledged for his intellectual contributions.

5.1. Introduction

The manganese ion, with its broad range of oxidation states and considerable Earth-abundance, is an appropriate choice for the study of the electron transfer processes involved in catalytic water oxidation. It has been proposed that incorporation of phenolate moieties into manganese species could lead to catalytic activity,[91, 201-202] As described in Chapter 1, Akermark[93, 95, 203] and coworkers have used the phenolate ligand moiety with bimetallic [Mn_2] and heterometallic [RuMn] to study electron transfer rates. A similar approach based on modifications of the triaza-cyclononane ligand was undertaken by Wieghardt[96] and collaborators.

Fujii[79, 98] *et al.* have shown remarkable examples of Mn(IV) stabilization using [N_2O_2] salen platforms. These systems build on an equilibrium between [Mn^{III}/phenoxyl] and [Mn^{IV}/phenolate] species. It was initially suggested by Åkermark[99] and coworkers that formation of Mn(IV) leads to a Mn^{III}/phenoxyl species where radical decay is prevented by coordination to the metal center, but Fujii[204] proposes that the [Mn^{III}/phenoxyl] state is favored upon coordination with water and the metal-centered high oxidation is only achieved by water deprotonation or formation of a Mn(IV)=O moiety. A study from Anxalabehere-Mallart *et al.*[205] proposed that an alternative and milder mechanism for water oxidation might involve the formation of Mn(III)-oxyl species in pentadentate ligands. It has been reported that valence tautomeric transitions can occur similarly via a stimulated intramolecular electron transfer, between redox-active ligands such as

www.manaraa.com

phenolates and a redox-active metal center, yielding two different valence tautomers or redox isomers.[206]

Continuing in the Verani group's success in designing mononucleated and pentadentate [N_2O_3] ligands containing three phenol moieties attached through rigid spacers that coordinate to trivalent 3*d* transition metals such as iron(III) and gallium(III), and form multiple phenoxyl radicals through sequential oxidations,[115, 207-211] we explore in this chapter the manganese chemistry of these ligands to improve our understanding of (i) how metal identity influences the physical and spectroscopic properties of complexes with these [N_2O_3] ligands, (ii) how valence tautomerism affects the coordination preferences in the formation of Mn(IV) species, and (iii) to determine if this pentadentate ligand framework is robust enough to support catalytic water oxidation at the vacant metal site.[209, 211]

To achieve these goals, we synthesized, and characterized two new trivalent manganese complexes, the hexacoordinate [$Mn^{III}(L^1)(CH_3OH)$] (**1**) and the pentacoordinate [$Mn^{III}(L^2)$] (**2**) **(Scheme 5.1)**, and evaluated their catalytic water oxidation properties.

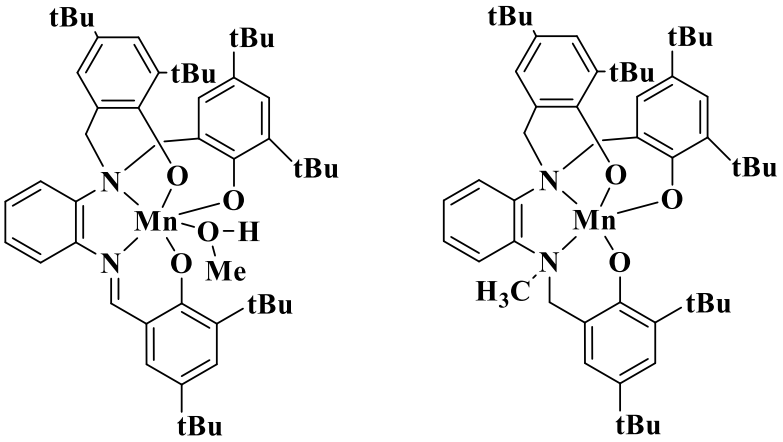

Scheme 5.1. Mononuclear manganese complexes hexacoordinate [$Mn^{III}(L^1)(CH_3OH)$] 1 (left) and the pentacoordinate [$Mn^{III}(L^2)$] 2 (right).

www.manaraa.com

Spectroelectrochemical measurements were combined with DFT calculations to provide detailed insight into the spectroscopy of these complexes as well as the balance between metal- and ligand-based oxidation.

5.2 Experimental Section

5.2.1 Materials and Methods

Spectroelectrochemical measurements were done in an optically transparent thin-layer cell (*ca.* 0.1 mm) constructed according to a procedure described as follows: a u-shaped flat platinum wire was sandwiched between two glass slides. The inner parts were coated with indium-tin oxide (ITO) (8-12 Ω/sq.). The Pt-wire acted as the working electrode and extended outside of the slides for electrical contact. The solutions were prepared and degassed under inert atmosphere (argon) and introduced into the cell through a capillary. The working electrode was located within 4-6 mm of the cell bottom to minimize ohmic potential (iR) drop. All potentials were measured vs. an Ag/AgCl reference electrode and a second platinum wire (counter electrode). Potentials were applied to the cell via a BASi 50W potentiostat/galvanostat, and the spectra were collected with a Varian Cary 50 apparatus at the room temperature.

5.2.2 X-Ray Structural Determinations

Diffraction studies were done on a Bruker *X8 APEX-II* kappa geometry diffractometer equipped with Mo radiation and a graphite monochromator. Diffraction patterns were collected at 100 K with the detector at 40 mm and 0.3 degrees between each reflection for 5-10 s. *APEX-II*[212] and *SHELX*[112] software were used for structure solution and refinement. A total 135,874 reflections were measured, yielding 35,599 unique data (R_{int} = 0.093). Hydrogen atoms were placed in calculated positions. The refinement included 26% racemic twinning. There were some partial occupancy (50/50) atoms placed in the disordered *tert*-butyl groups and held isotropically. Each

www.manaraa.com

complex coordinates to a neutral methanol ligand. The asymmetric unit contains 3 complexes and one methanol solvate. Compound **2** crystallized as dark needles and 79,319 *hkl* data points were harvested which averaged to 11,683 data (R_{int} = 0.107). Hydrogen atoms were calculated. The neutral complex crystallized without solvent. Selected crystallographic data are shown in **Table 5.1.**

Table 5.1. Summary of Crystallographic Data for complexes **1**·1/3CH_3OH and 2.

	1·1/3CH_3OH	**2**
Formula	$C_{52.33}H_{74.33}Mn_1N_2O_{4.33}$	$C_{52}H_{73}MnN_2O_3$
FW	855.74	829.06
Space group	*Cc*	*P21/c*
a (Å)	28.8966(17)	13.9076(7)
b (Å)	17.2405(17)	27.1291(14)
c (Å)	29.9927(19)	14.1947(7)
α (deg)	90	90
β (deg)	98.392(5)	117.731(2)
γ (deg)	90	90
V (Å^3)	14782.1(19)	4740.5(4)
Z	12	4
Temp (K)	100(2)	100(2)
λ (Å)	0.71073	0.71073
ρ(g cm^{-3})	1.154	1.162
μ (mm^{-1})	0.312	0.321
R(F) (%)	6.69	5.94
Rw(F)(%)	15.50	11.18

$R(F) = \sum \| F_o | - | F_c \| / \sum | F_o |$, $Rw(F) = [\sum w (F_o^2 - F_c^2)^2 / \sum w (F_o^2)^2]^{1/2}$

5.2.3 Computational Details

Electronic structure computations were performed using density functional theory (DFT)[122] as implemented in a development version of Gaussian.[143] Geometry optimizations were

www.manaraa.com

performed at the B3LYP/6-31G(d,p)[141, 213-214] level of theory employing the IEF-PCM[215] variant for the continuum solvation model (CH_2Cl_2) with no symmetry constraints. The ligand phenols were substituted with *tert*-butyl groups experimentally; we replaced the *tert*-butyl groups with methyl for computational efficiency while capturing the electronic properties of the alkyl substituents.[215] All optimized structures were confirmed to have stable wave functions, and to be local minima by analyzing the harmonic frequencies.[152] Cartesian coordinates and frequencies for all species can be found in the Appendix B. TD-DFT[214] was employed to estimate vertical electronic excitation energies and intensities, and the results were visualized and fit with Gaussians using GaussView.[23] Single point energies for thermodynamics and TD-DFT calculations were performed using a larger basis set, 6-311+G(d,p).[149]

5.2.4 Catalytic Studies

To test the catalytic activity of $[Mn^{III}L^1CH_3OH]$ (1) for water oxidation, bulk electrolysis was performed in a CH_3CN:phosphate 10:90% buffered solution at neutral pH. in a custom H-type cell. A 3-electrode system consisting of a 1.30 cm^2 FTO plate as the working electrode and Ag/AgCl and platinum wire as the reference and auxiliary electrodes, respectively. The quantification of oxygen was measured by gas chromatography and calculated from the ratio of O_2 and N_2 in the headspace according to equation 5.1.[155] A sample calculation is shown.

$$\Delta A = [(r_2 - r_1)]/r_0 \times A \qquad \text{(Equation 5.1)}$$

ΔA= number of moles of O_2 produced by catalyst (25 µM) after 10800 seconds

A = number of moles of O_2 in the headspace before electrolysis (113 µmol for 13 mL headspace)

r_0 = ratio of O_2 and N_2 in the headspace before electrolysis

r_1 = ratio of O_2 and N_2 in the headspace after electrolysis without catalyst

r_2 = ratio of O_2 and N_2 in the headspace after electrolysis with catalyst

www.manaraa.com

r_0, r_1, and r_2 are 0.257, 0.261, and 0.266, respectively. ΔA =2.20 µmol

TON = moles of O_2 produced/moles of catalyst used

TON = 2.20 µmol / 0.075 µmol =30

5.2.5 Synthetic Procedures

The ligands, *N*,*N*,*N*'-tris-(3,5-di-*tert*-butyl-2-hydroxybenzyl)-benzene-1,2-diamine ($H_3L^{1'}$), and, 6,6'-(((2-((3,5-di-*tert*-butyl-2-hydroxybenzyl)(methyl)amino)phenyl)azanediyl) bis(methylene))bis(2,4-di-tert-butylphenol) (H_3L^2) were prepared according to literature procedures.[115, 207-211] We demonstrated that $H_3L^{1'}$ transforms into the related L^1 containing an azomethine (C=N) group when coordinated to a trivalent metal under oxidizing conditions in earlier reports.[208-209, 211]

5.2.5.1 Synthesis of [$Mn^{III}(L^1)(CH_3OH)$] (1)

$H_3L^{1'}$ (0.380 g, 0.500 mmol) was dissolved in a solvent mixture of anhydrous CH_3OH:CH_2Cl_2 (20 mL, 1:1) and treated with $NaOCH_3$ (0.0810 g, 1.5000 mmol) under argon atmosphere. A methanol solution of $MnCl_2 \cdot 4H_2O$ (0.0990 g, 0.5000 mmol) was transferred via cannula, heated at 50 ^oC, and stirred for 2 h. The resulting light brown solution was cooled to room temperature. Oxygen gas was bubbled through the cooled solution for 15 min where the color immediately changed to dark brown. Upon slow solvent evaporation, dark brown crystals suitable for X-ray analysis were isolated from the solution. Yield: 70% (0.295 g, 0.350 mmol). ESI-MS (m/z^+; CH_3OH) = 813.4572, 100%, for [$C_{51}H_{69}N_2O_3Mn + H^+$]. IR (KBr, cm^{-1}) 2954(s), 2904(m), 2866(m), ν(C-H); 1610(m) ν(C=N), 1584(s), 1528(s), 1465(s), 1413(s), 1389(s),1360(s), ν(C=C); 1250(s), 1200(s), ν(C–O). Anal. calc. for $C_{52.33}$ $H_{74.33}$ $N_2O_{4.33}Mn$: C,73.45; H, 8.76; N, 3.27%. Found: C, 72.99; H, 8.13; N, 3.41%. UV-visible (λ / nm; ε / $M^{-1}cm^{-1}$): 290 (22,000); 440 (6,068); 527 (4,450); 609 (3,408).

www.manaraa.com

5.2.5.2 Synthesis of [$Mn^{III}(L^2)$] (2)

Complex **2** was prepared analogously to **1**, except that H_3L^2 was used as the ligand and anhydrous $MnCl_2$ was used as the salt. Brown X-ray suitable single crystals of **2** were obtained by slow crystallization in a CH_3OH : CH_2Cl_2 mixture (1 : 1). Yield: 70% (0.290 g, 0.350mmol). ESI (m/z^+) = 829.5061, 100%, for [$C_{52}H_{73}N_2O_3Mn + H^+$]. IR (KBr, cm^{-1}) 2955(s), 2904(m), 2867(m), ν(C-H); 1602(m), 1527(s), 1463(s), 1413(s), 1390(s),1360(s), ν(C=C); 1265(s), 1237(s), ν(C–O). Anal. calc. for C_{52} H_{73} N_2O_3Mn: C,75.33; H, 8.87; N, 3.38%. Found: C, 75.41; H, 8.78; N, 3.54%. UV-visible (λ / nm; ε / $M^{-1}cm^{-1}$): 285 (24,700); 390 (6,632); 532 (2,622); 815 (1,634).

5.3 Results and Discussion

5.3.1 Synthesis and Characterization

Ligands H_3L^1 and H_3L^2 were synthesized according to reported procedures.[115, 207-211] The hexacoordinate complex [$Mn^{III}(L^1)(CH_3OH)$] was synthesized by combining H_3L^1 with $MnCl_2{\cdot}4H_2O$ in the presence of $NaOCH_3$ followed by a 15 min O_2 purge. The IR spectrum of **1** lacked an N–H band at *ca.* 3200 cm^{-1} indicative of the amine group but did show an absorption band at 1610 cm^{-1} consistent with the C=N group. Oxidation of the amine $(L^1)^{3-}$ to form the imine $(L^1)^{3-}$ was previously observed for an iron(III) complex.[207, 209] Elemental analysis, ESI mass spectra, and the X-ray crystal structure confirmed a hexacoordinate manganese complex containing [$Mn^{III}(L^1)(CH_3OH)$], where the coordinated methanol occupies the last position.

Complex [$Mn^{III}L^2$] **(2)** was synthesized by reaction of equimolar amounts of H_3L^2 and anhydrous $MnCl_2$ under similar conditions. The ligands L^1 and L^2 are the 2,4-di-*tert*-butyl-6-[(2-[(3,5-di-tert-butylbenzyl)(methyl)amino]phenyl)imino]methylphenolate and 2,4-di-*tert*-butyl-6-(1-methyl-1*H*-benzo[*d*]imidazol-2-yl)phenolate, respectively. The use of anhydrous $MnCl_2$ yielded **2** as the only product. The compound showed an IR spectrum lacking the C=N band at

www.manaraa.com

1619 cm^{-1}, evidence that ligand oxidation was prevented by the N-attached methyl group present in $(L^2)^{3-}$. The $[M+H]^+$ peak was observed at 829.51 in the ESI mass spectrum along with an appropriate isotopic distribution pattern. Elemental analysis data supports that **2** has no coordinated CH_3OH or any other ligand occupying the sixth coordination site. The X-ray crystal structure determination confirmed **2** as a pentacoordinate manganese species.

5.3.2 Geometric and Electronic Structures

The molecular structures of hexacoordinate $[Mn^{III}L^1CH_3OH]$ **(1)** and pentacoordinate $[Mn^{III}L^2]$ **(2)** were solved by X-ray and are plotted as ORTEP[216] representations at 50% probability in **Figure 5.1**. The unit cell of **1** consists of an asymmetric unit with three $[Mn(L^1)(CH_3OH)]$ molecules and one uncoordinated methanol in the lattice.

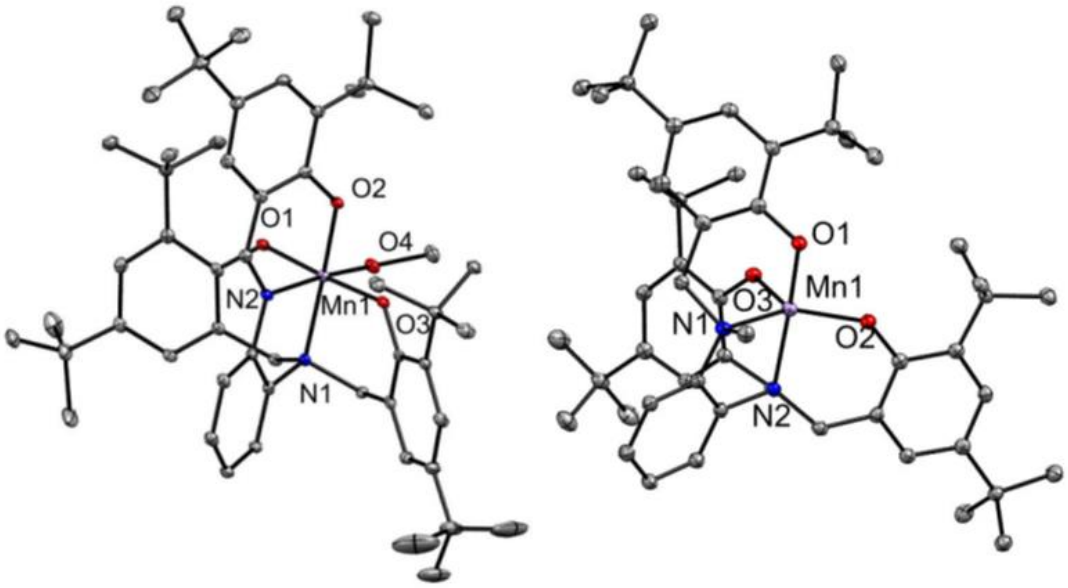

Figure 5.1. ORTEP[216] representations of **1** (left) and **2** (right).

These three manganese complexes are chemically equivalent with slight differences in the bond lengths and angles, with a notable exception for the Mn–O_{CH3OH} bond which shows a longer bond length. This elongation of the bond is consistent with the weak nature of the bound CH_3OH and rules out the possibility of the methoxylated coordination. The ORTEP[216] representation of **1**

www.manaraa.com

in **Figure 5.1** (left) contains a single molecule (Mn2 center). Complex **2** crystallized in the monoclinic space group $P2_1/c$, **(Figure 5.1)** (right). Selected bond lengths and angles for **1** and **2** are given in **Table 5.2.**

Table 5.2. Selected bond lengths (Å) and angles (°) from crystal data for **1** (Mn2 center) and **2**.

[$Mn^{III}(L^1)(CH_3OH)$]		**[$Mn^{III}(L^2)$]**	
Mn(2)-O(6)	1.865(3)	Mn(1)-O(2)	1.8934(17)
Mn(2)-O(5)	1.916(3)	Mn(1)-O(1)	1.8382(16)
Mn(2)-N(4)	2.126(3)	Mn(1)-N(2)	2.061(2)
Mn(2)-N(3)	2.151(4)	Mn(1)-N(1)	2.139(2)
Mn(2)-O(7)	1.887(3)	Mn(1)-O(3)	1.9235(16)
Mn(2)-O(8)	2.201(4)		
N(3)-C(59)	1.302(5)	N(1)-C(7)	1.493(3)
N(4)-C(73)	1.504(5)	N(2)-C(22)	1.508(3)
N(4)-C(66)	1.509(5)	N(2)-C(15)	1.511(3)
N(4)-C(65)	1.469(5)	N(2)-C(14)	1.473(3)
N(3)-C(60)	1.417(5)		
O(6)-C(72)	1.341(5)	O(2)-C(21)	1.338(3)
O(5)-C(53)	1.300(5)	O(1)-C(1)	1.350(3)
O(7)-C(79)	1.319(5)	O(3)-C(28)	1.344(3)
O(6)-Mn(2)-O(5)	90.58(13)	O(2)-Mn(1)-O(1)	90.06(7)
O(6)-Mn(2)-O(7)	170.00(14)	O(2)-Mn(1)-O(3)	121.62(7)
O(7)-Mn(2)-O(5)	89.16(13)	O(1)-Mn(1)-O(3)	96.13(7)
O(6)-Mn(2)-N(4)	92.32(13)	O(2)-Mn(1)-N(2)	92.21(7)
O(5)-Mn(2)-N(4)	166.90(13)	O(1)-Mn(1)-N(2)	168.20(7)
O(7)-Mn(2)-N(4)	90.17(12)	O(2)-Mn(1)-N(1)	132.36(7)
O(6)-Mn(2)-N(3)	92.08(14)	O(1)-Mn(1)-N(1)	87.09(7)
O(7)-Mn(2)-N(3)	97.91(13)	O(3)-Mn(1)-N(1)	105.95(7)
N(4)-Mn(2)-N(3)	78.41(13)	N(2)-Mn(1)-N(1)	82.82(7)
O(6)-Mn(2)-O(8)	86.54(13)		
O(5)-Mn(2)-O(8)	99.70(13)		
O(7)-Mn(2)-O(8)	83.65(13)		
N(4)-Mn(2)-O(8)	93.23(13)		
N(3)-Mn(2)-O(8)	171.47(13)		

In **[$Mn^{III}L^1CH_3OH$] (1),** the N_2O_3 moiety of L^1 consists of an amine nitrogen, an imine nitrogen, and three phenolate oxygens (based on C–O bond lengths of 1.30-1.34 Å) for an overall trianionic, pentadentate ligand. The three phenolates are chemically distinct, and display Mn–O

www.manaraa.com

bond lengths of 1.865(3), 1.887(3) and 1.916(3) Å, respectively. The π-withdrawing imine makes the iminophenolate less electron rich than the aminophenolates, as evidenced by a shorter C–O bond length of 1.300(5), which leads to weaker electrostatic interactions with the manganese(III) ion. The Mn–N_{amine} bond length (2.126(3) Å) is also shorter than Mn–N_{imine} (2.151(4) Å). Average Mn–N and Mn–O bond lengths of 2.14 and 1.89 Å are consistent with related manganese(III) complexes,[99, 217-218] and with those measured in an iron(III) complex that has an established $(L^1)^{3-}$ ligand oxidation state.[207] As discussed above, the Mn–O_{CH3OH} bond length of 2.201(4) Å is consistent with the presence of an axial CH_3OH rather than a methoxy anion.

Density functional theory (DFT) calculations were performed to evaluate the energetic and structural difference between a low spin $S = 1$ and high spin $S = 2$ manganese(III) center, denoted $3d^4$ $^{LS}Mn^{III}$ and $^{HS}Mn^{III}$, respectively. The computations predict the solution-phase free energy of the $^{HS}Mn^{III}$ complex to be 11.6 kcal mol^{-1} lower than for $^{LS}Mn^{III}$. Additionally, the computed geometry for $^{HS}Mn^{III}$ is more consistent with the X-ray structural information. Thus, we assign this species as pseudo-octahedral $[^{HS}Mn^{III}(L^1)(CH_3OH)]$, consistent with experimental evidence offered by similar compounds available in the literature.[217-218]

The N_2O_3 donor moiety for **$[Mn^{III}L^2]$ (2)** consists of two amine nitrogens and three phenolate oxygens to afford the pentadentate $(L^2)^{3-}$ ligand. **$[Mn^{III}L^2]$ (2)** crystallized as a pentacoordinate molecule with no methanol coordinated, although it was synthesized and recrystallized in a 1 : 1 CH_3OH : CH_2Cl_2 solvent mixture. The τ value[219] of 0.7 indicates that the manganese(III) ion is a distorted trigonal bipyramidal geometry. A similar geometry was observed for a related manganese(III) complex with an $[N_2O_3]$ pentadentate ligand. Average Mn–O and Mn–N bond lengths of 1.88 and 2.10 Å in **$[Mn^{III}L^2]$ (2)** are comparable to **$[Mn^{III}L^1CH_3OH]$ (1)** and other related complexes.[217-218]

www.manaraa.com

DFT computations were carried out in the case of **[$Mn^{III}L^2$] (2)** to evaluate the relative energetic difference between low-spin and high-spin configuration for a manganese(III) ion bound to the L^2 ligand environment as well. A Gibb's free energy difference of 22.9 kcal mol^{-1} favors species **[$Mn^{III}L^2$] (2)** as [$^{HS}Mn^{III}(L^2)$] consistent with the expectation that the high-spin state is favored due to a lower coordination number and, in good agreement with other five-coordinate species.[99, 101]

5.3.3 Electronic Spectroscopy

The electronic spectra of the hexacoordinate **[$Mn^{III}L^1CH_3OH$] (1)** and the pentacoordinate **[$Mn^{III}L^2$] (2)** in CH_2Cl_2 are illustrated in **Figure 5.2** (solid lines) along with TD-DFT simulations for each species (dotted lines). Both compounds demonstrate high energy ligand-centered transitions ($\pi \rightarrow \pi^*$) below 300 nm. Complex **[$Mn^{III}L^1CH_3OH$] (1)** shows an intense band at 440 nm that was initially associated with a phenolate-to-manganese charge transfer. According to TD-DFT results, however, this absorption band is predominantly associated with an intra-ligand-charge-transfer (ILCT) involving the phenolates and azomethine group (phenolate $\pi \rightarrow$ imine π^*) which overlaps the phenolate-to-manganese charge transfer. The nature of this ILCT was confirmed by spectroelectrochemical measurements **(Section 5.3.5).**

Compound **[$Mn^{III}L^2$] (2)** lacks an imine functionality and therefore the band observed at 390 nm is assigned as a phenolate $\pi \rightarrow {}^{HS}Mn^{III}$–$d\sigma^*$ ligand-to-metal charge transfer (LMCT).[217-218, 220-221] TD-DFT results support assignment. It is important to note that the TD-DFT results suggest that each transition involves multiple donor (and sometimes acceptor) orbitals. A full description of the low energy transitions with appreciable intensity can be found in **Appendix B**, Tables C3-C5. Lower energy LMCT bands between 500 and 900 nm are observed at 437, 527, and

www.manaraa.com

609 nm and at 532 and 815 nm, respectively for **[Mn^{III}L^{1}CH$_3$OH] (1)** and **[Mn^{III}L^{2}] (2)**. Similar features have been observed in related complexes reported in the literature.[218, 221-222]

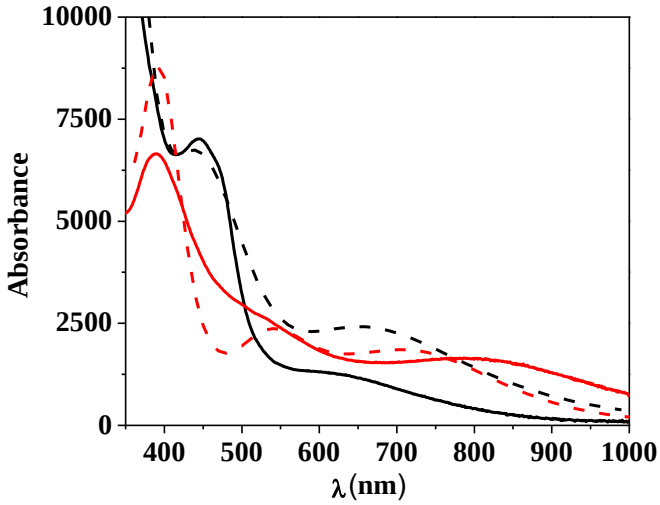

Figure 5.2. UV-visible spectra of [Mn^{III}L^{1}CH$_3$OH] **(1)** (black) and [Mn^{III}L^{2}] **(2)** (red) in CH_2Cl_2. Solid lines are experimental spectra, dotted lines are TD-DFT simulated spectra.

5.3.4 Electrochemical Properties

The redox behavior of the hexacoordinate [Mn^{III}L^{1}CH$_3$OH] **(1)** and the pentacoordinate [Mn^{III}L^{2}] **(2)** was studied by cyclic voltammetry (CV) in CH_2Cl_2 using tetrabutylammonium hexafluorophophate ($TBAPF_6$) as the supporting electrolyte. Redox potentials are reported versus Fc^+/Fc. Quasireversible one electron processes are observed at –0.88 and –0.92 V for **[Mn^{III}L^{1}CH$_3$OH] (1)** and **[Mn^{III}L^{2}] (2)**, respectively, and are attributed to the Mn(III/II) redox couple.[223] The potential difference of 0.04 V for the manganese reduction processes in **1** and **2** is likely associated to the different geometries of the metal ion. A first oxidative quasi-reversible process at 0.19 V is seen for **[Mn^{III}L^{1}CH$_3$OH] (1)**, whereas **[Mn^{III}L^{2}] (2)** shows the same process at a lower potential of 0.30 V. This process can be either attributed to the formation of a manganese(IV) species, or to ligand oxidation leading to a [Mn(III)/phenoxyl] species.

www.manaraa.com

DFT calculations for hexacoordinate **[Mn^{III}L^{1}CH$_3$OH] (1)** show ligand oxidation to be thermodynamically favored over metal-based oxidation by 2.8 kcal mol^{-1}. This energy difference is within the experimental error of the DFT method and therefore metal-based oxidation could be favored as well. This could be attributed to proximity in the energy of the ligand and metal redox-active orbitals. Therefore, one-electron oxidation of some M^{+}–phenolate complexes afford either the $M^{(n+1)+}$–phenolate or the M^{n+}–phenoxyl valence tautomer.[224-226] Interestingly, no metal-based oxidized state could be located for the pentadentate **[Mn^{III}L^{2}] (2)**.

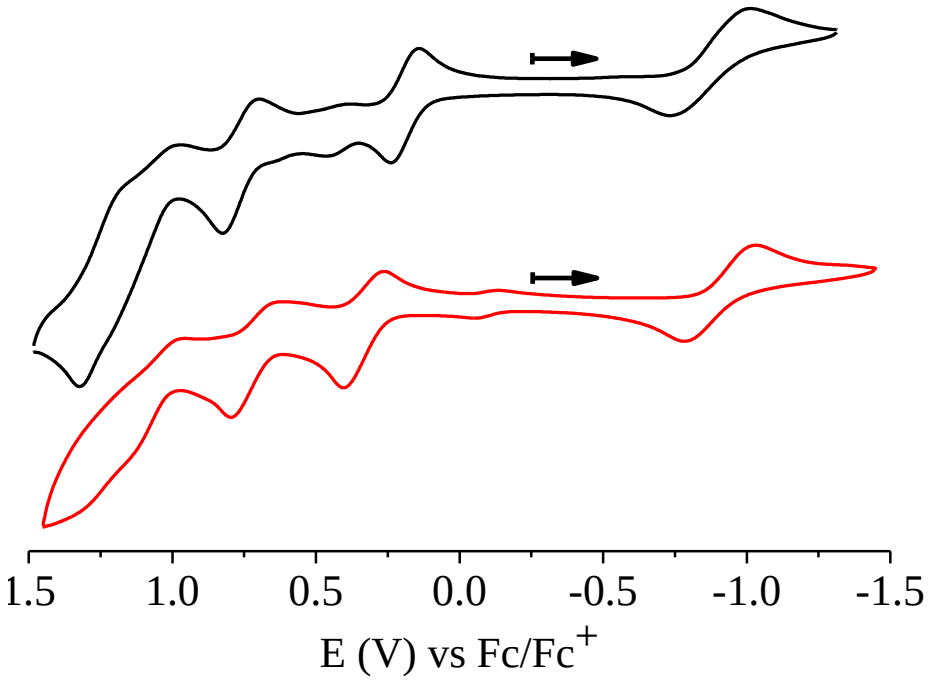

Figure 5.3. Cyclic voltammograms for **1** (top) and **2** (bottom) in CH_2Cl_2 with 0.1 M $TBAPF_6$ as supporting electrolyte.

Compound **[Mn^{III}L^{1}CH$_3$OH] (1)** also exhibits an anodic process at 0.42 V with a much smaller current response. The solution was prepared multiple times from isolated crystals and this redox process was reproducible. The amplitude of the process increases when the scan rate is decreased. This inverse proportionality could be associated with the formation of

www.manaraa.com

Mn(IV)/phenolate from a [Mn(III)/phenoxyl] species because the energy of their frontier orbitals is similar; a necessary condition for valence tautomerism.[224]

Another quasi-reversible redox process centered at 0.76 and 0.68 V is observed for **1** and **2**. Based on our previous study of [$Ga^{III}L^1$] and [$Fe^{III}L^1$] complexes[207, 209], as well as other literature reports[115, 227-230] and DFT calculations, we assign these processes to oxidation of a second phenolate group. A scheme of the computed spin densities for these redox states is included in **Figure 5.4** and summarizes the sequence of redox events for these two molecules. The first oxidation occurs at the aminophenolate instead of the iminophenolate in **1** due to the π-withdrawing nature of the imine, while the first oxidation of **2** occurs at the phenolate attached to the methylamine due to inductive effect. This sequence is also observed for iron(III) species with similar ligands,[115, 207] and suggests that ligand electronic properties precede coordination preferences. In both the hexa and pentadentate complexes DFT suggests an antiferromagnetic coupling between the phenoxyl radicals and the high-spin manganese(III) ion to be favored for coupling constants, in agreement with the results proposed by Fujii[98] and coworkers.

Table 5.3. Electrochemical parameters for compounds **1** and **2**.

Complexes					
1			**2**		
E (V) vs. Fc/Fc^+	ΔE_p (V)	i_{pa} / i_{pc}	E (V) vs. Fc/Fc^+	ΔE_p(V)	i_{pa} / i_{pc}
-0.88	0.28	1.42	-0.92	0.20	1.62
0.19	0.11	0.91	0.30	0.07	0.86
0.42	0.09	0.74	-	-	-
0.76	0.13	0.80	0.68	0.10	0.42
1.08	0.18	-	1.01	0.11	-

www.manaraa.com

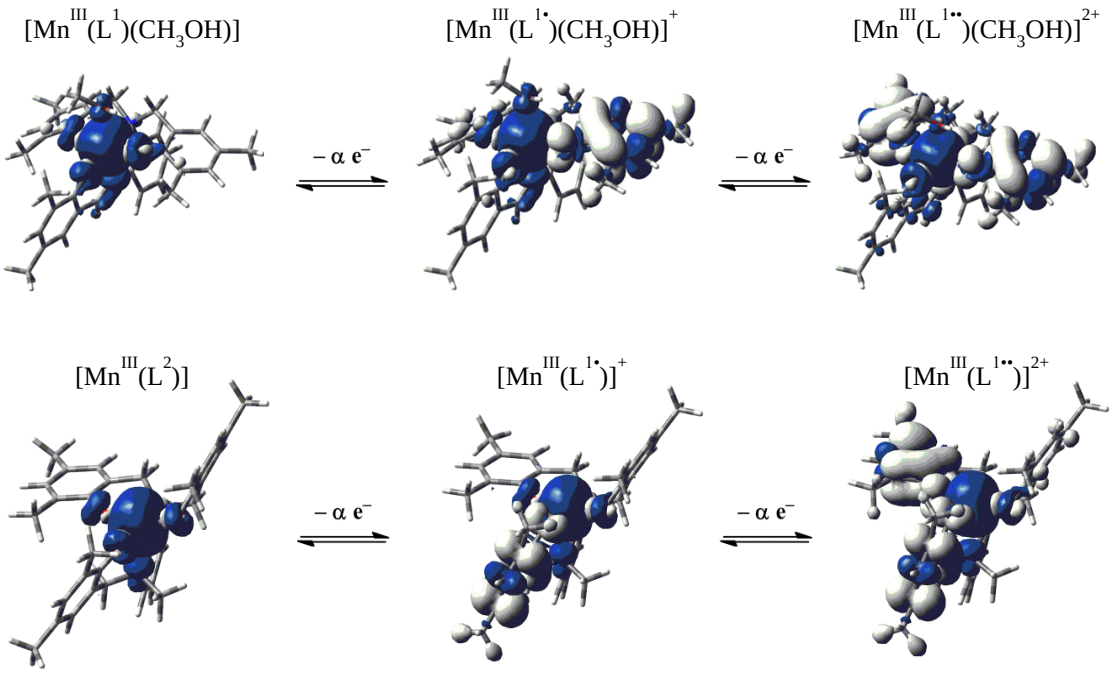

Figure 5.4. Summary of redox sequence based on predicted spin densities from DFT for **1** (top) and **2** (bottom). Spin densities are plotted with an isodensity value of 0.002 au, blue corresponds to excess α spin and white corresponding to excess β spin. The neutral species is on the left, the monocation is in the middle, and the dication is on the right.

5.3.5 Spectroelectrochemical Behavior

Spectral changes associated with electrochemical oxidations and reductions were collected under variable and stepwise potential conditions and were assessed to confirm the assignment of various bands in the UV-visible spectra. We were particularly interested in the ligand- versus metal-based character of the first anodic process. The spectral changes observed for the reduction of the hexacoordinate $[Mn^{III}L^{1}CH_3OH]$ **(1)** at an applied potential of –1.41 V vs. Fc^{+}/Fc are shown in **Figure 5.5** (left). The LMCT absorption bands decrease between 500 and 750 nm, in agreement with a Mn(III) + e^{-} → Mn(II) reduction process, where the unoccupied $d_{x^2-y^2}$-based molecular orbital accepts an electron and becomes half-filled. Isosbestic points are observed at 400 and 490 nm with an increase in the absorption band at 450 nm.

www.manaraa.com

No isosbestic points were observed for the reduction of the pentacoordinate $[Mn^{III}L^{2}]$ **(2)** under similar conditions (**Figure 5.5**, right), and instead, a continuous decrease of the spectral intensity is observed. Collectively, the disappearance of all LMCT bands in **1** and **2** upon reduction suggests the band at ~ 450 nm for **1** does not involve the metal, supporting the TD-DFT assignment of intraligand charge transfer ($\pi_{phenolate} \rightarrow \pi^*_{imine}$). This band has been commonly attributed to an LMCT in recent literature, but in view of these observations, it becomes apparent that an ILCT is more appropriate to explain the nature of the band.[115]

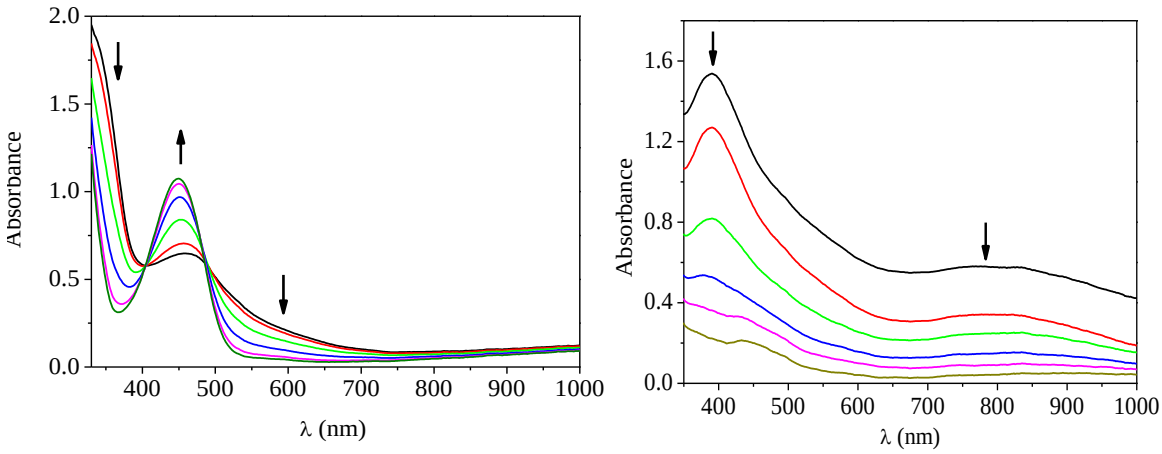

Figure 5.5. Spectral changes upon electrochemical reduction of **1** (left) and **2** (right) in CH_2Cl_2. The applied potential was –1.41 V vs. Fc^+/Fc for a period of 6 minutes.

We scanned the potential for oxidation of **1** instead of using a fixed potential due to the nearly overlapping oxidations at 0.19 and 0.42 V. This approach allows helps in deducing overlapping spectral contributions from the two oxidation processes. Oxidation between 0.20 to 0.30 V gives rise to two clear isosbestic points at 535 and 660 nm (**Figure 5.6**), with an increase in intensity below 535 nm and above 660 nm, and a decrease in between these values. The increased intensity in the low-energy region of the spectrum (> 660 nm) is consistent with ligand-based oxidation as phenolate π → phenoxyl radical π* transitions occur in this region.[96, 220 79, 208, 229]

www.manaraa.com

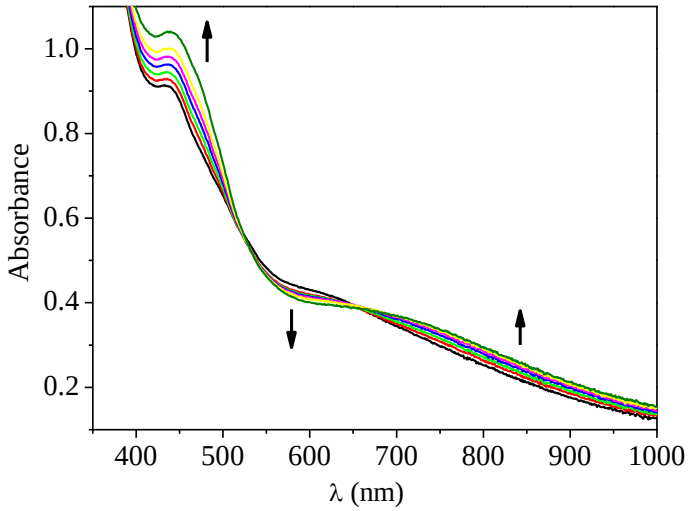

Figure 5.6. Spectral changes upon stepwise oxidation of **1** in CH_2Cl_2 in the potential range 0.20 to 0.30 $V_{Fc+/Fc.}$

Oxidation of pentadentate **2** at a fixed potential of 0.5 V vs. Fc^+/Fc **(Figure 5.7)** generates a spectral response similar to **1**. Two isosbestic points are seen at 435 and 500 nm, with increased intensity above 500 and below 435 nm and decreasing intensity between these regions. The intensity increase at low-energy is again consistent with a phenolate $\pi \rightarrow$ phenoxyl radical π^* charge transfer band, suggesting ligand-based oxidation, rather than manganese(IV) formation.

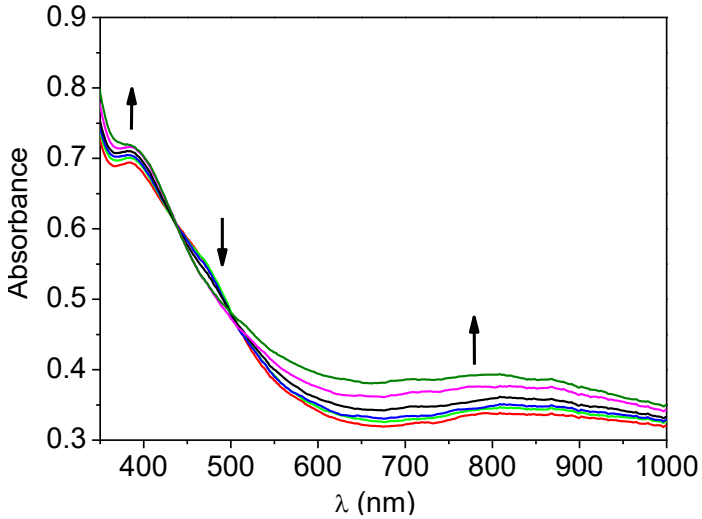

Figure 5.7. Spectral changes upon electrochemical oxidation of **2** in CH_2Cl_2. An applied potential of 0.5 V vs. Fc^+/Fc was applied for eight minutes.

www.manaraa.com

5.4. Catalytic Studies

Based on the spectroscopic results described in the sections above both [$Mn^{III}L^{1}CH_3OH$] **(1)** and [$Mn^{III}L^{2}$] **(2)** were screened for their catalytic activity towards water oxidation using a CH_3CN (10%) : phosphate (90%) buffered solution at neutral pH.[155, 170, 231] The experiment was conducted in a custom H-type cell with a 3-electrode system consisting of a 1.30 cm^2 FTO plate as the working electrode, and Ag/AgCl and a platinum wire as the reference and auxiliary electrodes, respectively. The quantification of oxygen was measured by gas chromatography and calculated from the ratio of O_2 and N_2 in the headspace according to **equation 5.1** described in the experimental **section 5.2.4**. Upon scanning the phosphate buffer without the catalyst, no current enhancement was observed until 1800 mV $_{Ag/AgCl}$.

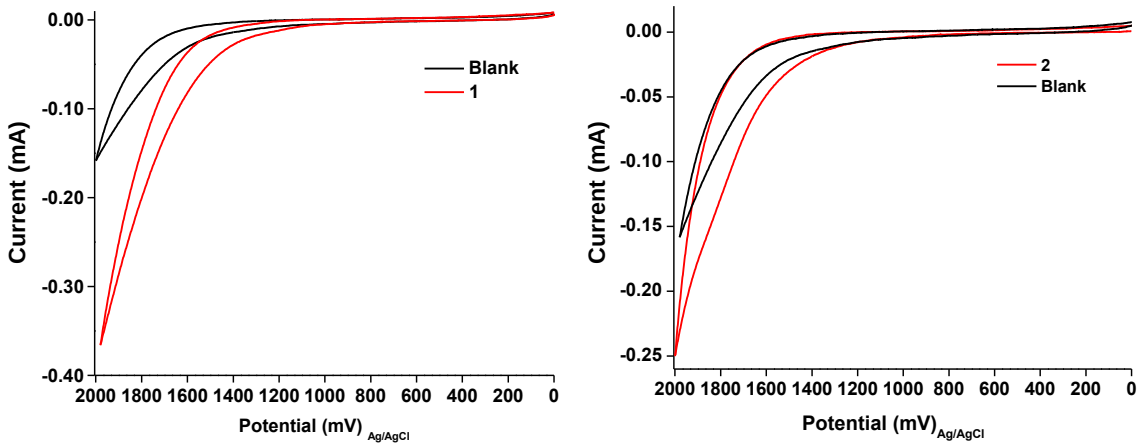

Figure 5.8. Catalytic water oxidation CV in (0.1 mol•L^{-1}) CH_3CN : Phosphate buffer at pH 7

Upon addition of **[$Mn^{III}L^{1}CH_3OH$] (1)** and the pentacoordinate **[$Mn^{III}L^{2}$] (2)** catalytic current enhancement was observed for **[$Mn^{III}L^{1}CH_3OH$]**, while **[$Mn^{III}L^{2}$]** gave a current enhancement comparable to the blank solution. These results suggest that **[$Mn^{III}L^{1}CH_3OH$]** can afford the $3d^3$ [Mn(IV)/phenolate] intermediate needed for water oxidation whilst [$Mn^{III}L^{2}$] is in capable of doing so (**Figure 5.8**). Bulk electrolysis was performed for [$Mn^{III}L^{1}CH_3OH$] **(1)** (**Figure 5.9**) under the same conditions, using 1.0 µmol•L^{-1} of catalyst and 1.30 cm^2 FTO as the

www.manaraa.com

working electrode, with an applied potential of 1.7 $V_{Ag/AgCl}$ for three hours.[231] It was observed after three hours that the catalyst operates at 85% Faradaic efficiency with a TON of 53.

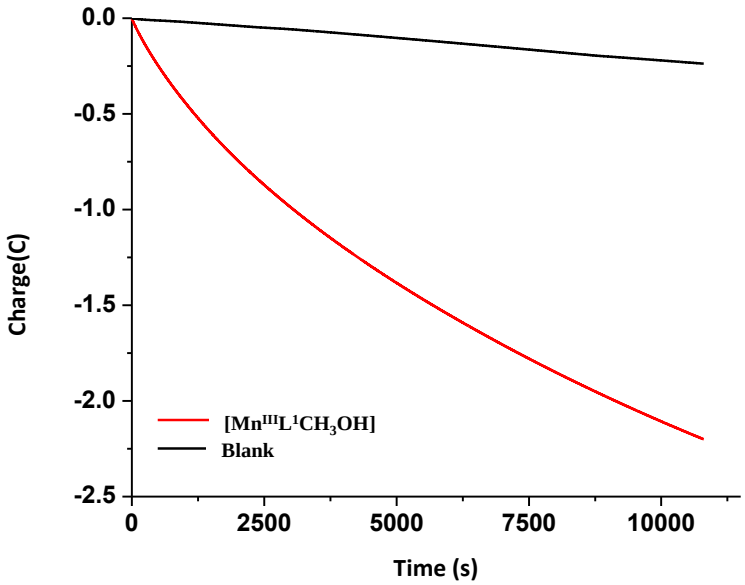

Figure 5.9. Charge consumption vs. time during BE with (0.1 mol•L^{-1} CH_3CN : phosphate buffer at pH 7 [1.0 umol•L^{-1}]) at 1.7 VAg/AgCl.

Even though the TON and %FE are considered low, they are better than others reported in the literature where TONs ranged from 16–24 with %FE of 74–81. [231-232] considering the fact that a thermodynamic barrier of 1.23 V needs to be overcome.[168]

5.5. Conclusions

I synthesized and investigated the effect of valence tautomerism on water oxidation in two manganese complexes, the hexacoordinate [$Mn^{III}L^1CH_3OH$] and the pentacoordinate [$Mn^{III}L^2$] using [N_2O_3] pentadentate ligands containing three phenolate donors. Detailed structural, electrochemical, and spectroscopic measurements suggest that whilst both complexes show ligand-based oxidations favoring formation of a [Mn(III)/phenoxyl] species, the hexacoordinate analog also shows a possibility of forming a [Mn(IV)/phenolate] species specifically due to the

www.manaraa.com

degree of the interaction between the metal center and the redox-active phenolate ligands, and the similarity between the energy of their frontier orbitals (>5 kcal/mol), essential attributes of valence tautomerism. I, therefore, tested the hexacoordinate [$Mn^{III}L^{1}CH_3OH$] for water oxidation catalysis and observed an overpotential of 0.77 V and TON of 53 in three hours with the catalyst operating at a Faradaic efficiency of 85%. Such a compound is thus particularly useful to better understand the way in which ligands could be designed to favor either a radical or a high-valent metal pathway for catalytic water oxidation.

www.manaraa.com

CHAPTER 6:

CONCLUSIONS

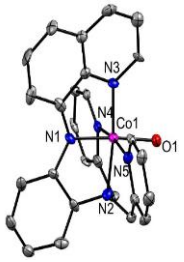

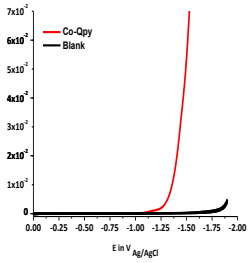

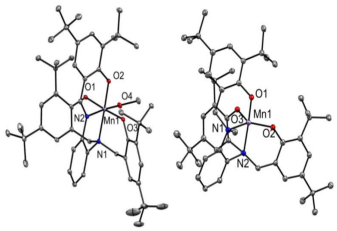

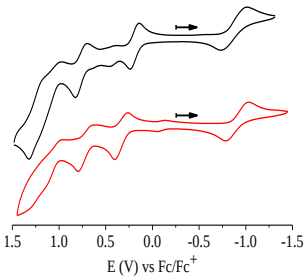

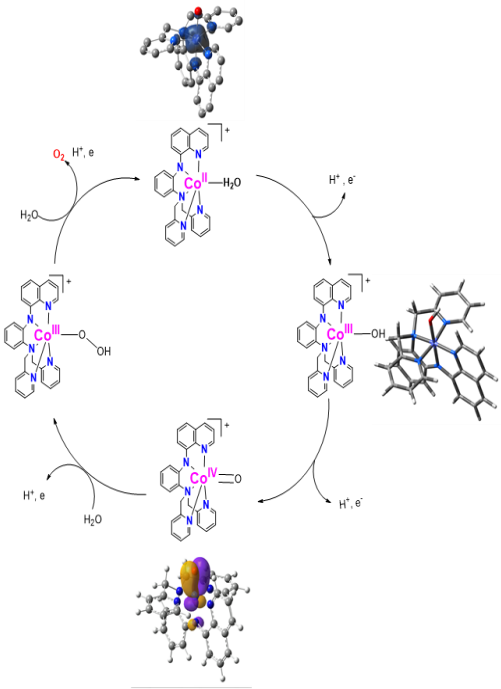

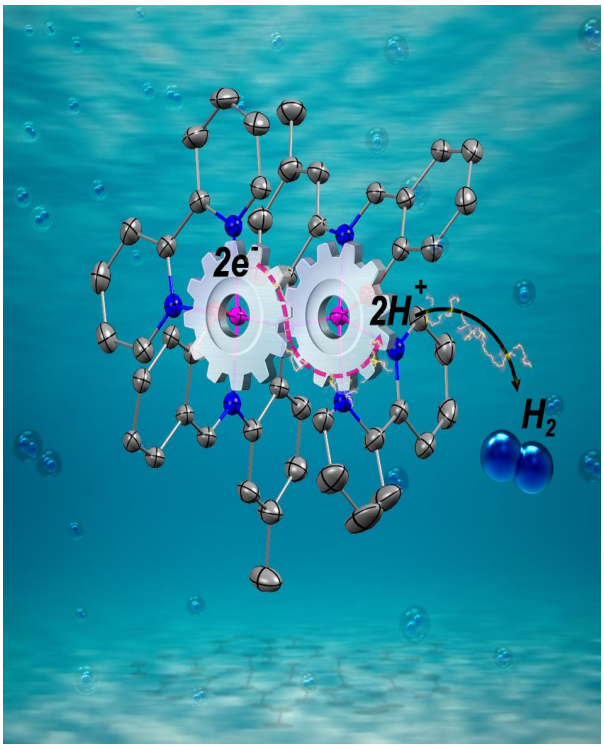

www.manaraa.com

CHAPTER 6: CONCLUSIONS

The focus of this dissertation was to design and evaluate the redox, electronic, catalytic, and mechanistic pathways of $3d^7$ Co^{II}, and $3d^4$ Mn^{III} complexes with various redox-active ligand frameworks in an effort towards efficient electrocatalytic water oxidation and reduction. These systematic studies were geared towards the eventual design of excellent photocatalysts based on affordable Earth-abundant metal complexes.

In Chapter 3, I described the synthesis and characterization an asymmetric, pentadentate quinolyl-bispyridine ligand $\mathbf{HL^{Qpy}}$ with a phenylenediamine backbone and its water-soluble $3d^7$ $^{HS}Co^{II}$ complex $\mathbf{[Co^{II}(L^{Qpy})H_2O]ClO_4}$. The complex is active as an electrocatalyst **(Figure 6.1)**, as well as a photocatalyst.

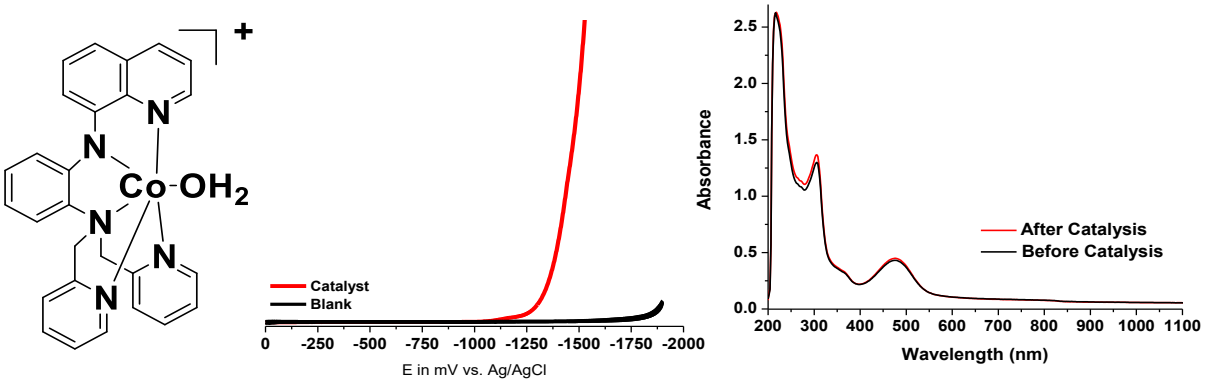

Figure 6.1. Robust and stable $\mathbf{[Co^{II}(L^{Qpy})H_2O]ClO_4}$ complex and its electrocatalytic water reduction activity.

$\mathbf{[Co^{II}(L^{Qpy})H_2O]ClO_4}$ is catalytic towards H_2O reduction at a low overpotential of 0.63 V, giving a TON of 2900 with a Faradaic efficiency of 98%. An 18 h catalytic TON of 12,100 suggests a highly robust and stable catalyst. $\mathbf{[Co^{II}(L^{Qpy})H_2O]ClO_4}$ serves as a robust water oxidation catalyst as well, with a TON of 97 at 91% FE.

www.manaraa.com

By using a series of experimental methods as well as DFT techniques, I isolated and characterized the catalytic oxidized intermediates for **$[Co^{II}(L^{Qpy})H_2O]ClO_4$** and proposed a 'water nucleophilic-attack' (WNA) mechanism of water oxidation **(Figure 6.2)**. The highly electrophilic $3d^5$ [$^{HS}Co^{IV}$=O] intermediate is attacked by a nucleophilic water molecule thus forming the essential O-O bond and releasing dioxygen.

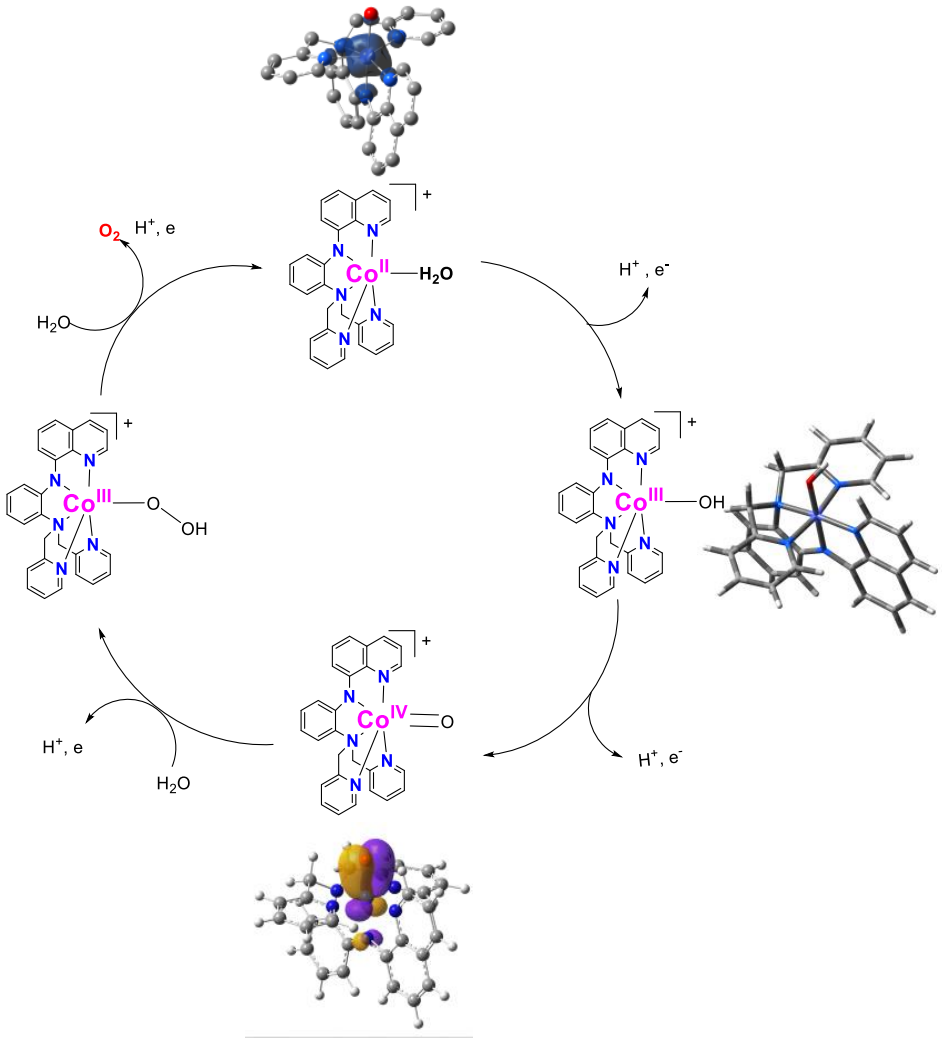

Figure 6.2. Proposed catalytic mechanism of O_2 generation by **$[Co^{II}(L^{Qpy})H_2O]ClO_4$**.

Finally, the photocatalytic activity of **$[Co^{II}(L^{Qpy})H_2O]ClO_4$** in the presence of $[Ru(bpy)_3]^{2+}$ and ascorbic acid acetate buffer (pH 4) shows a TON of 295 with a TOF of 50/h.

www.manaraa.com

In Chapter 4, the principal objective was to study the effect that distance and topology have on the electronic communication, and thereby cooperativity between two cobalt centers in a dicobalt complex towards efficient proton reduction **(Figure 6.3)**. In collaboration with the Fiedler group of Marquette University, I investigated both experimentally and theoretically the catalytic properties of the bimetallic complex **$[Co^{II}_2(L^{1'})(bpy)_2]ClO_4$**, a dicobalt(II) complex in which the metal centers lie at a short distance of 2.70 Å away from each other and bridged by a nitrogen atom of a diarylamido unit with a Co1-N3-Co2 at an angle of 86.9°.

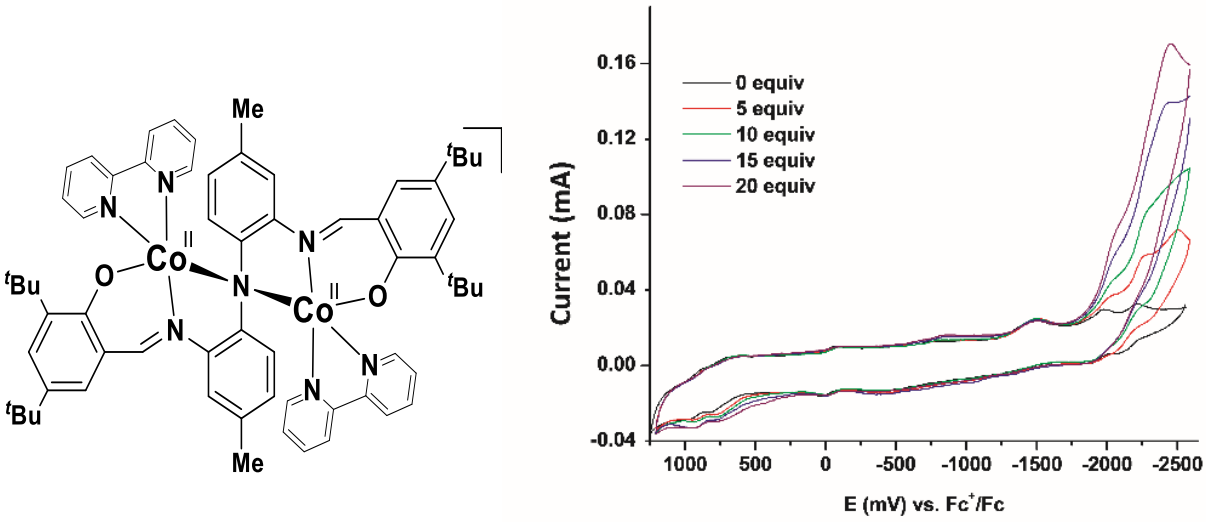

Figure 6.3. $[Co^{II}_2(L^{1'})(bpy)_2]ClO_4$ and its catalytic response to H^+ in CH_3CN.

Each metal center is a five-coordinate Co^{II} bonded to two N atoms and the O atom of a phenolate, with a bidentate bipyridine (bpy) completing the coordination. **$[Co^{II}_2(L^{1'})(bpy)_2]ClO_4$** supports the catalytic reduction of H^+ to H_2 in CH_3CN in the presence of a weak acid such as HOAc at an overpotential of 0.63 V. This catalytic activity relies on a $2e^-$ reduction of the parent species $[Co^{II}Co^{II}]$ to form a $[Co^{I}Co^{I}]$ complex with each of these Co^{I} centers contributing cooperatively with the donation of $1e^-$ to an incoming H^+, thus forming a reactive Co(II)-hydride.

www.manaraa.com

The novel bimetallic cooperativity exhibited by this system arises from the close proximity of the cobalt centers and an appropriate orbital topology that allows interaction between the frontier orbitals and facilitate intramolecular electron transfer between the two centers thus avoiding the formation of the Co^{III}–H^- moiety required for proton reduction in monometallic catalysts. The second Co^I center plays a pivotal role in the catalytic reduction of H^+, acting as an electron reservoir to donate the second electron necessary for formation of the Co^{II}–H^- unit that favorably accepts another H^+ and releases H_2 **(Figure 6.4)**.

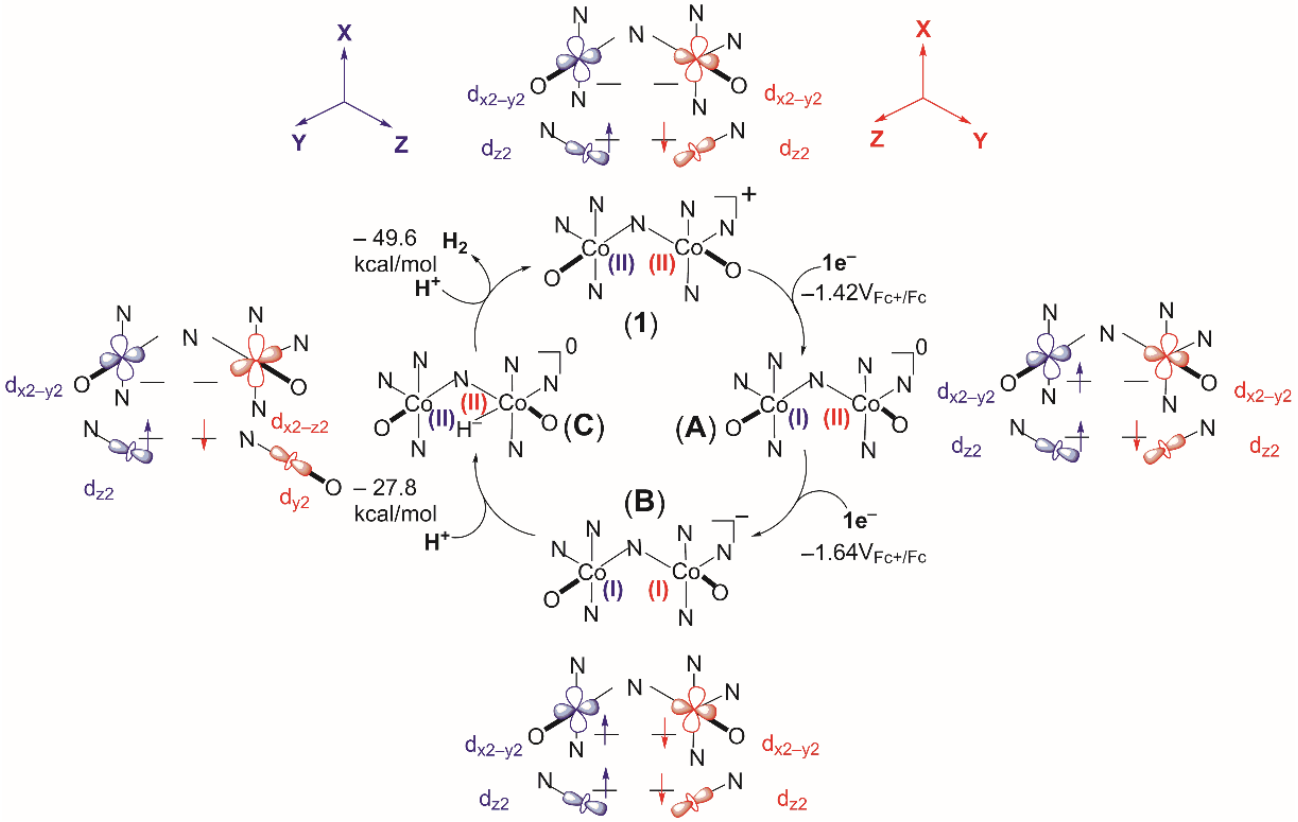

Figure 6.4. Catalytic mechanism of H_2 generation by **$[Co^{II}_2(L^{1'})(bpy)_2]ClO_4$** in CH_3CN.

Post-catalytic SEM and EDX analyses support the molecular nature of the catalyst. I utilized a wide array of experimental techniques aided by extensive theoretical computations to conclude that (i) topology, (ii) orbital overlap, and (iii) oxidation states play relevant roles in a cooperative mechanism and not merely the distance between two metals. Being the first report of

www.manaraa.com

the evaluation of mechanistic cooperativity for proton reduction,[233] the implications of this study are essential to the design of ligand platforms that can support the appropriate topology, afford the crucial orbital overlap necessary for cooperative catalysis, and ensure that the metals used maintain low oxidation states, which is essential for affordable catalytic proton and water reduction

In Chapter 5, the principal objective was to investigate whether the coordination environments around a manganese center can determine high-valent states relevant for electrocatalytic water oxidation. I synthesized two manganese complexes, the hexacoordinate [$Mn^{III}L^{1}CH_3OH$] and the pentacoordinate [$Mn^{III}L^{2}$] using [N_2O_3] pentadentate ligands containing three phenolate donors, and probed the implications of valence tautomerism in these complexes on water oxidation **(Figure 6.5)**.

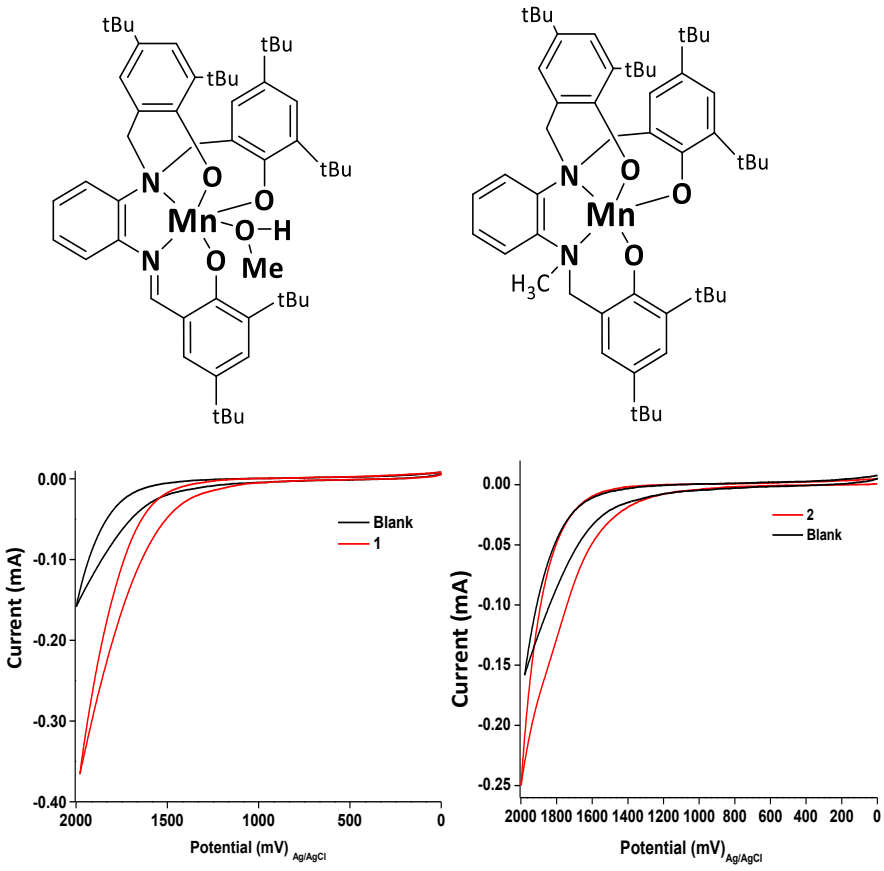

Figure 6.5. [$Mn^{III}L^{1}CH_3OH$] (1) and**[$Mn^{III}L^{2}$] (2)** and their respective catalytic responses to water oxidation.

www.manaraa.com

Detailed structural, electrochemical, and spectroscopic measurements suggest that whilst both complexes show ligand-based oxidations favoring formation of a [Mn^{III}/phenoxyl] species, the hexacoordinate analog could form a [Mn^{IV}/phenolate] species. This is specifically due to the low energy difference between the frontier orbitals (<5 kcal/mol) of the metal center, and the redox-active phenolate ligands. This low energy barrier allows electronic interaction between the Mn ion, and the phenolate ligand, causing valence tautomerism through electron transfer. We therefore tested the hexacoordinate [$Mn^{III}L^1CH_3OH$] for water oxidation catalysis and observed an overpotential of 0.77 V and TON of 53 in three hours with the catalyst operating at a Faradaic efficiency of 85%. This study is particularly useful because it provides a basis for ligand design that favors either a radical or a high-valent metal pathway for catalytic water oxidation.

In summary, I have evaluated molecular Earth-abundant monometallic and bimetallic complexes for their efficient activity towards catalytic water reduction and oxidation during the course of my stay in the Verani group and the results are reported in this dissertation. Results from these evaluations are critically important for the future design of molecular catalysts capable of producing dioxygen and dihydrogen as fuels from water using the sun's energy.

www.manaraa.com

APPENDIX A (CHAPTER 4)

Bimetallic Cooperativity in Proton Reduction with an Amido-bridged Cobalt Catalyst

1. Copyright Details

JOHN WILEY AND SONS LICENSE TERMS AND CONDITIONS

Jul 23, 2017

This Agreement between WAYNE STATE UNIVERSITY -- Kenneth KPOGO ("You") and John Wiley and Sons ("John Wiley and Sons") consists of your license details and the terms and conditions provided by John Wiley and Sons and Copyright Clearance Center.

License Number	4154920231119
License date	Jul 23, 2017
Licensed Content Publisher	John Wiley and Sons
Licensed Content Publication	Chemistry - A European Journal
Licensed Content Title	Bimetallic Cooperativity in Proton Reduction with an Amido-Bridged Cobalt Catalyst

www.manaraa.com

Licensed Content Author	Kenneth K. Kpogo, Shivnath Mazumder, Denan Wang, H. Bernhard Schlegel, Adam T. Fiedler, Cláudio N. Verani
Licensed Content Date	Jun 23, 2017
Licensed Content Pages	8
Type of use	Dissertation/Thesis
Requestor type	Author of this Wiley article
Format	Print and electronic
Portion	Full article
Will you be translating?	No
Title of your thesis / dissertation	EVALUATION OF EARTH-ABUNDANT MONOMETALLIC AND BIMETALLIC COMPLEXES FOR CATALYTIC WATER SPLITTING
Expected completion date	Dec 2017
Expected size (number of pages)	206
Requestor Location	WAYNE STATE UNIVERSITY 5101 CASS AVENUE DETROIT, MI 48202

www.manaraa.com

	United		States
	Attn: KENNETH KPOGO		
Publisher Tax ID	EU826007151		
Billing Type	Invoice		
Billing Address	WAYNE	STATE	UNIVERSITY
	5101	CASS	AVENUE
	DETROIT,	MI	48202
	United		States
	Attn: KENNETH KPOGO		
Total	0.00 USD		

Terms and Conditions

TERMS AND CONDITIONS

This copyrighted material is owned by or exclusively licensed to John Wiley & Sons, Inc. or one of its group companies (each a “Wiley Company") or handled on behalf of a society with which a Wiley Company has exclusive publishing rights in relation to a particular work (collectively "WILEY"). By clicking "accept" in connection with completing this licensing transaction, you agree that the following terms and conditions apply to this transaction (along with the billing and payment terms and conditions established by the Copyright Clearance Center Inc., ("CCC's Billing and Payment terms

www.manaraa.com

and conditions"), at the time that you opened your Rights Link account (these are available at any time at http://myaccount.copyright.com).

Terms and Conditions

The materials you have requested permission to reproduce or reuse (the "Wiley Materials") are protected by copyright.

You are hereby granted a personal, non-exclusive, non-sub licensable (on a stand-alone basis), non-transferable, worldwide, limited license to reproduce the Wiley Materials for the purpose specified in the licensing process. This license, **and any CONTENT (PDF or image file) purchased as part of your order,** is for a one-time use only and limited to any maximum distribution number specified in the license. The first instance of republication or reuse granted by this license must be completed within two years of the date of the grant of this license (although copies prepared before the end date may be distributed thereafter). The Wiley Materials shall not be used in any other manner or for any other purpose, beyond what is granted in the license. Permission is granted subject to an appropriate acknowledgement given to the author, title of the material/book/journal and the publisher. You shall also duplicate the copyright notice that appears in the Wiley publication in your use of the Wiley Material. Permission is also granted on the understanding that nowhere in the text is a previously published source acknowledged for all or part of this Wiley Material. Any third party content is expressly excluded from this permission.

With respect to the Wiley Materials, all rights are reserved. Except as expressly granted by the terms of the license, no part of the Wiley Materials may be copied, modified,

www.manaraa.com

adapted (except for minor reformatting required by the new Publication), translated, reproduced, transferred or distributed, in any form or by any means, and no derivative works may be made based on the Wiley Materials without the prior permission of the respective copyright owner.

For STM Signatory Publishers clearing permission under the terms of the STM Permissions Guidelines only, the terms of the license are extended to include subsequent editions and for editions in other languages, provided such editions are for the work as a whole in situ and does not involve the separate exploitation of the permitted figures or extracts, You may not alter, remove or suppress in any manner any copyright, trademark or other notices displayed by the Wiley Materials. You may not license, rent, sell, loan, lease, pledge, offer as security, transfer or assign the Wiley Materials on a stand-alone basis, or any of the rights granted to you hereunder to any other person.

The Wiley Materials and all of the intellectual property rights therein shall at all times remain the exclusive property of John Wiley & Sons Inc, the Wiley Companies, or their respective licensors, and your interest therein is only that of having possession of and the right to reproduce the Wiley Materials pursuant to Section 2 herein during the continuance of this Agreement. You agree that you own no right, title or interest in or to the Wiley Materials or any of the intellectual property rights therein. You shall have no rights hereunder other than the license as provided for above in Section 2. No right, license or interest to any trademark, trade name, service mark or other branding ("Marks") of WILEY or its licensors is granted hereunder, and you agree that you shall not assert any such right, license or interest with respect thereto

www.manaraa.com

NEITHER WILEY NOR ITS LICENSORS MAKES ANY WARRANTY OR REPRESENTATION OF ANY KIND TO YOU OR ANY THIRD PARTY, EXPRESS, IMPLIED OR STATUTORY, WITH RESPECT TO THE MATERIALS OR THE ACCURACY OF ANY INFORMATION CONTAINED IN THE MATERIALS, INCLUDING, WITHOUT LIMITATION, ANY IMPLIED WARRANTY OF MERCHANTABILITY, ACCURACY, SATISFACTORY QUALITY, FITNESS FOR A PARTICULAR PURPOSE, USABILITY, INTEGRATION OR NON-INFRINGEMENT AND ALL SUCH WARRANTIES ARE HEREBY EXCLUDED BY WILEY AND ITS LICENSORS AND WAIVED BY YOU.

WILEY shall have the right to terminate this Agreement immediately upon breach of this Agreement by you.

You shall indemnify, defend and hold harmless WILEY, its Licensors and their respective directors, officers, agents and employees, from and against any actual or threatened claims, demands, causes of action or proceedings arising from any breach of this Agreement by you.

IN NO EVENT SHALL WILEY OR ITS LICENSORS BE LIABLE TO YOU OR ANY OTHER PARTY OR ANY OTHER PERSON OR ENTITY FOR ANY SPECIAL, CONSEQUENTIAL, INCIDENTAL, INDIRECT, EXEMPLARY OR PUNITIVE DAMAGES, HOWEVER CAUSED, ARISING OUT OF OR IN CONNECTION WITH THE DOWNLOADING, PROVISIONING, VIEWING OR USE OF THE MATERIALS REGARDLESS OF THE FORM OF ACTION, WHETHER FOR BREACH OF CONTRACT, BREACH OF WARRANTY, TORT, NEGLIGENCE, INFRINGEMENT OR OTHERWISE (INCLUDING, WITHOUT LIMITATION, DAMAGES BASED ON

www.manaraa.com

LOSS OF PROFITS, DATA, FILES, USE, BUSINESS OPPORTUNITY OR CLAIMS OF THIRD PARTIES), AND WHETHER OR NOT THE PARTY HAS BEEN ADVISED OF THE POSSIBILITY OF SUCH DAMAGES. THIS LIMITATION SHALL APPLY NOTWITHSTANDING ANY FAILURE OF ESSENTIAL PURPOSE OF ANY LIMITED REMEDY PROVIDED HEREIN.

Should any provision of this Agreement be held by a court of competent jurisdiction to be illegal, invalid, or unenforceable, that provision shall be deemed amended to achieve as nearly as possible the same economic effect as the original provision, and the legality, validity and enforceability of the remaining provisions of this Agreement shall not be affected or impaired thereby.

The failure of either party to enforce any term or condition of this Agreement shall not constitute a waiver of either party's right to enforce each and every term and condition of this Agreement. No breach under this agreement shall be deemed waived or excused by either party unless such waiver or consent is in writing signed by the party granting such waiver or consent. The waiver by or consent of a party to a breach of any provision of this Agreement shall not operate or be construed as a waiver of or consent to any other or subsequent breach by such other party.

This Agreement may not be assigned (including by operation of law or otherwise) by you without WILEY's prior written consent.

Any fee required for this permission shall be non-refundable after thirty (30) days from receipt by the CCC.

These terms and conditions together with CCC's Billing and Payment terms and conditions (which are incorporated herein) form the entire agreement between you and

www.manaraa.com

WILEY concerning this licensing transaction and (in the absence of fraud) supersedes all prior agreements and representations of the parties, oral or written. This Agreement may not be amended except in writing signed by both parties. This Agreement shall be binding upon and inure to the benefit of the parties' successors, legal representatives, and authorized assigns.

In the event of any conflict between your obligations established by these terms and conditions and those established by CCC's Billing and Payment terms and conditions, these terms and conditions shall prevail.

WILEY expressly reserves all rights not specifically granted in the combination of (i) the license details provided by you and accepted in the course of this licensing transaction, (ii) these terms and conditions and (iii) CCC's Billing and Payment terms and conditions. This Agreement will be void if the Type of Use, Format, Circulation, or Requestor Type was misrepresented during the licensing process.

This Agreement shall be governed by and construed in accordance with the laws of the State of New York, USA, without regards to such state's conflict of law rules. Any legal action, suit or proceeding arising out of or relating to these Terms and Conditions or the breach thereof shall be instituted in a court of competent jurisdiction in New York County in the State of New York in the United States of America and each party hereby consents and submits to the personal jurisdiction of such court, waives any objection to venue in such court and consents to service of process by registered or certified mail, return receipt requested, at the last known address of such party.

WILEY OPEN ACCESS TERMS AND CONDITIONS

www.manaraa.com

Wiley Publishes Open Access Articles in fully Open Access Journals and in Subscription journals offering Online Open. Although most of the fully Open Access journals publish open access articles under the terms of the Creative Commons Attribution (CC BY) License only, the subscription journals and a few of the Open Access Journals offer a choice of Creative Commons Licenses. The license type is clearly identified on the article.

The Creative Commons Attribution License

The Creative Commons Attribution License (CC-BY) allows users to copy, distribute and transmit an article, adapt the article and make commercial use of the article. The CC-BY license permits commercial and non-

Creative Commons Attribution Non-Commercial License

The Creative Commons Attribution Non-Commercial (CC-BY-NC)License permits use, distribution and reproduction in any medium, provided the original work is properly cited and is not used for commercial purposes.(see below)

Creative Commons Attribution-Non-Commercial-NoDerivs License

The Creative Commons Attribution Non-Commercial-NoDerivs License (CC-BY-NC-ND) permits use, distribution and reproduction in any medium, provided the original work is properly cited, is not used for commercial purposes and no modifications or adaptations are made. (see below)

Use by commercial "for-profit" organizations

Use of Wiley Open Access articles for commercial, promotional, or marketing purposes requires further explicit permission from Wiley and will be subject to a fee.

Further details can be found on Wiley Online Library http://olabout.wiley.com/WileyCDA/Section/id-410895.html

www.manaraa.com

Other Terms and Conditions:

v1.10 Last updated September 2015

Questions? customercare@copyright.com or +1-855-239-3415 (toll free in the US) or +1-978-646-2777.

2. Results from DFT Calculations

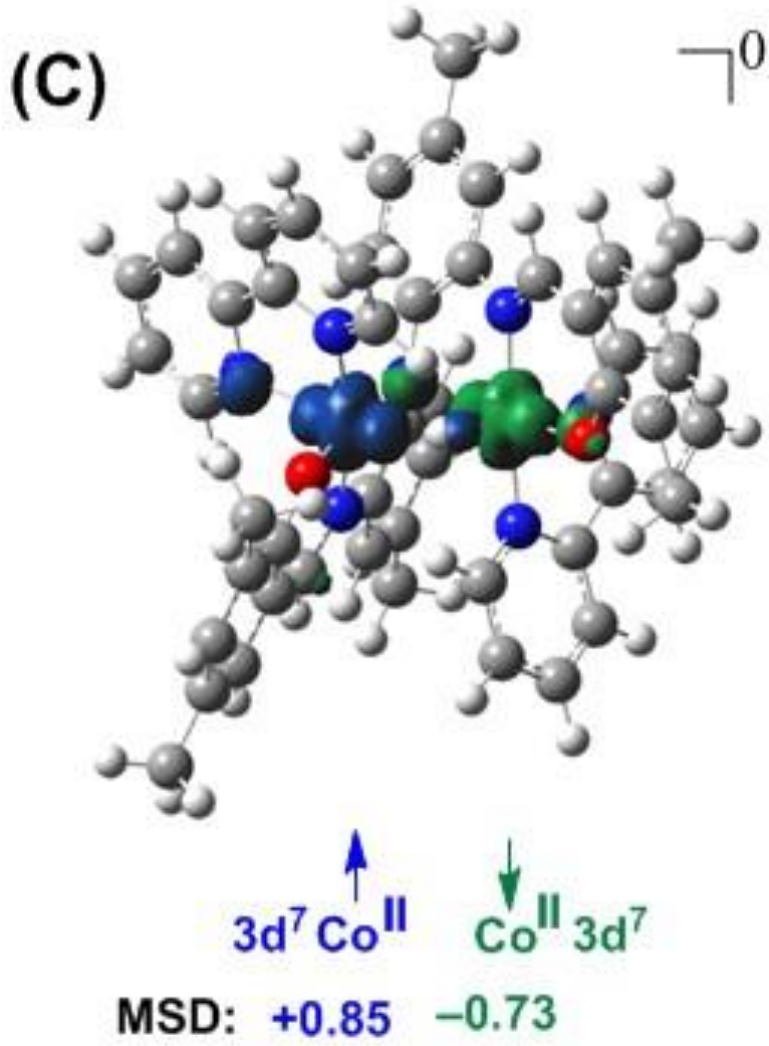

Figure A1. Spin density plot (isovalue = 0.004 au) with Mulliken spin density (MSD) values for $[Co^{II}(H^{-})Co^{II}]$ complex **C.**

www.manaraa.com

Table A1. The XYZ coordinates of the calculated structures

Complex 1

C	-3.951477000	-1.891537000	-5.683427000
C	-1.807016000	-0.739353000	-4.948893000
C	-3.143563000	-1.107098000	-4.673090000
C	-1.061485000	0.010015000	-4.036197000
C	2.099288000	-3.170152000	-3.579661000
C	0.514639000	3.992578000	-3.848998000
C	2.759769000	-1.944622000	-3.408098000
C	2.737539000	5.221416000	-3.708622000
C	-4.324957000	4.777346000	-2.867479000
C	-3.677739000	5.953272000	-2.459893000
C	-0.377411000	3.007615000	-3.418425000
C	-3.704631000	-0.705685000	-3.451762000
C	0.936086000	-3.419010000	-2.845266000
C	1.759857000	4.180988000	-3.208076000
C	-1.631463000	0.420849000	-2.814755000
C	-3.948918000	3.566872000	-2.277559000
C	-2.965367000	0.059090000	-2.522814000
C	-2.691630000	5.873696000	-1.472255000
C	2.220955000	-1.012316000	-2.516419000
C	-0.052453000	2.175708000	-2.328713000
C	0.461069000	-2.440704000	-1.953768000
C	2.075731000	3.358336000	-2.116495000
C	-2.376551000	4.622780000	-0.912044000
C	1.184414000	2.357734000	-1.671148000
C	-1.413988000	-3.820237000	-0.928108000
C	-0.717974000	-2.608821000	-1.081881000
C	-4.629095000	0.197210000	-0.808628000
C	-2.455075000	-3.906993000	0.000655000
C	-1.397555000	4.419042000	0.173743000
C	-0.787988000	5.466252000	0.886035000
C	2.446864000	1.603262000	0.215847000
C	-2.769742000	-2.779109000	0.769861000
C	-2.049737000	-1.599159000	0.560363000
C	-5.191291000	0.555112000	0.447694000
C	-6.514176000	0.102609000	0.748541000
C	0.047211000	5.173508000	1.967994000
C	-0.380142000	2.836495000	1.569615000
C	-4.449073000	1.299390000	1.433094000
C	2.752646000	0.814688000	1.359556000
C	0.243770000	3.833268000	2.325735000
C	-7.115186000	0.356885000	1.971033000
C	-8.518673000	-0.104721000	2.291310000
C	1.879203000	-0.235071000	1.818501000
C	3.937484000	1.124931000	2.097945000
C	-5.065111000	1.545387000	2.710033000
C	-6.356552000	1.080918000	2.937277000
C	2.228042000	-0.936990000	3.025105000
C	4.280137000	0.440764000	3.253438000
C	1.318133000	-2.031770000	3.521989000
C	3.397046000	-0.588791000	3.693786000
C	5.535871000	0.754368000	4.034798000
C	-4.293597000	2.308774000	3.756790000
H	-4.169304000	-1.284834000	-6.578057000
H	-3.405289000	-2.783646000	-6.028617000
H	-1.349058000	-1.042364000	-5.894431000
H	-4.912588000	-2.225002000	-5.266738000
H	2.484335000	-3.920378000	-4.273097000
H	0.246875000	4.621721000	-4.702309000
H	-0.032202000	0.289260000	-4.266107000
H	-3.937216000	6.916613000	-2.903291000
H	3.166861000	4.929891000	-4.681664000
H	-5.106729000	4.792710000	-3.628685000
H	2.246699000	6.196313000	-3.855574000
H	3.675326000	-1.710369000	-3.953740000
H	-1.329757000	2.868801000	-3.932396000
H	0.403611000	-4.362737000	-2.968324000
H	-4.741513000	-0.979495000	-3.245432000
H	3.572681000	5.366409000	-3.008382000
H	-4.417514000	2.624034000	-2.565089000
H	-2.171137000	6.774895000	-1.146236000
H	-1.124606000	-4.696398000	-1.508831000
H	2.692818000	-0.041536000	-2.354540000
H	3.046566000	3.490225000	-1.634464000
H	-5.250488000	-0.456835000	-1.431675000
H	-0.989018000	6.502970000	0.615176000
H	-2.997046000	-4.845351000	0.134544000
H	-7.058221000	-0.458004000	-0.019238000
H	3.131982000	2.436851000	0.021823000
H	-3.558249000	-2.801131000	1.523020000
H	0.519242000	5.979516000	2.533437000
H	-2.258190000	-0.694859000	1.133252000
H	4.585108000	1.926453000	1.726876000
H	-0.257169000	1.779777000	1.809254000
H	0.868107000	3.551993000	3.174536000
H	-6.815444000	1.288193000	3.910203000
H	3.652865000	-1.138840000	4.605981000
Co	-2.250355000	1.763026000	-0.417932000
Co	0.134366000	0.047288000	-0.497465000
N	-0.923875000	1.160753000	-1.809047000
N	1.098860000	-1.244316000	-1.803110000
N	-2.998657000	3.480574000	-1.323189000
N	-3.436380000	0.544583000	-1.275141000
N	-1.062065000	-1.500601000	-0.357505000
N	1.410298000	1.454425000	-0.599288000
N	-1.163212000	3.111913000	0.502590000
O	-3.232132000	1.750827000	1.234646000
O	0.768454000	-0.573029000	1.204929000
H	6.092727000	1.589282000	3.585538000
H	5.304587000	1.027285000	5.077623000
H	6.212673000	-0.115134000	4.075257000
H	1.713938000	-2.490155000	4.439194000
H	0.307659000	-1.646633000	3.734734000
H	1.195301000	-2.820618000	2.762581000
H	-3.996502000	3.302434000	3.384719000
H	-4.890473000	2.442418000	4.669835000
H	-3.360585000	1.787285000	4.025860000
H	-8.537912000	-0.750382000	3.184708000
H	-9.185286000	0.748483000	2.499669000
H	-8.955949000	-0.673039000	1.457738000

==========

Complex A

C	-4.154663000	-1.710038000	-5.781181000
C	-1.897384000	-0.806544000	-5.032106000
C	-3.265551000	-1.025840000	-4.764453000
C	-1.090922000	-0.138566000	-4.107685000
C	1.953436000	-3.274462000	-3.552647000
C	0.576171000	3.860282000	-4.009580000
C	2.680916000	-2.084560000	-3.387450000
C	2.658661000	5.299178000	-3.726022000
C	-4.038342000	4.926390000	-2.942650000
C	-3.415015000	6.106681000	-2.490079000
C	-0.270386000	2.826066000	-3.615038000
C	-3.779196000	-0.578523000	-3.538953000
C	0.799897000	-3.471702000	-2.788923000
C	1.751943000	4.170558000	-3.284399000
C	-1.608340000	0.334047000	-2.881732000
C	-3.713307000	3.718722000	-2.329390000
C	-2.976948000	0.081391000	-2.577592000
C	-2.506067000	6.017503000	-1.434677000
C	2.216619000	-1.137949000	-2.470064000

www.manaraa.com

C	0.028530000	2.041843000	-2.472956000
C	0.402934000	-2.482185000	-1.870554000
C	2.048313000	3.401629000	-2.152378000
C	-2.235088000	4.768187000	-0.844282000
C	1.215919000	2.333484000	-1.750433000
C	-1.493021000	-3.776861000	-0.774467000
C	-0.768118000	-2.589773000	-0.981301000
C	-4.582305000	0.111147000	-0.835582000
C	-2.534928000	-3.794978000	0.156932000
C	-1.335541000	4.565179000	0.296771000
C	-0.813916000	5.610351000	1.083267000
C	2.499392000	1.600207000	0.133541000
C	-2.821252000	-2.625458000	0.874488000
C	-2.071547000	-1.473404000	0.615185000
C	-5.155607000	0.416512000	0.438507000
C	-6.445488000	-0.133307000	0.717145000
C	-0.025691000	5.315684000	2.197091000
C	-0.326824000	2.976788000	1.689922000
C	-4.469294000	1.177991000	1.464184000
C	2.793222000	0.842025000	1.306114000
C	0.213108000	3.965249000	2.512452000
C	-7.085669000	0.041952000	1.934935000
C	-8.458878000	-0.529134000	2.212142000
C	1.885849000	-0.148642000	1.823857000
C	4.002110000	1.124994000	2.010405000
C	-5.137110000	1.339759000	2.737504000
C	-6.397785000	0.789470000	2.934674000
C	2.225715000	-0.807932000	3.057303000
C	4.338109000	0.477025000	3.191168000
C	1.270324000	-1.831928000	3.616666000
C	3.420988000	-0.488199000	3.694921000
C	5.623076000	0.774042000	3.932571000
C	-4.428692000	2.122027000	3.814445000
H	-4.220401000	-1.129224000	-6.716602000
H	-3.766496000	-2.706212000	-6.051708000
H	-1.464971000	-1.151533000	-5.976172000
H	-5.177832000	-1.843169000	-5.399953000
H	2.276711000	-4.032482000	-4.269363000
H	0.318907000	4.450649000	-4.894372000
H	-0.038200000	0.043171000	-4.333882000
H	-3.632785000	7.070560000	-2.955022000
H	3.059747000	5.126645000	-4.739278000
H	-4.764211000	4.943337000	-3.758167000
H	2.121758000	6.262270000	-3.756162000
H	3.590395000	-1.889660000	-3.958843000
H	-1.181332000	2.621595000	-4.179225000
H	0.205840000	-4.378116000	-2.914942000
H	-4.844738000	-0.723371000	-3.344039000
H	3.515542000	5.418620000	-3.046207000
H	-4.165931000	2.777120000	-2.646768000
H	-1.997568000	6.913099000	-1.073118000
H	-1.222606000	-4.684200000	-1.316028000
H	2.737650000	-0.191377000	-2.311900000
H	2.952301000	3.640218000	-1.587340000
H	-5.165594000	-0.610070000	-1.429283000
H	-1.049056000	6.647426000	0.837455000
H	-3.102842000	-4.711728000	0.330569000
H	-6.940235000	-0.708921000	-0.074564000
H	3.224943000	2.385129000	-0.111851000
H	-3.617350000	-2.588191000	1.618768000
H	0.379977000	6.118123000	2.817241000
H	-2.265549000	-0.534380000	1.137093000
H	4.675734000	1.884188000	1.597069000
H	-0.160021000	1.917584000	1.893113000
H	0.812964000	3.678355000	3.377886000
H	-6.885556000	0.937944000	3.905583000
H	3.666092000	-1.008003000	4.628324000
Co	-2.220517000	1.911879000	-0.410328000
Co	0.148831000	0.070102000	-0.505380000
N	-0.808461000	1.042871000	-1.940834000
N	1.108642000	-1.323112000	-1.721761000
N	-2.832314000	3.615329000	-1.301743000
N	-3.433322000	0.554599000	-1.326658000
N	-1.081037000	-1.443235000	-0.303684000
N	1.442590000	1.465143000	-0.656456000
N	-1.075114000	3.246436000	0.590040000
O	-3.285368000	1.698396000	1.311921000
O	0.757269000	-0.472757000	1.238415000
H	6.208451000	1.554991000	3.424543000
H	5.428983000	1.120240000	4.962051000
H	6.263354000	-0.121054000	4.013691000
H	1.661843000	-2.276190000	4.543713000
H	0.286915000	-1.383474000	3.833544000
H	1.084433000	-2.639829000	2.890514000
H	-4.200557000	3.145301000	3.474634000
H	-5.036231000	2.181081000	4.729913000
H	-3.457485000	1.664857000	4.065480000
H	-8.452225000	-1.209362000	3.081373000
H	-9.193607000	0.263447000	2.436167000
H	-8.838766000	-1.096893000	1.349312000

==========

Complex B

C	-4.319398000	-1.430997000	-5.828205000
C	-2.058631000	-0.501166000	-5.107525000
C	-3.413942000	-0.768152000	-4.811295000
C	-1.232903000	0.141483000	-4.184266000
C	2.015408000	-3.413404000	-3.697098000
C	0.776486000	3.864086000	-3.987597000
C	2.650371000	-2.157433000	-3.550427000
C	3.100169000	4.903495000	-3.867525000
C	-4.169841000	5.050811000	-2.940678000
C	-3.550721000	6.245163000	-2.502449000
C	-0.187653000	2.958501000	-3.543495000
C	-3.891011000	-0.391241000	-3.548603000
C	0.893486000	-3.683511000	-2.915094000
C	2.033193000	3.961719000	-3.349829000
C	-1.710542000	0.551015000	-2.913014000
C	-3.817586000	3.851720000	-2.330288000
C	-3.067838000	0.241177000	-2.588490000
C	-2.617793000	6.167671000	-1.469095000
C	2.125985000	-1.244169000	-2.642069000
C	0.045826000	2.101931000	-2.437351000
C	0.416183000	-2.721987000	-2.000152000
C	2.264858000	3.141482000	-2.237273000
C	-2.312329000	4.923457000	-0.879815000
C	1.296195000	2.230956000	-1.755650000
C	-1.393036000	-4.151153000	-0.932595000
C	-0.735680000	-2.916302000	-1.120908000
C	-4.572911000	0.109082000	-0.765724000
C	-2.446017000	-4.247669000	-0.023743000
C	-1.369058000	4.736610000	0.222062000
C	-0.794696000	5.790325000	0.964335000
C	2.410181000	1.632416000	0.248987000
C	-2.822076000	-3.096758000	0.700554000
C	-2.138732000	-1.904962000	0.463236000
C	-5.119769000	0.394951000	0.530205000
C	-6.347048000	-0.242134000	0.876980000
C	0.050699000	5.506076000	2.036343000
C	-0.290133000	3.160798000	1.583488000
C	-4.444721000	1.223345000	1.509916000
C	2.676911000	0.890078000	1.448531000
C	0.302306000	4.156251000	2.359647000
C	-6.950684000	-0.087785000	2.119758000
C	-8.265437000	-0.755284000	2.461227000
C	1.816446000	-0.173732000	1.927908000
C	3.798379000	1.291679000	2.231551000
C	-5.071890000	1.362605000	2.807479000
C	-6.281965000	0.729948000	3.072858000
C	2.154141000	-0.779633000	3.198693000
C	4.125629000	0.690557000	3.441743000
C	1.258926000	-1.879155000	3.712167000
C	3.275294000	-0.352837000	3.902781000
C	5.333636000	1.115822000	4.248350000
C	-4.371833000	2.213237000	3.837218000
H	-4.384164000	-0.849108000	-6.764496000
H	-3.956322000	-2.436585000	-6.104728000
H	-1.647141000	-0.797246000	-6.078480000
H	-5.342957000	-1.546646000	-5.439415000
H	2.388017000	-4.152740000	-4.410237000
H	0.553565000	4.506018000	-4.846640000
H	-0.190152000	0.341614000	-4.437212000
H	-3.789365000	7.205543000	-2.965821000
H	3.520208000	4.564298000	-4.831823000
H	-4.910838000	5.054825000	-3.743366000
H	2.699910000	5.917917000	-4.035722000
H	3.535583000	-1.895257000	-4.134485000
H	-1.151557000	2.898805000	-4.051771000
H	0.371128000	-4.637115000	-3.019071000
H	-4.945846000	-0.563617000	-3.315766000
H	3.938161000	4.991291000	-3.158679000
H	-4.262387000	2.902124000	-2.636569000
H	-2.110109000	7.070315000	-1.121929000
H	-1.060646000	-5.034839000	-1.481678000
H	2.578946000	-0.260131000	-2.500037000
H	3.241688000	3.191184000	-1.747470000
H	-5.099508000	-0.686965000	-1.318368000
H	-1.031437000	6.826404000	0.712661000
H	-2.957778000	-5.200979000	0.131799000
H	-6.828014000	-0.873781000	0.119324000
H	3.038147000	2.529855000	0.119617000
H	-3.635277000	-3.117392000	1.428258000
H	0.496722000	6.315730000	2.619776000
H	-2.400897000	-0.988089000	0.994104000
H	4.422892000	2.108897000	1.848770000
H	-0.116030000	2.103346000	1.791596000
H	0.953003000	3.877075000	3.190204000
H	-6.737067000	0.865720000	4.062393000
H	3.510168000	-0.841092000	4.857288000
Co	-2.268407000	2.055261000	-0.442937000
Co	0.133192000	-0.188209000	-0.608247000
N	-0.906158000	1.187091000	-1.946340000
N	1.034588000	-1.490515000	-1.868995000

www.manaraa.com

N	-2.913306000	3.757596000	-1.319630000
N	-3.501240000	0.655562000	-1.311481000
N	-1.126601000	-1.788372000	-0.431279000
N	1.475610000	1.375513000	-0.648113000
N	-1.099936000	3.419565000	0.527203000
O	-3.310031000	1.821974000	1.300068000
O	0.758479000	-0.592903000	1.299506000
H	5.841097000	1.976277000	3.784535000
H	5.061130000	1.408892000	5.277955000
H	6.079114000	0.304909000	4.338754000
H	1.609322000	-2.260290000	4.684388000
H	0.220733000	-1.525548000	3.824058000
H	1.212318000	-2.718247000	2.998432000
H	-4.215993000	3.238846000	3.464091000
H	-4.946226000	2.259789000	4.775852000
H	-3.365391000	1.820708000	4.058064000
H	-8.180301000	-1.409350000	3.347500000
H	-9.057815000	-0.019245000	2.688463000
H	-8.625716000	-1.377122000	1.626754000

==========

Complex C

C	-4.153755000	-1.825119000	-5.626349000
C	-2.099237000	-0.411265000	-5.108478000
C	-3.339148000	-0.954179000	-4.693899000
C	-1.334881000	0.390739000	-4.261920000
C	2.018149000	-2.992001000	-3.757397000
C	0.879487000	4.027705000	-3.823643000
C	2.585981000	-1.722593000	-3.553693000
C	3.244593000	4.918739000	-3.523313000
C	-4.283331000	4.629950000	-3.112538000
C	-3.525162000	5.792990000	-2.904228000
C	-0.162778000	3.170809000	-3.461507000
C	-3.785415000	-0.661121000	-3.398345000
C	0.898917000	-3.351719000	-3.004784000
C	2.099365000	4.017437000	-3.113589000
C	-1.789465000	0.702639000	-2.954924000
C	-4.030878000	3.513769000	-2.307786000
C	-3.041597000	0.169795000	-2.532276000
C	-2.559307000	5.795176000	-1.893913000
C	2.006071000	-0.867571000	-2.615475000
C	-0.040777000	2.275410000	-2.374977000
C	0.364613000	-2.443942000	-2.072100000
C	2.222907000	3.140642000	-2.025705000
C	-2.382862000	4.639073000	-1.110136000
C	1.169234000	2.286503000	-1.619696000
C	-1.423379000	-3.963402000	-1.097494000
C	-0.785390000	-2.714929000	-1.206560000
C	-4.589552000	0.231563000	-0.711071000
C	-2.467712000	-4.131537000	-0.186742000
C	-1.434984000	4.546490000	0.017645000
C	-0.919662000	5.672957000	0.683862000
C	2.167125000	1.600624000	0.410220000
C	-2.841049000	-3.038812000	0.613476000
C	-2.177444000	-1.821999000	0.455661000
C	-5.067849000	0.536213000	0.598459000
C	-6.355060000	0.045100000	0.974715000
C	-0.101779000	5.498128000	1.803567000
C	-0.378481000	3.118515000	1.535052000
C	-4.295705000	1.302038000	1.545645000
C	2.498348000	0.788534000	1.533487000
C	0.165161000	4.194416000	2.243498000
C	-6.892884000	0.261189000	2.235581000
C	-8.256058000	-0.264378000	2.628555000
C	1.881923000	-0.497206000	1.805345000
C	3.500729000	1.291945000	2.423342000
C	-4.852723000	1.517676000	2.858081000
C	-6.108521000	1.003382000	3.163768000
C	2.331182000	-1.219562000	2.980896000
C	3.920746000	0.594713000	3.543879000
C	1.700579000	-2.557481000	3.270676000
C	3.310845000	-0.671675000	3.795456000
C	4.985951000	1.129520000	4.475101000
C	-4.046236000	2.305107000	3.859926000
H	-4.473027000	-1.272045000	-6.526402000
H	-3.576462000	-2.696989000	-5.977820000
H	-1.723219000	-0.635775000	-6.111572000
H	-5.061060000	-2.205117000	-5.133414000
H	2.440944000	-3.685501000	-4.487449000
H	0.749806000	4.705578000	-4.672769000
H	-0.369063000	0.772227000	-4.596159000
H	-3.678078000	6.679194000	-3.524301000
H	3.513881000	4.776619000	-4.582971000
H	-5.055772000	4.584820000	-3.882848000
H	2.983424000	5.983798000	-3.401109000
H	3.464818000	-1.395464000	-4.112406000
H	-1.099490000	3.181125000	-4.022532000
H	0.436331000	-4.330258000	-3.141983000
H	-4.732417000	-1.094408000	-3.067292000
H	4.144962000	4.728330000	-2.920643000
H	-4.586688000	2.582632000	-2.437898000
H	-1.935231000	6.674966000	-1.728214000
H	-1.086649000	-4.801741000	-1.709150000
H	2.412854000	0.126439000	-2.427039000
H	3.181801000	3.094946000	-1.503325000
H	-5.285190000	-0.337237000	-1.341159000
H	-1.192632000	6.674781000	0.349273000
H	-2.969478000	-5.096770000	-0.090719000
H	-6.924977000	-0.527901000	0.233981000
H	2.723576000	2.547721000	0.357151000
H	-3.639989000	-3.118200000	1.352334000
H	0.299135000	6.363711000	2.335922000
H	-2.432473000	-0.948343000	1.052371000
H	3.951590000	2.264543000	2.191874000
H	-0.207187000	2.084387000	1.834764000
H	0.783974000	4.000992000	3.121087000
H	-6.512594000	1.183816000	4.166769000
H	3.632287000	-1.239093000	4.677149000
Co	-2.156774000	1.755096000	-0.387516000
Co	-0.017012000	-0.105532000	-0.494714000
N	-1.067959000	1.395984000	-1.983001000
N	0.915051000	-1.199775000	-1.885942000
N	-3.107203000	3.505962000	-1.325342000
N	-3.410080000	0.556034000	-1.224083000
N	-1.181248000	-1.637568000	-0.448174000
N	1.265311000	1.378230000	-0.539905000
N	-1.140447000	3.278031000	0.430767000
O	-3.122003000	1.816788000	1.284691000
O	0.963758000	-1.026852000	1.065829000
H	5.342270000	2.119156000	4.151100000
H	4.612254000	1.232643000	5.508591000
H	5.862771000	0.460541000	4.521158000
H	2.108014000	-3.000457000	4.191787000
H	0.607439000	-2.464636000	3.376481000
H	1.864973000	-3.262438000	2.438976000
H	-3.824794000	3.317614000	3.484268000
H	-4.580590000	2.395774000	4.817216000
H	-3.069771000	1.829178000	4.047563000
H	-8.199782000	-0.931904000	3.505546000
H	-8.948211000	0.552689000	2.895724000
H	-8.717948000	-0.833731000	1.807867000
H	-0.945698000	0.653413000	0.467688000

==========

www.manaraa.com

APPENDIX B (CHAPTER 5)

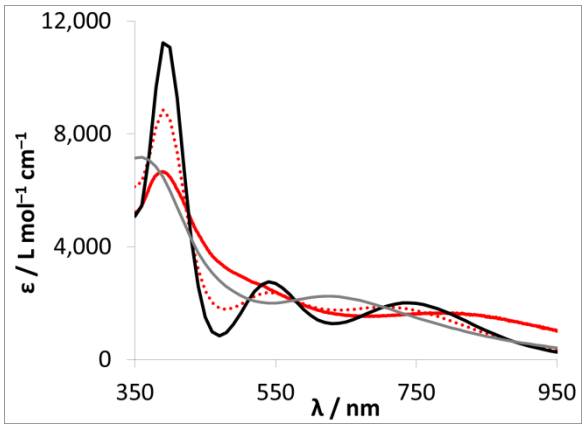

Figure B1. Plot of TD-DFT predicted spectrum of isomer 1 (black) and isomer 2 (gray) for species **2**.

Neither individual isomer's spectrum matched the intensities well for the experimental spectrum (solid red). These two species are predicted to be isoenergetic $\Delta G \sim 0.4$ kcal mol^{-1}, so we averaged their spectra (dotted red), and this average spectrum matches experiment quite well.

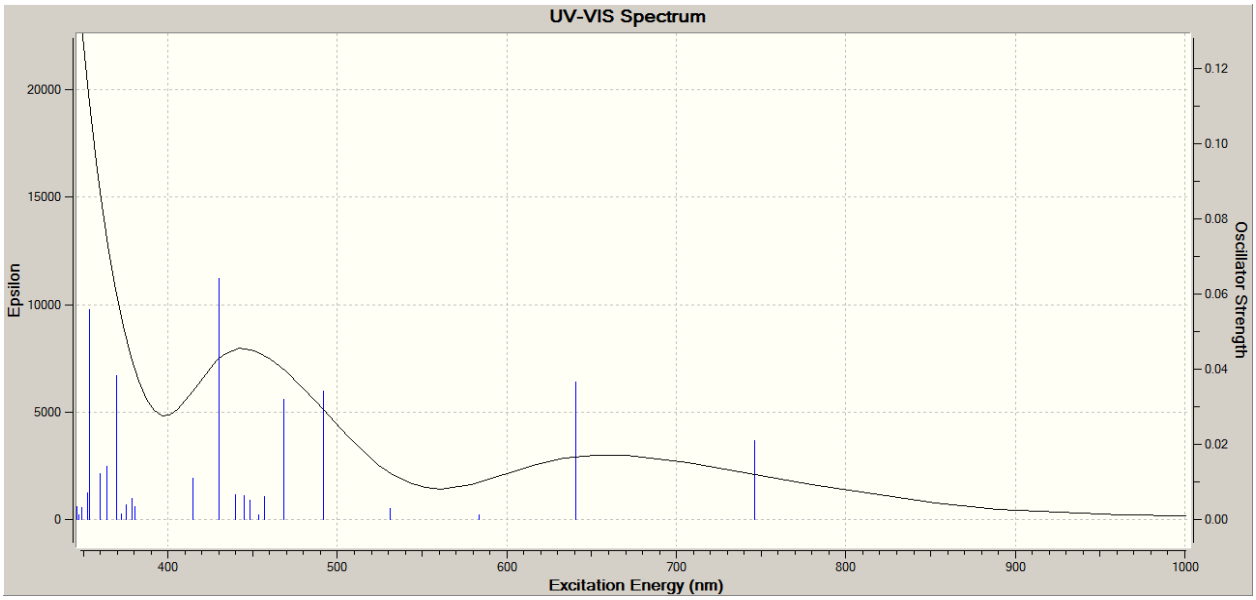

www.manaraa.com

Figure B2. Simulated UV-visible spectrum for **1** with individual transitions shown as sticks. A half-width at half-max of 0.2 eV was employed for the Gaussian fittings.

Table B1. Assignments for TD-DFT transitions of **1**. Contributions > 10% are shown. Orbitals are only listed once with label, then labels are repeated thereafter.

Excited State	**λ / nm**	**Osc. Str.**	**% Cont.**	**Occ. MO**	**Unocc. MO**
2	746	0.0211	43	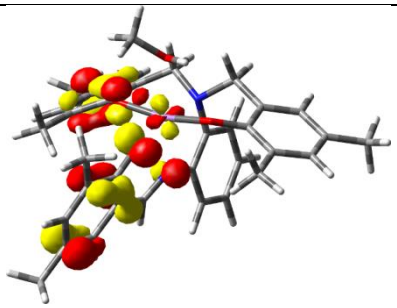 157α	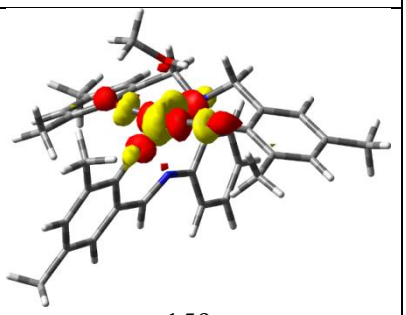 159α
			31	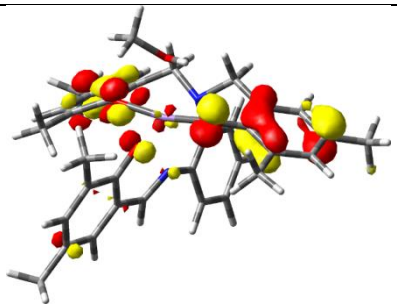 158α	159α
			18	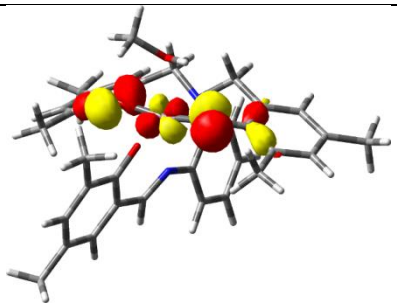 151α	159α
3	640	0.0367	64	158α	159α
			21	157α	159α
			10	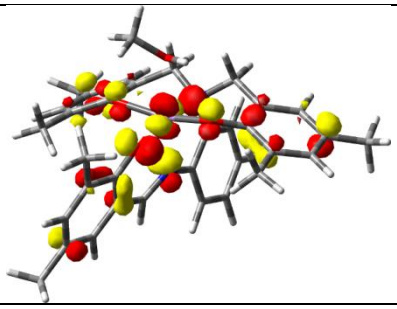	159α

www.manaraa.com

				156α	
6	492	0.0342	63	151α	159α
			17	157α	159α
			10	156α	159α
7	468	0.0320	44	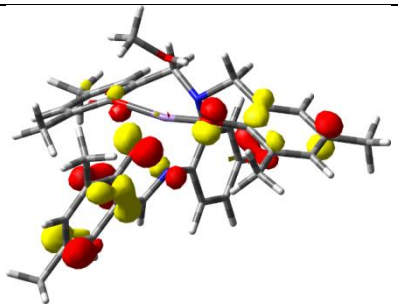 154β	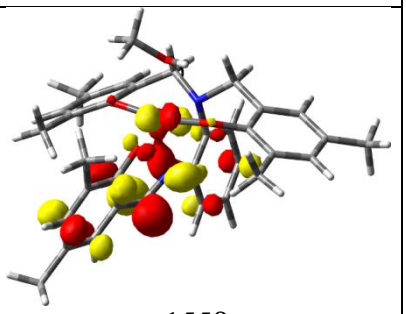 155β
			21	157α	159α
			16	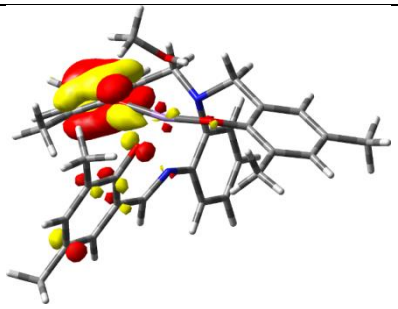 153β	155β
13	430	0.0640	35	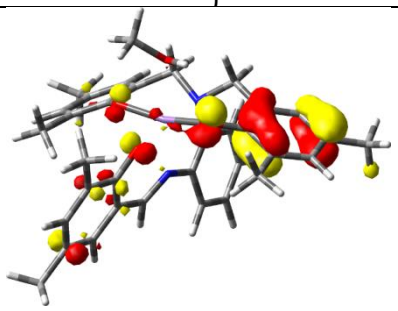 152β	155β

www.manaraa.com

			19	157α	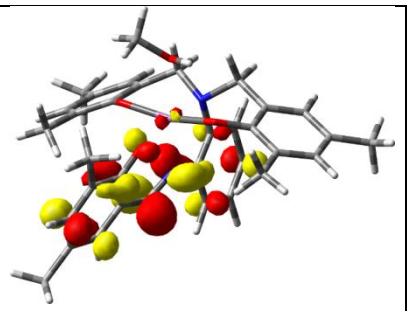 160α
			15	156α	160α
			10	153β	155β

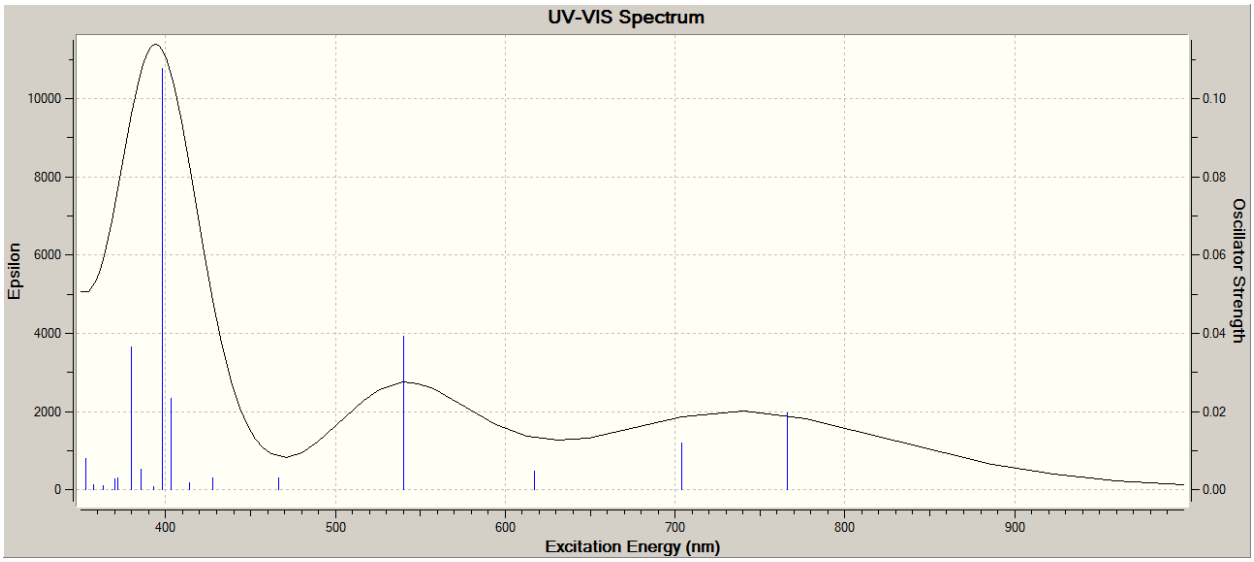

Figure B3. Simulated UV-visible spectrum for isomer 1 of **2** with individual transitions shown as sticks. A half-width at half-max of 0.2 eV was employed for the Gaussian fittings.

www.manaraa.com

Table B2. Assignments for TD-DFT transitions of Isomer 1 for **2**. Contributions > 10% are shown. Orbitals are only listed once with label, then labels are repeated thereafter.

Excited State	**λ / nm**	**Osc. Str.**	**% Cont.**	**Occ. MO**	**Unocc. MO**
1	766	0.0196	44	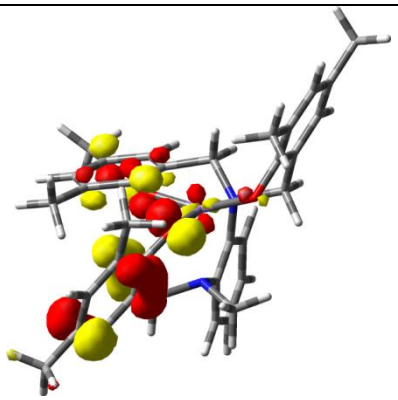 154α	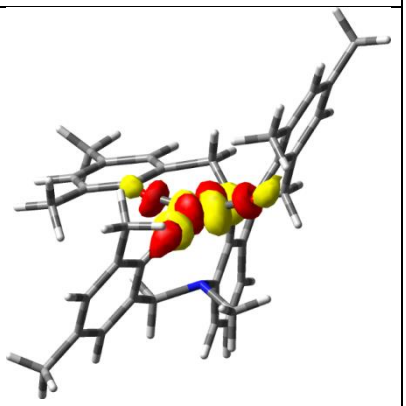 155α
			19	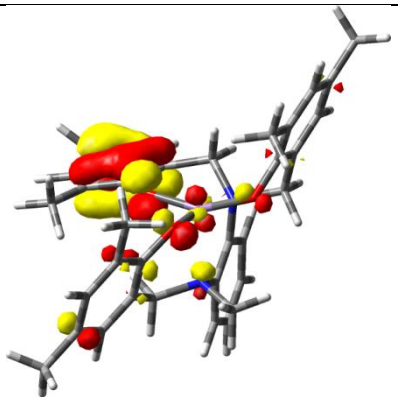 153α	155α
			18	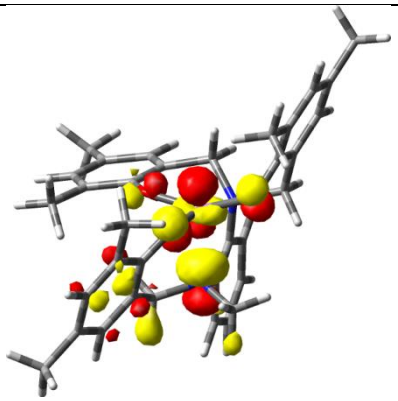 151α	155α

www.manaraa.com

			10	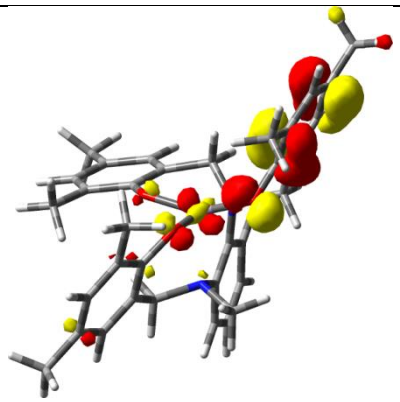 152α	155α
2	704	0.0119	38	154α	155α
			28	153α	155α
			20	151α	155α
4	540	0.0392	49	153α	155α
			28	151α	155α
			18	152α	155α
9	398	0.1078	68	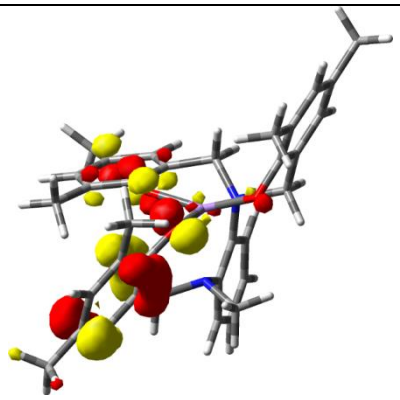 150β	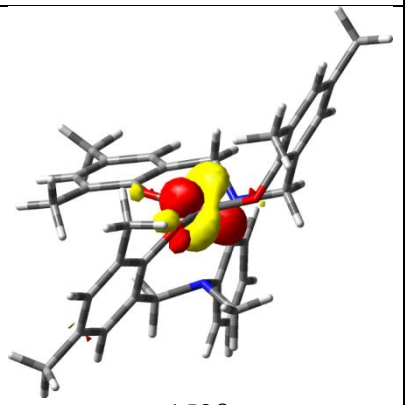 152β

www.manaraa.com

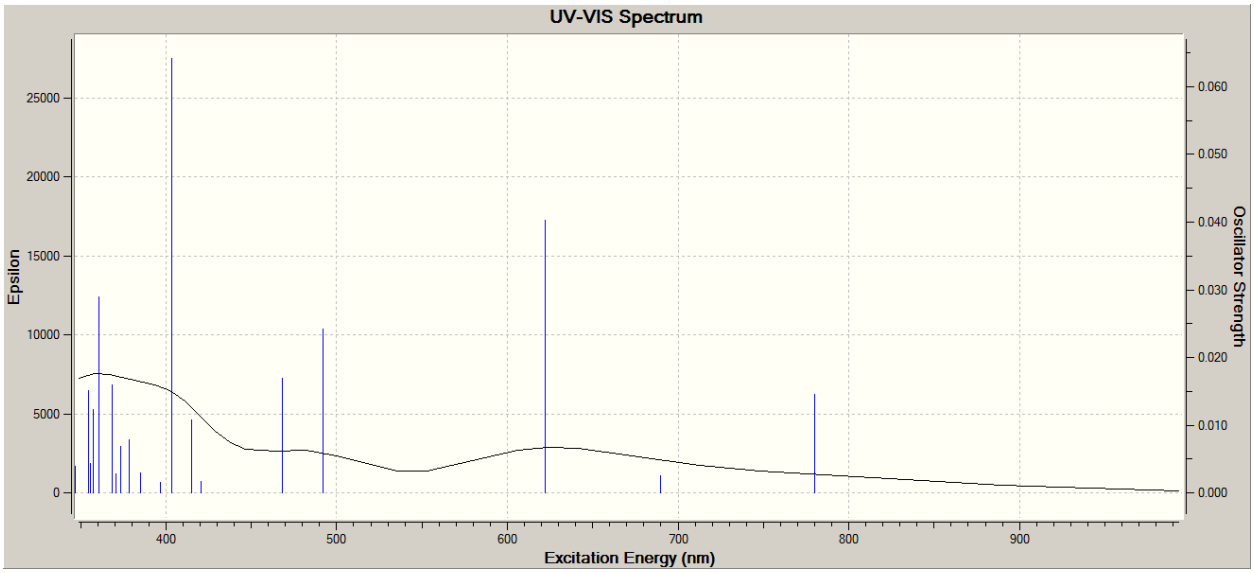

Figure B4. Simulated UV-visible spectrum for isomer 2 of **2** with individual transitions shown as sticks. A half-width at half-max of 0.2 eV was employed for the Gaussian fittings

Table B3. Assignments for TD-DFT transitions of Isomer 2 for **2**. Contributions > 10% are shown. Orbitals are only listed once with label, then labels are repeated thereafter.

Excited State	**λ / nm**	**Osc. Str.**	**% Cont.**	**Occ. MO**	**Unocc. MO**
1	780	0.0145	46	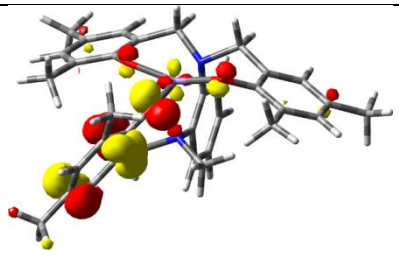 154α	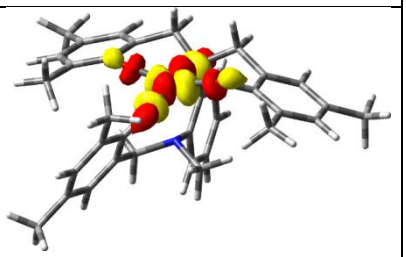 155α
			30	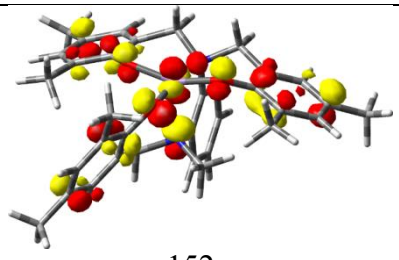 152α	155α

www.manaraa.com

			17	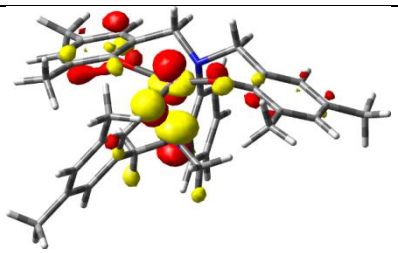 150α	155α
3	622	0.0403	68	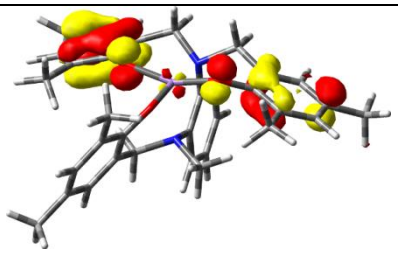 153α	155α
			19	154α	155α
4	492	0.0242	46	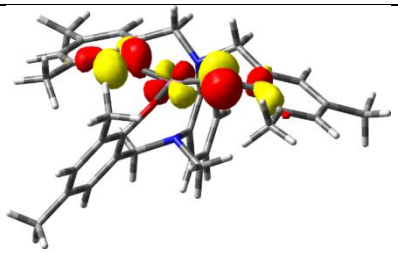 147α	155α
			22	150α	155α
			14	153α	155α
5	468	0.0170	37	150α	155α
			23	152α	155α
			21	147α	155α

Table B4. Cartesian coordinates (Å) for all optimized structures.

[^{HS}Mn^{III}(L^{1})(CH$_3$OH)]^0 *S*=2

Mn	0.01004400	-0.44509200	1.01807900
N	1.38563600	1.24523400	0.69499500
N	-0.15048800	-0.15029800	-1.13460200
C	1.52526000	1.52439700	-0.74095000
C	2.41602700	2.49683900	-1.19806400
C	0.75065800	0.79025400	-1.66374700
C	2.57244300	2.73498300	-2.56218100
H	3.00139200	3.07113800	-0.48754100
C	0.94289600	1.01630100	-3.03865800
C	1.83988600	1.98175500	-3.48225100
H	3.27315200	3.49036300	-2.90251700
H	0.40231600	0.41663300	-3.76267900
H	1.97437700	2.13908900	-4.54789800
C	0.83118700	2.43652300	1.43923600
H	0.76571500	2.11968100	2.48617200
H	1.55258300	3.26017200	1.38567400
C	2.71571100	0.87349700	1.31325500
H	2.49026900	0.63654100	2.35855900
H	3.37525200	1.74879900	1.31018500
C	-0.50996400	2.88981600	0.93669600
C	-1.58398600	1.97764300	0.97064800
C	-0.71882200	4.20220300	0.50157300
C	-2.87821500	2.41074600	0.59310800
C	-1.98402600	4.64892400	0.11271300
H	0.12407200	4.89006300	0.47708800
C	-3.04515800	3.73279000	0.17696500
H	-4.04247700	4.06180100	-0.11033600
O	-1.40403400	0.72253700	1.40897600
C	-1.18802600	-0.56273600	-1.80497000
H	-1.37530600	-0.15385500	-2.80288400
C	-2.16542300	-1.51239300	-1.35306100
C	-3.21689100	-1.81477400	-2.26092500
C	-2.13890900	-2.14837000	-0.06625300
C	-4.22142700	-2.71257600	-1.96075700
H	-3.21533600	-1.31508800	-3.22758400

www.manaraa.com

C	-3.18248100	-3.07813100	0.24292500
C	-4.17384300	-3.33342400	-0.68981300
H	-4.95613700	-4.04457700	-0.42904100
O	-1.20701700	-1.95253300	0.83134100
O	0.37453200	-0.59385800	3.28366100
C	-0.65314600	-0.66438200	4.28500400
H	-1.22674700	-1.59256500	4.20062000
H	-0.21935100	-0.58868000	5.28706400
H	-1.31450200	0.18226500	4.10525800
C	-3.16603900	-3.75832500	1.58674800
H	-2.25090500	-4.34553000	1.72384200
H	-3.18777500	-3.02644200	2.40207500
H	-4.02407200	-4.42640100	1.69861600
C	-5.33267500	-3.03161300	-2.93215100
H	-5.34711000	-4.09675100	-3.19230600
H	-6.31663400	-2.79401400	-2.51056400
H	-5.22253900	-2.46396800	-3.86026300
C	-4.04162700	1.45529200	0.66876400
H	-3.87591500	0.57194100	0.04349400
H	-4.18890100	1.08772600	1.69096100
H	-4.96692200	1.93966500	0.34473600
C	-2.20501800	6.06145800	-0.37742700
H	-2.34143300	6.09541500	-1.46581900
H	-3.10035900	6.50740400	0.06928400
H	-1.35369700	6.70435900	-0.13535100
C	3.38553100	-0.28251100	0.62666300
C	4.67789800	-0.17283400	0.10476300
C	2.69619400	-1.50908600	0.55017700
C	5.32099300	-1.26295600	-0.48710200
H	5.19309800	0.78346200	0.16923100
C	3.32506300	-2.62669200	-0.04895900
C	4.62081900	-2.47760400	-0.54659700
H	5.10283000	-3.34140300	-1.00154000
O	1.47205300	-1.64229000	1.08212200
C	2.59571600	-3.94352600	-0.12137900
H	2.34277800	-4.31722900	0.87764600
H	1.64845900	-3.84460200	-0.66277700
H	3.20251900	-4.70082700	-0.62528000
C	6.71025900	-1.13635100	-1.06880200
H	7.32739400	-2.00903400	-0.82982500
H	6.68486700	-1.05323500	-2.16290100
H	7.22237200	-0.24824400	-0.68691000
H	0.93609300	-1.38297200	3.31884100

[^{LS}Mn^{III}(L^{1})(CH$_3$OH)]^0 *S*=1

Mn	-0.11291200	-0.26236000	-0.92202600
N	1.39461000	1.17756700	-0.69014400
N	-0.30011900	-0.08734900	1.01366400
C	1.55512900	1.40712200	0.75155100
C	2.54312500	2.25258200	1.25572800
C	0.67126000	0.74613400	1.62312200
C	2.67258000	2.44490700	2.62916700
H	3.21953800	2.76147000	0.57723700
C	0.81974100	0.93533700	3.00813700
C	1.80828600	1.77971000	3.50200000
H	3.44585400	3.10117200	3.01457300
H	0.17622100	0.41776800	3.70955000
H	1.90790900	1.91232900	4.57466500
C	2.66948000	0.66763600	-1.32298100
H	2.40053600	0.45122100	-2.36206400
H	3.41000900	1.47540100	-1.33731300
C	1.02100600	2.45965000	-1.40225100
H	0.90703800	2.18053900	-2.45524400
H	1.86327700	3.15731500	-1.33606300
C	3.24469600	-0.54191100	-0.64485300
C	2.41789500	-1.66365900	-0.43647600
C	4.59247200	-0.58347600	-0.27071800
C	2.97448000	-2.83575700	0.13700100
C	5.16071600	-1.72639800	0.29470500
H	5.21094100	0.29712300	-0.43474900
C	4.32541300	-2.83915000	0.48364400
H	4.74411500	-3.74367300	0.92235700
O	1.13092500	-1.65992500	-0.79390800
C	-1.25763600	-0.66083800	1.69715900
H	-1.32838600	-0.45070400	2.76403100
C	-2.24518200	-1.55887300	1.19755900
C	-3.18262500	-2.06289100	2.14553500
C	-2.31783000	-1.98705800	-0.17331500
C	-4.16815100	-2.96097700	1.80201600
H	-3.10229800	-1.71953800	3.17485000
C	-3.34305600	-2.92880300	-0.52243900
C	-4.21933500	-3.37908300	0.44703700
H	-4.98984300	-4.09057700	0.15401300
O	-1.52143500	-1.57439600	-1.11505900
O	0.03807700	-0.25664900	-3.02009600
C	0.03929600	-1.48899200	-3.77329000
H	-0.82827600	-2.09709900	-3.51243900
H	0.04815100	-1.26127600	-4.84216600
H	0.95033800	-2.01623900	-3.49660500
C	-3.43443000	-3.39764200	-1.95059300
H	-3.59114700	-2.55665300	-2.63553400
H	-2.50677800	-3.88713600	-2.26802700
H	-4.25804200	-4.10500700	-2.07875300
C	-5.16050400	-3.49462100	2.80692500
H	-6.19160200	-3.25589300	2.52011500
H	-5.09922000	-4.58608400	2.89306800
H	-4.98485900	-3.07192500	3.80002100
C	2.10244200	-4.04676600	0.34783900
H	1.23580500	-3.81092900	0.97523100
H	1.70179900	-4.42271800	-0.60090500
H	2.66299300	-4.85563200	0.82480800
C	6.61506500	-1.76687400	0.70451200
H	6.72867800	-1.82848300	1.79410000
H	7.13004700	-2.63763200	0.28252600
H	7.14682800	-0.87146000	0.36963900
C	-0.22891000	3.10277100	-0.87726200
C	-0.24594800	4.43384400	-0.44834200
C	-1.41507100	2.34431100	-0.88390900
C	-1.43034300	5.04929300	-0.03632400
H	0.68292900	5.00114500	-0.44779700
C	-2.62850100	2.94765800	-0.47379600
C	-2.60576400	4.28213100	-0.06436300
H	-3.54168200	4.74236200	0.24885200
O	-1.40606100	1.07491400	-1.31297600
C	-3.90802300	2.15130500	-0.50119400
H	-4.16409600	1.84007700	-1.52099200
H	-3.82066000	1.23162000	0.08736000
H	-4.74314200	2.73668500	-0.10650900
C	-1.45016000	6.48291500	0.44235200
H	-2.26758900	7.05008300	-0.01664700
H	-1.59031000	6.54573600	1.52894400
H	-0.51322000	6.99485500	0.20403700
H	-0.77220100	0.24642600	-3.20917300

www.manaraa.com

[$^{HS}Mn^{III}(L^1)(CH_3OH)]^+$ S=3/2

Mn	-0.02484200	-0.43457900	0.98078100
N	1.34076900	1.23802600	0.67982500
N	-0.21368300	-0.13279900	-1.14603800
C	1.48700000	1.51292000	-0.76259200
C	2.38476300	2.47953700	-1.21764400
C	0.70409200	0.78526200	-1.68344800
C	2.54583300	2.70729200	-2.58258400
H	2.97040600	3.05606800	-0.50961800
C	0.90028400	1.00242000	-3.05896400
C	1.80799200	1.95709600	-3.50197600
H	3.25351000	3.45474200	-2.92483600
H	0.35051800	0.41074900	-3.78220100
H	1.94522800	2.11168600	-4.56725200
C	0.77977900	2.44015500	1.41648400
H	0.73799200	2.14258800	2.46982000
H	1.48943200	3.26929600	1.32980900
C	2.66670900	0.89428500	1.30911300
H	2.44471100	0.60899800	2.34276600
H	3.30177400	1.78521700	1.34374600
C	-0.57450300	2.85794700	0.92449700
C	-1.63077400	1.93057400	1.01792000
C	-0.81749800	4.14724100	0.44420100
C	-2.94358400	2.31347000	0.65715200
C	-2.10276600	4.54836500	0.06972000
H	0.00828700	4.85128400	0.37278800
C	-3.14449500	3.61508600	0.19581700
H	-4.15371400	3.91544300	-0.07848600
O	-1.39976900	0.69676900	1.50529700
C	-1.23998700	-0.57720900	-1.81360500
H	-1.42287800	-0.20524100	-2.82520200
C	-2.20612100	-1.52178500	-1.32767600
C	-3.27999700	-1.83893400	-2.19993900
C	-2.14306500	-2.14047500	-0.03707000
C	-4.27424600	-2.73301400	-1.85014200
H	-3.30974900	-1.35526700	-3.17341700
C	-3.16867800	-3.06022000	0.32829400
C	-4.18857200	-3.33110100	-0.57215700
H	-4.96178100	-4.03735000	-0.27602200
O	-1.16281000	-1.94046600	0.82209200
O	0.52201100	-0.70204200	3.19343800
C	-0.40045400	-0.51363100	4.28814600
H	-1.04117400	-1.39104900	4.41179400
H	0.14744400	-0.31729900	5.21372800
H	-1.01339600	0.34640600	4.02547200
C	-3.10978200	-3.72225900	1.67988300
H	-2.19700400	-4.31806400	1.79081200
H	-3.09798900	-2.97940000	2.48476700
H	-3.96927800	-4.38004500	1.82952900
C	-5.41448000	-3.06902100	-2.78006900
H	-5.43222500	-4.13850500	-3.01937100
H	-6.38296300	-2.82705500	-2.32763500
H	-5.33644000	-2.51666000	-3.72004400
C	-4.08542200	1.34052000	0.79953200
H	-3.92742200	0.44450600	0.19116400
H	-4.19023900	1.00073700	1.83589100
H	-5.02857700	1.80101800	0.49480400
C	-2.36801100	5.93418300	-0.46899600
H	-2.53458100	5.91634000	-1.55320500
H	-3.26207300	6.37541800	-0.01620200
H	-1.52573600	6.60455500	-0.27721800
C	3.40348500	-0.21135700	0.60583900
C	4.72098100	-0.07749500	0.23311400
C	2.74082800	-1.47539300	0.39018900
C	5.43949900	-1.14951000	-0.35730000
H	5.23250700	0.86599600	0.39882500
C	3.46247200	-2.57975500	-0.21055500
C	4.78408800	-2.38357500	-0.56108900
H	5.33895800	-3.20127600	-1.01163800
O	1.51759700	-1.65505400	0.74212800
C	2.74990000	-3.87996900	-0.42663400
H	2.37976400	-4.28404800	0.52160700
H	1.87311000	-3.74087900	-1.06807300
H	3.41053600	-4.61577000	-0.88808600
C	6.86303900	-0.95625200	-0.78408900
H	7.39423700	-1.90732400	-0.86014100
H	6.89568600	-0.47929700	-1.77310200
H	7.40080500	-0.29878800	-0.09528500
H	1.03766200	-1.50588400	3.34982100

[$Mn^{IV}(L^1)(CH_3OH)]^+$ S=3/2

Mn	0.01636700	-0.42313600	-0.89047400
N	-1.33940000	1.19092100	-0.72527700
N	0.20523300	-0.17191200	1.03248300
C	-1.53441000	1.44092100	0.71133300
C	-2.45561000	2.37322600	1.18439500
C	-0.76627100	0.68825000	1.60803000
C	-2.63554800	2.53492900	2.55669800
H	-3.04322800	2.96591900	0.49272400
C	-0.97655700	0.82650600	2.98753700
C	-1.90432500	1.75203500	3.45337100
H	-3.35889000	3.25522700	2.92275600
H	-0.43651300	0.20822900	3.69454800
H	-2.06273400	1.85442300	4.52155200
C	-0.79385900	2.41560300	-1.43892100
H	-0.69072800	2.11574300	-2.48678900
H	-1.55126800	3.20339500	-1.39149800
C	-2.65343300	0.82159100	-1.40123300
H	-2.38430200	0.55811700	-2.42809100
H	-3.27717400	1.71859600	-1.44790700
C	0.50871000	2.90659200	-0.88521800
C	1.58812300	2.00930800	-0.83308400
C	0.68699400	4.23538200	-0.49249300
C	2.86698700	2.45208900	-0.42648200
C	1.93582800	4.70054800	-0.07184800
H	-0.15784300	4.91877300	-0.53077400
C	3.00556900	3.79150500	-0.05848000
H	3.98776400	4.14104900	0.25243100
O	1.41602500	0.72850200	-1.22171100
C	1.22237400	-0.63969100	1.71210700
H	1.32035100	-0.32076200	2.74793000
C	2.22527500	-1.52652800	1.23162500
C	3.29141100	-1.86473600	2.10746400
C	2.16847400	-2.10431600	-0.06976100
C	4.28517300	-2.74436600	1.72640100
H	3.31291500	-1.41310100	3.09541200
C	3.17651100	-3.02073700	-0.46614100
C	4.19645200	-3.30836800	0.43163700
H	4.96860400	-4.00767300	0.11833800
O	1.17609600	-1.86000000	-0.90964100
O	-0.28552000	-0.60091400	-2.90797100
C	0.79074500	-0.57302400	-3.88663800
H	1.44386900	-1.43522200	-3.74564300
H	0.34873200	-0.57608700	-4.88367500

www.manaraa.com

H	1.33997900	0.34782600	-3.71088700
C	3.11646500	-3.65214400	-1.83160400
H	2.17301000	-4.18796300	-1.97929500
H	3.18024100	-2.89520800	-2.62093900
H	3.93868700	-4.35759400	-1.96936100
C	5.42911600	-3.10751500	2.64071900
H	5.45504700	-4.18561100	2.83392400
H	6.39309000	-2.83775600	2.19526200
H	5.34759600	-2.59458600	3.60212600
C	4.04085100	1.50744700	-0.42127200
H	3.88471400	0.67211000	0.26867800
H	4.20190300	1.06958400	-1.41233200
H	4.95496100	2.02815400	-0.12597000
C	2.13620300	6.13351700	0.36061000
H	2.35087600	6.19973400	1.43385900
H	2.98092900	6.59420200	-0.16276000
H	1.24689300	6.73758200	0.16266100
C	-3.38804400	-0.28564700	-0.70847700
C	-4.74030300	-0.17122100	-0.37448400
C	-2.69526200	-1.47183600	-0.41720400
C	-5.42681500	-1.22666600	0.23103800
H	-5.26601200	0.75372100	-0.59928600
C	-3.35803500	-2.55234300	0.20920700
C	-4.71087900	-2.40204600	0.51234600
H	-5.22765100	-3.23045500	0.99227600
O	-1.39900400	-1.60712700	-0.75371500
C	-2.60810500	-3.82070900	0.52133900
H	-2.22212600	-4.29061200	-0.39012900
H	-1.74187000	-3.62388200	1.16229600
H	-3.25446800	-4.54086200	1.02874900
C	-6.89357900	-1.11748900	0.57320000
H	-7.49930600	-1.78519000	-0.05107000
H	-7.08235800	-1.39712800	1.61529300
H	-7.26309200	-0.09946100	0.42454800
H	-0.82271600	-1.40197900	-3.02753100

[^{HS}Mn^{III}(L^{1})(CH$_3$OH)]$^{+}$ *S*=5/2

Mn	-0.00859900	-0.29982600	1.11033800
N	1.46873800	1.24866200	0.68379600
N	-0.19091200	-0.13737500	-1.06258200
C	1.61668500	1.42923000	-0.76147600
C	2.57930400	2.29777700	-1.27663700
C	0.77893500	0.70757700	-1.64014500
C	2.74147800	2.44246300	-2.65207500
H	3.21537900	2.86144300	-0.60316500
C	0.97789200	0.83791300	-3.02859000
C	1.94463200	1.69922900	-3.52773900
H	3.49691800	3.11847400	-3.03807700
H	0.39404800	0.24390400	-3.72157600
H	2.08503600	1.78351800	-4.60012300
C	1.00469800	2.51772000	1.36148200
H	0.92717200	2.27022200	2.42627700
H	1.77992100	3.28423300	1.25631300
C	2.76475400	0.79245400	1.31751900
H	2.52704800	0.61367400	2.37211200
H	3.49510900	1.60786100	1.28268500
C	-0.30676600	3.02767700	0.83315300
C	-1.43933800	2.19330600	0.90703300
C	-0.43167100	4.32507900	0.32711800
C	-2.70157000	2.67694900	0.49261900
C	-1.66572500	4.82630400	-0.09404100
H	0.45154000	4.95730600	0.27142700
C	-2.78302800	3.98236400	0.00635000
H	-3.75508300	4.35644600	-0.30900700
O	-1.33914000	0.95060200	1.41932300
C	-1.19098200	-0.58300800	-1.76160100
H	-1.31426500	-0.25536000	-2.79538800
C	-2.20969400	-1.50452700	-1.31688500
C	-3.17902800	-1.87163300	-2.25082000
C	-2.27348800	-2.08395100	0.02432100
C	-4.20198500	-2.78544700	-1.95289400
H	-3.13611100	-1.44113900	-3.24713500
C	-3.32996600	-3.04494900	0.32295600
C	-4.24547900	-3.35880700	-0.65477700
H	-5.03538200	-4.07001700	-0.42933400
O	-1.45306300	-1.78828200	0.94302500
O	0.17274600	-0.52908700	3.26217600
C	-0.85659200	-0.34766300	4.25806600
H	-1.50280500	-1.22780000	4.31155400
H	-0.40022200	-0.15585500	5.23217200
H	-1.43688500	0.51570600	3.93873500
C	-3.37657000	-3.64286500	1.69662600
H	-2.44641300	-4.17556100	1.92136500
H	-3.48068500	-2.86164600	2.45715300
H	-4.21161200	-4.33912600	1.79091500
C	-5.23224300	-3.16194100	-2.97494300
H	-5.21673900	-4.24279300	-3.15782000
H	-6.23872100	-2.92006200	-2.61357400
H	-5.07188200	-2.64711800	-3.92369700
C	-3.92103900	1.79764000	0.60070200
H	-3.81754100	0.89112700	-0.00530300
H	-4.08427600	1.46751000	1.63248200
H	-4.81574300	2.32923000	0.26697400
C	-1.79955000	6.22465900	-0.64968700
H	-2.04028100	6.21000200	-1.71960200
H	-2.60150200	6.77940700	-0.15043300
H	-0.87265100	6.79146900	-0.52743200
C	3.33030700	-0.43881200	0.66532800
C	4.63551700	-0.45762400	0.16707500
C	2.53964500	-1.60503500	0.59711800
C	5.18582100	-1.61256100	-0.39603500
H	5.23571300	0.44733000	0.22666100
C	3.07069500	-2.78644600	0.02575000
C	4.38064600	-2.76153500	-0.45148100
H	4.79066200	-3.67112900	-0.88570500
O	1.29917000	-1.62862400	1.11326600
C	2.22732000	-4.03300400	-0.03819200
H	1.95066600	-4.38002600	0.96392200
H	1.28974600	-3.85243700	-0.57513900
H	2.76281600	-4.84119400	-0.54254600
C	6.59019900	-1.62367300	-0.95075500
H	7.13705700	-2.51939800	-0.63808700
H	6.58704100	-1.61811800	-2.04788100
H	7.15649600	-0.74900600	-0.61942700
H	0.68606300	-1.33047800	3.44379500

[^{HS}Mn^{III}(L^{1})(CH$_3$OH)]$^{2+}$ *S*=1

Mn	0.11718800	-0.38456500	-0.94109200
N	-1.32620400	1.16990200	-0.70708900
N	0.23556400	-0.22711100	1.03831000
C	-1.51258900	1.39587800	0.73922200
C	-2.44058300	2.31739800	1.22385500
C	-0.73548300	0.63339500	1.62393600
C	-2.62313900	2.46205400	2.59693000

www.manaraa.com

H	-3.03133000	2.91748400	0.54086100
C	-0.95053100	0.76043300	3.00534900
C	-1.88508800	1.67267900	3.48232600
H	-3.34966200	3.17434900	2.97170100
H	-0.40759200	0.14415200	3.71142200
H	-2.04158600	1.76156400	4.55190800
C	-0.85889300	2.43067200	-1.42051400
H	-0.69284000	2.14135500	-2.46243800
H	-1.67466800	3.15757900	-1.40471200
C	-2.63730900	0.76502400	-1.37027700
H	-2.38527000	0.52104100	-2.40583600
H	-3.29864000	1.63494800	-1.39171000
C	0.38001500	3.04958300	-0.83907400
C	1.59360200	2.26625500	-0.82667000
C	0.40852900	4.34429300	-0.38387000
C	2.82632500	2.84700800	-0.33163200
C	1.61561000	4.93092100	0.09262700
H	-0.49761300	4.94343400	-0.39032500
C	2.79678000	4.15923200	0.10446000
H	3.71104100	4.61289800	0.47520700
O	1.57452900	1.06075000	-1.26241900
C	1.19516100	-0.77883800	1.74538800
H	1.24913700	-0.53622400	2.80480100
C	2.19583000	-1.66819800	1.26793300
C	3.16694500	-2.13573100	2.19511800
C	2.24046400	-2.11631200	-0.08344600
C	4.15461000	-3.02298100	1.81770700
H	3.11681100	-1.77981800	3.22018900
C	3.24511000	-3.03088200	-0.48261100
C	4.16496000	-3.45329300	0.46986300
H	4.93644400	-4.15311800	0.15677500
O	1.35383000	-1.72830700	-0.99225800
O	-0.13054400	-0.45317900	-3.01695000
C	0.95794300	-0.33061800	-3.97665900
H	1.62678800	-1.18882900	-3.89471100
H	0.53360900	-0.26206400	-4.97897300
H	1.48757800	0.58507200	-3.72588800
C	3.29102000	-3.51586200	-1.90716300
H	2.35898300	-4.01979500	-2.18398300
H	3.42106000	-2.68117600	-2.60428200
H	4.11652800	-4.21554400	-2.05262100
C	5.19200800	-3.52997700	2.78872400
H	5.14723700	-4.62067300	2.88040400
H	6.20398100	-3.27685100	2.45427900
H	5.04809200	-3.10172300	3.78350900
C	4.07028700	2.01372100	-0.31473400
H	3.92091700	1.10333000	0.27534200
H	4.33372000	1.68904600	-1.32716200
H	4.90916900	2.57207900	0.10364800
C	1.61890800	6.35527200	0.55446900
H	0.74121600	6.57207000	1.17130600
H	2.52137800	6.59718000	1.11837200
H	1.57029600	7.02982000	-0.31083000
C	-3.34209700	-0.38354700	-0.70504000
C	-4.63599300	-0.28914200	-0.25828300
C	-2.65085500	-1.64781800	-0.60383100
C	-5.30995700	-1.41480400	0.29779400
H	-5.17024700	0.65339500	-0.33177200
C	-3.31795100	-2.79659900	-0.02164100
C	-4.62628100	-2.64395900	0.40042100
H	-5.14652200	-3.49481600	0.82966800
O	-1.45275000	-1.75480400	-1.04591600
C	-2.57344100	-4.09086800	0.08799100
H	-2.25145400	-4.43933100	-0.89917700
H	-1.66376700	-3.96606200	0.68544700
H	-3.19335100	-4.86184400	0.54789800
C	-6.72474700	-1.27147400	0.76602600
H	-7.12240000	-2.20968000	1.15537800
H	-6.79349100	-0.50907200	1.55149600
H	-7.36798500	-0.93143300	-0.05442700
H	-0.65633300	-1.24132800	-3.22983700

$[^{HS}Mn^{III}(L^1)(CH_3OH)]^{2+}$ *S*=3

Mn	-0.01419800	-0.29926600	-1.06081100
N	1.38208600	1.34197500	-0.66463600
N	-0.34714400	0.02026500	1.07598700
C	1.44987600	1.60711100	0.77650300
C	2.37301300	2.52100200	1.28583700
C	0.56541400	0.93565600	1.64936200
C	2.44696100	2.76436900	2.65488600
H	3.04300000	3.04771500	0.61532500
C	0.67078500	1.17273100	3.03245200
C	1.59686200	2.08063900	3.52784900
H	3.17123000	3.47495300	3.03779100
H	0.04480300	0.63036800	3.73064300
H	1.66255000	2.24763400	4.59749300
C	2.71483000	0.93158500	-1.23232200
H	2.53015600	0.65592600	-2.27666500
H	3.39585800	1.78850500	-1.24377500
C	0.89545600	2.56116800	-1.42746400
H	0.92387600	2.28020900	-2.48564400
H	1.60597300	3.38004800	-1.27999800
C	3.37194400	-0.21311200	-0.50605500
C	2.65462700	-1.45449100	-0.29724600
C	4.68238700	-0.13798200	-0.10946300
C	3.33372200	-2.59750100	0.29778400
C	5.35626100	-1.24547100	0.48788200
H	5.23585800	0.78448200	-0.25742500
C	4.65504000	-2.45603900	0.67048600
H	5.17215000	-3.29742900	1.12091300
O	1.42302200	-1.59176300	-0.62870700
C	-1.34954400	-0.45127800	1.74992800
H	-1.54188500	-0.08868200	2.76067300
C	-2.28724000	-1.46260000	1.30272300
C	-3.28074700	-1.83649900	2.19527500
C	-2.23117300	-2.13012200	0.00168500
C	-4.23114300	-2.84377200	1.89772200
H	-3.33160500	-1.34692900	3.16354800
C	-3.20573300	-3.17693700	-0.29799400
C	-4.16009200	-3.49574100	0.64592700
H	-4.88480100	-4.27253300	0.42177800
O	-1.37262900	-1.84419800	-0.88492100
O	0.38799300	-0.71829300	-3.13917200
C	0.67568200	-1.99687700	-3.75814400
H	-0.22515300	-2.61326000	-3.79928600
H	1.07277000	-1.83440200	-4.76181400
H	1.42704200	-2.48112300	-3.13748400
C	-3.12970200	-3.85450100	-1.62979100
H	-3.28159700	-3.13170200	-2.43913500
H	-2.13897000	-4.29358300	-1.78662800
H	-3.88358500	-4.63839200	-1.71293600
C	-5.29745400	-3.18901200	2.88941500
H	-6.10861300	-2.45010100	2.83642800
H	-5.73014200	-4.17122400	2.69092800

www.manaraa.com

H	-4.91197200	-3.16485500	3.91256800
C	2.56825200	-3.86921300	0.48777000
H	1.70954000	-3.71008800	1.14929400
H	2.16511100	-4.22556700	-0.46614200
H	3.20226700	-4.64629800	0.91655200
C	6.78334600	-1.10056600	0.90840200
H	6.87805600	-0.31257300	1.66618700
H	7.18578400	-2.02800600	1.31748200
H	7.40429900	-0.78871300	0.05996800
C	-0.48817300	2.98594500	-1.02818600
C	-0.75687500	4.26000500	-0.52957200
C	-1.54416300	2.06984500	-1.20428400
C	-2.06534800	4.65269700	-0.22213600
H	0.06255400	4.95966200	-0.38687900
C	-2.87435900	2.43259600	-0.89885000
C	-3.10003400	3.72554000	-0.42406600
H	-4.12196400	4.02256200	-0.20036300
O	-1.27532700	0.84996800	-1.72339400
C	-4.00605600	1.46272400	-1.11738500
H	-4.03082700	1.10588300	-2.15212300
H	-3.90563400	0.57866500	-0.47901400
H	-4.96663100	1.93226100	-0.89411500
C	-2.35963100	6.02603100	0.32899300
H	-3.23198600	6.47174600	-0.15917900
H	-2.58074300	5.98158600	1.40234600
H	-1.51081700	6.70108400	0.19402600
H	-0.26202800	-0.23515400	-3.67251800

[^{HS}Mn^{III}(L^{2})]^{0} *S*=2, Isomer 1

Mn	-0.13126200	-0.74263400	-0.03845000
N	-1.53124300	0.70980300	0.67375800
N	1.04323100	0.03484600	1.73469600
C	-0.87729900	1.59293800	1.65357400
C	-1.52154200	2.75352100	2.09907300
C	0.35938500	1.23269400	2.20724100
C	-0.94634300	3.55313000	3.08200700
H	-2.47897500	3.03703400	1.67710500
C	0.92400200	2.03834700	3.20483900
C	0.28006600	3.19170300	3.64170600
H	-1.45769700	4.45181800	3.41107400
H	1.87701800	1.75959900	3.64148200
H	0.73416000	3.80505600	4.41317100
C	-2.04655100	1.46554100	-0.53321300
H	-2.42845300	0.69459300	-1.21150100
H	-2.90737100	2.07420700	-0.23727800
C	-2.69949000	0.02811600	1.37461000
H	-3.43292600	0.79596900	1.64147500
H	-2.28625000	-0.38059100	2.30113100
C	-1.00939400	2.32522100	-1.19839500
C	0.21787500	1.75208800	-1.58525900
C	-1.27454000	3.66962200	-1.48434600
C	1.16489100	2.54223700	-2.28322600
C	-0.35446500	4.46843000	-2.16534300
H	-2.22669400	4.09578800	-1.17434900
C	0.85629800	3.87500200	-2.55560200
H	1.58816700	4.47529900	-3.09360000
O	0.50074400	0.46539300	-1.33844100
C	2.38287500	0.39045700	1.16531500
H	2.19132200	1.17252900	0.42503900
C	3.15825100	-0.74792800	0.53276900
C	4.55618300	-0.70904200	0.65858600
C	2.56617400	-1.77375500	-0.23968900
C	5.39340600	-1.63269200	0.03564600
H	4.99883600	0.07934900	1.26483800
C	3.40373100	-2.72379700	-0.88443600
C	4.78506400	-2.63397400	-0.73656600
H	5.40955100	-3.37326900	-1.23550800
O	1.24295500	-1.95757600	-0.35256000
C	2.77269900	-3.81901800	-1.70537500
H	2.12896300	-4.45847300	-1.09068000
H	2.13393000	-3.40791100	-2.49508800
H	3.53633300	-4.44771000	-2.17151100
C	6.89584900	-1.56693100	0.18356300
H	7.30126000	-2.49228500	0.60994200
H	7.39125500	-1.42037900	-0.78383300
H	7.19512900	-0.74203800	0.83650900
C	2.46302700	1.92409000	-2.73561700
H	3.02251900	1.49477700	-1.89774400
H	2.28683100	1.10131600	-3.43832100
H	3.09749200	2.66452900	-3.23021900
C	-0.63717400	5.92318600	-2.46148400
H	-0.00501500	6.58893300	-1.86063000
H	-0.44393100	6.16503200	-3.51256600
H	-1.67895400	6.17787600	-2.24629900
C	-3.33598700	-1.06125900	0.56475900
C	-4.69067900	-1.04761400	0.21675500
C	-2.52310900	-2.15643200	0.21682700
C	-5.27007600	-2.11963200	-0.46599000
H	-5.30180400	-0.19107200	0.49400500
C	-3.08715100	-3.25395200	-0.47578000
C	-4.44495800	-3.20802500	-0.79584400
H	-4.87840900	-4.05232800	-1.32936300
O	-1.22470500	-2.16042400	0.56978000
C	-2.22056000	-4.43043500	-0.84280400
H	-1.35091000	-4.11347600	-1.42837400
H	-1.82657000	-4.93027700	0.04976200
H	-2.78178700	-5.16607600	-1.42513800
C	-6.73310200	-2.11589800	-0.84515000
H	-6.86849500	-2.18176900	-1.93121700
H	-7.26536700	-2.96807200	-0.40650300
H	-7.22942600	-1.20309700	-0.50390300
H	3.00716700	0.83381000	1.95099800
C	1.15346000	-0.99202800	2.80193900
H	0.15710600	-1.22671200	3.17882800
H	1.59227700	-1.89449800	2.37646800
H	1.78047900	-0.64680500	3.63307700

[^{HS}Mn^{III}(L^{2})]^{0} *S*=2, Isomer 2

Mn	-0.09986100	-0.43873600	-1.11740800
N	-1.22053000	1.37417500	-0.80449200
N	-0.08811100	-0.42569000	1.14708400
C	-1.26745900	1.69379900	0.63305800
C	-1.87869200	2.87686100	1.06661300
C	-0.71125100	0.81979900	1.57917200
C	-1.93747300	3.19643900	2.41939200
H	-2.31330800	3.55823900	0.34358400
C	-0.77604200	1.15114900	2.93932700
C	-1.38264600	2.32939300	3.36172800
H	-2.41475000	4.11873300	2.73415400
H	-0.34936000	0.47626500	3.67362000
H	-1.42289200	2.56804400	4.41958000
C	-0.55278800	2.48233100	-1.60072200
H	-0.53859800	2.11483400	-2.63364100
H	-1.19094400	3.37152500	-1.57863700

www.manaraa.com

C	-2.61876100	1.21863400	-1.37416600
H	-2.47091900	1.06935600	-2.44957300
H	-3.15695800	2.16269100	-1.24247700
C	0.83425800	2.82091700	-1.14978700
C	1.80037600	1.79759000	-1.17525400
C	1.19562900	4.12491400	-0.79754200
C	3.15148200	2.10853800	-0.88530200
C	2.51710100	4.45119100	-0.48472400
H	0.43129800	4.89905400	-0.78136000
C	3.47249900	3.42468900	-0.54711600
H	4.51173700	3.66026700	-0.32405800
O	1.45775600	0.54569900	-1.51388900
C	1.36912900	-0.45182100	1.49124700
H	1.79847700	0.46711700	1.08138900
C	2.14071300	-1.66227800	0.99518600
C	3.20658900	-2.09918200	1.79848000
C	1.90898700	-2.30343800	-0.24561400
C	4.06416500	-3.12987200	1.41764200
H	3.36872300	-1.60504400	2.75481500
C	2.77344600	-3.35671300	-0.65010600
C	3.82263900	-3.74300000	0.17896200
H	4.47303400	-4.55210600	-0.14925400
O	0.87274700	-2.02796000	-1.05050200
C	2.52634800	-4.03970700	-1.97087400
H	1.54233600	-4.52167400	-1.99353700
H	2.53632100	-3.32241900	-2.79923000
H	3.28611000	-4.80175900	-2.16548700
C	5.20588900	-3.57853500	2.30015400
H	5.10237600	-4.63037200	2.59303000
H	6.17159400	-3.48596500	1.78895200
H	5.25812700	-2.98349300	3.21649600
C	4.20697100	1.03549400	-0.96664000
H	4.00301000	0.21209000	-0.27464200
H	4.24508000	0.59267700	-1.96832300
H	5.19506000	1.44297900	-0.73600700
C	2.90848800	5.85353900	-0.07933500
H	3.08467600	5.92781400	1.00131100
H	3.83158100	6.17250000	-0.57511600
H	2.12535200	6.57424500	-0.33209300
C	-3.40707000	0.07961800	-0.80385200
C	-4.66521300	0.26801000	-0.22454600
C	-2.88603500	-1.21873500	-0.96657700
C	-5.44324100	-0.81764500	0.18649200
H	-5.04767400	1.27988200	-0.10704200
C	-3.66404500	-2.33505000	-0.57630000
C	-4.92082800	-2.10538600	-0.01192500
H	-5.51699800	-2.96594800	0.28691400
O	-1.67785400	-1.39437300	-1.52081000
C	-3.13013100	-3.72886100	-0.78117400
H	-2.90401900	-3.91885300	-1.83642700
H	-2.19432000	-3.88079400	-0.23245600
H	-3.85104600	-4.47878500	-0.44467800
C	-6.79212500	-0.61761800	0.83802500
H	-7.52384100	-1.34910700	0.47934100
H	-6.73517500	-0.73053100	1.92826600
H	-7.18809400	0.38169600	0.63486500
H	1.48362100	-0.39592500	2.58174900
C	-0.78849900	-1.60688700	1.71548000
H	-1.85272900	-1.53537000	1.49269600
H	-0.38602700	-2.50830300	1.25398900
H	-0.64952200	-1.67054600	2.80153000

$[^{LS}Mn^{III}(L^{2})]^{0}$ S=1

Mn	-0.06177200	-0.37226600	-1.00527800
N	-1.23602700	1.37668400	-0.76666500
N	0.00775300	-0.42642000	1.04000400
C	-1.26933200	1.66545800	0.67147000
C	-1.91758300	2.80100400	1.16947400
C	-0.62901600	0.79346000	1.55935300
C	-1.92481900	3.07159800	2.53441100
H	-2.41643500	3.48112600	0.48782900
C	-0.63951700	1.06912600	2.93138000
C	-1.28068000	2.20414300	3.41823500
H	-2.43004200	3.95724000	2.90550900
H	-0.15156300	0.39385900	3.62520200
H	-1.28002800	2.40689100	4.48411400
C	-0.61513300	2.52127200	-1.54451400
H	-0.58584600	2.17064300	-2.58290200
H	-1.28987400	3.38320300	-1.50891500
C	-2.62594700	1.19460900	-1.33417900
H	-2.47202200	1.04954900	-2.40985400
H	-3.18581700	2.12752600	-1.20720900
C	0.75697000	2.91520900	-1.09378300
C	1.75738600	1.92615300	-1.10101900
C	1.07421200	4.23786400	-0.77121400
C	3.09896600	2.28970000	-0.82978100
C	2.38553800	4.61573900	-0.47162900
H	0.28433000	4.98626700	-0.76954500
C	3.37624700	3.62266100	-0.51900900
H	4.40790600	3.89919800	-0.30834500
O	1.45442600	0.65586500	-1.40363300
C	1.47491000	-0.47674800	1.39850000
H	1.91342300	0.44404100	1.00911600
C	2.20569500	-1.70387800	0.89564700
C	3.21388200	-2.22640500	1.72182400
C	1.96055400	-2.29853200	-0.36829400
C	4.01201900	-3.30375400	1.34265800
H	3.37766900	-1.76460500	2.69419000
C	2.76176200	-3.40787600	-0.76242400
C	3.75935400	-3.87708400	0.08623200
H	4.35931600	-4.72564900	-0.23926300
O	0.99536300	-1.91426500	-1.20211700
C	2.50384000	-4.05297600	-2.09989100
H	1.48416500	-4.45031500	-2.16212600
H	2.60096900	-3.32972700	-2.91745900
H	3.20392100	-4.87355600	-2.28067700
C	5.10245700	-3.83958400	2.24125900
H	4.97439500	-4.91015400	2.44098800
H	6.09551800	-3.71848700	1.79095700
H	5.11336000	-3.32147300	3.20471200
C	4.19248300	1.25528900	-0.91237200
H	3.99970600	0.40205700	-0.25453700
H	4.27281700	0.84700800	-1.92657100
H	5.15990000	1.68793900	-0.64336500
C	2.72892100	6.03878900	-0.09622800
H	2.88096900	6.14614800	0.98535200
H	3.65242600	6.37080500	-0.58231700
H	1.93088600	6.72986500	-0.38298400
C	-3.40253300	0.04187100	-0.77483100
C	-4.70058400	0.20759400	-0.28220100
C	-2.84055300	-1.24491700	-0.87623400
C	-5.47939100	-0.88902400	0.09604600
H	-5.11386600	1.21166200	-0.20919200
C	-3.62106200	-2.37368600	-0.52544900

www.manaraa.com

C	-4.91735400	-2.16689600	-0.04897400
H	-5.51299200	-3.03718900	0.22124500
O	-1.58900200	-1.41174100	-1.32534300
C	-3.04955500	-3.75895100	-0.68488200
H	-2.77591300	-3.95922500	-1.72705500
H	-2.13449600	-3.88621700	-0.09689100
H	-3.76943300	-4.51867500	-0.36871200
C	-6.87226900	-0.71129800	0.65468800
H	-7.56691700	-1.45204300	0.24473300
H	-6.88802400	-0.82823900	1.74584300
H	-7.26855400	0.28281700	0.42810600
H	1.56119700	-0.44271900	2.48979900
C	-0.68414400	-1.63396900	1.59397500
H	-1.75278300	-1.55183400	1.40738500
H	-0.29120200	-2.51933900	1.09993600
H	-0.50550000	-1.70824100	2.67074700

$[^{HS}Mn^{III}(L^{2})]^{+}$ *S*=3/2, Isomer 1

Mn	0.02472400	-0.59484800	-0.16905500
N	-1.62808200	0.31104000	0.77354500
N	1.12146100	0.28191100	1.61171500
C	-1.13530200	1.30912000	1.73804700
C	-2.01372400	2.24794200	2.28952600
C	0.20303800	1.27958300	2.16145400
C	-1.57154600	3.15845400	3.24459500
H	-3.05050100	2.27232300	1.97550400
C	0.63373700	2.19378000	3.13038800
C	-0.24293400	3.13146500	3.66778000
H	-2.26577800	3.88287800	3.65686300
H	1.66202900	2.17142100	3.47394900
H	0.11058100	3.83385900	4.41511800
C	-2.49380400	0.92523600	-0.30911100
H	-2.73968900	0.10243600	-0.98903900
H	-3.44124300	1.24524300	0.13479800
C	-2.44358000	-0.73391000	1.52964100
H	-3.35799600	-0.25298000	1.89038000
H	-1.84043700	-1.00763800	2.39891800
C	-1.85198800	2.07494200	-1.03467200
C	-0.53449600	1.96712100	-1.51462900
C	-2.59038300	3.23660800	-1.29044900
C	0.02937000	3.02589400	-2.26436500
C	-2.06070600	4.29286500	-2.03275000
H	-3.60625800	3.30751600	-0.90810900
C	-0.74708000	4.15890300	-2.50748600
H	-0.31009000	4.96921600	-3.08774000
O	0.21189200	0.86498700	-1.29710500
C	2.33906100	0.93720200	1.03647000
H	1.98241200	1.63251300	0.27154600
C	3.34687500	-0.00762300	0.42044200
C	4.68245300	0.16252100	0.69581600
C	2.96827200	-1.03673300	-0.53258900
C	5.69697900	-0.60899000	0.06282100
H	4.98439100	0.92020800	1.41355200
C	3.99893300	-1.82924100	-1.19021200
C	5.32188700	-1.59116400	-0.87557300
H	6.09654500	-2.17879900	-1.35833000
O	1.75057200	-1.30680000	-0.81400200
C	3.57959200	-2.87631400	-2.17519300
H	2.92953400	-3.61882100	-1.70024900
H	2.99991200	-2.43195900	-2.99131100
H	4.44785600	-3.38575600	-2.59608200
C	7.13493400	-0.35672200	0.39472200
H	7.79649000	-1.08242600	-0.08069700
H	7.42986700	0.64773200	0.06520900
H	7.29419800	-0.38792700	1.47841800
C	1.43279600	2.90464300	-2.80072600
H	2.16382100	2.76078300	-1.99716000
H	1.53095300	2.04173800	-3.46900200
H	1.71468600	3.80128800	-3.35839100
C	-2.86909700	5.53519300	-2.32545800
H	-2.32431500	6.44402900	-2.04696700
H	-3.10350300	5.61856300	-3.39352500
H	-3.81627800	5.53160900	-1.77912900
C	-2.75855900	-1.95009600	0.70898800
C	-4.06667900	-2.37935700	0.46831000
C	-1.67065800	-2.70067800	0.22547500
C	-4.31671600	-3.56211000	-0.23338400
H	-4.89872300	-1.78938200	0.84533200
C	-1.89332600	-3.89719000	-0.49040500
C	-3.21453400	-4.29859200	-0.69733700
H	-3.39360900	-5.22103000	-1.24601700
O	-0.41061300	-2.27374400	0.48393700
C	-0.72693000	-4.70903000	-0.99121800
H	-0.06859200	-4.11068800	-1.63001200
H	-0.11102600	-5.07342900	-0.16113700
H	-1.07016300	-5.57360300	-1.56453900
C	-5.72580500	-4.04603000	-0.48196200
H	-5.89695600	-4.25202400	-1.54418400
H	-5.92908100	-4.97704000	0.06039800
H	-6.46362100	-3.30671100	-0.15936600
H	2.85847600	1.52133800	1.80285600
C	1.47827100	-0.73021600	2.64478600
H	0.56607700	-1.18403000	3.03025100
H	2.08797000	-1.51278800	2.19157000
H	2.03539600	-0.27754000	3.47279100

$[^{HS}Mn^{III}(L^{2})]^{+}$ *S*=3/2, Isomer 2

Mn	-0.11305000	-0.35034200	-1.15092200
N	-1.24299500	1.40912200	-0.78397000
N	-0.03695000	-0.41104200	1.11901400
C	-1.25950500	1.70397900	0.65945500
C	-1.88207900	2.86895800	1.12267200
C	-0.65210800	0.83489200	1.57812300
C	-1.89984000	3.17621800	2.47925300
H	-2.35570000	3.54626300	0.42091900
C	-0.67513700	1.15405000	2.94183500
C	-1.29095200	2.31626600	3.39381400
H	-2.38698500	4.08429100	2.81824100
H	-0.21453300	0.48335100	3.65887300
H	-1.29875100	2.54564500	4.45409400
C	-0.59863100	2.53945200	-1.57532800
H	-0.58813500	2.18485000	-2.61255600
H	-1.25044300	3.41658400	-1.53189500
C	-2.64814100	1.23124700	-1.33424300
H	-2.51715500	1.11463200	-2.41583900
H	-3.20583300	2.15725900	-1.16766400
C	0.78778500	2.89061000	-1.12927500
C	1.76793900	1.88161000	-1.16420900
C	1.13814100	4.19294100	-0.76746900
C	3.11717900	2.19628100	-0.88439600
C	2.46035400	4.52702500	-0.45722400
H	0.36832900	4.96048200	-0.74093400
C	3.42651600	3.51359500	-0.53576800
H	4.46437800	3.75913600	-0.32059400

www.manaraa.com

O	1.42879000	0.62230800	-1.50249400
C	1.41751900	-0.45123900	1.45805700
H	1.87585500	0.44145500	1.02277700
C	2.16396500	-1.68532800	0.98785100
C	3.15808000	-2.19137000	1.79473700
C	1.93541600	-2.32715500	-0.29756700
C	3.97776200	-3.28518700	1.40651300
H	3.33270400	-1.73774200	2.76661200
C	2.76580400	-3.45399200	-0.70025400
C	3.75636100	-3.89267100	0.15411400
H	4.37976500	-4.73104200	-0.14126400
O	0.99452900	-1.98422000	-1.09567200
C	2.50544700	-4.09643900	-2.02811900
H	1.48297500	-4.48550500	-2.07855500
H	2.60042700	-3.36679200	-2.83921900
H	3.20359600	-4.91584900	-2.20644300
C	5.05088500	-3.77541900	2.32929600
H	5.60144500	-4.61468100	1.90179500
H	5.76038400	-2.97101500	2.55693300
H	4.62010000	-4.09106300	3.28707900
C	4.18670000	1.14058600	-1.00027200
H	4.00095100	0.29219400	-0.33307700
H	4.23067700	0.73190400	-2.01605400
H	5.16846700	1.55406300	-0.75694100
C	2.83627300	5.92742600	-0.03394400
H	2.88218700	6.01583700	1.05886100
H	3.81979400	6.21136100	-0.42071000
H	2.10724700	6.66133900	-0.38899800
C	-3.40118800	0.05955500	-0.77839600
C	-4.66911900	0.20670800	-0.21122200
C	-2.85047500	-1.22560700	-0.94292300
C	-5.42193000	-0.90566600	0.17846000
H	-5.08109800	1.20546100	-0.08724600
C	-3.59635500	-2.36842200	-0.57722300
C	-4.86639100	-2.17746600	-0.02774600
H	-5.44481200	-3.05554500	0.25191700
O	-1.62305100	-1.36781300	-1.48029700
C	-3.02780300	-3.74517100	-0.80195600
H	-2.83800200	-3.92784000	-1.86563700
H	-2.06835400	-3.87108100	-0.28908500
H	-3.71416900	-4.51505600	-0.44115000
C	-6.78191300	-0.74680100	0.81606400
H	-7.47743100	-1.51829000	0.47127700
H	-6.72362700	-0.83143300	1.90849900
H	-7.21773500	0.22975200	0.58728700
H	1.54901600	-0.37919200	2.54375200
C	-0.74747100	-1.58732800	1.69680100
H	-1.81281000	-1.49914300	1.48952000
H	-0.37294000	-2.50035700	1.23418100
H	-0.59458800	-1.65128300	2.77962500

[^{HS}Mn^{III}(L^{2})]$^{+}$ *S*=5/2, Isomer 1

Mn	-0.09007000	0.51898200	-0.22879800
N	1.64918300	-0.09312600	0.76072200
N	-1.08386000	-0.43033400	1.56812900
C	1.28634800	-1.15457000	1.71469500
C	2.27708600	-1.96796000	2.27353700
C	-0.05056900	-1.30881900	2.11856200
C	1.94986400	-2.93634200	3.21829800
H	3.31081800	-1.84954600	1.97085400
C	-0.36532300	-2.28003800	3.07600500
C	0.62409800	-3.09333400	3.62128400
H	2.73040100	-3.56220400	3.63751200
H	-1.39092600	-2.39966800	3.40693700
H	0.35905200	-3.84174100	4.36051500
C	2.61642800	-0.56255000	-0.30851400
H	2.71238300	0.27946500	-1.00325300
H	3.60434900	-0.69980700	0.14170900
C	2.27219800	1.06566300	1.53257500
H	3.24726000	0.73714100	1.90511700
H	1.62074500	1.22981100	2.39439200
C	2.18934500	-1.82283400	-1.00946200
C	0.87141100	-1.96146500	-1.47963800
C	3.11802500	-2.84562200	-1.23856300
C	0.49638600	-3.12378500	-2.19252900
C	2.77625100	-3.99996900	-1.94379000
H	4.13187700	-2.72966400	-0.86184100
C	1.45734500	-4.11072400	-2.41049100
H	1.16580800	-5.00218400	-2.96238500
O	-0.05545200	-1.00148400	-1.28076800
C	-2.22827900	-1.21520200	1.00499800
H	-1.80568700	-1.87146400	0.23890500
C	-3.33239500	-0.37890400	0.39648500
C	-4.63886900	-0.63134000	0.73938500
C	-3.07130500	0.61848500	-0.63022800
C	-5.73495600	0.02822700	0.11434700
H	-4.85318500	-1.36991300	1.50674200
C	-4.18809300	1.28392000	-1.29059300
C	-5.47454800	0.97252900	-0.89905000
H	-6.31064300	1.47101700	-1.38006500
O	-1.89191400	0.95624400	-0.98574100
C	-3.89047700	2.29227400	-2.35668900
H	-3.29486800	3.11875900	-1.95425000
H	-3.29707700	1.84431500	-3.16084100
H	-4.81188000	2.69563800	-2.77952000
C	-7.13399900	-0.29485100	0.53896000
H	-7.87345000	0.27542100	-0.02518400
H	-7.33946800	-1.36376400	0.40519400
H	-7.26965100	-0.08344300	1.60653500
C	-0.91142300	-3.26646700	-2.71143700
H	-1.64572800	-3.25162200	-1.89789300
H	-1.17461600	-2.44268500	-3.38421200
H	-1.03151000	-4.20557700	-3.25743300
C	3.78188100	-5.09955700	-2.19337700
H	3.46155400	-6.04665000	-1.74373500
H	3.91571100	-5.28518800	-3.26527000
H	4.75975000	-4.84649900	-1.77475900
C	2.39570500	2.32529200	0.72585800
C	3.61724100	2.97425000	0.52461100
C	1.20817600	2.88875300	0.22274600
C	3.67982300	4.19170600	-0.15913700
H	4.52795500	2.52807700	0.91702800
C	1.24161800	4.11514500	-0.47595200
C	2.48001300	4.73777300	-0.64357300
H	2.51317900	5.68458500	-1.17877900
O	0.03396100	2.24441900	0.43689800
C	-0.03171400	4.72052100	-1.00707300
H	-0.54313300	4.03553800	-1.69210400
H	-0.73694600	4.93860800	-0.19728700
H	0.17176300	5.65172800	-1.54140000
C	4.99289700	4.90668100	-0.37463500
H	5.17464300	5.09747100	-1.43824000
H	5.00529000	5.87944800	0.13054600
H	5.83279000	4.32172100	0.00922000

www.manaraa.com

H	-2.67810700	-1.84599600	1.77806700
C	-1.54765700	0.53939900	2.59996500
H	-0.69213600	1.09532800	2.98009400
H	-2.24440200	1.24580000	2.14774900
H	-2.04536800	0.02628700	3.43071300

$[^{HS}Mn^{III}(L^2)]^+$ *S*=5/2, Isomer 2

Mn	-0.10351900	-0.29351700	-1.17826400
N	-1.23870500	1.44620600	-0.76625900
N	-0.01370600	-0.40608900	1.09360800
C	-1.23981100	1.71680600	0.68196600
C	-1.86097800	2.87204000	1.17080200
C	-0.61418700	0.83753600	1.57839700
C	-1.85786300	3.16106700	2.53143200
H	-2.34907900	3.55619000	0.48580000
C	-0.61558600	1.13922400	2.94634900
C	-1.22837000	2.29272400	3.42389800
H	-2.34416300	4.06177800	2.89062700
H	-0.14211400	0.46050100	3.64721600
H	-1.21909000	2.50813400	4.48708900
C	-0.61065900	2.59659600	-1.54272800
H	-0.60929700	2.26482400	-2.58708000
H	-1.26672800	3.46859300	-1.47292400
C	-2.64693900	1.26025900	-1.30446300
H	-2.52703700	1.16860200	-2.38991200
H	-3.21514100	2.17513100	-1.11300600
C	0.77942600	2.94511300	-1.10584100
C	1.76239400	1.94153200	-1.17735700
C	1.12956200	4.23895400	-0.71331100
C	3.11206300	2.25020700	-0.89886600
C	2.45374100	4.56818900	-0.40794700
H	0.35783600	5.00305700	-0.65798700
C	3.42154900	3.55916900	-0.51995200
H	4.46048000	3.80141800	-0.30604300
O	1.41928300	0.69149400	-1.55046100
C	1.44461800	-0.47148400	1.42051300
H	1.91926900	0.39921800	0.95938700
C	2.14753400	-1.73749600	0.97156600
C	3.08380500	-2.30166700	1.80609800
C	1.93331800	-2.35010900	-0.33180300
C	3.86144300	-3.43323600	1.43339300
H	3.24711800	-1.86800600	2.78887000
C	2.71994500	-3.51649100	-0.71759300
C	3.65494500	-4.01460900	0.16642400
H	4.24551400	-4.88047900	-0.11693500
O	1.05634200	-1.93735400	-1.16332900
C	2.47620600	-4.12841400	-2.06246100
H	1.43683700	-4.46064400	-2.15618700
H	2.64031600	-3.39503700	-2.85913900
H	3.13561500	-4.98214900	-2.22657100
C	4.88021700	-3.98050100	2.38467200
H	4.42812900	-4.18709400	3.36134900
H	5.33759100	-4.89638000	2.00730300
H	5.67415200	-3.24333500	2.55868800
C	4.18121600	1.19760700	-1.04605700
H	3.99168800	0.32856800	-0.40698700
H	4.22818000	0.82190700	-2.07438700
H	5.16282700	1.60143100	-0.78642100
C	2.83081900	5.95871400	0.04639600
H	2.90025400	6.01714200	1.13993200
H	3.80391400	6.25988900	-0.35362600
H	2.09001100	6.69745800	-0.27235100
C	-3.38227900	0.06886600	-0.76409400
C	-4.65220500	0.19741000	-0.19503700
C	-2.82367700	-1.21051000	-0.94810100
C	-5.39806800	-0.92492400	0.17704200
H	-5.07107400	1.19134300	-0.05627500
C	-3.56366600	-2.36324500	-0.60242100
C	-4.83462300	-2.18964500	-0.05002700
H	-5.40704000	-3.07602100	0.21552500
O	-1.59265500	-1.34113200	-1.48248100
C	-2.98655500	-3.73298100	-0.84795000
H	-2.78408700	-3.89391000	-1.91275200
H	-2.03262500	-3.86578300	-0.32650300
H	-3.67377500	-4.51241400	-0.51001200
C	-6.75959400	-0.78547400	0.81602000
H	-7.46044500	-1.53281200	0.43071700
H	-6.70731400	-0.92470500	1.90307500
H	-7.18584200	0.20485400	0.63341800
H	1.58991200	-0.37860200	2.50260000
C	-0.73385400	-1.58008500	1.66513100
H	-1.80051300	-1.47194500	1.47617200
H	-0.38132300	-2.49213400	1.18374700
H	-0.56518400	-1.66241600	2.74438300

$[^{HS}Mn^{III}(L^2)]^{2+}$ *S*=1, Isomer 1

Mn	-0.14988700	0.51702000	-0.18597200
N	1.62176600	-0.02411000	0.86841300
N	-1.11807700	-0.50136500	1.57345900
C	1.27944500	-1.10288500	1.81408700
C	2.28976800	-1.86371100	2.41119800
C	-0.06302800	-1.32999400	2.16174800
C	1.97566600	-2.85515900	3.33651900
H	3.32932000	-1.68518500	2.16212200
C	-0.36406500	-2.32254300	3.10056000
C	0.64479500	-3.08601800	3.68150100
H	2.77099500	-3.43835400	3.78767200
H	-1.39330100	-2.49898500	3.39109000
H	0.38980000	-3.85208700	4.40561100
C	2.67377200	-0.44305800	-0.12509200
H	2.80894100	0.40251900	-0.80953400
H	3.63047300	-0.56763600	0.38857300
C	2.14716300	1.18458000	1.64609500
H	3.12496400	0.92299900	2.06038200
H	1.45247800	1.32363900	2.47683900
C	2.36097400	-1.69205400	-0.90610900
C	1.04732400	-1.90731800	-1.46998300
C	3.34808400	-2.60691700	-1.17467900
C	0.79896100	-3.04712300	-2.33603300
C	3.11823200	-3.73557300	-2.01477100
H	4.33884000	-2.47173900	-0.75018200
C	1.83881500	-3.92179400	-2.57916600
H	1.66948700	-4.78024600	-3.22117400
O	0.06367600	-1.11540800	-1.21763900
C	-2.22435200	-1.34299000	1.00707500
H	-1.77042500	-2.01691500	0.27465000
C	-3.34174700	-0.55902500	0.35648000
C	-4.64587800	-0.84453100	0.67533800
C	-3.08779600	0.43166600	-0.67281300
C	-5.74577100	-0.22126100	0.01570700
H	-4.85750100	-1.57685100	1.44900600
C	-4.20132300	1.06285800	-1.36716000
C	-5.48780800	0.71878600	-1.00200800
H	-6.32589700	1.19076700	-1.50497600

www.manaraa.com

O	-1.90238500	0.79836200	-0.99969100
C	-3.90762000	2.07420600	-2.43043700
H	-3.35931900	2.92578500	-2.01285900
H	-3.27178600	1.64515800	-3.21188300
H	-4.82933800	2.43982800	-2.88509200
C	-7.14222400	-0.57874800	0.41333400
H	-7.88530900	-0.00262400	-0.13917100
H	-7.32628100	-1.64650800	0.24046000
H	-7.28997100	-0.40991400	1.48666400
C	-0.56498700	-3.23254700	-2.92424900
H	-1.30945700	-3.40256700	-2.13864600
H	-0.88028700	-2.33651700	-3.46842300
H	-0.57974000	-4.08419700	-3.60556400
C	4.23526000	-4.68932700	-2.29142400
H	4.65930500	-5.06752100	-1.35398700
H	3.91079900	-5.53405500	-2.90016900
H	5.05127500	-4.17413100	-2.81389700
C	2.22486100	2.42861700	0.80941200
C	3.41266000	3.13081100	0.60165300
C	1.02220000	2.90930800	0.25414400
C	3.42119200	4.31996700	-0.13736100
H	4.33835900	2.75415200	1.02858200
C	1.00051900	4.09678100	-0.50987600
C	2.20718400	4.77758900	-0.67673400
H	2.20477600	5.69919300	-1.25404300
O	-0.12140500	2.21922400	0.48992600
C	-0.29244300	4.60719400	-1.08936600
H	-0.77279000	3.85093400	-1.71885200
H	-1.00713300	4.85956800	-0.29826000
H	-0.12248700	5.50157900	-1.69255800
C	4.69503000	5.10033100	-0.34954600
H	4.84402800	5.33828700	-1.40795700
H	4.66668200	6.05345700	0.19125500
H	5.56792300	4.54444200	0.00106000
H	-2.66693000	-1.96294200	1.79193100
C	-1.65055700	0.45578800	2.59027900
H	-0.82890700	1.04085600	2.99930200
H	-2.35858900	1.13540600	2.11556200
H	-2.15454500	-0.07965500	3.40198200

$[^{HS}Mn^{III}(L^{2})]^{2+}$ *S*=1, Isomer 2

Mn	-0.11541900	-0.37259300	-1.12032100
N	-1.25579900	1.39732900	-0.74537600
N	0.03722500	-0.36658400	1.14822300
C	-1.24647100	1.71272400	0.69676900
C	-1.88377600	2.87059500	1.15655500
C	-0.57912600	0.87989100	1.60666900
C	-1.85831000	3.20506200	2.50653300
H	-2.40050900	3.52216900	0.46092500
C	-0.55727900	1.22810400	2.96286200
C	-1.18795800	2.38307600	3.41308800
H	-2.35809100	4.10582200	2.84578000
H	-0.05204200	0.58646600	3.67595800
H	-1.16018100	2.63603400	4.46739500
C	-0.62630300	2.52817100	-1.55705600
H	-0.65003800	2.18321800	-2.59611200
H	-1.26457400	3.41212000	-1.48275100
C	-2.65873400	1.22250500	-1.28261100
H	-2.54848200	1.08334600	-2.36413500
H	-3.21592300	2.15102000	-1.13324900
C	0.77703200	2.85876000	-1.15547200
C	1.74825900	1.83635700	-1.25495200
C	1.15902200	4.13679700	-0.76350800
C	3.11849500	2.11357100	-1.00841800
C	2.50371100	4.43676000	-0.49504800
H	0.40770800	4.91658300	-0.67781300
C	3.45626100	3.41247700	-0.63425000
H	4.50174300	3.64067000	-0.44313900
O	1.37145700	0.60571700	-1.61742300
C	1.50757300	-0.38517900	1.42981800
H	1.94299500	0.49858800	0.95384900
C	2.23931600	-1.63149200	0.97031400
C	3.26509400	-2.11220000	1.75124800
C	1.95786100	-2.31291500	-0.28164300
C	4.06644600	-3.22153800	1.36304500
H	3.48032600	-1.62908400	2.70028000
C	2.76702100	-3.45320700	-0.68603200
C	3.79155100	-3.86722100	0.14012000
H	4.40061600	-4.71595700	-0.15474700
O	0.97759500	-1.99205800	-1.04830600
C	2.44963400	-4.13621100	-1.98023800
H	1.42720300	-4.52888600	-1.97229600
H	2.50692800	-3.43183500	-2.81675500
H	3.14134400	-4.95957900	-2.16338600
C	5.17445000	-3.68447000	2.25574900
H	5.70224700	-4.54264300	1.83798100
H	5.89581200	-2.87547700	2.42275400
H	4.78255500	-3.95883600	3.24263200
C	4.16071700	1.04348100	-1.19086400
H	3.96410700	0.16832500	-0.56305200
H	4.17846500	0.68680100	-2.22647900
H	5.15351100	1.42458300	-0.94357700
C	2.92425100	5.82836100	-0.10009900
H	3.72929600	5.80581500	0.64016700
H	3.30130400	6.38207600	-0.96902000
H	2.08815900	6.39736500	0.31395800
C	-3.44690500	0.07551400	-0.71728200
C	-4.72431600	0.25184800	-0.24370300
C	-2.91739400	-1.26195400	-0.81286700
C	-5.54292100	-0.85699600	0.11317900
H	-5.13448400	1.25409100	-0.16198200
C	-3.74795400	-2.40402700	-0.49383400
C	-5.03012700	-2.16316500	-0.03599500
H	-5.66529100	-3.00519400	0.22035500
O	-1.69610100	-1.46481000	-1.18273500
C	-3.19579900	-3.78629100	-0.66138700
H	-2.87304900	-3.95094200	-1.69484000
H	-2.31437800	-3.94042500	-0.03019100
H	-3.94443700	-4.53650700	-0.40328800
C	-6.93758700	-0.62351800	0.60070600
H	-7.39245300	-1.53588900	0.98896500
H	-6.95536300	0.14678700	1.37885000
H	-7.56406200	-0.25114000	-0.22070400
H	1.67970000	-0.27665000	2.50590500
C	-0.62726100	-1.53569900	1.79875300
H	-1.70702100	-1.43676700	1.70058800
H	-0.30539500	-2.45619200	1.31293000
H	-0.37719700	-1.58888600	2.86315200

$[^{HS}Mn^{III}(L^{2})]^{2+}$ *S*=3, Isomer 1

Mn	-0.17863500	0.47724300	-0.21311300
N	1.61071500	0.08999600	0.83354800
N	-1.08031700	-0.56811900	1.56203600
C	1.35255900	-1.01281400	1.77897700

www.manaraa.com

C	2.41795500	-1.70078700	2.36706700
C	0.03041400	-1.33328800	2.13369100
C	2.17926500	-2.71537100	3.29025600
H	3.44008300	-1.44601900	2.11268400
C	-0.19470000	-2.34885200	3.06879500
C	0.86976400	-3.04150000	3.64021400
H	3.01583400	-3.24241700	3.73572100
H	-1.20745400	-2.59804600	3.36417900
H	0.67369600	-3.82679200	4.36217300
C	2.67960300	-0.23710700	-0.17859000
H	2.70878000	0.60984000	-0.87389000
H	3.65456400	-0.25295600	0.31620500
C	2.04369300	1.33300900	1.61162500
H	3.03807800	1.14354800	2.02523400
H	1.34209500	1.41758600	2.44365700
C	2.48213000	-1.53252100	-0.92118800
C	1.17962400	-1.91348800	-1.42307300
C	3.55438200	-2.34535100	-1.19201200
C	1.02652900	-3.12888100	-2.20905300
C	3.42015600	-3.53777500	-1.96265600
H	4.53917100	-2.08065200	-0.81732800
C	2.14638000	-3.89613100	-2.45423700
H	2.04918900	-4.80388100	-3.04106400
O	0.12924000	-1.20836000	-1.19232700
C	-2.14966800	-1.46270900	1.00788400
H	-1.66891600	-2.11957100	0.27738800
C	-3.30218900	-0.73044000	0.35617400
C	-4.59126600	-1.03576000	0.71615900
C	-3.09757700	0.21675500	-0.72657900
C	-5.72294300	-0.47402200	0.05419100
H	-4.76616300	-1.74048900	1.52375100
C	-4.24517900	0.77779300	-1.42768600
C	-5.51291700	0.41919700	-1.01569000
H	-6.37405400	0.84048400	-1.52453600
O	-1.93076100	0.58851200	-1.10943000
C	-4.00303600	1.73368200	-2.55337000
H	-3.47802200	2.62683300	-2.19710900
H	-3.36449900	1.28038100	-3.31873100
H	-4.94386900	2.03993800	-3.01268100
C	-7.09992000	-0.84133400	0.50644000
H	-7.86969600	-0.41569000	-0.13857100
H	-7.21941200	-1.93051800	0.53426100
H	-7.26883300	-0.48537300	1.53089700
C	-0.33037900	-3.48902900	-2.72829900
H	-1.04621200	-3.60941500	-1.90817900
H	-0.72273700	-2.69408500	-3.37173700
H	-0.29400300	-4.41745900	-3.29956500
C	4.62344600	-4.38188100	-2.23236500
H	5.08528000	-4.70163100	-1.29022600
H	4.37952200	-5.26641200	-2.82182000
H	5.38476700	-3.80054300	-2.76692700
C	2.02617000	2.58433900	0.78321600
C	3.15364400	3.38527100	0.60003400
C	0.79193600	2.97780300	0.22765100
C	3.07061500	4.58623400	-0.11442500
H	4.10369500	3.07657100	1.02794200
C	0.67699200	4.17854400	-0.50666600
C	1.82563300	4.95718500	-0.65082100
H	1.75193100	5.88777200	-1.20855400
O	-0.29137900	2.18601700	0.43269300
C	-0.64992400	4.59537200	-1.08332100
H	-1.06615000	3.81490700	-1.72862700
H	-1.38540700	4.77625300	-0.29173200
H	-0.54920300	5.51088800	-1.67000000
C	4.27935400	5.46893600	-0.30321900
H	4.41971500	5.73062700	-1.35728000
H	4.16866600	6.41020400	0.24757000
H	5.19033600	4.98033300	0.05081600
H	-2.56198100	-2.09571500	1.79894800
C	-1.64766700	0.35909400	2.58780500
H	-0.85463200	0.99083500	2.98415800
H	-2.40068000	0.99584000	2.12392300
H	-2.10445100	-0.20378700	3.40873100

[$^{HS}Mn^{III}(L^2)]^{2+}$ *S*=3, Isomer 2

Mn	-0.07140400	-0.28814100	-1.14904400
N	-1.22571800	1.45258000	-0.73875600
N	0.03907800	-0.37490000	1.11459400
C	-1.20014900	1.74126100	0.70955100
C	-1.81367300	2.90150100	1.19505700
C	-0.54350400	0.87885100	1.59950800
C	-1.77328000	3.20987500	2.55086600
H	-2.32205700	3.57585900	0.51520100
C	-0.50661100	1.20100900	2.96167600
C	-1.11225700	2.35910200	3.43744100
H	-2.25381200	4.11335100	2.91004400
H	-0.01059100	0.53593600	3.65955800
H	-1.07289800	2.59182600	4.49600700
C	-0.61315000	2.60459300	-1.53915500
H	-0.64949600	2.28120700	-2.58445900
H	-1.25827200	3.48057100	-1.43847000
C	-2.63483400	1.27446800	-1.25823900
H	-2.54178700	1.16087900	-2.34399100
H	-3.19713400	2.19443300	-1.07751200
C	0.79138000	2.93325300	-1.13875400
C	1.75991800	1.91819000	-1.25573900
C	1.16923000	4.20454000	-0.71045300
C	3.12071100	2.18182200	-0.98207100
C	2.50849200	4.49753100	-0.42412700
H	0.41471400	4.97983200	-0.60995000
C	3.45740600	3.47448600	-0.57540800
H	4.50201000	3.69358600	-0.36774700
O	1.37695400	0.69398300	-1.67693800
C	1.51076400	-0.44512700	1.39822800
H	1.97899600	0.41265600	0.90640300
C	2.18211200	-1.73133700	0.95887200
C	3.11865500	-2.30542000	1.78373900
C	1.92914400	-2.35752500	-0.32872500
C	3.86078200	-3.46429900	1.41155400
H	3.31293100	-1.86355800	2.75683300
C	2.67609300	-3.54884400	-0.71647000
C	3.61373400	-4.05884600	0.15746600
H	4.17529500	-4.94404200	-0.12400500
O	1.04149200	-1.93220000	-1.14915500
C	2.38865600	-4.17260500	-2.04623300
H	1.33976200	-4.48123700	-2.11171600
H	2.55328500	-3.45439500	-2.85650400
H	3.02346800	-5.04415200	-2.21139800
C	4.88740800	-4.01733900	2.34751300
H	5.26048900	-4.98734700	2.01601700
H	5.73927400	-3.32828900	2.42005400
H	4.48068600	-4.11530400	3.35985400
C	4.16781600	1.11463500	-1.16918300
H	4.00097300	0.25556400	-0.51081900

www.manaraa.com

H	4.16181700	0.73089600	-2.19477200
H	5.16351400	1.51032000	-0.95815500
C	2.92875600	5.88069200	0.00758000
H	3.71923200	5.83936400	0.76278500
H	3.32276300	6.45379000	-0.84063700
H	2.08779100	6.44331300	0.42110000
C	-3.40575400	0.10716200	-0.70711100
C	-4.66557700	0.26491900	-0.19035900
C	-2.87963900	-1.23128400	-0.86447700
C	-5.48021600	-0.85795200	0.15248000
H	-5.07376800	1.26242900	-0.05854000
C	-3.71200900	-2.38607800	-0.56119900
C	-4.97779500	-2.16066300	-0.05855600
H	-5.60826100	-3.00924200	0.18747700
O	-1.67504800	-1.42731000	-1.26578800
C	-3.16117200	-3.75767900	-0.79216600
H	-2.88571500	-3.88974100	-1.84413000
H	-2.24797300	-3.91761200	-0.20920700
H	-3.89074700	-4.52129000	-0.51993500
C	-6.85729300	-0.63458500	0.68573900
H	-7.30074900	-1.55307600	1.07229200
H	-6.85281300	0.12602600	1.47347500
H	-7.50683100	-0.24994400	-0.11259300
H	1.68805600	-0.32638200	2.47201200
C	-0.66373100	-1.53510500	1.74183200
H	-1.73946300	-1.38921600	1.65945800
H	-0.38537100	-2.45629100	1.23043700
H	-0.40541600	-1.62595300	2.80176000

Table B5. Frequencies (cm^{-1}) for all optimized structures.

$[^{HS}Mn^{III}(L^1)(CH_3OH)]^0$ S=2

15.6294 27.6272 29.8376 32.3668 34.8929 40.7550
42.3807 45.6158 48.5643 61.8792 74.5846 83.7317
90.3141 95.6249 104.2071 110.8661 118.1023 128.1257
131.9099 134.5866 135.0096 144.6642 148.7101 161.5423
174.6856 182.4604 188.5920 196.0452 201.1499 207.6627
218.2090 221.4539 223.0363 238.1232 243.3590 255.4313
265.1722 267.7617 282.6182 298.7640 303.0286 306.0318
310.4176 321.9974 329.8860 345.9204 357.9405 359.2917
369.5879 405.3065 422.5024 428.7050 440.3768 449.1116
481.3315 494.7620 501.1562 506.9326 522.0654 523.0502
530.5068 533.2055 542.8196 545.8328 553.6227 560.3966
570.1073 576.4368 580.9760 586.2255 587.2963 606.1792
615.0349 624.0813 633.0900 680.5852 686.6503 706.0243
751.7752 756.1026 762.9302 769.5545 781.2307 782.5448
820.4740 830.5602 833.4693 873.7556 878.5207 879.7345
881.1006 886.8286 906.6156 907.6392 924.4063 941.8322
954.7036 961.1770 970.3006 980.3684 980.6304 987.9248
990.0136 992.3236 995.3938 1009.7089 1030.2899 1035.6878
1036.3160 1038.1052 1040.3444 1046.0760 1059.6433 1060.1585
1061.4153 1061.9290 1062.4006 1064.2822 1066.5626 1067.8109
1075.2048 1076.1110 1080.1285 1127.5960 1180.0975 1185.6106
1186.8390 1188.6749 1190.6443 1204.4361 1230.7329 1239.9736
1266.5392 1273.1516 1280.3101 1280.7616 1289.7014 1296.1295
1302.6161 1312.8181 1326.4529 1336.0902 1343.4747 1347.9196
1350.5050 1354.3863 1357.2764 1360.5653 1398.9041 1417.9601
1418.7388 1419.7398 1420.7696 1423.1200 1424.6718 1424.8888
1427.6473 1450.3071 1453.4778 1454.0064 1457.0831 1477.0068
1477.4081 1480.3752 1483.8291 1485.2585 1488.4452 1489.5556
1490.6659 1491.0391 1492.0174 1497.1621 1499.8571 1502.4346
1508.5203 1509.6491 1510.5034 1512.0447 1513.3897 1516.9618
1520.3528 1529.4361 1579.7469 1619.0656 1620.4725 1628.9183
1636.6534 1658.8292 1659.1203 1660.9231 1671.7456 3030.6281
3030.8126 3032.8980 3038.6096 3039.5563 3039.8749 3041.6691
3045.6075 3046.4103 3084.8303 3085.9389 3086.8473 3088.1147
3089.0608 3091.4189 3092.0632 3093.0491 3096.3061 3116.2177
3117.6770 3117.8384 3121.3847 3123.3004 3124.2283 3125.0617
3157.9720 3158.0601 3158.9281 3164.0322 3164.2473 3165.0457
3175.5824 3192.3533 3199.4758 3210.7498 3218.0846 3786.1401

$[^{LS}Mn^{III}(L^1)(CH_3OH)]^0$ S=1

11.6241 24.6320 30.2606 33.9605 37.4899 40.9336
45.6484 52.4249 67.7882 77.9549 80.1408 88.3137
97.1325 99.1076 104.7993 116.2948 122.4420 131.1341
141.8333 148.4766 150.8510 161.1158 175.1151 181.2239
189.2458 195.6490 199.1287 204.2166 210.9726 216.8056
223.9451 233.7675 246.0401 253.4486 263.3176 267.7887
292.0270 297.4226 300.3949 311.9002 318.4130 328.5647
332.7671 343.5051 354.0359 361.9964 366.7415 387.0409
408.5493 426.5560 429.9649 437.6890 441.3438 468.9920
484.5642 494.4806 503.8590 510.2317 518.2446 531.1833
536.8464 537.9930 546.2754 558.3102 574.9959 575.8956
578.9107 583.2771 585.6163 587.4632 609.1885 614.6490
635.6606 654.7612 671.6276 682.7768 690.1941 709.7194
750.6700 753.7703 761.0427 767.4063 778.1996 784.7294
826.4279 830.6265 839.9669 868.9077 874.4799 880.1644
880.4781 898.5838 905.6777 906.5794 927.2808 942.1982
952.8448 964.1668 970.1529 972.0724 979.8887 982.1437
989.8012 990.1788 992.6970 1014.7318 1020.3765 1028.5730
1035.7073 1038.1537 1038.5389 1047.8579 1056.4698 1059.5711
1060.9203 1062.0219 1062.6780 1064.4150 1067.1106 1070.0560
1077.4534 1086.0602 1087.5712 1130.1678 1185.1506 1185.8571
1189.4702 1191.2741 1192.3242 1208.6421 1226.8285 1243.6620
1271.4044 1276.1507 1280.2446 1282.0183 1293.6723 1303.2364
1305.5409 1314.9367 1325.6035 1340.6235 1348.0282 1352.0447
1356.3149 1357.7474 1364.2189 1370.2254 1410.8186 1417.4347
1419.7804 1419.9117 1421.4201 1422.9248 1424.4750 1426.2718
1433.3688 1448.6605 1453.9276 1456.1300 1459.7223 1472.3788
1477.7802 1479.1183 1480.5465 1485.0976 1488.1168 1489.7807
1490.4699 1490.7782 1491.4517 1496.3769 1501.1731 1503.2910
1510.3362 1511.1169 1511.4262 1513.4444 1515.6265 1516.7174
1523.1861 1533.0418 1580.0395 1618.5722 1621.4573 1634.9311
1638.4274 1657.7063 1660.4906 1662.5309 1677.2792 3029.8265
3030.2193 3032.6067 3035.8607 3037.4352 3038.9746 3046.8454
3049.4961 3068.5170 3081.9106 3084.2725 3084.3597 3089.1952
3090.1479 3091.6056 3093.7231 3096.2664 3115.8256 3116.6851
3121.1408 3121.3254 3121.7321 3125.8566 3148.9062 3154.4673
3154.7741 3155.5718 3159.5578 3160.6858 3162.8528 3167.5115
3189.5708 3195.4355 3204.3398 3216.0697 3224.7681 3734.7110

$[^{HS}Mn^{III}(L^1)(CH_3OH)]^+$ S=3/2

15.9194 27.8867 30.4978 38.9541 40.8575 42.7179
43.9014 49.3042 50.2016 68.0759 75.2789 85.4297
95.5912 96.5821 112.4559 115.6286 121.6781 124.4874
125.9883 134.2891 136.2442 148.0592 154.8773 155.8453
171.4726 178.1114 190.1879 192.6380 193.7964 199.2805
207.2185 216.7210 223.5261 229.5622 240.0817 248.1080
263.8823 269.5019 285.2641 294.9676 302.2139 307.2472
308.5117 324.6672 332.1984 340.5949 344.1986 358.3761
369.0744 400.7051 417.0175 427.4469 439.1881 447.1745
473.0589 479.4215 487.0920 488.8810 498.2553 512.6210
520.1469 523.8388 530.8878 542.9055 552.1838 554.8839
567.0302 573.3472 575.0518 580.8246 585.7347 595.8250
606.8425 623.7328 637.6339 674.4970 684.6647 704.7045
749.9932 753.0442 759.9755 769.6720 777.3925 781.3568
811.0952 822.5369 826.4267 877.4526 881.8117 883.1186
888.0704 892.3646 907.7658 912.4976 931.2343 940.0491
958.1346 962.8757 967.2465 979.5380 983.0194 987.5734
989.0028 996.5898 1000.9020 1009.4037 1018.1573 1024.8923
1036.7016 1039.4956 1040.0181 1042.8424 1046.9610 1051.9456
1058.6171 1061.6226 1062.7463 1064.8551 1067.1502 1067.4589
1076.7008 1081.9739 1086.9737 1126.6341 1176.4551 1180.1078
1185.0737 1186.8014 1192.7588 1205.8822 1229.7647 1247.8803
1266.3479 1271.9236 1278.9496 1281.7014 1288.5148 1303.7124
1308.4167 1316.2118 1328.7859 1336.6893 1341.3150 1346.7264
1353.0923 1366.2758 1367.5423 1394.1157 1404.2006 1411.4498
1417.3718 1420.5612 1421.6668 1422.1743 1423.9800 1426.2438
1426.7549 1447.7149 1451.2513 1451.7605 1455.7503 1472.1546
1473.0606 1476.6093 1480.4174 1481.5602 1485.9921 1488.2053
1489.2490 1490.8729 1491.3491 1493.4163 1497.8790 1502.3271

www.manaraa.com

1503.0923 1505.1232 1506.6002 1509.2965 1509.5630 1512.7218
1513.9272 1526.6116 1528.1229 1577.7972 1617.6724 1627.8042
1633.3290 1639.5391 1652.2513 1656.0359 1664.1280 3035.9085
3036.3415 3039.2924 3043.9123 3046.8170 3052.3118 3053.0164
3055.5026 3057.4994 3093.2383 3093.5975 3098.1120 3102.6984
3103.5940 3104.3282 3104.6402 3108.0250 3110.5129 3125.0055
3128.6216 3131.8706 3132.0089 3133.2625 3148.0112 3151.3530
3168.2951 3169.2089 3174.2702 3177.7768 3190.0042 3191.1013
3197.1009 3198.1537 3204.4613 3216.3612 3223.5274 3810.9636

1502.9790 1509.2334 1510.3043 1511.2550 1511.6490 1513.4385
1516.7080 1522.9036 1531.9585 1603.0715 1612.2015 1619.4546
1626.5279 1633.3017 1649.7413 1653.8763 1657.8342 3035.6444
3036.6874 3041.8309 3041.9111 3043.0928 3044.1673 3051.6130
3051.9005 3062.1359 3090.8371 3091.5178 3092.5632 3095.2565
3095.3593 3096.4581 3098.1819 3107.3185 3124.6610 3125.1439
3125.4489 3129.3906 3129.9473 3139.5404 3149.9271 3150.9558
3166.0298 3167.0193 3171.5744 3174.8494 3191.8838 3192.9429
3193.4592 3203.6379 3211.6465 3220.5997 3227.3529 3798.6288

$[Mn^{IV}(L^1)(CH_3OH)]^+$ S=3/2

16.2635 30.5743 32.4211 36.1537 43.3006 44.9738
52.2827 57.2760 76.6418 84.3497 88.2642 92.3895
96.0229 113.1535 118.2175 130.0802 131.3847 132.5491
141.1493 146.3845 150.8219 160.5993 173.0423 181.7910
190.0914 197.7552 203.7537 207.6845 213.4967 223.0429
233.0577 242.4657 246.9727 259.2057 266.2893 273.5894
291.4274 298.6788 304.3452 307.4813 328.7719 331.4651
338.5652 342.4783 356.0654 363.0036 365.4020 391.9203
413.4185 426.5819 435.0490 442.7188 443.4878 461.8589
489.4188 494.9948 511.5774 514.3592 523.7283 532.9483
536.1049 541.0293 549.5530 560.2072 572.4140 574.5014
578.3044 583.7344 585.2930 593.1773 609.8684 614.7448
633.7533 647.9068 665.0145 682.0628 686.5177 708.0189
744.6279 748.8981 751.4572 764.5039 777.6757 782.3974
834.3052 839.3014 846.1341 873.7446 881.1741 883.4197
887.9395 901.5664 913.1964 915.5404 936.2773 938.8347
960.3723 962.6602 968.7780 978.8541 981.6383 983.2110
988.3501 989.1351 992.2597 1003.6484 1004.4908 1018.0153
1038.3562 1040.2022 1041.2601 1043.4208 1060.8683 1061.1865
1062.4967 1062.8222 1063.1349 1065.4863 1068.9501 1072.4139
1075.5793 1093.5099 1093.6389 1125.1119 1175.5470 1182.9716
1186.4217 1188.8756 1193.6129 1208.4374 1231.4193 1238.0482
1265.1956 1271.6276 1275.3569 1282.5161 1284.2961 1296.3099
1306.8592 1315.1524 1323.5690 1335.0421 1341.8166 1350.3246
1352.2890 1355.2053 1358.0988 1361.3430 1398.2236 1416.0183
1418.3357 1421.7977 1422.4777 1423.5852 1425.7692 1427.6981
1428.6406 1446.3599 1451.4222 1451.5973 1452.7015 1466.7242
1481.1419 1481.7634 1482.8264 1484.6046 1486.1019 1488.5509
1489.4147 1489.5213 1489.7262 1494.1117 1495.8325 1501.8286
1507.1051 1509.0785 1510.0786 1511.1477 1511.9756 1512.5306
1515.8777 1531.7118 1581.0337 1622.7118 1624.7599 1625.9549
1642.9501 1650.3328 1654.2404 1655.1060 1663.7684 3039.3343
3039.4659 3044.1353 3044.3770 3048.3772 3048.5050 3064.3258
3070.2417 3087.0206 3095.0297 3095.1573 3097.8373 3100.8728
3104.1495 3105.7740 3114.4610 3117.1918 3127.4682 3127.4969
3133.1808 3133.7096 3133.9059 3140.3591 3170.2684 3170.4401
3172.5851 3175.5199 3175.7875 3176.6938 3177.8260 3190.5469
3206.6709 3214.8213 3218.1851 3223.8057 3229.9514 3759.7097

$[^{HS}Mn^{III}(L^1)(CH_3OH)]^{2+}$ S=1

13.0242 32.2204 34.0591 40.7640 43.3763 45.8227
54.0839 59.9638 69.0895 76.4293 80.8273 88.2434
91.5540 106.0513 111.8737 116.2903 120.3710 131.0814
139.1919 142.1891 144.1836 159.8717 168.5405 170.9270
173.8637 181.3039 189.0063 191.3692 202.3936 206.1223
206.6940 212.9179 225.6131 235.6526 246.4558 261.2000
283.2565 286.1825 292.2569 293.6579 296.2530 315.5261
325.1923 330.7363 339.8016 348.9699 350.7369 371.2138
374.0384 389.8404 399.6122 430.6278 435.3918 450.0106
473.2039 479.8880 481.3095 483.5446 500.2797 513.2982
517.7708 522.7903 537.2769 546.6887 565.6375 567.1596
572.1740 573.8862 575.9285 585.8102 588.4580 602.8966
626.5391 630.3880 660.8081 668.9249 674.6299 709.1812
741.1293 751.0165 754.1146 765.5680 775.0354 781.1415
806.5174 810.4547 848.5120 869.1205 878.0712 894.0026
903.5896 904.4150 910.7636 923.2690 938.9033 940.7617
954.3637 957.3079 961.6833 976.2146 983.6754 984.8996
986.7098 990.8032 993.2126 1004.1516 1007.5072 1009.4307
1029.1924 1036.1819 1040.3476 1040.6707 1042.7101 1044.1019
1050.0096 1053.2630 1055.0500 1065.6814 1068.4743 1069.4823
1076.0103 1096.3025 1107.7375 1121.4860 1178.2330 1178.4356
1180.9941 1187.7604 1195.0219 1211.4694 1227.5224 1259.8528
1261.0275 1277.2482 1279.1495 1297.3837 1303.6163 1311.2515
1311.9187 1332.6096 1338.5508 1339.7972 1343.4515 1357.5433
1368.4000 1371.9259 1400.3725 1407.1432 1408.2647 1410.8906
1414.2944 1417.6660 1421.3798 1423.3457 1424.6738 1429.5489
1440.5349 1442.7494 1450.8083 1459.5053 1464.5045 1471.9597
1473.8198 1475.4036 1475.4493 1477.9187 1481.4147 1483.0217
1484.9586 1485.8111 1487.2724 1494.7540 1496.0987 1501.1442
1505.0522 1506.6081 1508.5363 1509.1320 1509.7718 1514.1497
1517.4010 1528.4967 1529.6731 1531.0622 1579.3649 1622.8468
1638.6922 1645.3874 1647.5150 1648.9289 1663.9425 3037.6718
3040.4453 3046.2561 3049.4290 3052.6693 3054.9911 3077.4329
3081.2055 3084.0779 3092.9687 3102.6758 3103.5017 3104.8535
3107.4327 3111.8577 3127.1355 3132.2606 3135.6675 3143.1467
3153.8327 3153.8663 3155.4734 3155.6898 3172.9651 3176.2334
3180.7070 3193.5536 3197.3909 3199.0686 3200.3395 3204.1546
3209.0922 3210.4987 3216.2371 3226.5209 3233.2788 3770.0199

$[^{HS}Mn^{III}(L^1)(CH_3OH)]^+$ S=5/2

9.6679 21.6790 27.0645 30.7028 32.2638 33.9808
35.7944 43.5697 49.4118 53.3967 74.8491 77.9203
84.2436 88.5693 102.8254 109.1525 121.3851 123.2156
126.2924 130.7640 135.5974 138.1158 140.8563 163.8381
170.6704 176.0939 183.8530 191.6779 197.1039 203.8414
210.0400 221.6773 236.1075 239.2378 244.0749 255.6023
269.0649 272.3866 282.0253 292.2383 297.9462 305.5347
315.8735 317.9932 330.3150 343.6469 356.7109 360.5581
371.0640 390.9149 425.4405 427.0698 438.3673 445.8903
460.3416 481.0590 495.5864 498.3339 505.7147 512.8606
523.6293 525.9519 538.2462 544.9640 549.2231 554.7542
564.6389 568.4959 572.3151 584.4757 586.3770 608.2505
611.2055 626.7058 628.6562 678.4427 681.5462 695.2367
748.5247 751.8634 761.3725 770.9956 777.1828 782.7039
806.3994 828.5701 831.4184 875.2655 881.3401 882.3974
886.0628 894.1446 910.9227 913.1373 920.9096 944.0154
960.9220 964.2760 969.9751 974.2804 979.3321 979.5433
990.5571 995.1641 1004.5349 1008.4384 1019.2934 1030.6822
1036.6133 1037.4206 1040.7006 1044.4481 1045.4777 1054.3767
1059.5967 1059.7019 1060.8837 1061.3494 1062.6341 1064.9865
1068.2987 1080.6267 1088.2852 1131.2221 1180.3300 1181.1044
1184.5950 1188.1957 1194.7703 1196.6898 1226.7732 1241.5685
1268.7304 1271.4250 1277.1058 1284.3781 1285.8475 1290.4817
1301.7050 1309.5314 1317.5358 1330.3405 1343.3088 1346.8929
1352.1217 1356.7851 1361.6492 1367.6281 1392.5810 1411.6990
1414.4933 1417.6656 1419.9936 1421.8614 1423.5600 1425.6543
1438.4454 1450.0540 1452.3250 1453.7386 1470.7500 1472.0571
1472.9104 1474.8082 1476.6585 1480.7667 1481.2853 1484.9761
1489.8747 1490.3445 1492.0692 1494.6617 1497.3028 1500.4916

$[^{HS}Mn^{III}(L^1)(CH_3OH)]^{2+}$ S=3

17.3001 23.6165 32.3020 38.5294 40.8628 45.7709
48.1886 50.0887 59.2296 70.2038 75.3489 84.1030
89.4766 93.0117 94.2844 102.9788 109.6525 114.5771
124.6458 132.5549 135.7758 142.5462 149.0772 159.4875
168.1081 173.4192 181.6238 190.6212 191.3731 197.9810
200.3277 210.8004 226.0107 235.7589 245.6769 253.5777
265.3389 271.1508 276.3411 292.8465 296.5487 306.8110
317.0349 322.0614 332.2305 339.8371 349.0440 359.5692
370.2148 391.1238 408.4855 428.1017 437.4802 449.5507
471.6916 482.0664 483.6573 488.9002 503.4787 510.6056
518.1107 523.3089 528.3365 539.2208 546.0006 553.0285
562.0511 567.3969 571.3680 572.7876 585.6496 603.0910
608.3651 626.5127 633.1224 673.1001 681.7462 696.7917
746.5298 751.3919 759.4398 769.6374 777.4651 785.6295
806.3934 807.8621 821.8466 878.8048 885.8953 890.0265
896.8113 902.6440 914.7466 918.6738 924.6000 941.7776
958.1652 967.0328 973.6732 976.0794 978.8238 985.3750
992.8060 997.9513 1003.8686 1010.4239 1012.9515 1023.2694
1033.8827 1036.6790 1037.1972 1039.4024 1046.0162 1048.9970
1049.8854 1050.1919 1060.3724 1061.4405 1062.3056 1065.7373
1067.2791 1085.9374 1101.5626 1131.8506 1178.5810 1179.2875
1181.8097 1186.8599 1198.3266 1200.8164 1232.0772 1246.9018
1261.6972 1278.8287 1279.5805 1284.1052 1304.7574 1310.5251
1313.3188 1321.7938 1327.0080 1340.7044 1345.8197 1354.0168
1356.5979 1369.7759 1374.4211 1397.0916 1404.8880 1408.6819
1413.7283 1414.9011 1418.7764 1421.4888 1425.4952 1436.2128
1442.8984 1448.8716 1453.7060 1457.3397 1470.3760 1470.8868
1472.5018 1473.3452 1476.6955 1479.5942 1480.3105 1481.9883
1484.9089 1489.7923 1491.2217 1495.0732 1496.9454 1498.7434

المنارة للاستشارات
www.manaraa.com

1500.5392 1505.6088 1506.4485 1511.3967 1515.9031 1517.0773
1522.4109 1528.6303 1534.3478 1538.1497 1615.9517 1620.4801
1630.3971 1631.3600 1647.4646 1657.9337 1662.0268 3037.0750
3037.9904 3041.5221 3052.3573 3052.6737 3052.9624 3062.0862
3063.7583 3072.0542 3089.8174 3100.6234 3105.8699 3107.3136
3107.8072 3108.1691 3108.6056 3115.6156 3133.1910 3138.2410
3143.0588 3154.2475 3155.7661 3158.2150 3158.8716 3159.7521
3177.3953 3183.3351 3193.5983 3199.0066 3203.4741 3206.2505
3207.2941 3208.2600 3214.6828 3225.0066 3233.4662 3789.9558

$[^{HS}Mn^{III}(L^2)]^0$ *S*=2, Isomer 1

17.2891 19.9290 31.7210 32.4164 35.1855 39.5812
44.8975 52.4879 59.6220 68.8617 80.8836 89.0324
107.0478 122.5975 126.9280 139.2357 142.0424 147.2061
152.4303 161.6735 169.7939 181.4163 183.9808 195.1925
200.4185 205.8232 211.2194 219.8727 224.7452 227.7589
235.0681 245.8375 255.9524 263.5729 272.3979 287.1771
287.6695 305.4073 316.8173 322.1902 327.3102 345.9449
355.7430 360.2183 363.8136 374.3039 411.4240 425.4402
435.8477 456.5288 467.8642 486.2597 498.6223 505.8209
508.6305 520.9134 523.6549 532.3073 548.9064 551.8852
555.7846 567.4650 574.8226 584.3613 585.6705 586.8321
588.9458 604.1804 623.3427 628.1545 637.6651 667.3319
683.7124 705.8070 739.9638 750.1570 762.7850 776.5661
783.6399 795.9458 809.8295 817.9023 833.0730 838.3284
876.7099 881.2820 882.4583 887.1556 902.3207 908.6472
910.8537 916.2852 923.3128 952.5849 965.9926 969.2914
974.1699 976.6940 977.2082 985.0392 1002.0849 1006.2610
1011.2253 1021.4803 1036.1337 1037.8478 1038.2114 1042.8685
1052.0518 1060.4320 1060.7767 1061.1688 1061.8627 1062.0224
1063.0867 1064.3065 1064.7643 1074.1640 1086.6085 1127.6639
1158.8730 1183.1065 1184.3988 1188.7041 1189.4894 1191.0933
1198.9754 1248.8113 1254.3012 1269.4427 1270.5510 1281.8807
1286.7659 1290.8326 1296.5266 1299.5602 1300.3616 1305.4662
1330.2474 1336.2025 1336.6781 1346.0922 1351.8592 1354.3458
1357.8423 1392.4312 1398.9836 1402.9711 1419.4755 1419.8638
1420.8849 1422.9490 1424.5043 1425.0451 1452.8189 1453.6970
1455.3722 1460.9340 1479.3816 1482.1938 1482.7819 1482.8737
1483.4374 1486.3687 1487.0497 1489.2797 1489.8376 1490.5745
1490.6512 1498.0477 1500.1489 1506.1455 1507.7050 1508.9417
1511.4087 1512.4422 1514.7061 1517.2890 1520.3136 1533.4924
1614.2469 1619.6167 1620.6167 1638.9958 1649.2344 1658.8448
1660.2070 1661.3213 3031.1458 3031.4673 3034.1057 3035.5375
3038.6807 3040.2960 3040.6999 3041.3577 3058.2411 3061.5563
3082.4036 3085.4286 3086.6474 3091.2715 3094.7539 3095.8619
3098.4226 3099.8408 3114.6098 3117.1307 3117.8772 3119.6890
3122.5873 3125.1426 3126.4079 3136.1288 3156.9678 3158.2728
3159.0801 3159.5523 3163.1694 3165.5423 3176.4717 3198.1170
3207.5268 3215.8444 3223.0747

$[^{HS}Mn^{III}(L^2)]^0$ *S*=2, Isomer 2

18.4648 19.8284 33.4256 36.5357 37.4713 39.9346
48.6223 53.1270 56.2592 71.9662 83.0861 96.4056
108.8271 121.9785 132.9193 137.2222 145.0363 149.4275
152.2230 169.7531 174.4612 181.7011 187.3523 192.4284
197.0609 208.7528 220.0430 223.0981 229.5808 240.6914
246.3267 253.8697 261.6119 263.7337 269.0012 286.2719
297.6624 305.5835 309.8399 323.7597 336.8889 344.7790
357.9028 366.2965 367.9372 377.3204 419.1736 429.1243
435.9079 445.1575 457.9793 490.4219 496.7453 507.1467
508.4590 520.7081 526.6318 535.4096 543.7446 550.1752
554.5735 563.1554 576.8179 584.6224 586.0582 586.9361
588.7110 606.6900 615.4058 625.4506 636.1922 684.2377
687.4220 695.3817 737.3141 750.4674 762.3285 769.2964
778.3049 785.6477 811.0230 825.9837 832.0409 835.5153
877.7147 878.6465 880.9503 885.4196 902.6647 908.3317
909.3726 919.4328 934.1571 961.9375 966.3656 969.6265
970.4941 976.2062 981.2424 987.5474 1003.4753 1005.1150
1012.5696 1025.1533 1036.0022 1037.9295 1038.5798 1049.2739
1049.7740 1059.5528 1059.7648 1060.7480 1062.0601 1062.1827
1062.3327 1063.6942 1072.0427 1076.3353 1087.7959 1126.2491
1161.6762 1181.4537 1185.4229 1186.9308 1187.9907 1189.4941
1196.2145 1244.5206 1251.3028 1269.2529 1271.4849 1281.5004
1282.9240 1291.3051 1296.8501 1298.5886 1302.3419 1310.4620
1331.0216 1333.3564 1341.0564 1347.8779 1350.7079 1354.6183
1358.2015 1364.4158 1396.4299 1419.3454 1420.6534 1422.1705
1422.7743 1423.9473 1425.2129 1427.7968 1453.1574 1453.4409
1455.0040 1462.8868 1479.4380 1479.9198 1481.6229 1483.8778
1485.6291 1487.0202 1489.2684 1489.8823 1491.1034 1492.3501
1496.5652 1498.2645 1506.4311 1509.0133 1509.6839 1510.4948

1511.5177 1513.5215 1516.7075 1517.3546 1520.8908 1532.6732
1611.9023 1619.7947 1620.9554 1638.4603 1649.9660 1658.9091
1659.5540 1660.7449 3028.2061 3031.0184 3031.0828 3031.4263
3037.6193 3038.8091 3039.4717 3041.6507 3043.0982 3050.9629
3082.2064 3087.3771 3088.0831 3090.2399 3092.9482 3093.2690
3095.7451 3099.9217 3101.6328 3116.7309 3118.7638 3119.4531
3121.6014 3124.5487 3125.8723 3142.6318 3155.6515 3158.3053
3159.3076 3159.3618 3166.1449 3167.2890 3184.1548 3197.4512
3206.4308 3214.4054 3221.5069

$[^{LS}Mn^{III}(L^2)]^0$ *S*=1

11.3350 27.3000 32.3487 33.8985 34.8320 40.8095
44.1114 45.6070 54.7394 75.3769 81.8973 90.9440
99.9138 112.8631 134.8564 139.0054 146.7706 147.6295
156.0884 174.7112 187.4176 189.0315 189.6684 198.8805
205.1102 215.9205 222.4270 230.5083 236.9487 244.9422
256.4418 265.5318 273.0705 280.9143 286.4566 294.5369
303.8934 311.4748 313.7970 320.7333 330.3179 354.3964
359.0240 369.0414 375.0166 381.2148 424.8535 431.1074
440.0761 447.4897 468.1094 489.8431 496.3642 505.9952
509.5792 518.8170 528.3087 538.4106 546.6683 550.2337
555.3882 569.5254 578.0699 585.0138 586.6148 588.1821
592.2389 608.8737 613.1759 632.5458 651.2995 686.0417
686.4664 698.9996 737.7232 751.4355 760.7151 773.6731
775.8131 785.6445 811.2223 824.7294 831.7715 840.2172
877.3867 877.7917 880.4947 885.0409 901.4974 907.8875
909.1833 911.0193 936.5341 961.2755 964.8526 966.7662
970.0727 974.8498 982.9611 989.4920 1004.4819 1007.5412
1012.8428 1025.9199 1035.8015 1036.9010 1038.7060 1045.7990
1049.5555 1054.8209 1060.0638 1060.8647 1061.6297 1062.1779
1062.4617 1063.6029 1066.2718 1074.0231 1078.4599 1120.9739
1159.1938 1178.0308 1185.9730 1188.8167 1189.2162 1190.9640
1199.8443 1240.7987 1247.7533 1268.8384 1272.2478 1282.1471
1286.3853 1291.3944 1297.4679 1298.8336 1306.3024 1313.6145
1328.8638 1331.0414 1345.3044 1349.9542 1351.2046 1357.4624
1361.1760 1367.0121 1392.1954 1416.9472 1421.8671 1422.1604
1422.8015 1424.2584 1427.0006 1429.3472 1453.0860 1453.4820
1455.6098 1459.9127 1474.4503 1481.3391 1483.0543 1483.7085
1484.0236 1489.1992 1489.2553 1490.5262 1491.2356 1492.1148
1492.2984 1497.3904 1503.3055 1505.3445 1507.3026 1510.5449
1511.3653 1512.1092 1515.9611 1517.0314 1522.2238 1532.6207
1608.6768 1620.9073 1622.1536 1644.5074 1649.6659 1659.0814
1659.9792 1662.0636 3028.7530 3031.1863 3031.3479 3032.5621
3037.8033 3042.3153 3043.6666 3044.9772 3059.1630 3070.1125
3079.3300 3084.4636 3087.7271 3087.7559 3087.8375 3091.7859
3096.0873 3099.9698 3114.5695 3118.3695 3119.0242 3119.4540
3125.3515 3125.6840 3127.3266 3152.5248 3155.0645 3159.4730
3159.8674 3164.0309 3164.6187 3167.2255 3200.0710 3208.0335
3208.9622 3216.8545 3223.6104

$[^{HS}Mn^{III}(L^2)]^+$ *S*=3/2, Isomer 1

15.2707 27.6326 31.5109 35.4190 37.9722 42.9877
51.3625 53.4555 63.7792 67.4787 82.3468 92.1938
111.0346 116.6624 120.9708 122.9391 131.6975 137.8289
145.6311 160.6292 170.8220 176.9971 182.0007 190.8938
195.8207 211.0596 214.0067 218.7821 224.6868 230.2302
238.7419 242.1084 255.9583 265.7440 269.8634 289.7331
293.6264 301.7619 314.6235 327.9102 343.4559 352.7772
356.3752 362.4355 372.0877 377.7273 401.3781 417.3947
428.2490 456.5442 463.9917 477.2021 485.1535 494.3704
513.0443 514.7730 523.7428 527.5026 543.9989 548.6028
560.4273 560.6530 572.4031 579.0092 583.7369 585.3262
591.0826 605.3659 616.5623 635.2463 640.2297 661.3894
680.6240 700.0130 743.4211 750.6601 759.7544 771.4245
783.8417 793.8161 806.6244 814.6077 821.0173 842.7236
881.3176 883.8986 888.6701 896.2039 901.2577 911.2885
914.0356 923.5415 934.4983 952.6688 958.8065 970.7188
974.9760 976.7064 976.8863 985.7942 1002.4197 1005.9454
1008.9187 1033.7733 1034.5904 1037.6539 1038.9335 1039.3935
1044.5672 1050.8389 1052.2293 1059.8664 1061.0805 1063.1125
1063.4231 1063.8612 1065.5928 1075.1860 1089.5635 1124.0191
1157.7093 1178.6822 1182.5985 1182.6428 1189.5465 1194.8109
1199.3770 1246.1273 1252.8795 1269.6203 1271.5719 1275.7102
1283.9114 1293.2873 1301.2000 1301.9070 1309.1975 1321.9328
1329.0195 1331.7547 1341.1796 1344.2131 1349.2600 1353.9303
1389.4711 1396.5904 1406.8788 1408.1235 1416.4905 1421.4980
1422.1167 1424.8860 1425.5212 1431.3208 1451.4220 1453.5938
1457.6598 1469.0468 1470.7669 1475.0508 1478.7997 1481.2982
1481.5016 1482.5548 1485.3387 1486.4535 1488.6771 1489.7891
1490.2226 1495.3246 1498.2627 1500.3852 1505.9504 1509.4791

www.manaraa.com

1510.8138 1512.8766 1515.8357 1521.9894 1528.2343 1532.3997
1548.1666 1621.7493 1624.8444 1639.1524 1645.7746 1649.6908
1655.5134 1659.8401 3036.5559 3038.9779 3039.7623 3041.0990
3042.9115 3050.8079 3052.2153 3059.6362 3063.6604 3066.2236
3091.0209 3092.6633 3094.3632 3095.2710 3096.5640 3098.8417
3108.3617 3118.6541 3120.3237 3122.9732 3126.0469 3128.4658
3132.1301 3142.4476 3152.3700 3153.1279 3165.7390 3168.9739
3170.5511 3174.7822 3178.1272 3193.3326 3201.6746 3203.2397
3211.8851 3220.6141 3228.3355

$[^{HS}Mn^{III}(L^2)]^+$ *S*=3/2, Isomer 2

13.0812 29.1292 36.0060 38.2574 43.0148 48.2850
50.9552 53.3057 64.6355 76.5139 87.9234 93.6757
106.4849 113.9840 125.6586 126.6945 130.5331 134.6098
150.8096 168.1510 172.2009 179.1798 183.5772 187.4267
195.0099 203.8407 210.7186 217.8522 226.2971 233.8754
239.8771 253.9243 260.6160 266.1061 267.2810 285.2345
294.7024 302.9487 305.6454 308.9060 339.5006 348.5595
356.1517 359.1735 375.8881 385.6229 413.2131 431.0107
435.5115 440.1136 456.1056 476.8030 482.4924 496.4470
509.4305 511.5923 523.0113 529.3361 542.8989 546.3055
552.2073 557.5765 571.3518 577.7990 583.4593 585.5800
587.6660 604.6637 617.8810 625.0209 633.0186 672.4357
685.8403 693.4881 736.4459 750.7746 758.9578 766.7106
775.2744 786.4805 800.1340 820.0324 833.1253 838.4664
881.3117 883.5729 887.8312 895.9076 902.7703 912.5704
914.0947 929.1853 933.4003 960.9460 962.4602 969.3255
971.1018 975.5385 982.0250 987.3586 1002.4794 1005.9747
1010.1862 1024.8468 1034.2049 1037.5301 1039.3307 1040.5995
1048.9822 1051.5541 1053.3653 1059.7285 1060.2088 1061.5177
1062.5389 1063.5150 1070.7829 1076.7223 1088.2883 1123.0049
1162.5001 1178.3389 1182.0876 1185.0536 1188.2176 1188.8705
1197.8105 1239.6389 1247.5102 1269.6834 1272.0259 1279.6552
1286.2033 1286.8591 1297.9317 1299.7529 1312.3294 1316.6726
1328.7048 1339.1188 1340.4412 1343.6118 1344.5961 1355.7934
1360.4616 1388.1592 1409.7975 1415.8413 1421.0252 1422.2321
1423.4880 1425.7796 1427.9102 1429.6668 1451.2666 1453.0494
1457.3924 1471.6918 1471.8655 1474.9081 1476.6408 1480.5285
1482.0508 1484.3377 1486.0265 1487.3905 1491.3486 1491.7808
1492.3819 1493.6725 1499.9952 1503.8084 1507.4520 1508.8897
1511.1125 1511.7894 1513.9562 1517.2101 1520.7356 1527.4946
1531.4097 1620.3737 1621.7362 1639.3792 1640.4842 1649.5668
1653.9251 1656.3552 3035.4856 3035.9581 3042.2479 3042.7120
3044.2100 3044.8355 3048.8813 3051.2187 3052.9574 3056.3168
3095.2450 3095.2907 3095.2922 3097.5529 3097.6400 3106.4906
3106.9480 3108.8190 3111.7941 3125.3508 3125.9891 3131.4858
3132.4586 3148.1112 3152.7472 3153.2382 3168.6183 3169.0907
3175.1065 3175.3935 3187.1769 3189.6442 3199.3706 3203.1057
3211.1829 3218.7122 3226.1377

$[^{HS}Mn^{III}(L^2)]^+$ *S*=5/2, Isomer 1

14.4380 30.7642 34.8666 37.7907 42.6222 46.8353
51.0074 54.2977 68.7584 72.1763 79.8204 99.0098
108.6559 118.0303 119.7176 133.1155 139.3912 146.0523
150.7721 154.8142 171.3915 178.6342 181.6190 184.4619
192.4261 194.0171 211.3024 215.9796 222.7771 228.8710
236.7636 240.9387 253.8982 264.3587 270.2788 290.3859
294.5414 302.3438 313.3881 320.2609 327.1200 348.7325
352.7286 357.3210 361.9785 372.3315 403.4786 415.9668
430.8358 455.4501 464.7677 478.7505 488.3232 494.8713
510.7338 515.3536 523.9973 524.7371 542.7004 548.6812
558.6116 560.0281 571.0230 577.5221 584.0704 587.2523
589.9587 602.4614 615.3456 634.1299 637.2462 661.4262
678.2227 700.3891 740.8164 750.2457 759.1103 770.6183
782.4218 791.6682 803.8412 812.1941 818.0366 843.4374
881.0638 885.3486 888.7887 897.3277 901.1469 911.2215
914.4895 922.6596 931.6488 953.1323 958.1663 969.5528
973.9518 975.5237 976.6371 985.6113 1003.4590 1006.5198
1008.3573 1026.7277 1034.3209 1037.9378 1038.8680 1039.3071
1042.1652 1051.1645 1053.0308 1060.0685 1061.4468 1062.7078
1063.4727 1063.7019 1064.3404 1073.9006 1087.3755 1120.7987
1155.7240 1179.2749 1180.2245 1183.7745 1188.3228 1191.8834
1195.8089 1243.2507 1248.8751 1264.9070 1272.5425 1272.9962
1282.6671 1289.8576 1291.6593 1298.1816 1307.2463 1319.6930
1322.7965 1330.2355 1339.4777 1341.2642 1347.2567 1354.7307
1382.7801 1391.6662 1395.2081 1408.5891 1417.4662 1421.6651
1422.0698 1425.4827 1425.6231 1428.8098 1451.8553 1454.3270
1458.3687 1464.3456 1473.5489 1475.2305 1478.8216 1480.6625
1481.8862 1483.5984 1484.5462 1485.5296 1489.0450 1489.4486
1489.9483 1494.5956 1496.5236 1498.7423 1503.1334 1509.8753

1510.9727 1513.5083 1515.6016 1520.4691 1524.6118 1529.7125
1532.3658 1621.2154 1625.0961 1637.9054 1645.4846 1649.1132
1656.1302 1660.2251 3037.1595 3039.5256 3039.7296 3040.1954
3043.1066 3050.1749 3052.1266 3054.0043 3060.0412 3070.4041
3090.9410 3091.5190 3092.5672 3094.3627 3096.8441 3098.7650
3107.7296 3116.2268 3123.7446 3124.3164 3126.5836 3128.5264
3131.9405 3144.0374 3153.4584 3153.9770 3165.9975 3168.5857
3170.6736 3176.4394 3181.9292 3196.7536 3202.2125 3204.1661
3212.8016 3220.8522 3227.3935

$[^{HS}Mn^{III}(L^2)]^+$ *S*=5/2, Isomer 2

13.9676 26.0731 31.1391 34.6761 37.2637 42.6136
45.7947 50.5884 53.5980 75.9835 87.9678 94.6908
106.3927 114.7235 127.5186 129.7505 131.5895 134.2921
149.3509 168.3614 171.6519 179.1391 183.8552 186.4623
194.5181 202.1578 209.0543 216.6049 224.7360 233.4465
245.8093 251.4910 259.2084 265.3309 267.1119 283.1748
295.2995 301.8522 306.6946 312.1567 330.8188 347.6036
357.1724 359.7221 373.2497 375.4460 407.0479 430.8064
435.4857 439.1471 454.2173 476.9368 483.7609 497.0669
510.2983 512.4002 523.0246 528.9672 543.9628 547.6284
552.6753 559.0416 569.6989 577.4399 583.1704 585.4721
587.4576 606.9815 617.0704 628.4436 635.6974 670.3115
686.0570 692.9766 736.4093 750.5512 758.6881 766.9508
775.5903 786.4514 798.6488 817.4052 833.9127 840.6446
881.3352 882.9126 887.8423 895.6631 902.0766 912.6936
914.0848 927.9407 933.6198 959.4509 961.1542 969.0076
971.2016 975.6630 981.9131 987.5099 1002.5901 1004.1252
1010.2287 1026.4283 1033.7126 1037.2425 1039.5106 1039.5708
1048.5032 1050.1459 1051.3041 1059.7943 1060.2717 1062.3084
1062.6456 1063.5413 1070.3217 1074.7009 1085.8459 1122.1156
1158.9069 1176.1921 1180.9937 1185.2999 1188.5183 1188.7702
1197.3692 1241.3567 1246.2425 1267.2361 1271.7503 1279.0186
1285.6916 1287.8744 1297.6939 1298.3955 1311.6442 1314.7268
1330.5588 1338.1598 1340.8798 1344.2498 1345.4881 1355.3644
1363.3834 1388.3762 1409.6647 1414.6633 1420.8526 1422.2494
1423.5312 1426.3152 1428.5316 1429.9606 1451.5377 1453.1570
1456.0666 1469.8264 1471.2730 1475.0948 1477.2764 1481.3029
1482.3371 1484.9539 1486.2788 1487.8279 1490.9812 1491.7017
1493.2738 1498.4461 1499.1378 1505.0933 1508.0923 1508.1945
1511.2324 1511.8712 1512.7553 1515.6446 1520.4290 1528.0839
1530.9595 1621.3670 1623.8591 1639.3241 1642.0792 1649.4926
1655.4240 1658.1193 3035.5673 3036.2040 3039.1830 3040.5186
3044.6243 3044.8083 3052.3201 3053.0089 3056.2072 3065.3779
3094.8701 3094.9417 3095.0840 3097.4004 3097.7803 3107.4259
3107.8211 3110.0217 3117.1636 3125.0136 3125.6788 3131.7183
3132.8138 3148.2428 3153.1339 3153.3337 3168.2884 3169.0974
3174.8329 3175.2464 3188.6205 3188.9176 3200.6607 3202.8986
3210.1396 3217.4509 3225.5622

$[^{HS}Mn^{III}(L^2)]^{2+}$ *S*=1, Isomer 1

6.5153 22.0422 25.6704 35.3287 38.7835 42.8569
51.4821 57.4979 59.5104 72.8294 77.0882 88.2780
101.2841 112.8351 120.7068 125.6652 134.6083 137.8518
143.7252 161.6275 163.7401 169.2450 179.5697 186.7014
194.5275 203.4405 211.0664 213.2364 222.7137 227.9853
231.7410 236.7790 244.2942 259.7016 270.7704 280.4652
286.9900 302.8426 313.9471 323.4333 333.6760 341.4809
351.2016 358.1672 364.5107 368.1672 400.8506 405.3706
415.2728 455.7741 461.3779 475.3547 486.1814 490.3217
493.4123 509.3943 515.3246 517.7824 530.1182 545.6525
547.8740 556.0046 566.7569 570.9513 576.0308 586.8758
587.8003 598.9142 613.7479 616.8560 634.0374 659.6295
669.9368 695.6153 739.4161 747.6639 756.7307 765.8996
781.8777 791.6277 800.3092 809.8368 813.9773 821.6154
883.8659 891.8293 894.5994 898.8002 899.8944 913.3994
919.8644 928.6616 932.7454 944.1672 957.9055 969.1837
972.2911 975.3289 976.3915 983.5710 1002.6020 1006.1282
1012.7205 1020.3176 1033.4779 1034.9289 1036.1087 1037.0117
1041.0751 1048.5789 1050.1617 1051.2646 1054.8762 1059.2068
1061.8003 1063.9216 1064.1521 1070.3330 1086.1966 1119.4311
1156.2179 1179.1782 1179.5259 1180.7837 1181.6601 1192.9889
1199.7019 1241.9411 1251.3504 1266.2258 1274.5632 1275.2560
1291.4925 1293.8366 1297.7248 1310.6461 1314.4251 1317.9263
1324.9828 1341.7995 1342.8836 1345.0898 1348.2419 1382.5634
1386.6965 1396.2751 1404.6154 1404.8813 1413.6717 1416.9426
1423.0073 1424.5733 1426.4038 1426.7913 1449.4484 1456.1284
1456.8429 1464.8259 1469.4192 1470.8516 1472.2345 1473.0678
1476.2463 1476.4507 1477.9185 1483.6906 1484.8088 1488.8500
1490.1255 1493.8222 1496.5432 1498.2102 1499.3744 1506.0613

www.manaraa.com

1507.6410 1510.2755 1512.5422 1518.6607 1524.4477 1530.4656
1531.3644 1534.6370 1614.6954 1638.5973 1647.2925 1647.5393
1653.2690 1654.8428 3039.8838 3041.0845 3044.3249 3049.0667
3053.5880 3054.5951 3058.2665 3068.0596 3068.3940 3083.8988
3092.9619 3093.3628 3101.1930 3104.5340 3109.0719 3111.0196
3112.7923 3120.7174 3134.5413 3140.1037 3140.4515 3150.5423
3157.6143 3157.7036 3159.4418 3159.5767 3178.2135 3188.0979
3188.9872 3197.2420 3202.6420 3208.4778 3208.5428 3208.6400
3215.6249 3223.0814 3230.1626

$[^{HS}Mn^{III}(L^{2})]^{2+}$ *S*=1, Isomer 2

21.7719 27.2301 37.9815 39.4706 45.7315 49.1233
50.3007 67.1331 67.9866 70.5963 74.4269 96.7012
103.4436 107.5387 117.6976 127.6160 132.8283 136.1174
148.8124 158.9902 173.0206 178.2127 183.9374 188.8632
193.5479 197.1534 211.1867 216.8906 220.1747 232.0104
248.3992 260.5899 263.5273 266.1787 271.8484 284.5392
297.6754 302.8590 310.8439 316.0927 331.8695 340.6679
351.5214 361.6228 375.2041 377.4246 403.1952 414.7735
428.4010 434.4002 450.1314 472.7432 483.4676 486.5161
487.1709 508.3414 510.8756 520.2308 523.2970 533.9388
546.1244 550.6712 567.9180 570.6633 573.4171 582.1636
583.7391 596.4221 601.7304 618.4831 629.0709 672.3914
678.6203 686.1075 735.5799 749.4335 756.4436 764.7663
772.9949 787.0558 800.4633 811.2733 816.9027 822.2178
884.0027 889.5380 897.0128 897.9870 906.0752 912.0971
918.6534 928.8444 933.1878 957.5266 962.7283 967.2091
971.5498 976.0878 981.0354 983.8340 1003.4630 1006.5459
1015.4977 1020.9887 1032.4055 1034.9523 1037.7767 1039.1939
1043.6594 1050.2478 1050.7263 1052.2583 1056.0041 1057.0522
1059.2914 1063.6637 1068.3875 1074.3698 1085.6615 1121.3325
1159.6390 1174.3142 1177.7507 1178.9023 1181.7308 1190.5122
1199.0170 1246.6249 1249.0499 1254.5516 1271.3878 1272.8039
1287.7842 1299.7379 1300.3455 1306.2030 1316.3096 1319.1699
1328.6698 1342.7434 1344.6239 1347.5732 1356.1936 1369.5370
1388.4658 1398.8362 1406.5465 1406.8231 1414.5772 1419.3642
1421.1396 1423.2382 1430.3124 1435.0622 1442.7497 1451.7129
1454.5557 1466.4098 1469.0218 1472.2606 1472.5605 1473.0485
1473.2943 1475.7511 1479.5874 1482.9368 1487.9375 1488.8284
1492.0447 1492.6752 1496.5967 1501.0350 1502.5058 1504.5261
1509.6550 1510.2509 1513.0361 1516.7136 1518.4712 1528.4152
1528.8523 1530.9039 1590.0904 1628.6480 1639.8693 1643.2680
1648.0991 1651.1155 3038.8118 3041.8197 3042.0318 3053.0646
3053.6694 3055.5029 3055.5813 3062.5755 3064.7010 3073.3975
3094.4854 3097.6094 3103.9693 3105.1629 3108.0987 3109.2427
3111.3190 3118.9103 3131.2331 3137.3874 3145.9528 3151.0634
3157.3285 3157.3934 3157.6148 3157.8304 3185.5393 3185.7582
3192.2596 3196.1562 3196.7128 3204.2547 3207.9299 3208.8149
3215.7509 3223.2929 3230.6729

$[^{HS}Mn^{III}(L^{2})]^{2+}$ *S*=3, Isomer 1

16.2417 29.1455 32.5139 37.6795 45.2359 47.7161
48.6551 52.1769 67.7027 81.2059 92.0098 98.9111
112.3002 120.3874 130.0911 135.3167 138.0687 144.0535
150.8627 156.8509 165.4290 169.0063 180.5204 187.9909
191.0661 202.3787 207.6236 214.0305 221.8341 227.2781
232.1028 238.5398 253.5053 266.7151 273.5008 292.0119
297.9453 301.7943 319.0838 329.8122 335.5424 344.4197
360.2754 362.6407 369.9084 389.8665 405.5158 411.9605
424.6516 454.5073 460.5114 474.5552 488.5176 489.5411
495.4126 511.8117 517.3314 517.9615 531.5363 548.1551
551.0349 557.4597 567.0612 572.0152 576.0233 586.5234
589.2039 602.8459 616.6443 620.2662 634.6538 658.8654
669.5664 696.4734 742.2334 750.2411 757.2335 768.2099
784.4305 794.6120 801.0423 808.8281 811.5894 828.4334
885.9447 892.1338 896.2328 901.2225 902.4911 916.4782
923.4893 929.6415 932.7550 945.6971 956.8764 970.5709
972.7989 974.3455 976.7949 983.9686 1003.4529 1007.5866
1013.9418 1026.5108 1034.8378 1035.9491 1036.8692 1038.9342
1043.1518 1049.8609 1050.1380 1051.2664 1055.3952 1061.3511
1061.9004 1064.0345 1066.2811 1072.9404 1088.1665 1119.6329
1159.9947 1177.9468 1178.5015 1180.9449 1181.9621 1192.7258
1199.0206 1244.6779 1248.2359 1261.3984 1271.6960 1279.2429
1288.7163 1299.9905 1305.5121 1311.7098 1317.6653 1322.0345
1323.7143 1341.5015 1341.9530 1345.2319 1348.5181 1380.5861
1395.8120 1400.4851 1405.0925 1405.6916 1414.4209 1416.4846
1421.0420 1424.7562 1425.3703 1429.4090 1448.2759 1453.4442
1455.6179 1468.8999 1469.8814 1470.9324 1471.1308 1472.2270
1475.0866 1475.6438 1476.8759 1483.4309 1483.9721 1488.6749
1490.5387 1493.2096 1495.7791 1497.0734 1503.4607 1507.2363
1509.5765 1509.9764 1511.3818 1516.7450 1529.7102 1530.7858
1533.6616 1606.7867 1619.4637 1637.8438 1646.0611 1647.4167
1651.7124 1654.6705 3039.1309 3040.9611 3043.6985 3047.9879
3052.1815 3053.1170 3061.1478 3066.8368 3070.6375 3079.4600
3092.6831 3093.2973 3100.6956 3103.1181 3107.7007 3108.4113
3111.9990 3121.4778 3133.8162 3138.0144 3140.5652 3153.8586
3156.5409 3158.2910 3158.3971 3159.2722 3178.1259 3186.4369
3189.3732 3196.5731 3200.4521 3207.7876 3209.3875 3210.0404
3216.9957 3224.5439 3231.0870

$[^{HS}Mn^{III}(L^{2})]^{2+}$ *S*=3, Isomer 2

15.1781 29.8838 39.3339 40.3733 44.5614 50.4958
55.8389 61.4773 63.2494 73.3434 82.2198 95.0630
98.1358 106.2203 123.0878 129.8825 133.0023 140.8708
149.9165 164.9971 171.1468 173.1504 178.5738 181.3743
190.1637 197.9387 205.4875 212.7403 216.4897 232.2453
238.9035 254.3899 262.4818 267.8769 279.8566 289.8178
293.8984 299.5296 307.6572 315.1666 323.5307 340.7036
347.5315 355.6206 362.8667 375.1101 399.4506 411.8117
434.6626 438.6460 448.6041 473.3068 481.6710 485.7335
488.1650 504.7280 512.8640 521.3488 527.6980 541.2977
548.6186 553.5894 566.0385 569.2972 572.6765 582.2342
584.4928 599.2843 607.1918 619.8557 628.8724 668.5978
676.1202 684.0647 733.2379 748.3199 756.0066 765.8017
771.4775 786.9788 798.6530 806.0127 815.4511 826.1792
882.3668 888.2994 895.6440 900.3283 902.2421 914.0765
922.1405 926.5895 934.1188 956.1488 959.0387 965.0533
971.0232 976.9509 980.8128 985.0460 1004.3353 1005.0679
1015.8678 1018.0322 1029.7590 1034.1240 1034.8181 1035.2480
1042.2274 1047.8651 1050.3898 1050.7731 1053.1606 1058.9674
1061.8727 1062.2264 1068.6104 1069.4706 1083.0070 1119.2159
1153.9059 1174.7385 1175.4461 1177.2862 1183.5839 1187.9213
1197.6001 1245.6173 1249.2459 1263.8919 1267.8261 1271.5154
1286.8099 1297.6558 1299.2440 1310.9627 1314.4412 1319.2578
1330.9623 1340.7536 1341.0375 1345.3886 1355.1363 1366.9238
1388.4259 1401.5543 1405.8287 1410.9404 1413.7610 1420.8477
1423.3608 1427.3938 1429.8260 1432.5762 1448.9962 1450.5293
1451.8968 1466.8849 1468.7109 1469.6548 1471.6262 1472.2806
1473.2382 1474.4259 1478.6210 1487.9686 1489.6266 1492.3390
1493.4013 1493.7814 1496.7723 1498.8485 1505.0810 1508.0450
1508.5564 1512.6670 1513.1272 1515.5529 1519.2249 1529.7325
1530.6615 1534.0486 1615.5332 1639.7045 1647.6703 1647.8194
1649.9047 1657.7286 3035.2754 3037.9833 3042.2849 3050.7571
3052.7822 3053.9151 3057.9260 3062.2844 3065.1922 3078.8442
3096.6108 3097.0527 3103.3781 3104.5846 3108.0997 3108.6113
3108.8134 3119.7094 3133.9719 3134.5727 3141.6625 3151.9135
3157.1043 3158.1654 3159.7958 3160.6163 3180.6414 3188.5244
3190.6708 3192.6767 3203.3004 3207.1100 3207.5222 3210.4235
3213.3316 3220.6698 3229.1704

www.manaraa.com

Table B6. Energetics for all optimized structures. Energies are in Hartree, coupling constant J is in cm^{-1}.

Species	S^2	E(sol) 6-31G(d,p)	E(sol) 6-311+G(d,p)	G_{corr} 6-31G(d,p)	G(sol)	J
$[^{HS}Mn^{III}(L^1)(CH_3OH)]^0$ *S*=2	6.06	-2879.455014	-2879.923775	0.561075	-2879.362700	-
$[^{LS}Mn^{III}(L^1)(CH_3OH)]^0$ *S*=1	2.02	-2879.441113	-2879.910207	0.565973	-2879.344234	-
$[^{HS}Mn^{III}(L^1)(CH_3OH)]^+$ *S*=3/2	4.78	-2879.270648	-2879.730538	0.561932	-2879.168606	–154
$[Mn^{IV}(L^1)(CH_3OH)]^+$ *S*=3/2	3.82	-2879.277296	-2879.733024	0.568829	-2879.164195	-
$[^{HS}Mn^{III}(L^1)(CH_3OH)]^+$ *S*=5/2	8.84	-2879.267185	-2879.727694	0.558832	-2879.168862	-
$[^{HS}Mn^{III}(L^1)(CH_3OH)]^{2+}$ *S*=1	3.90	-2879.072052	-2879.524129	0.565731	-2878.958398	–310
$[^{HS}Mn^{III}(L^1)(CH_3OH)]^{2+}$ *S*=3	12.17	-2879.059247	-2879.512424	0.561623	-2878.950801	-
$[^{HS}Mn^{III}(L^2)]^0$ *S*=2, Isomer 1	6.05	-2804.214938	-2804.656154	0.563796	-2804.092358	-
$[^{HS}Mn^{III}(L^2)]^0$ *S*=2, Isomer 2	6.05	-2804.215057	-2804.656437	0.564745	-2804.091692	-
$[^{LS}Mn^{III}(L^2)]^0$ *S*=1	2.26	-2804.178296	-2804.621514	0.565626	-2804.055888	-
$[^{HS}Mn^{III}(L^2)]^+$ *S*=3/2, Isomer 1	4.79	-2804.032027	-2804.464697	0.564892	-2803.899805	–84
$[^{HS}Mn^{III}(L^2)]^+$ *S*=3/2, Isomer 2	4.80	-2804.031785	-2804.464757	0.565196	-2803.899561	–79
$[^{HS}Mn^{III}(L^2)]^+$ *S*=5/2, Isomer 1	8.82	-2804.030311	-2804.463153	0.564531	-2803.898622	-
$[^{HS}Mn^{III}(L^2)]^+$ *S*=5/2, Isomer 2	8.84	-2804.029951	-2804.463300	0.563908	-2803.899392	-
$[^{HS}Mn^{III}(L^2)]^{2+}$ *S*=1, Isomer 1	4.03	-2803.825411	-2804.250566	0.562924	-2803.687642	–106
$[^{HS}Mn^{III}(L^2)]^{2+}$ *S*=1, Isomer 2	4.07	-2803.822777	-2804.248523	0.565508	-2803.683015	–156
$[^{HS}Mn^{III}(L^2)]^{2+}$ *S*=3, Isomer 1	12.13	-2803.820741	-2804.246651	0.565357	-2803.681294	-
$[^{HS}Mn^{III}(L^2)]^{2+}$ *S*=3, Isomer 2	12.16	-2803.816046	-2804.242754	0.564375	-2803.678379	-

$$E(sol) = E(SCF) + \Delta G_{solv} \qquad \text{(Equation B1)}$$

$$G(sol) = E(sol) + G_{corr} \qquad \text{(Equation B2)}$$

E(SCF) is the electronic energy, ΔG_{solv} is the solvation free energy, and G_{corr} is the thermal free energy corrections (0 K → 298 K) for a given species. Tabulated G(sol) values combine the triple-zeta E(sol) with the double-zeta free energy corrections G_{corr}. Coupling constants for the broken symmetry wavefunctions[1,2] were computed using equation 3.

$$J = -(E^{HS} - E^{BS}) / (\langle S^2 \rangle^{HS} - \langle S^2 \rangle^{BS}) \qquad \text{(Equation B3)}$$

www.manaraa.com

REFERENCES

1. Lewis, N. S.; Nocera, D. G., Powering the Planet: chemical challenges in solar energy utilization. *Proc. Natl. Acad. Sci. U. S. A.* **2006,** *103* (43), 15729-35.
2. OECD, *Energy: The Next Fifty Years*. OECD Publishing.
3. Landsberg, H. H., Policy Elements of US Resource Supply Problems. *Resources Policy* **1974,** *1* (2), 104-114.
4. Thoi, V. S.; Karunadasa, H. I.; Surendranath, Y.; Long, J. R.; Chang, C. J., Electrochemical Generation of Hydrogen from Acetic acid using a Molecular Molybdenum–oxo catalyst. *Energy & Environ. Sci.* **2012,** *5* (7), 7762.
5. Du, P.; Knowles, K.; Eisenberg, R., A Homogeneous System for the Photogeneration of Hydrogen from Water Based on a Platinum(II) Terpyridyl Acetylide Chromophore and a Molecular Cobalt Catalyst. *J. Am. Chem. Soc.* **2008,** *130* (38), 12576-12577.
6. Cady, C. W.; Crabtree, R. H.; Brudvig, G. W., Functional Models for the Oxygen-Evolving Complex of Photosystem II. *Coord. Chem. Rev.* **2008,** *252* (3-4), 444-455.
7. Cady, C. W.; Shinopoulos, K. E.; Crabtree, R. H.; Brudvig, G. W., [(H_2O)(terpy)Mn(mu-O)$_2$Mn(terpy)(OH_2)](NO3)3 (terpy = 2,2':6,2"-terpyridine) and its Relevance to the Oxygen-Evolving Complex of Photosystem II Examined through pH Dependent Cyclic Voltammetry. *Dalton Trans.* **2010,** *39* (16), 3985-9.
8. Pal, R.; Negre, C. F.; Vogt, L.; Pokhrel, R.; Ertem, M. Z.; Brudvig, G. W.; Batista, V. S., S0-State Model of the Oxygen-Evolving Complex of Photosystem II. *Biochemistry* **2013,** *52* (44), 7703-6.
9. Walter, M. G.; Warren, E. L.; McKone, J. R.; Boettcher, S. W.; Mi, Q.; Santori, E. A.; Lewis, N. S., Solar Water Splitting Cells. *Chem. Rev.* **2010,** *110* (11), 6446-6473.

www.manaraa.com

10. Kaveevivitchai, N.; Kohler, L.; Zong, R.; El Ojaimi, M.; Mehta, N.; Thummel, R. P., A Ru(II) Bis-terpyridine-like Complex that Catalyzes Water Oxidation: The Influence of Steric Strain. *Inorg. Chem.***2013,** *52* (18), 10615-10622.

11. Liu, F.; Concepcion, J. J.; Jurss, J. W.; Cardolaccia, T.; Templeton, J. L.; Meyer, T. J., Mechanisms of Water Oxidation from the Blue Dimer to Photosystem II. *Inorg. Chem.* **2008,** *47* (6), 1727-1752.

12. Wanniarachchi, D. C.; Heeg, M. J.; Verani, C. N., Effect of Substituents on the Water Oxidation Activity of [RuII(terpy)(phen)Cl]+ Procatalysts. *Inorg. Chem.* **2014,** *53* (7), 3311-3319.

13. Cline, E. D.; Adamson, S. E.; Bernhard, S., Homogeneous Catalytic System for Photoinduced Hydrogen Production Utilizing Iridium and Rhodium Complexes. *Inorg. Chem.* **2008,** *47* (22), 10378-10388.

14. Connolly, P.; Espenson, J. H., Cobalt-catalyzed Evolution of Molecular Hydrogen. *Inorg. Chem.* **1986,** *25* (16), 2684-2688.

15. Baffert, C.; Artero, V.; Fontecave, M., Cobaloximes as Functional Models for Hydrogenases. 2. Proton Electroreduction Catalyzed by Difluoroborylbis(Dimethylglyoximato)Cobalt(II) Complexes in Organic Media. *Inorg. Chem.* **2007,** *46* (5), 1817-24.

16. Hu, X.; Brunschwig, B. S.; Peters, J. C., Electrocatalytic Hydrogen Evolution at Low Overpotentials by Cobalt Macrocyclic Glyoxime and Tetraimine Complexes. *J. Am. Chem. Soc.* **2007,** *129* (29), 8988-8998.

www.manaraa.com

17. Jacques, P. A.; Artero, V.; Pecaut, J.; Fontecave, M., Cobalt and Nickel Diimine-Dioxime Complexes as Molecular Electrocatalysts for Hydrogen Evolution with Low Overvoltages. *Proc. Natl. Acad. Sci. U. S. A.* **2009,** *106* (49), 20627-32.

18. Bigi, J. P.; Hanna, T. E.; Harman, W. H.; Chang, A.; Chang, C. J., Electrocatalytic Reduction of Protons to Hydrogen by a Water-compatible Cobalt Polypyridyl Platform. *Chem. Commun.* **2010,** *46* (6), 958-60.

19. Caramori, S.; Husson, J.; Beley, M.; Bignozzi, C. A.; Argazzi, R.; Gros, P. C., Combination of Cobalt and Iron Polypyridine Complexes for Improving the Charge Separation and Collection in Ru(Terpyridine)(2)-Sensitised Solar Cells. *Chemistry* **2010,** *16* (8), 2611-8.

20. Losse, S.; Vos, J. G.; Rau, S., Catalytic Hydrogen Production at Cobalt Centres. *Coord. Chem. Rev.* **2010,** *254* (21-22), 2492-2504.

21. Wasylenko, D. J.; Ganesamoorthy, C.; Borau-Garcia, J.; Berlinguette, C. P., Electrochemical evidence for catalytic water oxidation mediated by a high-valent cobalt complex. *Chem. Commun.* **2011,** *47* (14), 4249-51.

22. Zhang, M.; Zhang, M. T.; Hou, C.; Ke, Z. F.; Lu, T. B., Homogeneous electrocatalytic water oxidation at neutral pH by a robust macrocyclic nickel(II) complex. *Angew. Chem. Int. Ed.* **2014,** *53* (48), 13042-8.

23. Zhang, P.; Wang, M.; Yang, Y.; Zheng, D.; Han, K.; Sun, L., Highly efficient molecular nickel catalysts for electrochemical hydrogen production from neutral water. *Chem. Commun.* **2014,** *50* (91), 14153-6.

24. Martin, D. J.; McCarthy, B. D.; Donley, C. L.; Dempsey, J. L., Electrochemical hydrogenation of a homogeneous nickel complex to form a surface adsorbed hydrogen-evolving species. *Chem. Commun.* **2015,** *51* (25), 5290-5293.

www.manaraa.com

25. Tatematsu, R.; Inomata, T.; Ozawa, T.; Masuda, H., Electrocatalytic Hydrogen Production by a Nickel(II) Complex with a Phosphinopyridyl Ligand. *Angew. Chem. Int. Ed.* **2016,** *55* (17), 5247-50.

26. Zhang, M. T.; Chen, Z.; Kang, P.; Meyer, T. J., Electrocatalytic water oxidation with a copper(II) polypeptide complex. *J. Am. Chem. Soc.* **2013,** *135* (6), 2048-51.

27. Gerlach, D. L.; Bhagan, S.; Cruce, A. A.; Burks, D. B.; Nieto, I.; Truong, H. T.; Kelley, S. P.; Herbst-Gervasoni, C. J.; Jernigan, K. L.; Bowman, M. K.; Pan, S.; Zeller, M.; Papish, E. T., Studies of the pathways open to copper water oxidation catalysts containing proximal hydroxy groups during basic electrocatalysis. *Inorg. Chem.* **2014,** *53* (24), 12689-98.

28. Fillol, J. L.; Codola, Z.; Garcia-Bosch, I.; Gomez, L.; Pla, J. J.; Costas, M., Efficient water oxidation catalysts based on readily available iron coordination complexes. *Nature Chem.* **2011,** *3* (10), 807-13.

29. Hong, D.; Mandal, S.; Yamada, Y.; Lee, Y. M.; Nam, W.; Llobet, A.; Fukuzumi, S., Water oxidation catalysis with nonheme iron complexes under acidic and basic conditions: homogeneous or heterogeneous? *Inorg. Chem.* **2013,** *52* (16), 9522-31.

30. Acuna-Pares, F.; Codola, Z.; Costas, M.; Luis, J. M.; Lloret-Fillol, J., Unraveling the mechanism of water oxidation catalyzed by nonheme iron complexes. *Chemistry* **2014,** *20* (19), 5696-707.

31. Artero, V.; Chavarot-Kerlidou, M.; Fontecave, M., Splitting Water with Cobalt. *Angew. Chem. Int. Ed.* **2011,** *50* (32), 7238-7266.

32. Cook, T. R.; Dogutan, D. K.; Reece, S. Y.; Surendranath, Y.; Teets, T. S.; Nocera, D. G., Solar Energy Supply and Storage for the Legacy and Nonlegacy Worlds. *Chem. Rev.* **2010,** *110* (11), 6474-6502.

www.manaraa.com

33. Britt, R. D.; Campbell, K. A.; Peloquin, J. M.; Gilchrist, M. L.; Aznar, C. P.; Dicus, M. M.; Robblee, J.; Messinger, J., Recent pulsed EPR studies of the photosystem II oxygen-evolving complex: implications as to water oxidation mechanisms. *Biochim Biophys Acta* **2004,** *1655* (1-3), 158-71.

34. Messinger, J., Evaluation of different mechanistic proposals for water oxidation in photosynthesis on the basis of Mn4OxCa structures for the catalytic site and spectroscopic data. *PCCP* **2004,** *6* (20), 4764.

35. Zong, R.; Thummel, R. P., A New Family of Ru Complexes for Water Oxidation. *J. Am. Chem. Soc.* **2005,** *127* (37), 12802-12803.

36. Meelich, K.; Zaleski, C. M.; Pecoraro, V. L., Using small molecule complexes to elucidate features of photosynthetic water oxidation. *Phil. Trans. Soc. B, Biological sciences* **2008,** *363* (1494), 1271-9; discussion 1279-81.

37. Mullins, C. S.; Pecoraro, V. L., Reflections on Small Molecule Manganese Models that Seek to Mimic Photosynthetic Water Oxidation Chemistry. *Coord. Chem. Rev.* **2008,** *252* (3-4), 416-443.

38. Concepcion, J. J.; Jurss, J. W.; Norris, M. R.; Chen, Z.; Templeton, J. L.; Meyer, T. J., Catalytic water oxidation by single-site ruthenium catalysts. *Inorg. Chem.* **2010,** *49* (4), 1277-9.

39. Wang, L. P.; Wu, Q.; Van Voorhis, T., Acid-base mechanism for ruthenium water oxidation catalysts. *Inorg. Chem.* **2010,** *49* (10), 4543-53.

40. Wasylenko, D. J.; Ganesamoorthy, C.; Koivisto, B. D.; Berlinguette, C. P., Examination of Water Oxidation by Catalysts Containing Cofacial Metal Sites. *Eur. J. Inorg. Chem.* **2010,** *2010* (20), 3135-3142.

www.manaraa.com

41. Wasylenko, D. J.; Ganesamoorthy, C.; Koivisto, B. D.; Henderson, M. A.; Berlinguette, C. P., Insight into water oxidation by mononuclear polypyridyl Ru catalysts. *Inorg. Chem.* **2010,** *49* (5), 2202-9.

42. Yamazaki, H.; Shouji, A.; Kajita, M.; Yagi, M., Electrocatalytic and photocatalytic water oxidation to dioxygen based on metal complexes. *Coord. Chem. Rev.* **2010,** *254* (21-22), 2483-2491.

43. Rutherford, A. W.; Boussac, A., Biochemistry. Water photolysis in biology. *Science* **2004,** *303* (5665), 1782-4.

44. Rappaport, F.; Guergova-Kuras, M.; Nixon, P. J.; Diner, B. A.; Lavergne, J., Kinetics and Pathways of Charge Recombination in Photosystem II. *Biochemistry* **2002,** *41* (26), 8518-8527.

45. Parent, A. R.; Crabtree, R. H.; Brudvig, G. W., Comparison of primary oxidants for water-oxidation catalysis. *Chem. Soc. Rev.* **2013,** *42* (6), 2247-52.

46. Solis, B. H.; Hammes-Schiffer, S., Theoretical analysis of mechanistic pathways for hydrogen evolution catalyzed by cobaloximes. *Inorg. Chem.* **2011,** *50* (21), 11252-62.

47. Marinescu, S. C.; Winkler, J. R.; Gray, H. B., Molecular mechanisms of cobalt-catalyzed hydrogen evolution. *Proc. Natl. Acad. Sci. U. S. A.* **2012,** *109* (38), 15127-31.

48. Mandal, S.; Shikano, S.; Yamada, Y.; Lee, Y. M.; Nam, W.; Llobet, A.; Fukuzumi, S., Protonation equilibrium and hydrogen production by a dinuclear cobalt-hydride complex reduced by cobaltocene with trifluoroacetic acid. *J. Am. Chem. Soc.* **2013,** *135* (41), 15294-7.

www.manaraa.com

49. Roberts, J. A. S.; Bullock, R. M., Direct Determination of Equilibrium Potentials for Hydrogen Oxidation/Production by Open Circuit Potential Measurements in Acetonitrile. *Inorg. Chem.* **2013,** *52* (7), 3823-3835.

50. Razavet, M.; Artero, V.; Fontecave, M., Proton Electroreduction Catalyzed by Cobaloximes: Functional Models for Hydrogenases. *Inorg. Chem.* **2005,** *44* (13), 4786-4795.

51. Wiedner, E. S.; Bullock, R. M., Electrochemical Detection of Transient Cobalt Hydride Intermediates of Electrocatalytic Hydrogen Production. *J. Am. Chem. Soc.* **2016,** *138* (26), 8309-8318.

52. Costentin, C.; Dridi, H.; Savéant, J.-M., Molecular Catalysis of H2 Evolution: Diagnosing Heterolytic versus Homolytic Pathways. *J. Am. Chem. Soc.* **2014,** *136* (39), 13727-13734.

53. Hu, X.; Cossairt, B. M.; Brunschwig, B. S.; Lewis, N. S.; Peters, J. C., Electrocatalytic hydrogen evolution by cobalt difluoroboryl-diglyoximate complexes. *Chem. Commun.* **2005,** (37), 4723-4725.

54. Basu, D.; Mazumder, S.; Niklas, J.; Baydoun, H.; Wanniarachchi, D.; Shi, X.; Staples, R. J.; Poluektov, O.; Schlegel, H. B.; Verani, C. N., Evaluation of the coordination preferences and catalytic pathways of heteroaxial cobalt oximes towards hydrogen generation. *Chem. Sci.* **2016,** *7* (5), 3264-3278.

55. Lei, H.; Fang, H.; Han, Y.; Lai, W.; Fu, X.; Cao, R., Reactivity and Mechanism Studies of Hydrogen Evolution Catalyzed by Copper Corroles. *ACS Catal.* **2015,** *5* (9), 5145-5153.

56. Zee, D. Z.; Chantarojsiri, T.; Long, J. R.; Chang, C. J., Metal–Polypyridyl Catalysts for Electro- and Photochemical Reduction of Water to Hydrogen. *Acc. Chem. Res.* **2015,** *48* (7), 2027-2036.

www.manaraa.com

57. Lehn, J., Chemical storage of light energy. Catalytic generation of hydrogen by visible light or sunlight. Irradiation of neutral aqueous solutions. *Nouveau Journal de Chimie* **1977,** *1* (6), 449-451.

58. Du, P.; Knowles, K.; Eisenberg, R., A homogeneous system for the photogeneration of hydrogen from water based on a platinum(II) terpyridyl acetylide chromophore and a molecular cobalt catalyst. *J. Am. Chem. Soc.* **2008,** *130* (38), 12576-7.

59. Chen, L.; Wang, M.; Gloaguen, F.; Zheng, D.; Zhang, P.; Sun, L., Tetranuclear iron complexes bearing benzenetetrathiolate bridges as four-electron transformation templates and their electrocatalytic properties for proton reduction. *Inorg. Chem.* **2013,** *52* (4), 1798-806.

60. Simmons, T. R.; Artero, V., Catalytic hydrogen oxidation: dawn of a new iron age. *Angew. Chem. Int. Ed.* **2013,** *52* (24), 6143-5.

61. Han, Z.; McNamara, W. R.; Eum, M. S.; Holland, P. L.; Eisenberg, R., A nickel thiolate catalyst for the long-lived photocatalytic production of hydrogen in a noble-metal-free system. *Angew. Chem. Int. Ed.* **2012,** *51* (7), 1667-70.

62. Smith, R. D.; Prevot, M. S.; Fagan, R. D.; Trudel, S.; Berlinguette, C. P., Water oxidation catalysis: electrocatalytic response to metal stoichiometry in amorphous metal oxide films containing iron, cobalt, and nickel. *J. Am. Chem. Soc.* **2013,** *135* (31), 11580-6.

63. Smith, R. D.; Berlinguette, C. P., Accounting for the Dynamic Oxidative Behavior of Nickel Anodes. *J. Am. Chem. Soc.* **2016,** *138* (5), 1561-7.

64. Zarkadoulas, A.; Field, M. J.; Papatriantafyllopoulou, C.; Fize, J.; Artero, V.; Mitsopoulou, C. A., Experimental and Theoretical Insight into Electrocatalytic Hydrogen Evolution with Nickel Bis(aryldithiolene) Complexes as Catalysts. *Inorg. Chem.* **2016,** *55* (2), 432-44.

www.manaraa.com

65. Cobo, S.; Heidkamp, J.; Jacques, P. A.; Fize, J.; Fourmond, V.; Guetaz, L.; Jousselme, B.; Ivanova, V.; Dau, H.; Palacin, S.; Fontecave, M.; Artero, V., A Janus cobalt-based catalytic material for electro-splitting of water. *Nat. Mater.* **2012,** *11* (9), 802-7.

66. Eckenhoff, W. T.; McNamara, W. R.; Du, P.; Eisenberg, R., Cobalt complexes as artificial hydrogenases for the reductive side of water splitting. *Biochimica et Biophysica Acta (BBA) - Bioenergetics* **2013,** *1827* (8), 958-973.

67. King, A. E.; Surendranath, Y.; Piro, N. A.; Bigi, J. P.; Long, J. R.; Chang, C. J., A mechanistic study of proton reduction catalyzed by a pentapyridine cobalt complex: evidence for involvement of an anation-based pathway. *Chem. Sci.* **2013,** *4* (4), 1578.

68. Schrauzer, G. N.; Holland, R. J., Hydridocobaloximes. *J. Am. Chem. Soc.* **1971,** *93* (6), 1505-1506.

69. Baffert, C.; Artero, V.; Fontecave, M., Cobaloximes as Functional Models for Hydrogenases. 2. Proton Electroreduction Catalyzed by Difluoroborylbis(dimethylglyoximato)cobalt(II) Complexes in Organic Media. *Inorg. Chem.* **2007,** *46* (5), 1817-1824.

70. Bigi, J. P.; Hanna, T. E.; Harman, W. H.; Chang, A.; Chang, C. J., Electrocatalytic reduction of protons to hydrogen by a water-compatible cobalt polypyridyl platform. *Chem. Commun.* **2010,** *46* (6), 958-960.

71. Vennampalli, M.; Liang, G.; Katta, L.; Webster, C. E.; Zhao, X., Electronic Effects on a Mononuclear Co Complex with a Pentadentate Ligand for Catalytic H2 Evolution. *Inorg. Chem.* **2014,** *53* (19), 10094-10100.

www.manaraa.com

72. Lewandowska-Andralojc, A.; Baine, T.; Zhao, X.; Muckerman, J. T.; Fujita, E.; Polyansky, D. E., Mechanistic Studies of Hydrogen Evolution in Aqueous Solution Catalyzed by a Tertpyridine–Amine Cobalt Complex. *Inorg. Chem.* **2015,** *54* (9), 4310-4321.

73. Basu, D.; Mazumder, S.; Shi, X.; Baydoun, H.; Niklas, J.; Poluektov, O.; Schlegel, H. B.; Verani, C. N., Ligand transformations and efficient proton/water reduction with cobalt catalysts based on pentadentate pyridine-rich environments. *Angew. Chem. Int. Ed.* **2015,** *54* (7), 2105-10.

74. Szymczak, N. K.; Berben, L. A.; Peters, J. C., Redox rich dicobalt macrocycles as templates for multi-electron transformations. *Chem. Commun.* **2009,** (44), 6729-6731.

75. Valdez, C. N.; Dempsey, J. L.; Brunschwig, B. S.; Winkler, J. R.; Gray, H. B., Catalytic hydrogen evolution from a covalently linked dicobaloxime. *Proc. Natl. Acad. Sci. U. S. A.* **2012,** *109* (39), 15589-93.

76. Valdez, C. N.; Dempsey, J. L.; Brunschwig, B. S.; Winkler, J. R.; Gray, H. B., Catalytic hydrogen evolution from a covalently linked dicobaloxime. *Proc. Natl. Acad. Sci. U. S. A.* **2012,** *109* (39), 15589-15593.

77. Kal, S.; Filatov, A. S.; Dinolfo, P. H., Electrocatalytic proton reduction by a dicobalt tetrakis-Schiff base macrocycle in nonaqueous electrolyte. *Inorg. Chem.* **2014,** *53* (14), 7137-45.

78. Gao, Y.; Crabtree, R. H.; Brudvig, G. W., Water oxidation catalyzed by the tetranuclear Mn complex [Mn(IV)4O5(terpy)4(H2O)2](ClO4)6. *Inorg. Chem.* **2012,** *51* (7), 4043-50.

79. Kurahashi, T.; Kikuchi, A.; Shiro, Y.; Hada, M.; Fujii, H., Unique Properties and Reactivity of High-Valent Manganese−Oxo versus Manganese−Hydroxo in the Salen Platform. *Inorg. Chem.* **2010,** *49* (14), 6664-6672.

www.manaraa.com

80. Lassalle-Kaiser, B.; Hureau, C.; Pantazis, D. A.; Pushkar, Y.; Guillot, R.; Yachandra, V. K.; Yano, J.; Neese, F.; Anxolabéhère-Mallart, E., Activation of a water molecule using a mononuclear Mn complex: from Mn-aquo, to Mn-hydroxo, to Mn-oxyl via charge compensation. *Energy & Environ. Sci.* **2010,** *3* (7), 924-938.

81. Wasylenko, D. J.; Palmer, R. D.; Schott, E.; Berlinguette, C. P., Interrogation of electrocatalytic water oxidation mediated by a cobalt complex. *Chem. Commun.* **2012,** *48* (15), 2107-9.

82. Cooper, S. R.; Calvin, M., Mixed valence interactions in di-.mu.-oxo bridged manganese complexes. *J. Am. Chem. Soc.* **1977,** *99* (20), 6623-6630.

83. Gersten, S. W.; Samuels, G. J.; Meyer, T. J., Catalytic oxidation of water by an oxo-bridged ruthenium dimer. *J. Am. Chem. Soc.* **1982,** *104* (14), 4029-4030.

84. Llobet, A.; Doppelt, P.; Meyer, T. J., Redox properties of aqua complexes of ruthenium(II) containing the tridentate ligands 2,2':6',2''-terpyridine and tris(1-pyrazolyl)methane. *Inorg. Chem.* **1988,** *27* (3), 514-520.

85. Zhang, G.; Zong, R.; Tseng, H.-W.; Thummel, R. P., Ru(II) Complexes of Tetradentate Ligands Related to 2,9-Di(pyrid-2‘-yl)-1,10-phenanthroline. *Inorg. Chem.* **2008,** *47* (3), 990-998.

86. Tseng, H.-W.; Zong, R.; Muckerman, J. T.; Thummel, R., Mononuclear Ruthenium(II) Complexes That Catalyze Water Oxidation. *Inorg. Chem.* **2008,** *47* (24), 11763-11773.

87. Greenwood, N. N.; Earnshaw, A., *Chemistry of the elements*. 1st ed.; Pergamon Press: Oxford ; New York, 1984; p xxi, 1542 p.

88. Limburg, J.; Brudvig, G. W.; Crabtree, R. H., O2 Evolution and Permanganate Formation from High-Valent Manganese Complexes. *J. Am. Chem. Soc.* **1997,** *119* (11), 2761-2762.

www.manaraa.com

89. Collomb, M.-N.; Deronzier, A., Electro- and Photoinduced Formation and Transformation of Oxido-Bridged Multinuclear Mn Complexes. *Eur. J. Inorg. Chem.* **2009,** *2009* (14), 2025-2046.

90. Karlsson, E. A.; Lee, B.-L.; Åkermark, T.; Johnston, E. V.; Kärkäs, M. D.; Sun, J.; Hansson, Ö.; Bäckvall, J.-E.; Åkermark, B., Photosensitized Water Oxidation by Use of a Bioinspired Manganese Catalyst. *Angew. Chem. Int. Ed.* **2011,** *50* (49), 11715-11718.

91. Hammarström, L.; Styring, S., Coupled electron transfers in artificial photosynthesis. *Phil. Trans. Soc. B: Bio.Sci.* **2008,** *363* (1494), 1283-1291.

92. Anderlund, M. F.; Zheng, J.; Ghiladi, M.; Kritikos, M.; Rivière, E.; Sun, L.; Girerd, J.-J.; Åkermark, B., A new, dinuclear high spin manganese(III) complex with bridging phenoxy and methoxy groups. Structure and magnetic properties. *Inorg. Chem. Commun.* **2006,** *9* (12), 1195-1198.

93. Anderlund, M. F.; Högblom, J.; Shi, W.; Huang, P.; Eriksson, L.; Weihe, H.; Styring, S.; Åkermark, B.; Lomoth, R.; Magnuson, A., Redox Chemistry of a Dimanganese(II,III) Complex with an Unsymmetric Ligand: Water Binding, Deprotonation and Accumulative Light-Induced Oxidation. *Eur. J. Inorg. Chem.* **2006,** *2006* (24), 5033-5047.

94. Anderlund, M. F.; Zheng, J.; Ghiladi, M.; Kritikos, M.; Rivière, E.; Sun, L.; Girerd, J.-J.; Åkermark, B., A new, dinuclear high spin manganese(III) complex with bridging phenoxy and methoxy groups. Structure and magnetic properties. *Inorg. Chem. Commun.* **2006,** *9* (12), 1195-1198.

95. Borgström, M.; Shaikh, N.; Johansson, O.; Anderlund, M. F.; Styring, S.; Åkermark, B.; Magnuson, A.; Hammarström, L., Light Induced Manganese Oxidation and Long-Lived

www.manaraa.com

Charge Separation in a Mn2II,II−RuII(bpy)3−Acceptor Triad. *J. Am. Chem. Soc.* **2005,** *127* (49), 17504-17515.

96. Burdinski, D.; Bothe, E.; Wieghardt, K., Synthesis and Characterization of Tris(bipyridyl)ruthenium(II)-Modified Mono-, Di-, and Trinuclear Manganese Complexes as Electron-Transfer Models for Photosystem II. *Inorg. Chem.* **1999,** *39* (1), 105-116.

97. Kurahashi, T.; Hada, M.; Fujii, H., Critical Role of External Axial Ligands in Chirality Amplification of trans-Cyclohexane-1,2-diamine in Salen Complexes. *J. Am. Chem. Soc.* **2009,** *131* (34), 12394-12405.

98. Kurahashi, T.; Fujii, H., One-Electron Oxidation of Electronically Diverse Manganese(III) and Nickel(II) Salen Complexes: Transition from Localized to Delocalized Mixed-Valence Ligand Radicals. *J. Am. Chem. Soc.* **2011,** *133* (21), 8307-8316.

99. Schmitt, H.; Lomoth, R.; Magnuson, A.; Park, J.; Fryxelius, J.; Kritikos, M.; Mårtensson, J.; Hammarström, L.; Sun, L.; Åkermark, B., Synthesis, Redox Properties, and EPR Spectroscopy of Manganese(III) Complexes of the Ligand N,N-Bis(2-hydroxybenzyl)-N′-2-hydroxybenzylidene-1,2-diaminoethane: Formation of Mononuclear, Dinuclear, and Even Higher Nuclearity Complexes. *Chem. Eur. J.* **2002,** *8* (16), 3757-3768.

100. Kurahashi, T.; Kikuchi, A.; Tosha, T.; Shiro, Y.; Kitagawa, T.; Fujii, H., Transient Intermediates from Mn(salen) with Sterically Hindered Mesityl Groups: Interconversion between MnIV-Phenolate and MnIII-Phenoxyl Radicals as an Origin for Unique Reactivity. *Inorg. Chem.* **2008,** *47* (5), 1674-1686.

101. Colpas, G. J.; Hamstra, B. J.; Kampf, J. W.; Pecoraro, V. L., The Preparation of VO3+ and VO2+ Complexes Using Hydrolytically Stable, Asymmetric Ligands Derived from Schiff Base Precursors. *Inorg. Chem.* **1994,** *33* (21), 4669-4675.

www.manaraa.com

102. Hong, D.; Jung, J.; Park, J.; Yamada, Y.; Suenobu, T.; Lee, Y.-M.; Nam, W.; Fukuzumi, S., Water-soluble mononuclear cobalt complexes with organic ligands acting as precatalysts for efficient photocatalytic water oxidation. *Energy & Environ. Sci.* **2012,** *5* (6), 7606-7616.

103. Rigsby, M. L.; Mandal, S.; Nam, W.; Spencer, L. C.; Llobet, A.; Stahl, S. S., Cobalt analogs of Ru-based water oxidation catalysts: overcoming thermodynamic instability and kinetic lability to achieve electrocatalytic O2 evolution. *Chem. Sci.* **2012,** *3* (10), 3058.

104. Stuart, B., Infrared Spectroscopy. In *Kirk-Othmer Encyclopedia of Chemical Technology*, John Wiley & Sons, Inc.: 2000.

105. Kebarle, P.; Verkerk, U. H., On the Mechanism of Electrospray Ionization Mass Spectrometry (ESIMS). In *Electrospray and MALDI Mass Spectrometry*, John Wiley & Sons, Inc.: 2010; pp 1-48.

106. Weil, J. A.; Bolton, J. R., Basic Principles of Paramagnetic Resonance. In *Electron Paramagnetic Resonance*, John Wiley & Sons, Inc.: 2006; pp 1-35.

107. Stoll, S.; Schweiger, A., EasySpin, a comprehensive software package for spectral simulation and analysis in EPR. *J Magn Reson* **2006,** *178* (1), 42-55.

108. Bruker Single Crystal X-ray Diffraction. https://www.bruker.com/products/x-ray-diffraction-and-elemental-analysis/single-crystal-x-ray-diffraction.html.

109.<Product_Sheet_31_APEX_II_CCD_Detector_DOC-S86EXS031_V2_en_low.pdf>.

110. <APEX2 User Manual.pdf>.

111. Bourhis, L. J.; Dolomanov, O. V.; Gildea, R. J.; Howard, J. A.; Puschmann, H., The anatomy of a comprehensive constrained, restrained refinement program for the modern

www.manaraa.com

computing environment - Olex2 dissected. *Acta Crystallogr A Found Adv* **2015,** *71* (Pt 1), 59-75.

112. Sheldrick, G., A short history of SHELX. *Acta Crystallogr. A* **2008,** *64* (1), 112-122.

113. <07_solving_phase_problem_mir_sir_lecture7.pdf>.

114. Bard, A. J.; Faulkner, L. R., *Electrochemical methods : fundamentals and applications*. Wiley: New York, 1980; p xviii, 718 p.

115. Basu, D.; Allard, M. M.; Xavier, F. R.; Heeg, M. J.; Schlegel, H. B.; Verani, C. N., Modulation of electronic and redox properties in phenolate-rich cobalt(III) complexes and their implications for catalytic proton reduction. *Dalton Trans.* **2015,** *44* (7), 3454-66.

116. Milner, G. W. C.; Phillips, G., *Coulometry in analytical chemistry*. 1st ed.; Pergamon Press: Oxford, New York, 1967; p x, 207 p.

117. Verani, C. N.; Kpogo, K.; Mazumder, S.; Wang, D.; Schlegel, H. B.; Fiedler, A., Bimetallic Cooperativity in Proton Reduction with an Amido-bridged Cobalt Catalyst. *Chem. Eur. J.* **2017**.

118. Zhou, W.; Apkarian, R.; Wang, Z. L.; Joy, D., Fundamentals of Scanning Electron Microscopy (SEM). In *Scanning Microscopy for Nanotechnology: Techniques and Applications*, Zhou, W.; Wang, Z. L., Eds. Springer New York: New York, NY, 2007; pp 1-40.

119. Vernon-Parry, K. D., Scanning electron microscopy: an introduction. *III-Vs Review* **2000,** *13* (4), 40-44.

120. McCarthy, J. J.; McMillan, D. J., Application of X-ray Optics to Energy-Dispersive Spectroscopy. *Microsc Microanal* **1998,** *4* (6), 632-639.

www.manaraa.com

121. Williams, T. J., Scanning electron microscopy and x-ray microanalysis, 3rd edition. By Joseph Goldstein, Dale Newbury, David Joy, Charles Lyman, Patrick Echlin, Eric Lifshin, Linda Sawyer, Joseph Michael Kluwer Academic Publishers, New York (2003) ISBN 0306472929; hardback; 688; $75.00. *Scanning* **2005,** *27* (4), 215-216.

122. Calais, J.-L., Density-functional theory of atoms and molecules. R.G. Parr and W. Yang, Oxford University Press, New York, Oxford, 1989. IX + 333 pp. *Intl. J. Quantum Chem.* **1993,** *47* (1), 101-101.

123. M. J. Frisch, G. W. T., H. B. Schlegel, G. E. Scuseria, M. A. Robb, J. R. Cheeseman, G. Scalmani, V. Barone, B. Mennucci, G. A. Petersson, H. Nakatsuji, M. Caricato, X. Li, H. P. Hratchian, A. F. Izmaylov, J. Bloino, G. Zheng, J. L. Sonnenberg, W. Liang, M. Hada, M. Ehara, K. Toyota, R. Fukuda, J. Hasegawa, M. Ishida, T. Nakajima, Y. Honda, O. Kitao, H. Nakai, T. Vreven, J. A. Montgomery, Jr., J. E. Peralta, F. Ogliaro, M. Bearpark, J. J. Heyd, E. Brothers, K. N. Kudin, V. N. Staroverov, T. Keith, R. Kobayashi, J. Normand, K. Raghavachari, A. Rendell, J. C. Burant, S. S. Iyengar, J. Tomasi, M. Cossi, N. Rega, J. M. Millam, M. Klene, J. E. Knox, J. B. Cross, V. Bakken, C. Adamo, J. Jaramillo, R. Gomperts, R. E. Stratmann, O. Yazyev, A. J. Austin, R. Cammi, C. Pomelli, J. W. Ochterski, R. L. Martin, K. Morokuma, V. G. Zakrzewski, G. A. Voth, P. Salvador, J. J. Dannenberg, S. Dapprich, P. V. Parandekar, N. J. Mayhall, A. D. Daniels, O. Farkas, J. B. Foresman, J. V. Ortiz, J. Cioslowski, and D. J. Fox, , Gaussian Development Version, Revision H.31. Gaussian, Inc: Wallingford, CT, 2010.

124. Becke, A. D., Density-functional exchange-energy approximation with correct asymptotic behavior. *Phys. Rev. A.* **1988,** *38* (6), 3098-3100.

www.manaraa.com

125. Becke, A. D., Density-functional exchange-energy approximation with correct asymptotic behavior. *Phys. Rev. A Gen. Phys.* **1988,** *38* (6), 3098-3100.

126. Pople, P. C. H. a. J. A., *Theoretica Chimica Act.* **1973,** *28*, 213-222.

127. M. M. Francl, W. J. P., W. J. Hehre, J. S. Binkley, M. S. Gordon, D. J. DeFrees and J. A. Pople *J. Chem. Phys.* **1982,** *77*, 3654-3665.

128. M. Dolg, U. W., H. Stoll and H. Preuss *J. Chem. Phys.* **1987,** *86*, 866-872.

129. Wilson, A. D.; Newell, R. H.; McNevin, M. J.; Muckerman, J. T.; Rakowski DuBois, M.; DuBois, D. L., Hydrogen oxidation and production using nickel-based molecular catalysts with positioned proton relays. *J. Am. Chem. Soc.* **2006,** *128* (1), 358-66.

130. Kankanamalage, P. H. A.; Mazumder, S.; Tiwari, V.; Kpogo, K. K.; Bernhard Schlegel, H.; Verani, C. N., Efficient electro/photocatalytic water reduction using a [NiII(N2Py3)]2+ complex. *Chem. Commun.* **2016**.

131. Solis, B. H.; Hammes-Schiffer, S., Substituent effects on cobalt diglyoxime catalysts for hydrogen evolution. *J. Am. Chem. Soc.* **2011,** *133* (47), 19036-9.

132. Muckerman, J. T.; Fujita, E., Theoretical studies of the mechanism of catalytic hydrogen production by a cobaloxime. *Chem. Commun.* **2011,** *47* (46), 12456-8.

133. Solis, B. H.; Yu, Y.; Hammes-Schiffer, S., Effects of ligand modification and protonation on metal oxime hydrogen evolution electrocatalysts. *Inorg. Chem.* **2013,** *52* (12), 6994-9.

134. Concepcion, J. J.; Jurss, J. W.; Templeton, J. L.; Meyer, T. J., One Site is Enough. Catalytic Water Oxidation by [Ru(tpy)(bpm)(OH2)]2+ and [Ru(tpy)(bpz)(OH2)]2+. *J. Am. Chem. Soc.* **2008,** *130* (49), 16462-16463.

www.manaraa.com

135. Concepcion, J. J.; Jurss, J. W.; Brennaman, M. K.; Hoertz, P. G.; Patrocinio, A. O. T.; Murakami Iha, N. Y.; Templeton, J. L.; Meyer, T. J., Making Oxygen with Ruthenium Complexes. *Acc. Chem. Res.* **2009,** *42* (12), 1954-1965.

136. Wasylenko, D. J.; Ganesamoorthy, C.; Henderson, M. A.; Koivisto, B. D.; Osthoff, H. D.; Berlinguette, C. P., Electronic modification of the [Ru(II)(tpy)(bpy)(OH(2))](2+) scaffold: effects on catalytic water oxidation. *J. Am. Chem. Soc.* **2010,** *132* (45), 16094-106.

137. Wang, L.-P.; Wu, Q.; Van Voorhis, T., Acid−Base Mechanism for Ruthenium Water Oxidation Catalysts. *Inorg. Chem.* **2010,** *49* (10), 4543-4553.

138. Tong, L.; Duan, L.; Xu, Y.; Privalov, T.; Sun , L., Structural Modifications of Mononuclear Ruthenium Complexes: A Combined Experimental and Theoretical Study on the Kinetics of Ruthenium-Catalyzed Water Oxidation. *Angew. Chem. Int. Ed.* **2011,** *50* (2), 445-449.

139. England, J.; Britovsek, G. J. P.; Rabadia, N.; White, A. J. P., Ligand Topology Variations and the Importance of Ligand Field Strength in Non-Heme Iron Catalyzed Oxidations of Alkanes. *Inorg. Chem.* **2007,** *46* (9), 3752-3767.

140. Bruker Corporation. Datamonitor.: New York, NY. http://proxy.lib.wayne.edu/login?url=http://search.ebscohost.com/direct.asp?db=bth&jid=BDE4&scope=site.

141. Becke, A. D., Density-functional exchange-energy approximation with correct asymptotic behavior. *Phys. Rev. A.* **1988,** *38* (6), 3098.

142. Perdew, J. P., Density-functional approximation for the correlation energy of the inhomogeneous electron gas. *Physical Review B* **1986,** *33* (12), 8822.

143. Frisch, M. J.; Trucks, G. W.; Schlegel, H. B.; Scuseria, G. E.; Robb, M. A.; Cheeseman, J. R.; Scalmani, G.; Barone, V.; Petersson, G. A.; Nakatsuji, H.; Li, X.; Caricato, M.;

www.manaraa.com

Marenich, A.; Bloino, J.; Janesko, B. G.; Gomperts, R.; Mennucci, B.; Hratchian, H. P.; Ortiz, J. V.; Izmaylov, A. F.; Sonnenberg, J. L.; Williams-Young, D.; Ding, F.; Lipparini, F.; Egidi, F.; Goings, J.; Peng, B.; Petrone, A.; Henderson, T.; Ranasinghe, D.; Zakrzewski, V. G.; Gao, J.; Rega, N.; Zheng, G.; Liang, W.; Hada, M.; Ehara, M.; Toyota, K.; Fukuda, R.; Hasegawa, J.; Ishida, M.; Nakajima, T.; Honda, Y.; Kitao, O.; Nakai, H.; Vreven, T.; Throssell, K.; Montgomery, J. A.; Jr.; Peralta, J. E.; Ogliaro, F.; Bearpark, M.; Heyd, J. J.; Brothers, E.; Kudin, K. N.; Staroverov, V. N.; Keith, T.; Kobayashi, R.; Normand, J.; Raghavachari, K.; Rendell, A.; Burant, J. C.; Iyengar, S. S.; Tomasi, J.; Cossi, M.; Millam, J. M.; Klene, M.; Adamo, C.; Cammi, R.; Ochterski, J. W.; Martin, R. L.; Morokuma, K.; Farkas, O.; Foresman, J. B.; Fox, D. J., Gaussian 09, revision E01. **2016**.

144. Andrae, D.; Häußermann, U.; Dolg, M.; Stoll, H.; Preuß, H., Energy-adjusted ab initio pseudopotentials for the second and third row transition elements. *Theoretica chimica acta* **1990,** *77* (2), 123-141.

145. Dolg, M.; Wedig, U.; Stoll, H.; Preuss, H., Energy-adjusted abinitio pseudopotentials for the first row transition elements. *J. Chem. Phys.* **1987,** *86* (2), 866-872.

146. Ditchfield, R.; Hehre, W. J.; Pople, J. A., Self-consistent molecular-orbital methods. IX. An extended Gaussian-type basis for molecular-orbital studies of organic molecules. *J. Chem. Phys.* **1971,** *54* (2), 724-728.

147. Francl, M. M.; Pietro, W. J.; Hehre, W. J.; Binkley, J. S.; Gordon, M. S.; DeFrees, D. J.; Pople, J. A., Self-Consistent Molecular Orbital Methods. XXIII. A Polarization-Type Basis Set for Second-Row Elements. *J. Chem. Phys.* **1982,** *77* (7), 3654-3665.

148. Hariharan, P. C.; Pople, J. A., The Influence of Polarization Functions on Molecular Orbital Hydrogenation Energies. *Theoretica chimica acta* **1973,** *28* (3), 213-222.

www.manaraa.com

149. Hehre, W. J.; Ditchfield, R.; Pople, J. A., Self-Consistent Molecular Orbital Methods. XII. Further Extensions of Gaussian-Type Basis Sets for Use in Molecular Orbital Studies of Organic Molecules. *J. Chem. Phys.* **1972,** *56* (5), 2257-2261.

150. Clark, T.; Chandrasekhar, J.; Spitznagel, G. W.; Schleyer, P. V. R., Efficient diffuse function-augmented basis sets for anion calculations. III. The 3-21+G basis set for first-row elements, Li-F. *J. Computational Chemistry* **1983,** *4* (3), 294-301.

151. Marenich, A. V.; Cramer, C. J.; Truhlar, D. G., Universal Solvation Model Based on Solute Electron Density and on a Continuum Model of the Solvent Defined by the Bulk Dielectric Constant and Atomic Surface Tensions. *J. Phys. Chem. B* **2009,** *113* (18), 6378-6396.

152. Dennington, R.; Keith, T.; Millam, J., GaussView, version 5. *Semichem Inc., Shawnee Mission, KS* **2009**.

153. Tong, L.; Zong, R.; Thummel, R. P., Visible light-driven hydrogen evolution from water catalyzed by a molecular cobalt complex. *J. Am. Chem. Soc.* **2014,** *136* (13), 4881-4.

154. <Ortep3.pdf>.

155. Wang, H. Y.; Mijangos, E.; Ott, S.; Thapper, A., Water oxidation catalyzed by a dinuclear cobalt-polypyridine complex. *Angew. Chem. Int. Ed.* **2014,** *53* (52), 14499-502.

156. Song, X.; Wen, H.; Ma, C.; Chen, H.; Chen, C., Hydrogen photogeneration catalyzed by a cobalt complex of a pentadentate aminopyridine-based ligand. *New J. Chem.* **2015,** *39* (3), 1734-1741.

157. Queyriaux, N.; Jane, R. T.; Massin, J.; Artero, V.; Chavarot-Kerlidou, M., Recent developments in hydrogen evolving molecular cobalt(II)–polypyridyl catalysts. *Coord. Chem. Rev.* **2015**.

www.manaraa.com

158. Stubbert, B. D.; Peters, J. C.; Gray, H. B., Rapid water reduction to H2 catalyzed by a cobalt bis(iminopyridine) complex. *J. Am. Chem. Soc.* **2011,** *133* (45), 18070-3.

159. Knijnenburg, Q.; Hetterscheid, D.; Kooistra, T. M.; Budzelaar, Peter H. M., The Electronic Structure of (Diiminopyridine)cobalt(I) Complexes. *Eur. J. Inorg. Chem.* **2004,** *2004* (6), 1204-1211.

160. Zhang, P.; Wang, M.; Gloaguen, F.; Chen, L.; Quentel, F.; Sun, L., Electrocatalytic hydrogen evolution from neutral water by molecular cobalt tripyridine-diamine complexes. *Chem. Commun.* **2013,** *49* (82), 9455-7.

161. Di Giovanni, C.; Gimbert-Surinach, C.; Nippe, M.; Benet-Buchholz, J.; Long, J. R.; Sala, X.; Llobet, A., Dinuclear Cobalt Complexes with a Decadentate Ligand Scaffold: Hydrogen Evolution and Oxygen Reduction Catalysis. *Chemistry* **2016,** *22* (1), 361-9.

162. Fukuzumi, S.; Mandal, S.; Mase, K.; Ohkubo, K.; Park, H.; Benet-Buchholz, J.; Nam, W.; Llobet, A., Catalytic four-electron reduction of O2 via rate-determining proton-coupled electron transfer to a dinuclear cobalt-mu-1,2-peroxo complex. *J. Am. Chem. Soc.* **2012,** *134* (24), 9906-9.

163. Nelson, J. H.; Nathan, L. C.; Ragsdale, R. O., Complexes of aromatic amine oxides. 4-Substituted quinoline 1-oxide complexes of cobalt(II) and nickel(II) perchlorates. *Inorg. Chem.* **1968,** *7* (9), 1840-1845.

164. Tong, L.; Kopecky, A.; Zong, R.; Gagnon, K. J.; Ahlquist, M. S.; Thummel, R. P., Light-Driven Proton Reduction in Aqueous Medium Catalyzed by a Family of Cobalt Complexes with Tetradentate Polypyridine-Type Ligands. *Inorg. Chem.* **2015,** *54* (16), 7873-84.

www.manaraa.com

165. Sun, Y.; Bigi, J. P.; Piro, N. A.; Tang, M. L.; Long, J. R.; Chang, C. J., Molecular cobalt pentapyridine catalysts for generating hydrogen from water. *J. Am. Chem. Soc.* **2011,** *133* (24), 9212-5.

166. Singh, W. M.; Baine, T.; Kudo, S.; Tian, S.; Ma, X. A.; Zhou, H.; DeYonker, N. J.; Pham, T. C.; Bollinger, J. C.; Baker, D. L.; Yan, B.; Webster, C. E.; Zhao, X., Electrocatalytic and photocatalytic hydrogen production in aqueous solution by a molecular cobalt complex. *Angew. Chem. Int. Ed.* **2012,** *51* (24), 5941-4.

167. Wasylenko, D. J.; Palmer, R. D.; Schott, E.; Berlinguette, C. P., Interrogation of electrocatalytic water oxidation mediated by a cobalt complex. *Chem. Commun.* **2012,** *48* (15), 2107-2109.

168. Karkas, M. D.; Akermark, B., Water oxidation using earth-abundant transition metal catalysts: opportunities and challenges. *Dalton Trans.* **2016,** *45* (37), 14421-14461.

169. Zhao, Y.; Lin, J.; Liu, Y.; Ma, B.; Ding, Y.; Chen, M., Efficient light-driven water oxidation catalyzed by a mononuclear cobalt(iii) complex. *Chem. Commun.* **2015,** *51* (97), 17309-17312.

170. Das, B.; Orthaber, A.; Ott, S.; Thapper, A., Water oxidation catalysed by a mononuclear CoII polypyridine complex; possible reaction intermediates and the role of the chloride ligand. *Chem. Commun.* **2015,** *51* (66), 13074-13077.

171. Lei, H.; Han, A.; Li, F.; Zhang, M.; Han, Y.; Du, P.; Lai, W.; Cao, R., Electrochemical, spectroscopic and theoretical studies of a simple bifunctional cobalt corrole catalyst for oxygen evolution and hydrogen production. *PCCP* **2014,** *16* (5), 1883-1893.

www.manaraa.com

172. Crandell, D. W.; Ghosh, S.; Berlinguette, C. P.; Baik, M. H., How a [Co(IV) a bond and a half O](2+) fragment oxidizes water: involvement of a biradicaloid [Co(II)-(O)](2+) species in forming the O-O bond. *ChemSusChem* **2015,** *8* (5), 844-52.

173. Dogutan, D. K.; McGuire, R., Jr.; Nocera, D. G., Electocatalytic water oxidation by cobalt(III) hangman beta-octafluoro corroles. *J. Am. Chem. Soc.* **2011,** *133* (24), 9178-80.

174. Schilling, M.; Patzke, G. R.; Hutter, J.; Luber, S., Computational Investigation and Design of Cobalt Aqua Complexes for Homogeneous Water Oxidation. *J. Phys. Chem. C* **2016,** *120* (15), 7966-7975.

175. Nguyen, A. I.; Ziegler, M. S.; Oña-Burgos, P.; Sturzbecher-Hohne, M.; Kim, W.; Bellone, D. E.; Tilley, T. D., Mechanistic Investigations of Water Oxidation by a Molecular Cobalt Oxide Analogue: Evidence for a Highly Oxidized Intermediate and Exclusive Terminal Oxo Participation. *J. Am. Chem. Soc.* **2015,** *137* (40), 12865-12872.

176. Brunschwig, B. S.; Chou, M. H.; Creutz, C.; Ghosh, P.; Sutin, N., Mechanisms of water oxidation to oxygen: cobalt(IV) as an intermediate in the aquocobalt(II)-catalyzed reaction. *J. Am. Chem. Soc.* **1983,** *105* (14), 4832-4833.

177. Gerken, J. B.; McAlpin, J. G.; Chen, J. Y. C.; Rigsby, M. L.; Casey, W. H.; Britt, R. D.; Stahl, S. S., Electrochemical Water Oxidation with Cobalt-Based Electrocatalysts from pH 0–14: The Thermodynamic Basis for Catalyst Structure, Stability, and Activity. *J. Am. Chem. Soc.* **2011,** *133* (36), 14431-14442.

178. Wasylenko, D. J.; Palmer, R. D.; Berlinguette, C. P., Homogeneous water oxidation catalysts containing a single metal site. *Chem. Commun.* **2013,** *49* (3), 218-227.

179. Lo, W. K. C.; Castillo, C. E.; Gueret, R.; Fortage, J.; Rebarz, M.; Sliwa, M.; Thomas, F.; McAdam, C. J.; Jameson, G. B.; McMorran, D. A.; Crowley, J. D.; Collomb, M.-N.;

www.manaraa.com

Blackman, A. G., Synthesis, Characterization, and Photocatalytic H2-Evolving Activity of a Family of [Co(N4Py)(X)]n+ Complexes in Aqueous Solution. *Inorg. Chem.* **2016,** *55* (9), 4564-4581.

180. Kankanamalage, P. H. A.; Mazumder, S.; Tiwari, V.; Kpogo, K. K.; Bernhard Schlegel, H.; Verani, C. N., Efficient electro/photocatalytic water reduction using a [NiII(N2Py3)]2+ complex. *Chem. Commun.* **2016,** *52* (91), 13357-13360.

181. Xie, J.; Zhou, Q.; Li, C.; Wang, W.; Hou, Y.; Zhang, B.; Wang, X., An unexpected role of the monodentate ligand in photocatalytic hydrogen production of the pentadentate ligand-based cobalt complexes. *Chem. Commun.* **2014,** *50* (49), 6520-6522.

182. Han, Z.; McNamara, W. R.; Eum, M.-S.; Holland, P. L.; Eisenberg, R., A Nickel Thiolate Catalyst for the Long-Lived Photocatalytic Production of Hydrogen in a Noble-Metal-Free System. *Angew. Chem. Int. Ed.* **2012,** *51* (7), 1667-1670.

183. Varma, S.; Castillo, C. E.; Stoll, T.; Fortage, J.; Blackman, A. G.; Molton, F.; Deronzier, A.; Collomb, M.-N., Efficient photocatalytic hydrogen production in water using a cobalt(iii) tetraaza-macrocyclic catalyst: electrochemical generation of the low-valent Co(I) species and its reactivity toward proton reduction. *PCCP* **2013,** *15* (40), 17544-17552.

184. Turner, J. A., Sustainable Hydrogen Production. *Science* **2004,** *305* (5686), 972-974.

185. Rountree, E. S.; Martin, D. J.; McCarthy, B. D.; Dempsey, J. L., Linear Free Energy Relationships in the Hydrogen Evolution Reaction: Kinetic Analysis of a Cobaloxime Catalyst. *ACS Catal.* **2016,** *6* (5), 3326-3335.

www.manaraa.com

186. Pilkington, N. H.; Robson, R., Complexes of binucleating ligands. III. Novel complexes of a macrocyclic binucleating ligand. *Australian Journal of Chemistry* **1970,** *23* (11), 2225-2236.

187. Ōkawa, H.; Furutachi, H.; Fenton, D. E., Heterodinuclear metal complexes of phenol-based compartmental macrocycles. *Coord. Chem. Rev.* **1998,** *174* (1), 51-75.

188. Laga, S. M.; Blakemore, J. D.; Henling, L. M.; Brunschwig, B. S.; Gray, H. B., Catalysis of Proton Reduction by a [BO4]-Bridged Dicobalt Glyoxime. *Inorg. Chem.* **2014,** *53* (24), 12668-12670.

189. Di Giovanni, C.; Gimbert-Suriñach, C.; Nippe, M.; Benet-Buchholz, J.; Long, J. R.; Sala, X.; Llobet, A., Dinuclear Cobalt Complexes with a Decadentate Ligand Scaffold: Hydrogen Evolution and Oxygen Reduction Catalysis. *Chem. Eur. J.* **2016,** *22* (1), 361-369.

190. Basu, D.; Mazumder, S.; Shi, X.; Staples, R. J.; Schlegel, H. B.; Verani, C. N., Distinct Proton and Water Reduction Behavior with a Cobalt(III) Electrocatalyst Based on Pentadentate Oximes. *Angew. Chem. Int. Ed.* **2015,** *54* (24), 7139-43.

191. Wang, D.; Lindeman, S. V.; Fiedler, A. T., Bimetallic Complexes Supported by a Redox-Active Ligand with Fused Pincer-Type Coordination Sites. *Inorg. Chem.* **2015,** *54* (17), 8744-54.

192. Perdew, J. P.; Wang, Y., Accurate and simple analytic representation of the electron-gas correlation energy. *Phys. Rev. B* **1992,** *45* (23), 13244-13249.

193. A. V. Marenich, C. J. C., D. G. Truhlar, , *J. Phys. Chem. B* **2009,** *113*, 6378-6396.

194. Neese, F. J., *Phys. Chem. Solids* **2004,** *65*, 781-785.

www.manaraa.com

195. R. Dennington, T. K., J. Millam, Version 5 ed ed.; Semichem Inc: Shawnee Mission, KS, 2009.

196. C. P. Kelly, C. J. C. a. D. G. T., *J. Phys. Chem. B.* **2006,** *110*, 16066-16081.

197. Fourmond, V.; Jacques, P. A.; Fontecave, M.; Artero, V., H2 evolution and molecular electrocatalysts: determination of overpotentials and effect of homoconjugation. *Inorg. Chem.* **2010,** *49* (22), 10338-47.

198. de Bruin, B.; Bill, E.; Bothe, E.; Weyhermüller, T.; Wieghardt, K., Molecular and Electronic Structures of Bis(pyridine-2,6-diimine)metal Complexes [ML2](PF6)n (n = 0, 1, 2, 3; M = Mn, Fe, Co, Ni, Cu, Zn). *Inorg. Chem.* **2000,** *39* (13), 2936-2947.

199. When referenced to the experimental acid, protonation of Co(I)-Co(I) B will be slightly uphill by 2.6 kcal/mol. Similarly, protonation and release of H2 from C will be downhill by 19.2 kcal/mol., When referenced to the experimental acid, acetic acid (pKa = 22.3), protonation of Co(I)-Co(I) B will be slightly uphill by 2.6 kcal/mol. Similarly, protonation and release of H2 from C will be downhill by 19.2 kcal/mol.

200. Hurst, J. K.; Roemeling, M. D.; Lymar, S. V., Mechanistic Insight into Peroxydisulfate Reactivity: Oxidation of the cis,cis-[Ru(bpy)2(OH2)]2O(4+) "Blue Dimer". *J. Phys. Chem. B* **2015,** *119* (24), 7749-60.

201. Karlsson, E. A.; Lee, B.-L.; Åkermark, T.; Johnston, E. V.; Kärkäs, M. D.; Sun, J.; Hansson, Ö.; Bäckvall, J.-E.; Åkermark, B., Photosensitized Water Oxidation by Use of a Bioinspired Manganese Catalyst. *Angew. Chem. Int. Ed.* **2011,** *50* (49), 11715-11718.

202. Gagliardi, C. J.; Wang, L.; Dongare, P.; Brennaman, M. K.; Papanikolas, J. M.; Meyer, T. J.; Thompson, D. W., Direct observation of light-driven, concerted electron–proton transfer. *Proc. Natl. Acad. Sci. U. S. A.* **2016,** *113* (40), 11106-11109.

www.manaraa.com

203. Xu, Y.; Eilers, G.; Borgström, M.; Pan, J.; Abrahamsson, M.; Magnuson, A.; Lomoth, R.; Bergquist, J.; Polívka, T.; Sun, L.; Sundström, V.; Styring, S.; Hammarström, L.; Åkermark, B., Synthesis and Characterization of Dinuclear Ruthenium Complexes Covalently Linked to RuII Tris-bipyridine: An Approach to Mimics of the Donor Side of Photosystem II. *Chem. Eur. J.* **2005,** *11* (24), 7305-7314.

204. Kurahashi, T.; Kikuchi, A.; Tosha, T.; Shiro, Y.; Kitagawa, T.; Fujii, H., Transient Intermediates from Mn(salen) with Sterically Hindered Mesityl Groups: Interconversion between MnIV-Phenolate and MnIII-Phenoxyl Radicals as an Origin for Unique Reactivity. *Inorg. Chem.* **2008,** *47* (5), 1674-1686.

205. Lassalle-Kaiser, B.; Hureau, C.; Pantazis, D. A.; Pushkar, Y.; Guillot, R.; Yachandra, V. K.; Yano, J.; Neese, F.; Anxolabehere-Mallart, E., Activation of a water molecule using a mononuclear Mn complex: from Mn-aquo, to Mn-hydroxo, to Mn-oxyl via charge compensation. *Energy & Environ. Sci.* **2010,** *3* (7), 924-938.

206. Tezgerevska, T.; Alley, K. G.; Boskovic, C., Valence tautomerism in metal complexes: Stimulated and reversible intramolecular electron transfer between metal centers and organic ligands. *Coord. Chem. Rev.* **2014,** *268*, 23-40.

207. Lanznaster, M.; Hratchian, H. P.; Heeg, M. J.; Hryhorczuk, L. M.; McGarvey, B. R.; Schlegel, H. B.; Verani, C. N., Structural and electronic behavior of unprecedented five-coordinate iron(III) and gallium(III) complexes with a new phenol-rich electroactive ligand. *Inorg. Chem.* **2006,** *45* (3), 955-7.

208. Allard, M. M.; Sonk, J. A.; Heeg, M. J.; McGarvey, B. R.; Schlegel, H. B.; Verani, C. N., Bioinspired five-coordinate iron(III) complexes for stabilization of phenoxyl radicals. *Angew. Chem. Int. Ed.* **2012,** *51* (13), 3178-82.

www.manaraa.com

209. Lanznaster, M.; Heeg, M. J.; Yee, G. T.; McGarvey, B. R.; Verani, C. N., Design of Molecular Scaffolds Based on Unusual Geometries for Magnetic Modulation of Spin-Diverse Complexes with Selective Redox Response. *Inorg. Chem.* **2007,** *46* 72-78.

210. Allard, M. M.; Xavier, F. R.; Heeg, M. J.; Schlegel, H. B.; Verani, C. N., Sequential Phenolate Oxidations in Octahedral Cobalt(III) Complexes with [N2O3] Ligands. *Eur. J. Inorg. Chem.* **2012,** *2012* (29), 4622-4631.

211. Lesh, F. D.; Shanmugam, R.; Allard, M. M.; Lanznaster, M.; Heeg, M. J.; Rodgers, M. T.; Shearer, J. M.; Verani, C. N., A Modular Approach to Redox-Active Multimetallic Hydrophobes of Discoid Topology. *Inorg. Chem.* 7226-7228.

212. <Bruker SMART X2S User Manual.pdf>.

213. Vosko, S. H.; Wilk, L.; Nusair, M., Accurate spin-dependent electron liquid correlation energies for local spin density calculations: a critical analysis. *Canadian Journal of Physics* **1980,** *58* (8), 1200-1211.

214. Stephens, P. J.; Devlin, F. J.; Chabalowski, C. F.; Frisch, M. J., Ab Initio Calculation of Vibrational Absorption and Circular Dichroism Spectra Using Density Functional Force Fields. *J. Phys. Chem.* **1994,** *98* (45), 11623-11627.

215. Scalmani, G.; Frisch, M. J.; Mennucci, B.; Tomasi, J.; Cammi, R.; Barone, V., Geometries and properties of excited states in the gas phase and in solution: Theory and application of a time-dependent density functional theory polarizable continuum model. *J. Chem. Phys.* **2006,** *124* (9), 094107.

216. Johnson Carroll K, "ORTEP: A FORTRAN Thermal-Ellipsoid Plot Program for Crystal Structure Illustrations". Oak Ridge, T., Oak Ridge National Laboratory., Ed. 1965.

www.manaraa.com

217. Dutta, A.; Biswas, S.; Dolai, M.; Shaw, B. K.; Mondal, A.; Saha, S. K.; Ali, M., Mononuclear manganese(iii) complexes of bidentate NO donor Schiff base ligands: synthesis, structural characterization, magnetic and catecholase studies. *RSC Advances* **2015,** *5* (30), 23855-23864.

218. Li, Q.-B.; Han, Y.-J.; Zhao, G.-Q.; Xue, L.-W., Synthesis, Crystal Structures and Catalytic Oxidation of Manganese(III) Complexes Derived from Salen-Type Schiff Base N,N'-Bis(5-nitrosalicylidene)ethane-1,2-diamine. *Acta Chimica Slovenica* **2017,** *64* (2), 500-505.

219. Addison, A. W.; Rao, T. N.; Reedijk, J.; van Rijn, J.; Verschoor, G. C., Synthesis, structure, and spectroscopic properties of copper(II) compounds containing nitrogen-sulphur donor ligands; the crystal and molecular structure of aqua[1,7-bis(N-methylbenzimidazol-2[prime or minute]-yl)-2,6-dithiaheptane]copper(II) perchlorate. *Dalton Trans.* **1984,** (7), 1349-1356.

220. <v17n8a09.pdf>.

221. Herrero, C.; Hughes, J. L.; Quaranta, A.; Cox, N.; Rutherford, A. W.; Leibl, W.; Aukauloo, A., Intramolecular light induced activation of a Salen-Mn(III) complex by a ruthenium photosensitizer. *Chem. Commun.* **2010,** *46* (40), 7605-7.

222. Ghachtouli, S. E.; Guillot, R.; Dorlet, P.; Anxolabehere-Mallart, E.; Aukauloo, A., Influence of second sphere hydrogen bonding interaction on a manganese(ii)-aquo complex. *Dalton Trans.* **2012,** *41* (6), 1675-1677.

223. Gandolfi, C.; Cotting, T.; Martinho, P. N.; Sereda, O.; Neels, A.; Morgan, G. G.; Albrecht, M., Synthesis and self-assembly of spin-labile and redox-active manganese(III) complexes. *Dalton Trans.* **2011,** *40* (9), 1855-65.

www.manaraa.com

224. Evangelio, E.; Ruiz-Molina, D., Valence Tautomerism: More actors than just electroactive ligands and metal ions. *Comptes Rendus Chimie* **2008,** *11* (10), 1137-1154.

225. Ruiz-Molina, D.; Veciana, J.; Wurst, K.; Hendrickson, D. N.; Rovira, C., Redox-Tunable Valence Tautomerism in a Cobalt Schiff Base Complex. *Inorg. Chem.* **2000,** *39* (3), 617-619.

226. Sedo, J.; Saiz-Poseu, J.; Busque, F.; Ruiz-Molina, D., Catechol-based biomimetic functional materials. *Adv. Mater.* **2013,** *25* (5), 653-701.

227. Shimazaki, Y.; Stack, T. D. P.; Storr, T., Detailed Evaluation of the Geometric and Electronic Structures of One-electron Oxidized Group 10 (Ni, Pd, and Pt) Metal(II)-(Disalicylidene)diamine Complexes. *Inorg. Chem.* **2009,** *48* (17), 8383-8392.

228. Franks, M.; Gadzhieva, A.; Ghandhi, L.; Murrell, D.; Blake, A. J.; Davies, E. S.; Lewis, W.; Moro, F.; McMaster, J.; Schröder, M., Five Coordinate M(II)-Diphenolate [M = Zn(II), Ni(II), and Cu(II)] Schiff Base Complexes Exhibiting Metal- and Ligand-Based Redox Chemistry. *Inorg. Chem.* **2013,** *52* (2), 660-670.

229. Ghorai, S.; Sarmah, A.; Roy, R. K.; Tiwari, A.; Mukherjee, C., Effect of Geometrical Distortion on the Electronic Structure: Synthesis and Characterization of Monoradical-Coordinated Mononuclear Cu(II) Complexes. *Inorg. Chem.* **2016,** *55* (4), 1370-1380.

230. Houmam, A., Electron Transfer Initiated Reactions: Bond Formation and Bond Dissociation. *Chem. Rev.* **2008,** *108* (7), 2180-2237.

231. Lee, W.-T.; Muñoz, S. B.; Dickie, D. A.; Smith, J. M., Ligand Modification Transforms a Catalase Mimic into a Water Oxidation Catalyst. *Angew. Chem. Int. Ed.* **2014,** *53* (37), 9856-9859.

www.manaraa.com

232. Han, Z.; Horak, K. T.; Lee, H. B.; Agapie, T., Tetranuclear Manganese Models of the OEC Displaying Hydrogen Bonding Interactions: Application to Electrocatalytic Water Oxidation to Hydrogen Peroxide. *J. Am. Chem. Soc.* **2017,** *139* (27), 9108-9111.

233. Kpogo, K. K.; Mazumder, S.; Wang, D.; Schlegel, H. B.; Fiedler, A. T.; Verani, C. N., Bimetallic Cooperativity in Proton Reduction with an Amido-Bridged Cobalt Catalyst. *Chem. Eur. J.* **2017,** *23* (39), 9272-9279.

www.manaraa.com

ABSTRACT

EVALUATION OF EARTH-ABUNDANT MONOMETALLIC AND BIMETALLIC COMPLEXES FOR CATALYTIC WATER SPLITTING

by

KENNETH KWAME KPOGO

December 2017

Advisor: Dr. Cláudio N. Verani

Major: Major (Inorganic Chemistry)

Degree: Doctor of Philosophy

The development of affordable water-splitting catalysts from Earth-abundant transition metal ions such as Co and Mn is of immense scientific interest. Aiming to develop an efficient water-splitting catalyst, a Co(II) complex featuring an asymmetric, pentadentate quinolyl-bispyridine ligand with a phenylenediamine backbone was synthesized and characterized by spectroscopic, spectrometric, and X-ray analysis. The Co ion was selected because of its ability to undergo redox conversions from $3d^5$ Co^{IV} through $3d^8$ Co^{I} thereby making it a suitable catalyst that can withstand harsh structural, and electronic changes during catalysis.

The electrocatalytic water reduction activity of the catalyst at neutral pH, gave a turnover frequency (TOF) of 970 moles of H_2/h at an overpotential of 0.65 V. Sustained catalytic water reduction over 18 hours gave a TON of 12,100 and (%FE) of 97% suggesting a stable catalyst. Post-catalytic analysis of a grafoil electrode using SEM, EDS, and UV-visible spectroscopy shows no evidence of catalyst degradation or transformation into other species thus confirming the molecular nature of the catalyst. **$[Co^{II}(L^{Qpy})H_2O]ClO_4$** is active towards water oxidation as well, operating with a %FE of 91% during catalysis in a 0.1 M borate buffer (pH 8.0), and giving a TON

www.manaraa.com

of 97, at an applied potential of 1.50 $V_{Ag/AgCl}$. By using a series of experimental methods as well as DFT techniques, I isolated and characterized the catalytic oxidized intermediates for **$[Co^{II}(L^{Qpy})H_2O]ClO_4$**, and proposed a 'water nucleophilic-attack' (WNA) mechanism of water oxidation where, the highly electrophilic $3d^5$ [$^{HS}Co^{IV}$=O] intermediate is attacked by a nucleophilic water molecule thus forming the essential O-O bond and releasing dioxygen. The photocatalytic activity in the presence of $[Ru(bpy)_3]^{2+}$ and ascorbic acid in acetate buffer (pH 4) shows a TON of 295 and TOF of 50 moles of O_2/h.

Monometallic cobalt complexes have been shown to efficiently catalyze water reduction and therefore, enhanced activity is expected from binuclear analogs of these monometallic catalysts. Close proximity between two Co centers could trigger cooperativity either by facilitating homolytic pathways or by enabling electron transfer between the metallic centers, thus avoiding formation of a Co^{III}–H^- species. We hypothesize that cooperativity will be dependent on (i) the distance between the Co centers, (ii) the relative topology of the coordination environments, and (iii) the degree of orientation and overlap between redox-active orbitals. I analyzed the catalytic potential of the bimetallic complex **$[Co^{II}_2(L^{1'})(bpy)_2]Cl_4$**, by means of electrochemical, spectroscopic, and computational methods and observed that it efficiently reduces H^+ to H_2 in acetonitrile in the presence of 100 equiv of acetic acid with a TON of 18 and %FE of 94 after 3 h at –1.6 $V_{Ag/AgCl}$. This observation allows us to propose that this bimetallic cooperativity is associated with distance, angle, and orbital alignment of the two Co centers, as promoted by the unique Co-N_{amido}-Co environment offered by $L^{1'}$.

Experimental results reveal that the parent [$Co^{II}Co^{II}$] complex undergoes two successive metal-based $1e^-$ reductions to generate the catalytically active species [$Co^{I}Co^{I}$], and DFT calculations suggest that addition of a proton to one Co^I triggers a cooperative $1e^-$ transfer by each

www.manaraa.com

of these Co^{I} centers. This $2e^{-}$ transfer is an alternative route to generate a more reactive [Co^{II}(Co^{II}–H^{-})] hydride avoiding the Co^{III}–H^{-} required in monometallic species. This [Co^{II}(Co^{II}–H^{-})] species then accepts another H^{+} in order to release H_2.

The manganese ion, with its broad range of oxidation states and considerable Earth-abundance, is an appropriate choice for the study of electron transfer processes involved in catalytic water oxidation as it has been used as an efficient electron donor in PS II. It has been proposed that incorporation of phenolate moieties into manganese species could lead to catalytic activity as well. I synthesized two manganese complexes, the hexacoordinate [$Mn^{III}L^{1}CH_3OH$] and the pentacoordinate [$Mn^{III}L^{2}$], with a pentadentate tris-phenolate ligands H_3L^{1} and H_3L^{2} respectively. Detailed results from the structural, spectroscopic, and electrochemical evaluation of the two Mn complexes suggest that whilst both complexes show ligand-based oxidations favoring formation of a [Mn^{III}/phenoxyl] species, the hexacoordinate analog could form a [Mn^{IV}/phenolate] species. This is specifically due to the low energy difference between the frontier orbitals (<5 kcal/mol) of the Mn center, and the redox-active phenolate ligands. This low energy barrier allows electronic interaction between the Mn ion, and the phenolate ligand, causing valence tautomerism through electron transfer.

We therefore tested the hexacoordinate [$Mn^{III}L^{1}CH_3OH$] for water oxidation catalysis and observed an overpotential of 0.77 V and TON of 53 in three hours with the catalyst operating at a %FE of 85. This study is particularly useful because it provides a basis for ligand design that favors either a radical or a high-valent metal pathway for catalytic water oxidation.

www.manaraa.com

AUTOBIOGRAPHICAL STATEMENT

EDUCATION

Ph.D. Degree (Inorganic Chemistry): Wayne State University, Detroit, MI (2012 – 2017)

M.Sc. Degree (Inorganic): East Tennessee State University (ETSU), Johnson City, TN (2012)

B.Sc. in Chemistry (Honors thesis): University of Cape Coast (UCC), Cape Coast, Ghana (2005)

PROFESSIONAL SOCIETY MEMBERSHIPS

American Chemical Society – ACS (2013 – Present)

AWARDS AND PROFESSIONAL MEMBERSHIP

- Wayne State University Summer Dissertation Fellowship–2017
- Mary G. Wood Award for Excellence in Research and Service – Wayne State University (2017)
- Graduate Thesis/Dissertation Scholarship – Wayne State University (2017)
- Thomas C. Rumble Graduate Fellowship – Wayne State University (2016 – 2017)
- Best Poster Presentation Award – Wayne State Graduate and Postdoc Research Symposium (2017)
- Graduate Thesis/Dissertation Scholarship – East Tennessee State University (2012)
- Best Oral Presentation – (Graduate Science Division) Appalachian Student Research Conference (2012)

PUBLICATIONS.

- **Kpogo, K. K.,** and Verani, C.N., "Efficient Electro/photocatalytic Water Splitting using a $[Co^{II}(L^{Qpy})]^{+}$ Complex" **2017,** *manuscript in preparation.*
- **Kpogo, K. K**., Wang, D., Mazumder, S., Schlegel, H.B., Fiedler, A., and Verani, C.N., *Chem. Eur. J.* **2017** *23*, 9272.
- Kankanamalage, P. H. A., Mazumder, S., Tiwari, V., **Kpogo, K. K.**, Schlegel, H. B. and Verani, C. N., *Chem. Commun.* **2016,** *52*, 13357-13360.
- Gonawala, S., Leopoldino, V. R., **Kpogo, K. K.,** and Verani, C. N., *Chem. Commun.* **2016,** *52*, 11155-11158.
- Wickramasinghe, L. D., Mazumder, S., **Kpogo, K. K.,** Staples, R. J., Schlegel, H.B., and Verani, C.N., *Chem. Eur. J.* **2016,** *22*, 10786-10790.
- Verani, C. N., Shanmugam, R., Xavier, F. R., Allard, M. M., **Kpogo, K. K**., *Dalton Trans.* **2013,** *42* (43), 15296-306

PRESENTATIONS/CONFERENCES

1. **Kpogo, K. K**., Wang, D., Mazumder, S., Schlegel, H.B., Verani, C.N., and Fiedler, A., 48th Central Regional Meeting (ACS), June 6-10, 2017, Dearborn, MI, USA (poster presentation)
2. **Kpogo, K. K.,** Wang, D., Mazumder, S., Schlegel, H.B., Verani, C.N., and Fiedler, A., Ohio Inorganic Weekend, November 4-5, 2016, University of Akron, Akron, OH, USA (oral presentation)
3. **Kpogo, K. K.,** Basu, D., Verani, C. N., Ohio Inorganic Weekend, November 13-14, 2015, Bowling Green State University, Bowling Green, OH, USA (poster presentation)
4. **Kpogo, K. K.,** Verani, C. N., 246th ACS National Meeting, September 8-12, 2013 Indianapolis, IN (oral presentation)
5. **Kpogo, K. K.,** Verani, C. N., 20th International Symposium on the Photophysics and Photochemistry of Coordination Compounds, July 7-11, 2013, Traverse city, Michigan, USA
6. **Kpogo, K. K.** Eagle, C. T. **Best Science Oral Presentation**, Appalachian Student Research Conference April 12-13, **2012**, Johnson City, Tennessee, USA (oral presentation)

www.manaraa.com